The role of odd chain fatty acids on hepatocyte and monocyte function

Ogwu John Ikwuobe

Doctor of Philosophy

Aston University

April 2018

Aston University

The role of odd chain fatty acids on hepatocyte and monocyte function

Ogwu John Ikwuobe

Doctor of Philosophy

2018

Thesis summary

Lipid-induced dysfunction of the liver is becoming increasingly prevalent and may be an essential link between obesity and type 2 diabetes (T2DM). Elevated circulating saturated fatty acids (FA) like palmitate have been shown to contribute to hepatic insulin resistance and chronic low-grade inflammation leading to T2DM while other plasma unsaturated FA appear protective. Strong emerging evidence point to the potentially protective effect of odd chain FA (OCSFA) on T2DM disease development; however, no study has looked at the cellular mechanisms underpinning its effect. The transcription factor PPAR alpha is involved in regulating hepatic lipid accumulation by upregulating genes responsible for FA transport and has been shown to alter hepatic insulin sensitivity, as well as an anti-inflammatory effect on monocytes. Therefore, the hypothesis that OCSFA predict fasting plasma glucose and their role in modulating hepatocyte and monocyte function (by activating PPAR alpha) has been examined. Analysis of the FA profile of a healthy and T2DM cohort showed that C15:0 occurred in higher proportions in healthy controls compared to T2DM (median difference 0.07%, $p = 0.05$) and was found to be negatively correlated with fasting blood glucose ($p = 0.002$). In a model of terminally differentiated HepG2 cells, the data showed that C15:0 ameliorated palmitate-induced dysfunction of glucose output ($p < 0.001$) and glycogen production ($p < 0.001$); and increased PPAR alpha transcriptional activity by 20% ($p < 0.01$). Furthermore, there was a 72% reduction in TNFα production in monocytes pre-exposed to C15:0 before LPS stimulation compared to controls ($p < 0.01$). Taken together, the potentially protective effect of C15:0 regarding T2DM development may be due to PPAR alpha-related attenuation of chronic inflammation and improvement of hepatocyte metabolism.

Acknowledgements

I would like to thank Prof. Helen Griffiths for her kindness, patience, mentorship, supervision, and support throughout my PhD. You were a rock when I needed one and a stellar example of a leader. I can only hope to be like you one day.

Many thanks to Prof. Clifford Bailey, Dr Srikanth Bellary, and Dr James Brown for their support throughout the development of this thesis. Your words of encouragement, supervision and constructive criticism were vital to the success of this work. I am incredibly grateful to James Brown and Srikanth Bellary for letting me use samples from their study for this thesis.

I will also like to acknowledge the tremendous amount of time and effort Dr Karan Rana and Nadia Lascar put into collecting samples used in this thesis.

To all the members of HRG 358, thank you for providing a familal atmosphere in the lab and for stimulating me academically every day. I hope that we have forged a friendship and scientific partnership that will last a long time.

Thank you Dr Chat Pararasa for the banter, the friendship and for showing me, a novice, the intricacies of biomedical research.

And to the best placement student ever, Kiran Shabir; your hard work and dedication to research is inspiring.

I appreciate my parents and siblings for their immense all-round support. You guys are the best!

A special thank you to all my friends, for willing me on; especially Dr Ehase Agyeno, for his critical eye and being that friend that is more like a brother.

And to my lovely wife, Yemisi, I wish it was possible to add you on as a co-author, because that is what you were and even more. Thank you for being ever present, especially at my lowest points.

And to my lovely children, Patani and Obiye, daddy did this for you to know you can achieve anything. And finally, I thank God for divine strength and inspiration.

Table of contents

List of Figures

List of Tables

ABBREVIATIONS

%wt	Percentage weight
µl	Microlitre
µM	Micromolar
ABCD1	ATP binding cassette subfamily D Member 1
ABCD2	ATP binding cassette subfamily D Member 2
ABCD3	ATP binding cassette subfamily D Member 3
ABCD4	ATP binding cassette subfamily D Member 4
ACAA2	Acetyl-CoA Acyltransferase 2
ACAD10	Acyl-CoA dehydrogenase family, member 10
ACADL	Acyl-CoA dehydrogenase, long chain
ACC	Acetyl-CoA carboxylase
ACC1	Acetyl-CoA carboxylase 1 or alpha
ACC2	Acetyl-CoA carboxylase 2 or beta

ACOX1	Acyl-coenzyme A oxidase 1
ACSL1	Long-chain-fatty-acid—CoA ligase 1
ADC	Atypical ductal cells
ADP	Adenosine diphosphate
AFP	alpha-fetoprotein
AGE	Advanced glycation end products
ALA	Alpha linolenic acid
ANOVA	Analysis of variance
anti- DNP	Anti-2,4-Dinitrophenol
APC	Allophycocyanin
ATP	Adenosine triphosphate
HRP	Horseradish peroxidase
BC	Biotin carboxylase
BCA	Bicinchoninic acid
BCL3	Boron trichloride
BF3	Boron trifluoride

BHT	Butylated hydroxytoluene
BMI	Body mass index
BSA	Bovine serum albumin
BSAox	Bovine serum albumin oxidised
BSAred	Bovine serum albumin reduced
c/EBPa	CCAAT/enhancer-binding protein alpha
C3b	Complement receptor type 1 receptors
CAT	Catalase
CD14	Cluster of differentiation 14
CD16	Cluster of differentiation 16
CD36	Cluster of differentiation 36/Fatty acid translocase
CDKAL1	CDK5 regulatory subunit associated protein 1-like 1
cDNA	Complementary DNA
CHD	Coronary heart disease
ChREBP	Carbohydrate response element binding protein
CPT1	Carnitine palmitoyltransferase 1

CPT2	Carnitine palmitoyltransferase 2
CRP	C-reactive protein
CT	carboxyltransferase
CT Method	Threshold cycle
DAG	Diacylglycerol
DHA	Docosahexaenoic acid
dHepG2	Differentiated HepG2 cells
DMEM	Dulbecco's modified eagle medium
DMSO	Dimethyl sulfoxide
DNA	Deoxyribonucleic acid
DNL	De novo lipogenesis
DNPH	2,4-Dinitrophenylhydrazine
dsDNA	double-stranded DNA
DTT	Dithiothreitol
EDTA	Ethylenediaminetetraacetic acid
ELISA	Enzyme-linked immunosorbent assay

ELOVL2	Elongase 2
ELOVL5	Elongase 5
EPA	Eicosapentaenoic acid
EPIC	European Prospective Investigation into Cancer and Nutrition
ER	endoplasmic reticulum
ERK	extracellular signal-regulated kinase
EVC-304	Umbilical vein endothelial cell line
FA	Fatty acid
FABP	Fatty acid binding protein
FACS	Fluorescence-activated cell sorting
FADS1	Fatty acid desaturase 1
FADS2	Fatty acid desaturase 2
FAME	Fatty acid methyl ester
FASN	Fatty acid synthase
FB	Fenofibrate
FBS	Foetal bovine serum

FCCP	Carbonyl cyanide-4-phenylhydrazone
Fc epsilon-RI	high-affinity IgE receptor
FDR	False discovery rate
Fe (II) SO4	Iron (II) Sulfate
FFA	Free fatty acid
FID	Flame ionisation detector
FITC	Fluorescein isothiocyanate
FTO	Fat mass and obesity-associated protein
G0/G1	Gap 0/Gap 1
G2/M	Gap 2/Mitosis
G6P	Glucose-6-Phosphate
GADPH	Glyceraldehyde phosphate dehydrogenase
GC	Gas chromatography
GK	Glucokinase
GLUT2	Glucose transporter 2
GLUT4	Glucose transporter 4

GPC	Glycerol-3-phosphocholine
GPR120	G-protein coupled receptor 120
GPR41	G-protein coupled receptor 41
GPR43	G-protein coupled receptor 43
GSK3β	Glycogen synthase kinase 3 beta
HCL	Hydrogen chloride
HDL	High density lipoprotein
HGF	Hepatocyte growth factor
HHEX	Hematopoietically-expressed homeobox protein
HLA	human leukocyte antigen
HNF	Hepatocytic nuclear factors
$HNF_{1\alpha}$	Hepatocytic nuclear factor 1 alpha
HNF1β	Hepatocytic nuclear factor 1 beta
HNF3β	Hepatocytic nuclear factor 3 beta
HNF4α	Hepatocytic nuclear factor 4 alpha
HNF6	Hepatocytic nuclear factor 6

HOMA-IR	Homeostatic model assessment-Insulin resistance
HPLC	High-performance liquid chromatography
HRP	Horseradish peroxidase
ICAM-1	(Intercellular Adhesion Molecule 1
IgE	Immunoglobulin E
IGF2BP2	Insulin like growth factor 2 binding protein 2
IκB	nuclear factor of kappa light polypeptide gene enhancer in B-cells inhibitor
IKKβ	IκB kinase-β
IKKβ	inhibitor of nuclear factor kappa
IL-1	Interleukin 1
IL-10	Interleukin 10
IL-4	Interleukin 4
IL-6	Interleukin 6
IL-8	Interleukin 8
IL-1β	Interleukin 1 beta
IRS-1	Insulin receptor substrate 1

IRS-2	Insulin receptor substrate 2
JAZF1	Juxtaposed with another zinc finger protein 1
JNK	c-Jun N-terminal kinases
KCNJ11	Potassium inwardly rectifying channel, subfamily J, member 11
KPNA2	Karyopherin subunit alpha 2
KPNB1	Karyopherin subunit beta 1
LDL	Low density lipoprotein
L-FABP	Liver specific fatty acid binding protein
LPC	Lysophosphatidylcholine
LPS	Lipopolysacharide
MAT	Malonyl-ACP by malonyl-CoA transferase
MCP-1	Monocyte chemotactic protein 1
MHO	Metabolically healthy obese
MLYCD	Malonyl-CoA decarboxylase
MMP-9	Matrix metallopeptidase 9
MoD	Median of difference

mRNA	Messenger RNA
MTT	3-(4,5-dimethylthiazol-2-yl)-2,5-diphenyltetrazolium bromide
MUFA	Monounsaturated fatty acid
NAD	Nicotinamide adenine dinucleotide oxidised
NADH	Nicotinamide adenine dinucleotide reduced
NADPH	Nicotinamide adenine dinucleotide phosphate
NAFLD	Non-alcoholic fatty liver disease
NASH	Non-alcoholic staetohepatitis
NCOA2	Nuclear receptor coactivator 2
NF-κB	Nuclear factor kappa-light-chain-enhancer of activated B cells
NHS	National Health Service
NLRP3	NLR family pyrin domain containing 3
nm	Nanometre
NO	Nitric oxide
NOTCH2	Neurogenic locus notch homolog protein 2
NOX3	NADPH oxidase 3

OCSFA	Odd-chain saturated fatty acid
OPD	o-phenylenediamine
OSM	Oncostatin M
P38MAPK	P38 mitogen-activated protein kinases
p53	TP53 or tumor protein
p65	Nuclear factor NF-kappa-B p65 subunit
PAS	Periodic acid-Schiff
PBS	Phosphate-buffered saline
PCR	Polymerase chain reaction
PEA	Palmitoylethanolamide
pH	Potential of Hydrogen
PI-3K	Phosphatidylinositide 3- kinase
PKC	Protein kinase C
PKC-Ɵ	Protein kinase C theta
PMA	Phorbol 12-myristate 13-acetate
PPAR	Peroxisome proliferator-activated receptor

PPARG	Peroxisome proliferator-activated receptor gamma gene
PPAR alpha	Peroxisome proliferator-activated receptor alpha
PPARγ	Peroxisome proliferator-activated receptor gamma
PPARδ	Peroxisome proliferator-activated receptor delta
PPRE	Peroxisome proliferator response element
PUFAs	Polyunsaturated fatty acids
qPCR	Quantitative polymerase chain reaction
RA	Retinoic acid
RIPA	Radioimmunoprecipitation assay
RNase	Ribonuclease free
ROS	Reactive oxygen species
RPMI 1640	Roswell Park Memorial Institute 1640 medium
RR	Relative risk
RT-qPCR	Real-time quantitative polymerase chain reaction
RXR	Retinoid X receptor
RxRa	Retinoid x receptor alpha

SAT	Subcutaenous adipose tissue
SCD	Stearoyl-CoA desaturase
SCD1	Stearoyl-CoA desaturase 1
SCD5	Stearoyl-CoA desaturase 5
SEM	Standard error of mean
SFA	Saturated fatty acid
Sirt1	Sirtuin 1
SLC30A8	Solute carrier family 30, member 8
S-Phase	Synthesis phase
SREBP1c	Sterol regulatory element binding protein 1c
STAT3	Signal transducer and activator of transcription 3
T2DM	Type 2 diabetes mellitus
TBX3	T-box transcription factor 3
TCA	Tricarboxylic acid
TCF7L2	Transcription factor 7-like 2
TLR1	Toll-like receptor 1

TLR2	Toll-like receptor 2
TLR4	Toll-like receptor 4
TLRs	Toll-like receptors
TNFα	Tumour necrosis factor α
UK	United Kingdom
UN	United Nations
US	United States
USA	United States of America
VAT	Visceral adipose tissue
VCAM-1	Vascular cell adhesion protein 1
VIF	Variance inflation factor
VLCFA	Very long-chain fatty acids
VLDL	Very low density lipoprotein
WAT	White adipose tissue
WFS1	Wolfram syndrome 1
WHO	World Health Organisation

β-ME	2-Mercaptoethanol
ω3-PUFA	Omega 3 fatty acid
ω6-PUFA	Omega 6 fatty acid

1 CHAPTER 1: GENERAL INTRODUCTION

1.1 Type 2 diabetes

There has been an alarming rise in the prevalence of diabetes over the last few decades. Statistics from the USA indicates more than 100% increase in diabetes incidence across all age groups between 1980 and 2011 [1]. The World Health Organisation (WHO) estimates that around 347 million people had diabetes in 2012, representing almost 10% of the global adult population. A more recent pooled analysis looking at data from more than 146 countries found that the global age-standardised prevalence of diabetes doubled in men (an increase from 4.3% to 9%) and increased by approximately 60% in women from 1980 to 2014 [2]. The same study also showed that the people living with diabetes rose from 108 million in 1980 to 422 million in 2014, age and population growth accounting for 40% of this rise. In the UK, the crude prevalence of diabetes increased by more than threefold between 1991 and 2014 as a result of an ageing population and a mean increase in survival from diabetes [3]. There are currently about 3.7 million confirmed diagnoses of diabetes with up to a million remaining undiagnosed and an expectation that more than 12 million people are at risk of developing the disease [4].

The disease has become a global epidemic with a 50% rise in incidence in the last ten years. In 2012, a global survey estimated that 1.5-5.1 million deaths were caused by diabetes and the WHO predicts it will be the seventh leading cause of death by 2030 [5]. Despite these daunting statistics, it is perhaps the economic burden of diabetes that has increased awareness towards it and other non-communicable diseases. It is estimated that the annual cost of diabetes (especially the complications) to the

healthcare system in the UK and US alone is in the region of £10 billion [6] and $250 billion respectively[7, 8].

The exact mechanism leading to diabetes mellitus is still unknown and widely debated [9]. However, it is well recognised that it is a disease of glucose homeostasis with two primary forms: Type 1, characterised by an absolute lack of insulin, accounting for 10% of cases; and Type 2 (T2DM), characterised by a relative lack of insulin or insulin resistance, accounting for 90% of cases. Monogenic diabetes and gestational diabetes (a derangement in glucose metabolism occurring in pregnancy, with an increased risk of T2DM in later life) are other less commonly recognised variants. T2DM is the most researched type of diabetes and centres around a dysfunction in insulin. The pathogenesis of T2DM is complex, involving factors such as high energy environments, elevated free FAs and inflammation. The consequence of this complex interaction is an inability of the pancreatic β-cells to produce insulin which is complicated by the widespread development of insulin resistance in peripheral tissues. The relationship between T2DM, sedentary lifestyle, and the so-called “western diet” is well established, highlighting the importance of the environmental and social risk factors for diabetes [10]. The genetic factors contributing to the onset and progression of T2DM is, however, less characterised.

Genetic factors have been consistently linked to an increased risk of T2DM. A family history of T2DM is a strong clinical predictor of the disease. Several genetic variants have been identified as reliable predictors of T2DM, independent of clinical risk factors. A review of genome-wide association studies over the last decade has revealed some

genes with a single-nucleotide polymorphism that appear to predict T2DM consistently. Some of the genes that have been shown to be predictive for T2DM at pre-diabetic states include: *TCF7L2, PPARG, FTO, KCNJ11, NOTCH2, WFS1, CDKAL1, IGF2BP2, SLC30A8, JAZF1,* and *HHEX* [11]. Despite this recent advancement in genetic studies, the specific mechanism by which these genetic factors interact to cause T2DM is still unknown. An increasing number of gene-specific candidate-driven studies for T2DM have identified more than 70 loci, mostly in non-coding regions of the genome. Consequently, research is now shifting towards identifying variants that affect the activity of enhancer elements regulating target gene expression [12]. Therefore, the interaction between environmental factors and epigenetic modifications are now being investigated to determine not just the mechanism of disease but also to determine why patients differ in disease progression and response to drug therapy [13].

T2DM is a highly heterogeneous disorder in onset and disease progression. A recent data-driven cluster analysis identified five different subgroups of individuals with T2DM with clear disease progression and risk of complications, highlighting the need for a more personalised approach to the management of T2DM [14]. Several publications from the Food4Me study have shown promise regarding the personalised management of T2DM tailored around the nutritional, environmental and genetic differences between individuals [15]. In these studies, personalised nutrition had a positive impact on behavioural change, which impacted on physical activity and other factors leading to the modification of obesity; regarded as one of the most important modifiable risks associated with T2DM.

1.2 Obesity

Obesity defines a complex, multifactorial, and preventable state of abnormal or disproportionate accumulation of body fat [16]. It increases the risk of chronic metabolic diseases and presents a substantial economic burden regarding morbidity and mortality. Regarding quantifying obesity, a body mass index (BMI) of more than 30kg/m^2 is considered obese. BMI is the most commonly used index for categorising disorders of weight, but it is not without bias in the context of predicting metabolic outcomes. The BMI cut-off for overweight and obesity is affected by several factors, especially age, gender, and race. For example, the BMI for Caucasians is significantly higher than that of Asians and people of sub-Saharan origin adjusted for body fat, age and gender, highlighting the need for population-specific BMI cut-off points for obesity [17]. Furthermore, BMI does not correctly account for muscle mass; therefore, a well-built athlete with a healthy body fat composition can be erroneously classed as obese by BMI. Consequently, the waist circumference is recommended in clinical and research settings for categorising obesity, as it accounts for abdominal obesity [18]. A pooled analysis of over 1600 population-based studies from almost 200 countries shows an alarming increase in the global prevalence of obesity over the last four decades. The global age-standardised BMI increased by more than 3kg/m^2 and 2kg/m^2 in men and women respectively from 1975 to 2014 [19]. This corresponded to a global tripling of obesity prevalence (from 3.2% to 10.4%) in men and a doubling (6.4% to 14.9%) in women. If this trend continues, at least 60% of the world's population would be obese or overweight by 2030 [20]; which is grave consequence in the US where it is expected that 85% of the population would be overweight or

obese [21]. A United Nations (UN) report in 2013 shows that at least one in four residents of the UK are obese, with the expectation that at least half the population will be obese by 2050 [22]. Obesity arises as a result of energy surplus, where energy consumption is not matched by calories expended. Although the complex interaction between genetic, environmental and socioeconomic factors contribute to obesity, the growing obesity epidemic is more likely due to changes in diet and lifestyle. The unexpected rise in obesity in developing countries exemplifies this. In addition to the adoption of the 'Western diet', which is high in carbohydrates and fat and low in fibres, urbanisation, associated with rapid industrialisation and mechanised transportation has reduced physical activity, consequently leading to obesity. Importantly, the dietary and lifestyle risks of obesity are modifiable; however, the prevalence of obesity has not been improved by enhanced campaigns to increase awareness of healthy dietary and physical activity recommendations [23]. The importance of developing effective strategies to modify these risks, reversing the obesity trend, relates to the numerous diseases associated with diabetes. Obesity is associated with diabetes, cardiovascular disease, cancer and many other disorders [24].

The link between obesity and T2DM received increased recognition in the early 1990's and now appears to be well established. There are excellent scientific reasons for this. Firstly, the prevalence of obesity tightly mirrors that of T2DM in the last three decades [25]. Furthermore, the relative risk (RR) of T2DM increases exponentially with increasing BMI; from an RR of 1 at 22kg/m^2 to 93.2 at a BMI of 35kg/m^2 [26]. Moreover, interventions aimed at reducing obesity, like bariatric surgery, low-calorie diets and increased physical activity have been shown to either cure T2DM or induce remission

[27]. Therefore, focus has switched to identifying the complex mechanisms that underpin the relationship between T2DM and obesity. Many theories have been suggested, including obesity-induced inflammation associated with a high energy state which is characterised by hyperglycaemia and hyperlipidaemia. However, not all obese people have insulin resistance or metabolic disease, the so-called 'metabolically healthy obese (MHO)' [28]. Despite high energy states, including hyperlipidaemia, the MHO show no signs of inflammation or hyperglycaemia. This contributes to the obesity-T2DM axis in two ways. Firstly, it confirms the importance of inflammation in the development of T2DM; however, it casts doubts on the requirement of obesity in the pathogenesis of T2DM. Secondly, it raised interest in the distribution of fat rather than its absolute quantity. Consequently, studies have found that visceral adipose tissue (VAT) fat predicts insulin resistance better than subcutaneous adipose tissue (SAT) fat, and within the SAT, abdominal distribution confers a higher risk of T2DM [29-31]. Naukkarinen and colleagues carried out a cross-sectional study where they measured several indices of metabolic disease including liver fat, markers of inflammation and insulin resistance in sixteen rare obesity-discordant monozygotic adult twin pairs to study the relationship between fat depots, MHO and metabolic disease [32]. In this robust study, the authors found liver fat accumulation, a downregulation of FA oxidation and a dysfunctional mitochondrial oxidative phosphorylation pathway as the differentiating factors between obese twins with insulin resistance MHO. Therefore, the liver is an essential organ in the pathogenesis of metabolic diseases. The factors that determine dysfunctional ectopic fat deposition are still poorly understood.

1.3 Liver

The liver is a major organ involved in glucose homeostasis. The gut and liver account for a third of glucose handling in humans under postprandial conditions [33-35]. During periods of glucose excess, as seen in post-prandial periods, glucose is phosphorylated to Glucose-6-Phosphate (G6P) within hepatocytes and channelled towards energy production via the tricarboxylic acid cycle (TCA) or mitochondrial oxidative phosphorylation. The glycolytic product, pyruvate, is also directed towards FA synthesis (de novo lipogenesis) and the production of Nicotinamide Adenine Dinucleotide Phosphate (NADPH) through the Pentose Phosphate Pathway. Furthermore, excess glucose converted to G6P is stored as glycogen in a process driven by glycogen synthase and facilitated by insulin, which simultaneously blocks endogenous glucose production (gluconeogenesis) by 50% in healthy humans [36]. Conversely, in the fasted state, glucose homeostasis is maintained by liver-driven gluconeogenesis; glucose is produced from glycogen on a short-term basis and from lactate, pyruvate, glycerol, and amino acids, long-term, in a process that follows a downregulation of insulin and the liver is more 'glucose-effective' than muscle cells. Glucose effectiveness denotes the ability of glucose to stimulate its metabolism independent of insulin. For example, glucose can move across hepatocyte membrane but not muscle cells through glucose transporter 2 (GLUT2), facilitated by glucokinase (GK), to suppress gluconeogenesis, independently of insulin signalling, in a bi-directional manner dependent on glucose concentration. Whereas, muscle cells require glucose transporter 4 (GLUT4) in an insulin-mediated pathway. However, the liver is still very insulin sensitive, requiring insulin for glycogen synthase derive

glycogen [37]. The subtle distinction between liver and muscle handling of glucose is made because of the effect it has on obesity-induced insulin resistance (or high-fat diet-induced dysregulation of glucose homeostasis). In addition to glucose metabolism, the liver is capable of de novo lipogenesis (DNL), a mechanism that is important in obesity-related insulin resistance. The justification for targeting the liver over muscle cells is highlighted in clinical studies where the resolution of hyperglycaemia in T2DM subjects after short-term calorie restriction was related to improved hepatic glucose metabolism rather than insulin-mediated glucose metabolism in muscle cells [38]. Furthermore, Brøns and colleagues showed that hepatic gluconeogenesis-induced elevation of plasma glucose precedes muscle insulin resistance in a cohort of young healthy lean individuals fed a high-fat diet for five days [39]. Their results are also corroborated by other studies [40].

1.4 Hepatocyte

The hepatocyte is the functional unit of the liver and accounts for up to 80% of liver cell mass. Hepatocytes are responsible for a wide range of metabolic activity, including carbohydrate, lipid and protein metabolism, as well as detoxification and immune surveillance. Hepatocytes are arranged around the portal-central axis. The metabolic functions of hepatocytes are highly differentiated and dependent upon their position in the portal-central axis. For example, periportal hepatocytes are mostly involved with gluconeogenesis, ammonia synthesis, cholesterol synthesis and FA degradation. Conversely, perivenous hepatocytes chiefly handle DNL, glycolysis and xenobiotic detoxification.

The diverse functions of hepatocytes necessitate a complex phenotype which is acquired progressively during foetal development by expression of a vast array of complement genes and maintained by tight regulation throughout adulthood [41]. Hepatocytes differentiate from hepatoblast upon stimulation by hepatocyte growth factor (HGF) and oncostatin M (OSM) in the early stages. TBX3 (T-box transcription factor 3) then stimulates hepatocyte maturation mediated expression of a host of transcriptional factors including several hepatocyte nuclear factors ($HNF_{1\alpha}$, $HNF_{1}\beta$, $HNF_{4\alpha}$, HNF3β, AND HNF6) and c/EBPa (CCAAT-enhancer binding protein α). The final steps of hepatocyte maturation involve the repression of oncofetal genes (like alpha-fetoprotein, hexokinase 2, and pyruvate kinase M2) and the full expression of genes like albumin, transferrin, fatty acid synthase. Hepatocytes exist in vivo as mostly quiescent cells but are capable of de-differentiation into foetal forms in cases of liver injury; however, this process is tightly regulated to assume a differentiated state upon regeneration. Hepatocytes are unique in their ability to regenerate in response to injury by cell growth and division and by facultative-stem cell-mediated recovery which involves the recruitment of atypical ductal cells (ADC) also known as oval cells [42]. Abnormal proliferation leads to conditions like hepatocellular cancer. In in vitro hepatocyte models, HepG2 cells, an immortalised cell line is often used in place of primary hepatocytes because they are relatively inexpensive and are more proliferative. However, HepG2 cells show significant differences in gene expression and metabolic function compared to primary hepatocytes. For example, metabolic network flexibility analysis of HepG2 cells under different glucose conditions shows that in comparison to primary hepatocytes, hepatoma cells favour glycolysis over

oxidative phosphorylation, due to their highly proliferative nature. Furthermore, gene expression levels of markers of differentiation, like albumin, transferrin, and fatty acid synthase are usually low, while xenobiotic enzyme gene expression is often absent. However, the feedback responses to energy availability, insulin stimulation, and end-products of glucose metabolism remain mostly the same. Moreover, HepG2 cells have been successfully differentiated by various methods to more closely resemble their primary counterpart in gene expression and functional phenotype.

1.5 NAFLD

Non-alcoholic liver fatty disease (NAFLD) describes a spectrum of disorders associated with the accumulation of fat in the liver in the absence of competing liver aetiologies [43]. It ranges from simple hepatic steatosis (liver fat accumulation) to steatohepatitis (NASH), where fatty deposits are associated with inflammation, and a small proportion may culminate in hepatic fibrosis, cirrhosis, or carcinoma. The current burden of NAFLD is as staggering as T2DM and obesity, and it is now increasingly recognised as the liver component of metabolic syndrome [44-47]. Indeed, up to 90% of people with NAFLD fulfil at least one component of metabolic syndrome, while up to a third fulfil three aspects of metabolic syndrome [48]. Many studies have reported a close association between NAFLD, obesity and T2DM. The prevalence of NAFLD in obese is as high as 90%, depending on the level of obesity [49-51]. Similarly, the prevalence of T2DM in a population of people with NAFLD was recorded to be as high as 85% (prevalence of T2DM and pre-diabetes combined) in one study [52] and 76% in another [50]; while another study showed that those with NAFLD are three times more likely to have T2DM [53]. The global prevalence of NAFLD is on the rise. In a

meta-analysis of 86 studies by Younossi and colleagues, the global prevalence of NAFLD was estimated from over eight million individuals in 22 countries, where NAFLD was diagnosed using a range of imaging studies [54]. The prevalence of NAFLD was estimated to be 25%; the prevalence of obesity and T2DM among people with NAFLD were 51% and 22% respectively. The prevalence of NAFLD is likely to be underestimated in this analysis considering the sensitivity of imaging is up to 20% less than the gold standard liver biopsy [55]. Moreover, NAFLD is ubiquitous among people with T2DM. In a meta-analysis by Dai and colleagues, the pooled prevalence of NAFLD among people diagnosed with T2DM was 60%, ranging from 29% to 87% in twenty-four studies involving more than thirty thousand participants [56].

Further justification for the importance of NAFLD in T2DM lies with the value of early intervention. Peripheral insulin resistance is already established and indeed plateaus by the time T2DM is diagnosed [57]. It is hypothesised that the onset of hepatic lipid accumulation and insulin resistance precedes T2DM by five to ten years and peripheral insulin resistance is entirely reversible at this stage [57]. Therefore, early diagnosis of NAFLD could provide a useful opportunity to halt the progression of impaired glucose tolerance to T2DM. NAFLD provides a useful link between obesity and T2DM and the effect of circulatory FAs could be key.

In patients with NAFLD, both saturated (SFA) and monounsaturated fatty acids (MUFA) are causally implicated in the pathogenesis of steatosis [58, 59]. However, SFA are more likely to induce hepatocellular dysfunction and a pro-inflammatory profile consistent with nonalcoholic fatty liver pathology [60]. Cellular dysfunction is the result of FAs promoting endoplasmic reticulum (ER) stress, uncoupling mitochondrial

respiration and increasing production of reactive oxygen species (ROS), culminating in hepatic inflammation and cell death [61-63]. In contrast to previous reports of SFA-mediated steatosis, some MUFA has been shown to reverse the lipotoxic effect of SFA on hepatocytes in vitro, despite a paradoxical increase in lipid accumulation. This variation in metabolic consequence has been suggested to be due to the ability of different classes of FAs to behave differently as signalling molecules.

1.6 Fatty acids

FA are the basic building blocks of lipids. They are made of a carbon skeleton attached to a carboxylic acid functional group. Natural occurring FA are usually monocarboxylic acids and are classified by chain length, saturation, carbon number, and chain nature. Classification by saturation is perhaps the most biologically relevant sub-division of FAs. On this basis, FA are designated as either saturated or unsaturated based on the presence of double bonds. Palmitic acid is a sixteen-chain FA, and is the most abundant saturated FA in humans, accounting for up to 30% of total FAs in plasma. Unsaturated FAs contain at least one double bond. They are further classified as monounsaturated fatty acids (MUFA) because they contain one double bond, or polyunsaturated fatty acids (PUFA), which contains at least two double bonds. The most abundant MUFA is oleic acid (C18:1n9), which occurs in diet, but can also be synthesised de novo by desaturation enzymes introducing double bonds to its saturated counterpart octadecanoic acid (C18:0). FAs can be straight chain (like most free FA in human plasma), branched chain, cyclic, or substituted (addition of hydroxyl, epoxy, dicarboxy groups attached to straight chain FA), by chain nature. Traditionally, FA were classified by carbon chain length as either short-chain (C4-C6), medium chain

(C8-C12), long-chain (C14-C20), and very long chain (>C22). The clinical importance of FA classification by chain length is highlighted in disorders such as Refsum disease and Zellweger syndrome, where the presence of very long FA can be both diagnostic and prognostic [64]. However, a new classification has been added by carbon number, whereby FA are either odd-chain FA or even-chain FA, depending on the number of carbon atoms.

Ancel keys helped to institute the epidemiologic link between lipids and cardiovascular disease as early as the 1940s. The link between fat and cardiovascular disease was then fully established in 1970 after the publication of results from Ancel Key's 'seven countries' study, which then led to a series of nutritional recommendation to reduce dietary fat [65, 66]. However, the significance of FA classification in health and disease gained momentum afterwards when many publications showed the potential benefits of replacing saturated fats with PUFA [67]. However, growing evidence from re-analysis of previous incomplete randomised control trials has shown that the effect of saturated fats on cardiovascular health, and the potential benefits of its replacement may have been overestimated [68]. Nevertheless, many in vitro and in vivo models have corroborated the lipotoxic effects of FA over the years. The deleterious effect of increased circulating FA, especially SFA on whole-body insulin resistance is well studied. Dresner et al. (1999) established that infusion of healthy human subjects with free fatty acids (FFA) resulted in insulin resistance in muscle cells [69]. Results from muscle biopsies from these subjects showed up to 60% reduction in glucose oxidation and glycogen synthesis associated with a 90% decrease in intramuscular G6P, suggesting a reduction in glucose transport across cells resulting from IRS-1 (insulin

receptor substrate 1) associated PI-3K (Phosphatidylinositide 3- kinase) activity. Subsequently, many other mechanisms of FA-induced insulin resistance in peripheral tissues have been described, including accumulation of lipid metabolites such as diacylglycerol (DAG) and ceramides. Similarly, in animal models, short-term high fat diet has been used to induce hepatic insulin resistance via many mechanisms including protein kinase C (PKC) activation [70] induced by accumulation of diacylglycerol (DAG) resulting in hepatic insulin resistance which occurs long before systemic insulin resistance or inflammation, suggesting the pivotal role of hepatic dysfunction on the development of T2DM [71]. Furthermore, Dan Gao and colleagues found a reduction in hepatic glycogen content as a result of a FA-induced increase in NADPH oxidase 3 (NOX3)-derived reactive oxygen species (ROS) in *db/db* mice fed high-fat diets and in palmitate-treated HepG2 cells, mediated via JNK and $P38^{MAPK}$ pathway [72]. Although evidence abounds on the general effect of FA on insulin resistance and consequently glucose metabolism, some studies have shown that there may be significant differences in metabolic outcome and signalling when unsaturated FA are used in place of the more commonly adopted palmitate treatment. There is so far no study done to understand if these differences exist within SFA with odd-numbered carbon chain length.

Emerging evidence from large-scale longitudinal studies over the last decade has drawn attention to the role of odd-chain saturated fatty acids (OCSFA) on health and disease in humans. Research interest in OCSFA has evolved from investigating factors that affect their composition in ruminant milk to measuring their association with metabolic diseases in human studies. OCSFA were initially thought to be

physiologically unimportant and non-existent in humans. Therefore, they were used as internal standards for the chromatographic identification of other FA. Earlier research into OCSFA focused on factors that influenced their composition in ruminant milk because of their potential to impact the melting point of milk and animal fat in a chain length-dependent manner. Furthermore, OCSFA was found to reduce total SFA in milk significantly; therefore, research intensified to influence their composition in milk given nutritional policies to keep SFA intake below 30%. Incidentally, these studies would provide further insight into its de novo synthesis, including the role of foliage ratios, propionate, the gut bacteria, and adipocytes in ruminants. Further interests in OCSFA developed as some studies showed its antitumor effect in vitro and in vivo reproducible for breast and prostate cancer. The antitumor activity was reported to be closely linked to the downregulation of de novo lipogenesis; however, this was never replicated in human studies. In the early 2000's, studies began to emerge correlating plasma OCSFA to dairy intake, which correlated positively with healthy eating habits and general lifestyle. Therefore, plasma OCSFA were used in nutritional studies as a marker for dairy intake. Despite this, it took some time to recognise their physiological importance for a few reasons. Most of the scepticism about the physiological significance of OCSFA have come from a lack of understanding regarding their metabolic fate in humans. The hypothesis regarding their catabolism have come from animals and bacteria, and these pathways are thought to be redundant in humans [73]. Peroxisome α-oxidation has been proposed but remains unproven in humans. However, some studies have shown that phytanic acid, a β-branched odd-chain fatty acid, can undergo both β-oxidation and α-oxidation,

offering fresh insight into the possible mechanisms for catabolising OCSFA [74, 75]. Furthermore, a recent in vitro study showed that OCSFA is produced in adipocytes during the early stages of differentiation, proposing a de novo lipogenesis pathway for OCSFA. Recent publications from the European Prospective Investigation into Cancer and Nutrition (EPIC) have shown an inverse correlation between the concentrations of OCSFA in plasma and red cell membranes and the incidence cardiovascular diseases and T2DM [76]. Other longitudinal and cross-sectional studies have also highlighted the potentially protective effect of OCSFA against a range of conditions such as T2DM and pre-diabetes, biotin deficiency, anorexia nervosa, atherosclerosis, disorders of propionate, and peroxisome disorders [77-84]. Although the benefits of OCSFA are clear from the studies above, the mechanisms by which they are protective is still unknown. Moreover, a recent study showed that OCSFA is heterogeneous in metabolism, biosynthesis, and relationship with glucose tolerance [85]. Therefore, further in vitro and in vivo studies are needed to define the benefit of specific OCSFAs.

1.7 Fatty acid metabolism

The liver plays a central role in the metabolism of FA [86]. Exogenous FA bound to albumin, are mostly transported into hepatocytes via FA transport proteins found in the membrane [87]. Intracellular trafficking of FA between organelles is further regulated by fatty acid binding proteins (FABP) [88]. The metabolic fate of intracellular FA is dependent upon several factors, including FA themselves, which act as signalling molecules. The most critical catabolic pathway for FA within the liver is mitochondrial β-oxidation, which results in the breakdown of FAs by two carbon atoms

in each cycle into acetyl CoA and carbon dioxide. This process is facilitated by activation of FAs into Acyl-CoA in the cytosol before transport into the mitochondria by carnitine palmitoyltransferase located in the mitochondrial membrane [89]. Minor pathways of FA oxidation, like α-oxidation and ω-oxidation, also occur in peroxisomes for odd-chain FAs and very long-chain FAs (VLCFA) respectively [90, 91]. FA produced de novo, or acquired exogenously, can also be directed towards other metabolic pathways, like acylation into cellular lipids (including triglycerides, phospholipids and lipoproteins), and elongation and desaturation into VLCFA and unsaturated FA respectively [92, 93]. These pathways are tightly controlled, with dysregulation leading to metabolic dysfunction such as an accumulation of lipids within hepatocytes (steatosis), which may lead to the clinical scenario of non-alcoholic fatty liver diseases (NAFLD) [94].

The ability of the liver to synthesise FA underpins its importance in lipid metabolism. The de novo lipogenesis (DNL) is a critical pathway in the liver that is tightly linked with glucose metabolism [95, 96]. In fact, the primary product of the glycolytic pathway acts as substrates for DNL. Therefore, a substantial carbohydrate diet provides a large substrate for the DNL pathway resulting in increased lipid production [97-99]. The biochemical process of DNL can be summarised as the condensation of acetyl Co-A subunits on to a glycerol backbone in a multiplex reaction regulated by enzymes and signalling molecules such as insulin [100]. In the first irreversible step, malonyl-CoA is produced by carboxylation of acetyl-CoA, catalysed by acetyl-CoA Carboxylase (ACC), mediated by its two catalytic activities; biotin carboxylase (BC) and carboxyltransferase (CT). ACC is a complex multifunctional enzyme regulated

transcriptionally and encoded by two genes: ACC1 (Acetyl-CoA Carboxylase 1 or alpha) and ACC2 (Acetyl-CoA Carboxylase 2 or beta), both coding for two distinct ACC isoenzymes with different functions. ACC1 is primarily involved with DNL and under short-term regulation by citrate and palmitoyl-CoA. Whereas, the malonyl-CoA produced via ACC2 interacts with FA oxidation by blocking carnitine palmitoyltransferase I, the rate-limiting step for β-oxidation [101], making it an essential anti-obesity drug target. In addition to the transcriptional and allosteric regulation of ACC, the DNL is regulated by insulin and glucose through sterol regulatory element binding protein 1c (SREBP1c) and carbohydrate response element binding protein (ChREBP) respectively [102]. The malonyl-CoA produced by ACC is then converted to malonyl-ACP by malonyl-CoA transferase (MAT), and a series of NADPH-mediated reduction reactions follows culminating in the formation of acyl-CoA, which is converted to palmitate in another series of sequential elongation by 2 carbon atoms involving fatty acid synthase (FASN) [Figure 1.1]. Palmitate is then desaturated by stearoyl-CoA desaturase (SCD) to MUFA. Fructose can indirectly fuel DNL by the interaction of its substrates (dihydroxy-acetone-phosphate and glyceraldehyde 3-phosphate) with glycolysis. Lipid accumulation is central to the development of NAFLD, and DNL is critical to this process. Radioisotope studies have shown that DNL contributes up to a quarter of liver fat in NAFLD [59, 103]. Adipocytes produce about 60%, while 15% is from the diet. Although the majority of this fat is from adipocytes, the absence of obesity in some individuals with NAFLD, and the role of hepatic insulin resistance (and mitochondrial dysfunction) in the pathogenesis of T2DM (as previously discussed) in NAFLD suggests a more prominent role for DNL.

Figure 1.1: Schematic of the de novo lipogenesis pathway, showing the interaction between glucose metabolism and FA synthesis. [104]

GKRP, glucokinase regulatory protein; G6Pase, glucose-6-phosphatase, catalytic subunit; GAPDH, glyceraldehyde-3-phosphate dehydrogenase; PKLR, pyruvate kinase, liver and RBC; PCK1, phosphoenolpyruvate carboxykinase1; LDH, lactate dehydrogenase A; DCT, dicarboxylate transporter; PDK2, pyruvate dehydrogenase kinase isozyme2; PDH, pyruvate dehydrogenase; SDHAP3, succinate dehydrogenase complex, subunit A; FASN, fatty acid synthase; SCD1, stearoyl-CoA desaturase 1; GPD1, glycerol-3-phosphate dehydrogenase 1 (soluble); MOGAT2, monoacylglycerol O-acyltransferase 2; DGAT2, diacylglycerol O-acyltransferase homolog 2.

1.8 Inflammation and T2DM

The connection between T2DM, obesity, and inflammation has been a historic topic of hot debate. Early recognition of this paradigm started over a century ago when a series of case studies showed that the use of high dose aspirin effectively treated glycosuria, followed by intervention studies that showed complete independence from insulin after high dose aspirin therapy [105-107]. Although well-designed efficacy trials further validated the hypoglycemic action of salicylates, it was not until early 21st century that mechanistic studies were able to identify IκB kinase-β (IKKβ)/NF-κB axis as the molecular target for salicylate-induced modification of insulin resistance [108, 109]. Previous studies on the effect of salicylates had measured insulin secretion from pancreatic islet cells with poor outcomes [110]. Further evidence to support the theory of inflammation in the pathogenesis of T2DM comes from the observation of a higher risk of T2DM among individuals with other chronic inflammatory disorders such as rheumatoid arthritis [111]. More so, chronic inflammation and mitochondrial oxidative stress are hallmarks of adipocyte expansion and remodelling with obesity, which is highly correlated with T2DM [112]. This chronic low-grade inflammatory state is then able to start an inflammatory cascade which is fuelled by reactive oxygen species. Consequently, expanding adipocytes have been shown to overproduce tumour necrosis factor α (TNFα), which impacts directly upon insulin resistance. In fact, some studies have been able to show that administration of recombinant TNFα to cells or animals impairs insulin function, whereas, TNFα knockdown mice are partially protected from high-fat diet-induced insulin resistance [113, 114]. Furthermore, chronic systemic inflammation increases leptin-resistance STAT3 (signal transducer

and activator of transcription 3) activation/phosphorylation in the hypothalamus and the gut, affecting appetite and food intake, which then fuels insulin resistance [115, 116]. More recent epidemiologic studies have now been able to establish a positive correlation between pro-inflammatory markers, like C-reactive protein (CRP), interleukin 6 (IL-6), interleukin 8 (IL-8), TNFα and the incidence of T2DM [117-121]. However, it is the mechanistic studies that have elucidated the specific links between inflammation and T2DM, especially the role of inflammatory cytokines. TNFα is able to stimulate the inhibitory phosphorylation of serine residues for insulin receptor substrate 1 (IRS-1) inhibiting downstream signalling and insulin sensitivity [122-125]. Furthermore, pro-inflammatory cytokines are able to induce insulin resistance by interacting with JNK (c-Jun N-terminal kinases), NF-ƙB and PKC-Ɵ. JNK is elevated in the liver with obesity, and upon activation by pro-inflammatory cytokines, or directly by FAs, it associates and phosphorylates IRS-1 on Ser307[126]. JNK knockdown in mouse models protects from development of hepatic insulin resistance, while overexpression produces the systemic effect of insulin resistance, underpinning its importance in T2DM pathogenesis [127, 128]. An accumulation of ceramides and other intermediates are known to interact directly with IKK (inhibitor of nuclear factor kappa), JNK, NF-ƙB and PKC-Ɵ. Ceramides can directly activate PKC-Ɵ which induces insulin resistance similarly to JNK, or by activating IKKβ. In addition to direct interaction with IRS-1, IKKβ activates NF-ƙB by phosphorylating its inhibitor (IƙB), which stimulates the production of pro-inflammatory cytokines [129].

There has also been interest regarding monocytes and macrophage contribution to the inflammatory theory of T2DM. The chronic inflammation associated with increasing

adiposity stimulates MCP-1 (monocyte chemotactic protein 1), which enhances monocyte recruitment to adipocytes, creating a snowball inflammatory effect [130]. The theory that monocytes and macrophages, as chief players in innate immunity, drive differential response to inflammatory stimuli in healthy individuals compared to people with T2DM is gaining popularity [131]. Monocytes infiltrate and interact with many organs and tissues such as the liver, gut, pancreas and adipose tissue, and are involved with local and systemic response to inflammatory stimuli such as infections and hyperglycaemia [132, 133]. Monocyte and macrophage phenotypes have been a particular interest. A more precise distinction between pro-inflammatory and anti-inflammatory monocytes and macrophages are now more possible due to improved flow cytometry techniques. Monocytes are classified as classical, intermediate, or non-classical; depending on the expression of CD14 (cluster of differentiation 14) and CD16 (cluster of differentiation 16) on the cell surface [134, 135]. The classical monocyte subset represents 80% of circulating monocytes and expresses high levels of CD14 and deficient levels of CD16 (otherwise denoted CD14++/CD16- population). This subpopulation of monocytes express anti-inflammatory phenotype characterised by high phagocytic function, but quick resolution post-inflammation, with reduced TNFα and increased IL-β secretion. Intermediate monocyte subset is characterised by high levels of CD14, and higher levels of CD16 compared to classical monocytes (denoted as CD14+/CD16+ monocytes) and have been denoted pro-atherogenic. Along with intermediate monocytes, the non-classical monocytes (or CD14-/CD16++ sub-population) are associated with increased production of pro-inflammatory cytokines and are increased in infectious diseases as well as chronic metabolic

disorders [136-139]. Similarly, macrophages express a pro-inflammatory classically generated (M1), or anti-inflammatory alternatively generated (M2) macrophage phenotype depending on the inflammatory environment [140]. The M2 macrophage has also been subdivided into M2a, M2b, M2c, and M2d subsets on the basis of induced transcriptional changes [141, 142]. Evidence for the deleterious effect of M1 macrophage leading up to T2DM abounds in literature. M1 macrophage numbers have been positively correlated with insulin resistance in models of high-fat feeding in rodents, and there is evidence of M1 macrophage recruitment around necrotic adipocytes in WAT (white adipose tissue [143-145]. Moreover, successful ablation of M1 macrophages was associated with improved insulin sensitivity [146]. In humans, the accumulation of M1 macrophages in adipose tissue is positively correlated with insulin resistance [147, 148]. Furthermore, M2 macrophages tend to replace M1 macrophages after bariatric surgery, associated with more anti-inflammatory cytokine production and improved insulin sensitivity, highlighting their importance in the inflammatory pathogenesis of T2DM [149-151].

1.9 PPAR alpha

Peroxisome proliferator-activated receptor alpha (PPAR alpha) is a nuclear receptor protein encoded for by the PPARA gene. PPAR alpha is part of the subfamily of PPAR along with PPARγ (Peroxisome proliferator-activated receptor gamma) and PPARδ (Peroxisome proliferator-activated receptor delta) [152]. It was the first PPAR to be discovered and was named on the basis of being activated by chemicals that cause peroxisome proliferation [153]. Located on chromosome 22q12.2-13.1, PPAR alpha is a transcriptional factor and regulator of lipid metabolism [154]. It is abundant in tissues

with high FA oxidation activity, like the liver, where it has been proposed to link glucose and lipid metabolism with inflammation, making it an attractive target for T2DM research [155]. In fact, its agonists, like Fenofibrate, have been used successfully as hypolipidaemic agents for decades [156]. PPAR alpha is activated in a ligand-dependent and independent manner [157, 158]. In the former, ligand-induced phosphorylation of receptors in the cytosol is followed by ligand-activated PPAR alpha translocation into the nucleus, forming a heterodimer with RXR (retinoid X receptor), which then attaches to the consensus sequence of peroxisome proliferator response element (PPRE) of target gene, activating transcription of target genes by direct genomic binding, in a process facilitated by co-factors and co-repressors [159]. Alternatively, a ligand-dependent activated PPAR alpha upon translocation to the nucleus binds indirectly to the target gene by forming complexes with other transcription factors which is probably regulated by histone acetylase and deacetylase activity [160]. Furthermore, a third mechanism (unbound nongenomic response) of action for ligand-dependent activation of PPAR alpha is described, where activated PPAR alpha's activate protein kinase cascades resulting in phosphorylation of kinases involved in different signalling pathways, that depends on phosphatidylinositol signalling [159]. Mapping of PPAR alpha regulatory network in primary hepatocytes show that most of the transcription activity is mediated by direct binding to PPRE [159]. PPAR alpha regulation is controlled at different levels including ligand availability, receptor abundance, and posttranslational modification [161, 162]. Subcellular compartmentalisation and intracellular trafficking achieve further regulation of PPAR. There is evidence of different subcellular localisation of PPAR in different cell lines

[163]. For example, PPAR alpha is reported to be cytoplasmic in macrophages and endothelial cell lines like the EVC-304 [164, 165]. Although it is predominantly nuclear in hepatocytes, reports have suggested a cytoplasmic subpopulation in rat hepatocytes [165]. Some authors have reported that ligands and certain conditions can affect subcellular localisation of PPAR, which shunts across the nuclear membrane with the help of importins and calcium-dependent calreticulin [166, 167]. The knowledge of PPAR alpha regulation and localisation is essential in correctly quantifying and analysing PPAR alpha transcriptional activity. Most mechanistic knowledge on PPAR alpha activity has come from mice and rat models. There are some subtle differences between human and rodent hepatocytes regarding PPAR alpha activity. For example, PPAR is a known carcinogen in rodents, but this has not been reported in humans [168]. However, the critical beneficial metabolic functions of PPAR alpha remains the same in both species, vis: improvement of glucose and energy homeostasis, reduction in inflammation and attenuation of age-related dysfunction [169]. PPAR alpha contributes positively to T2DM by suppressing VLDL (very low density lipoprotein) and LDL (low density lipoprotein) production, while simultaneously raising HDL (high density lipoprotein) levels (a distinct feature in humans, not seen in rodents) [170-172]. Furthermore, PPAR alpha potentiates FA oxidation by upregulating genes responsible for both mitochondrial and peroxisome oxidation of FAs. Further evidence of its benefits on old and emerging markers of insulin resistance reinforces its continuous usefulness [173-175]

2 CHAPTER 2: MATERIALS AND METHODS

2.1 Cell culture

2.1.1 Reagents

The THP-1 monocytic cell line (THP-1 ATCC® TIB-202™) and HepG2/C3A hepatocellular carcinoma cell line (C3A [HepG2/C3A, derivative of Hep G2 (ATCC HB-8065)] ATCC® CRL-10741™) were obtained from the American Type Culture Collection (ATCC). Gibco modified Roswell Park Memorial Institute medium (RPMI 1640) was obtained from Thermo fisher scientific (UK). The RPMI 1640 is supplied already supplemented with L-glutamine (2mM) and glucose (11.1mM). Foetal bovine serum, penicillin and streptomycin solutions were purchased from Sigma (UK). Cells utilised for experiments were within passage 6-20.

2.1.2 Background

2.1.2.1 THP-1 cells

THP-1 cells are a human monocytic cell line derived from the peripheral blood of a 1-year-old male infant with acute monocytic leukaemia. The cell line expresses HLA A2, A9, B5, DRw1, and DRw2 antigens, as well as Fc and C3b receptors, but they lack surface and cytoplasmic immunoglobulins. They are phagocytic against latex and sensitised erythrocytes. THP-1 cells can also be differentiated into macrophages by incubation with either phorbol 12-myristate 13-acetate (PMA) or vitamin D3. PMA differentiation of THP-1 cells increases cell surface expression of both CD14 and CD16.

2.1.2.2 HepG2/C3A

HepG2/C3A cells are a clonal derivative of HepG2 cells, acquired from the liver of a 15-year-old male Caucasian with hepatocellular carcinoma. The C3A clone is an epithelial adherent cell line selected for strong contact inhibition of growth, high albumin production, high production of alpha-fetoprotein (AFP) and ability to grow in a glucose-deficient medium. Increasing confluence leads to marked reduction in AFP production with an increase in albumin secretion. The cell line expresses many genes and proteins similar to primary hepatocytes including, but not limited to: AFP, albumin, alpha1 antitrypsin, transferrin, cytochrome P450 enzymes. HepG2 cells can be differentiated into a quiescent phenotype very similar to primary hepatocytes by incubation with either DMSO or retinoic acid.

2.1.3 Protocol

2.1.3.1 THP-1

The THP-1 monocytes were cultured in growth media made up of RPMI 1640 media with 2mM glutamine and 11mM glucose supplemented with foetal bovine serum (FBS) at a final concentration of 10% v/v, and penicillin (100 µg/ml)/ streptomycin (100 µg/ml) solution to a final concentration of 1% v/v. The THP-1 monocytes were cultured in 75cm^2 flasks (Corning® cell culture flasks) with vented caps incubated in a humidified environment at 37°C with 5% carbon dioxide. The THP-1 cells were seeded at 3 x 10^5 cells/ml in 20ml of growth media and subcultured after 3 days, or when the cells reach a density of 8 x 10^5 cells/ml by centrifuging at 800g for 5 minutes and resuspending in fresh warm growth media prior to being counted by trypan blue staining on a Neubauer haemocytometer and diluted to the desired cell density.

2.1.3.2 HepG2/C3A

HepG2/C3A cells were cultured in growth media made up of RPMI 1640 media with 2mM glutamine and 11mM glucose supplemented with foetal bovine serum (FBS) at a final concentration of 10% v/v, and penicillin (100 µg/ml)/ streptomycin (100 µg/ml) solution to a final concentration of 1% v/v. The cells were cultured in 150cm^2 flasks (Corning® cell culture flasks) with vented caps incubated in a humidified environment at 37°C with 5% carbon dioxide. The cells were seeded at 3 x 10^5 cells/ml in 30ml of growth media and subcultured after 5 days. To passage cells, old medium was discarded, and cells were washed three times with warm PBS or serum-free RPMI and then detached by adding 5ml of 0.2% Trypsin-EDTA solution incubated at 37˚C for 5 minutes. 10ml of growth media was added to inactivate trypsin and aspirated gently into a 20ml universal. The cell suspension was centrifuged at 800g for 5 minutes and the cell pellet was re-suspended in warm growth medium prior to being counted by trypan blue staining on a Neubauer haemocytometer and diluted to the desired cell density.

2.2 Differentiation of HepG2/C3A cells

2.2.1 Background

HepG2/C3A cells exhibit contact inhibition upon confluence becoming less proliferative and more quiescent. However, they still show important differences in gene expression and phenotype compared to primary hepatocytes. Primary hepatocytes are regarded as the gold standard and have more gene expression of albumin, transferrin and xenobiotic enzymes. Exogenous substances like DMSO and Retinoic acid have been used to differentiate HepG2 cells into more mature quiescent

phenotypes, but these processes may be associated with cellular stress and apoptosis [176]. On the other hand, growing cells in reduced cell media has been shown to offer a less stressful alternative for differentiation.

2.2.2 Protocol

Cells were seeded at a rate of 200 x 10^6 cells/ml in growth media supplemented with 10% FCS as indicated above until they achieve 80% confluency. After three washes with sterile PBS, cells are re-supplemented with growth media supplemented with 2% FCS for 10 days with changing media every two days.

2.3 THP-1 macrophage differentiation

2.3.1 Reagents

Phorbol 12-myristate 13-acetate (PMA) and lipopolysaccharide (LPS) were obtained from Sigma (UK).

2.3.2 Protocol

THP-1 cells were seeded in 6 well plates at a rate at 1 x 10^6 cells/ml (total number of cells 3 x 10^6 cells).The cells were treated then primed for 6 hours with FAs (palmitate or pentadecanoic acid) at 50µM, 150µM, and 300µM concentrations, or 5% BSA, followed by 320nM of PMA for 66 hours with total treatment time of 72 hours (Figure 2.1) as previously described [324]. The resultant macrophage phenotype was determined by measuring the cytokine secreted.

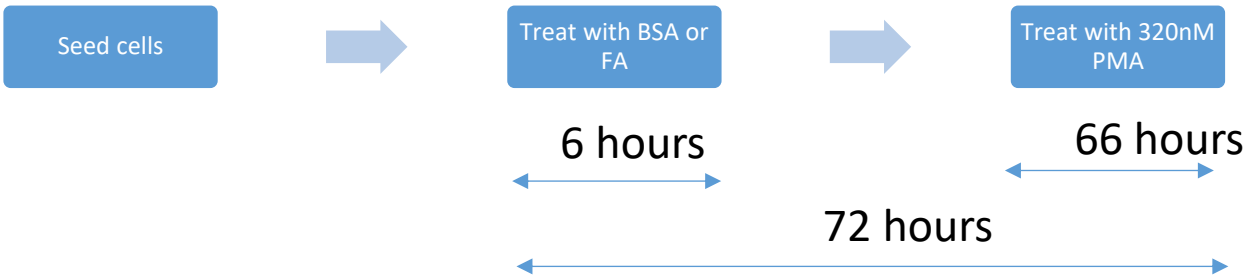

Figure 2.1: THP-1 macrophage differentiation protocol

2.4 Cell cycle analysis

2.4.1 Reagents

All reagents were obtained from Sigma (UK). Propidium iodide (PI) solution was made up at 50µg/ml in 0.1% Triton-X and 0.1% sodium citrate in distilled water.

2.4.2 Protocol

Upon cell treatments, cells were washed three times with PBS then centrifuged at 800g for five minutes to obtain a cell pellet. The cells were then resuspended in 1ml of PI solution overnight, washed three times with PBS to remove excess PI and analysed under flow conditions (excitation 518nm and emission 617nm) until 20,000 events was achieved (using Beckman Coulter Quanta or Epics XCL).

2.5 Flow cytometry measurement of THP-1 cell surface antigen

2.5.1 Reagents

Mouse anti-human CD14 RPE-Cy5 conjugated monoclonal antibody (clone 61D3, Abd Serotec); Mouse anti-human CD16-RPE Cy5 conjugated antibody (clone 3G8, Abd Serotec); Mouse-anti-human CD36-FITC conjugated antibody (clone SMO); Mouse IgG1 isotype control FITC and RPE-Cy5 antibodies were all obtained from Abd Serotec (UK).

2.5.2 Protocol

Upon completion of experimental conditions, cells were harvested and suspended in ice-cold serum in eppendorfs for 15 minutes to block receptors. Subsequently, cells were again harvested by centrifuging at 800g for 5 minutes, at $4°C$ and washed thrice with ice-cold PBS. Then, the cells were suspended in 500mls of antibodies or isotype control (details of antibodies used in section 2.5.1) at saturation concentrations for 30 minutes on ice in the dark before analysis of 20,000 events by flow cytometry (Beckman Coulter Quanta or Epics XCL). Data was analysed using the Flowing software (version 2.5). Median fluorescent intensity was used in preference to mean intensity as the data was not normally distributed and the median it is less likely to be influenced by outliers than mean values.

2.6 Trypan blue exclusion staining

2.6.1 Reagents

Trypan blue reagent, Neubauer haemocytometer, cover slides, and microscope.

2.6.2 Protocol

Cells suspended in growth media were diluted with trypan blue at a ratio of 1:2 and allowed to incubate at room temperature for 5 minutes. The suspension was mixed thoroughly by pipetting up and down several times. 10µl was added on to each side of a Neubauer haemocytometer and cells in 10 random square grids were counted. The cell density was determined by the formula: cells/ml = the average number of cells per grid x dilution factor x 10^4 and the viability was expressed in percentage as follows: percentage viability = the total number of viable cells (clear cells)/the total number of cells counted (included dead cells) x 100. Cell counting was done in technical replicates for each representative sample.

2.7 Measurement of metabolic activity by MTT assay

2.7.1 Reagents

The assay reagent was prepared by dissolving (3-(4,5-dimethylthiazol-2-yl)-2,5-diphenyltetrazolium bromide (MTT) in PBS at a concentration of (5mg/ml). 50% DMSO was used to lyse the cells.

2.7.2 Protocol

100µl of cells at a concentration of 2 x 10^5 cells/ml were seeded into a 96-well plate and treated with FA conjugated to BSA. 10µl of 5mg/ml MTT was added to each well 4 hours prior to the treatment endpoint and incubated in a cell incubator in the dark for a further four hours. DMSO was added to each well to a final concentration of 50% v/v to lyse the cells and the plate was placed on a rocker for one hour. The absorbance was read at a wavelength of 570nm on a microplate reader.

2.8 Determination of protein concentration by BCA

2.8.1 Reagents

Bicinchoninic acid solution (made up of bicinchoninic acid, sodium carbonate, sodium tartrate and sodium bicarbonate at pH 11.25), copper (II) sulphate pentahydrate (4% w/v) solution and 1mg/ml bovine serum albumin (BSA) protein standard solution purchased from Sigma-Aldrich.

2.8.2 Protocol

Prior to analysis, cell lysates and plasma samples were diluted 1:5 and 1:10 in PBS respectively. 10µl of the diluted samples were loaded onto a clear bottom 96-well plate in triplicates. A standard curve was created by adding 0µl, 2µl, 4µl, 6µl, 8µl, and 10µl of the 1mg/ml BSA protein standard in triplicates onto the 96-well plate. All wells were brought to a final volume of 10µl with PBS bringing the final concentration to 0mg/ml, 0.2, 0.4, 0.6, 0.8, and 1mg/ml of protein respectively. 200µl of BCA solution (made by mixing BCA reagent with copper (II) sulphate solution at a ratio of 50:1) was added to each standard and sample well. The plate was incubated at 37°C for 30 minutes prior to measurement of absorbance at 570nm on an absorbance microplate reader.

2.9 Conjugation of FA to bovine serum albumin

2.9.1 Reagents

FA-free bovine serum albumin (BSA) and sodium hydroxide were purchased from Sigma (UK). HPLC-grade ethanol (VWR, UK), palmitate sodium and pentadecanoate sodium were purchased from Nu-Check Prep (USA). Serum-free RPMI 1640 media was obtained from Gibco (UK).

2.9.2 Conjugation of FAs to BSA protocol

200mM stock solution of the FAs were prepared by dissolving the corresponding FA in 2ml 70% ethanol, 0.1M NaOH, 30% distilled water at 60˚C on a hot plate (112mg of sodium palmitate, 106mg of sodium pentadecanoate). The stock solution was stored in -20˚C until required.

A 5mM working solution was prepared by adding 0.5ml of the working solution to 19.5ml of 5% BSA in serum-free RPMI 1640 media and stirred at 37˚C on a hot plate for 4 hours, giving an FA/BSA ratio of 6:1. The solution was brought to a pH of 7.4 and sterilised through a 0.2µM filter. Sterile FA/BSA solution was stored at 4˚C until required and warmed to 37˚C before use. Working solutions were stored for up to one month.

2.9.3 Cell treatment

Stock solutions of FA were prepared and stored as previously described. To determine the metabolic activity and viability, cells were treated with 50µM, 150µM, 200µM, and 300µM FA for 4, 6, and 24 hours. For all other experiments, cells were treated with 300µM palmitate (C16:0), or 50µM pentadecanoate (C15:0) for 6 hours or 24 hours.

2.10 Analysis of free fatty acid profile in plasma and cell lysates

2.10.1 Reagents

Chloroform, methanol, HCl and BHT (2, 6 – Di-tert-butyl-4-methylphenol) were purchased from Sigma and stored at room temperature.12% boron trichloride-methanol w/w (BCl_3-methanol) was supplied by Sigma (UK) and stored at 4°C. Supelco

FAME 37 mix was obtained from Sigma (UK) and stored at -20˚C. A stock solution of 1mg/ml of the internal standards, undecanoic acid (C11:0) and heptadecanoic acid (C17:0), was made by dissolving 1mg of C11:0 or C17:0 in 1ml of ethanol and stored at -20˚ until required. A working solution of these internal standards were made by diluting the stock solution in chloroform/methanol up to a final concentration of 0.2mg/ml. C11:0 and C17:0 were purchased from Sigma (UK). Choloroform/methanol was made up in the ratio of 2:1 with 0.01% BHT (2, 6 – Di-tert-butyl-4-methylphenol), wrapped with foil paper and stored in the fridge. A stock solution of 8% w/v HCl solution was made from 8.5ml of conc HCl and 41.5ml of methanol and stored in the fridge. FAMEs were analysed using the Agilent 7820A gas chromatography (GC) machine with an Omegawax 250 Fused silica Bonded polyethylene phase Capillary column [30m x 0.25mm x 0.25µm], and a flame ionisation detector (FID).

2.10.2 Protocol

2.10.2.1 Folch lipid extraction

Plasma samples were added into a glass centrifuge tube using glass pipettes and mixed with 100µl of 0.2mg/ml internal standard (C11:0 and C17:0 solution). This was then made to a final volume of 600µl with 0.9% saline solution. 1.8ml of chloroform/methanol (2:1) with 0.01% BHT was added and vortexed for 30 seconds. The mixture was then spun down at 750g for 10 minutes forming three distinct layers. The chloroform layer (bottom layer) was eluted and placed into a glass vial after which it was dried down by liquid nitrogen and used immediately or stored at -80˚C for future use.

2.10.2.2 Methylation of FA by HCl method

Plasma samples were extracted by the Folch method as described above, then 0.2ml of toluene, 1.5ml of methanol and 0.3ml of 8% HCl solution were added to the dried lipid sample extract. The glass vial was sealed with a PTFE lid and heated on the heating block at 45˚C for 1 hour for FFA methylation. Once methylation was complete and the mixture was left to cool to room temperature, 1ml of hexane and 1ml of water was added. The mixture was then vortexed and spun at 750g for 2 minutes after which the floating hexane layer, which contains the lipids, was eluted into a glass vial. This was subsequently dried down completely by liquid nitrogen and re-suspended in 20µl of hexane for FAME analysis.

2.10.2.3 Methylation of FA by BCl_3 method

Plasma samples were added into a glass centrifuge tube using glass pipettes and mixed with 100µl of 0.2mg/ml internal standard. For cells, 1 x 10^6 cells were washed thrice with PBS and resuspended in 500µL of chloroform/methanol. Both plasma and cell lysates were made to a final volume of 600µl with 0.9% saline solution after which 2ml of 12% BCl_3-methanol was in a glass vial and heated on a heating block at 60˚C for 10 minutes. After cooling to room temperature, 1ml of water and 1ml of hexane was added to the mixture and vortexed for 30 seconds. It was then spun at 750g for 2 minutes and the top hexane layer eluted. This was then dried down and resuspended in 20µl of hexane. 1µl of the sample was injected into the GC for analysis. FA peaks were identified by comparing retention times and peak areas to that of the FAME 37 mix.

2.11 Protein carbonyl determination

2.11.1 Reagents

Anti-DNP antiserum (mouse IgE), peroxidase labelled rat anti-mouse IgE, o-phenylenediamine (OPD), NUNC-Immuno MaxiSorp 96 well plates, hydrogen peroxide, BSA, citrate phosphate buffer (50mM citric acid, 100mM sodium phosphate), 2N sulphuric acid and Tween-20, sodium borohydride, trichloroacetic acid, ferrous sulphate, desferal, DNPH, Sephadex PD10 column, o- Phenylenediamine (OPD) tablets, and guanidine HCl were all purchased from Sigma-Aldrich (UK).

2.11.2 Preparation of protein carbonyl standards

40mg of sodium borohydride was added gently into 20ml of BSA (10mg/ml in PBS) in a sealed universal at room temperature. It was then allowed to fizz for up to 30 minutes, as oxygen is eliminated. This was then referred to as reduced BSA (BSAred). It was subsequently neutralised by adding 1 N HCl using drops on pH paper. Afterwards, it was desalted using two separate PD10 columns of Sephadex G-25, which were pre-equilibrated with PBS according to manufacturer's instructions. Finally, the protein content of the BSAred column eluate was measured using the BCA method and adjusted to 2 mg/ml with PBS.

Oxidised BSA (BSAox) was then produced by a Fenton-type reaction using ferrous sulphate as follows: Freshly prepared iron solution was neutralised with sodium dihydrogen carbonate using a pH meter. The volume was then adjusted to 100ml to give an iron concentration of 10mM Fe (II) SO4.

0.1ml, 0.5ml and 2ml of the iron solution was then added to each of four separate tubes containing 5ml of BSA solution (10 mg/ml in PBS) and incubated for 30 min at room temperature. These were then termed BSAox solutions. Desferal was then added to a final concentration of 5 mM to chelate the iron and prevent any further oxidation. Four separate PD10 columns of Sephadex G-25, which were pre-equilibrated with PBS according to manufacturer's instructions, were then used to desalt the BSAox. The protein content in the BSAox column eluates was then measured using the BCA method and further adjusted to 2 mg/ml BSAox with PBS.

The remaining BSA (10mg/ml in PBS) was then adjusted to 2mg/ml. This meant there were now five oxidised protein standards, vis: BSAox, BSA, BSAox0.1, BSAox0.5, and BSAox2. The carbonyl content was then measured by the colourimetric technique described in section 2.11.2.1. All the standards were then aliquoted and stored at -20°C.

2.11.2.1 *Colourimetry method for protein carbonyl determination*

Half a millilitre of each of the albumin standards prepared above were aliquoted into Eppendorf tubes in duplicates for mixing with either 10mM DNPH in 2M HCl (in duplicates), or 2M HCl alone without DNPH (again in duplicates). This was incubated at room temperature for 1 hour, vortexing every 15 min. The proteins were then precipitated with a final concentration of 20% trichloroacetic acid (w/v) by adding 0.25ml of 100% TCA to 1ml of each BSA solution above, which was then subsequently vortexed and centrifuged at 13,000*g* for 3 min. After discarding the supernatant, the pellets were washed three times with 1ml ethanol-ethyl acetate (1:1 v/v) and re-

dissolved in 1ml of 6M guanidine HCl in 20mM potassium phosphate. The solution was vortexed and incubated for 30 minutes at 37°C to re-dissolve. After removing any remaining insoluble material by centrifugation (again at 13,000*g* for 1 minute), the supernatants were retained in a separate tube. The absorbance of the supernatants was measured at 360nm with a spectrophotometer, using plain 6M guanidine HCl in 20mM potassium sulphate as blank. The carbonyl content was calculated using the molar absorption coefficient of 22000 M-1 cm-1 for aliphatic hydrazones. The protein content of the samples was measured using BCA method again and the carbonyl content of samples was recorded as nmol carbonyl/mg protein.

2.11.2.2 Protein carbonyl ELISA

Five carbonyl standards previously prepared as described in section 2.11.2.1 and all plasma samples were diluted to 20µg/ml with carbonate buffer. 50µl of each diluted standard and sample were loaded on a Nunc Maxisorb 96 well plate in triplicates and incubated at 37˚C for 1 hour. After washing the wells three times with washing buffer, 50µl of 1mM DNPH in 2M HCl was loaded in each well and incubated at room temperature in the dark for 1 hour. The wash step was repeated and the wells were blocked with blocking buffer overnight at -4˚C. After another washing step, the plates were incubated with primary antibody (anti- DNP antiserum, mouse IgE), diluted 1:2000 with blocking buffer, at 37˚C for 2 hours. The plates were washed again and incubated with secondary antibody (peroxidase labelled rat anti-mouse IgE), diluted 1:5000 in blocking buffer, at 37˚C for 1 hour. After another washing step, the wells are developed with 50µl of OPD substrate (10ml 0.15M citrate phosphate buffer, 20mg OPD tablet and 10µl 8.8M hydrogen peroxide). with OPD substrate for approximately

15 minutes in the dark and the reaction with stopped with 2M sulphuric acid. The absorbance was read immediately on a microplate reader at 490nm wavelength. The carbonyl content was interpolated from a standard curve of the absorbance of the five carbonyl standards and expressed as nmol/mg.

2.12 Cytokine analysis

2.12.1 Reagents

Analysis of human TNFα, IL-10, IL-6, and C-reactive protein (CRP) were performed with representative ELISA kits purchased from Affymetrix (eBiosciences, UK). All the reagents needed for the ELISA were provided within the kits. ELISA kit numbers: CRP (88-7502-28), TNFα (88-7346-86), IL-10 (88-7106-86), IL-6 (88-7066-86).

2.12.2 Protocol

The protocol for all the ELISAs are the same and are therefore presented as one. The 96-well plate was coated with capture antibody overnight at 4˚C and washed 5 times, after which it was blocked with blocking buffer for 1 hour at room temperature. Following another wash step, the plates are incubated with standards and samples overnight at 4˚C and washed again 5 times. Subsequently, the plates are incubated with detection antibody at room temperature for 1 hour and then incubated with Avidin-HRP at room temperature for 30 minutes. Following another wash step, TMB solution is then added to the wells and incubated at room temperature for 15 minutes to allow for optimal colour development. The reaction was terminated by adding a stop solution and the absorbance reading is measured at 450nm using a microplate reader. The

concentration of cytokines in the sample was interpolated from an internal standard curve.

2.13 Cell Lysis

2.13.1 Reagents

Radioimmunoprecipitation assay (RIPA) buffer (150 mM sodium chloride, 1.0% triton-X, 0.5% sodium deoxycholate, 0.1% SDS, 50mM Tris, pH 8.0), protease inhibitor cocktail (Sigma-Aldrich, UK), 21-gauge needle, 1ml syringes (Appleton woods, UK).

2.13.2 Protocol

Treated cells were harvested by centrifugation at 800g for 5 minutes and washed with ice-cold PBS and centrifuged (HepG2/C3A cells trypsinized prior to this step). The pellet was lysed in 50µl RIPA buffer supplemented with 0.5µl protease inhibitor cocktail before lysis and incubated for 30 minutes on ice. The DNA in the lysate was then sheared using a 21-gauge needle attached to a syringe and centrifuged at 16,000xg for 30 minutes at 4°C to remove cellular debris.

2.14 PPAR alpha activation assay

2.14.1 Reagents

PPAR alpha Transcription Factor Assay Kit (ab133107) and a nuclear extraction kit (40410) were purchased from Abcam and Actif Motif respectively.

2.14.2 Nuclear extraction protocol

Cells were collected by centrifugation at 800g for 5 minutes (adherent cells were gently lifted with a cell scraper then centrifuged). 500µl of hypertonic buffer was added to the

cell pellet, resuspended by pipetting up and down several times, and incubating on ice for 15 minutes for cells to swell. The cells were lysed by adding 25µl detergent and vortexing for 1 minute. A sample of the cells was examined under the microscope to ensure lysis of cell membrane and expulsion of the nucleus (repeat lysis step if cells not lysed). The suspension was centrifuged at 16,000g for 15 minutes at 4˚C. The supernatant was collected as the cytoplasmic fraction. The pellet was resuspended in 50µl of complete lysis buffer and incubated on ice for a further 30 minutes after which 5µl of detergent was added and then vortexed for 1 minute. The suspension was centrifuged at 16,000g for 30 minutes. The supernatant was collected as the nuclear fraction and stored at -80˚C until required. Samples were diluted 1:20 before protein determination by BCA.

2.14.3 PPAR alpha activity assay protocol

The 96-well plate was purchased pre-coated with a dsDNA sequence containing PPRE. The samples were prepared and added to the plates along with a positive and negative control and then incubated overnight at 4˚C. The plates were washed 5 times and a PPAR alpha primary antibody was added and incubated at room temperature for 1 hour. After another 5 washes, the plates were subsequently incubated with a goat anti-rabbit HRP conjugated secondary antibody at room temperature for 1 hour. Following another wash step, the developing solution was then added to the wells and incubated at room temperature for 45 minutes after which a stop solution is added and the absorbance reading is taken at 450nm using a microplate reader.

2.15 Quantification of glucose output

2.15.1 Reagents

Glucose (hexokinase) quantification assay purchased from Sigma-Aldrich (UK) includes glucose standard (10mg/ml) and a lyophilised glucose assay reagent.

2.15.2 Protocol

After the indicative treatment endpoint, cells were washed three times with PBS to remove glucose and then incubated for 16 hours in glucose production medium (glucose- and phenol red-free DMEM containing gluconeogenic substrates, 20 mmol/l sodium lactate, and 2 mmol/l sodium pyruvate). The lyophilised glucose assay buffer was reconstituted with 20ml of distilled water. Glucose standards (0.05mg/ml – 5mg/ml) and samples (50µl) were added to a 96 well plate. The reconstituted glucose assay buffer (100µl) was added to each well. The plate was incubated for 15 minutes at room temperature prior to measuring absorbance at 340nm on a microplate reader.

2.16 Glycogen content determination

2.16.1 Reagents

0.2M sodium hydroxide (NaOH), 30mM HCl, 0.1mg/ml of amyloglucosidase (Sigma-Aldrich, UK) in 0.1M sodium acetate buffer pH 5.0, RIPA buffer, glucose assay kit (Sigma, UK).

2.16.2 Protocol

After the indicative endpoint, treated cells were glucose starved overnight to deplete glycogen stores and treated with RPMI media containing 11mM glucose for 48hrs with 100nM insulin in the final 1hr of incubation. Cells were washed in ice-cold PBS and

immediately lysed with RIPA buffer as previously described. 5ml of 0.2M NaOH was added to the suspension and boiled for 1 hour. The samples were brought down to a final volume of 500µl with a concentrator. The samples were divided into aliquots; one used for glycogen content determination, the other two for protein determination and baseline glucose content determination as previously described. To the aliquot for glycogen content determination, 0.1mg/ml of amyloglucosidase was added and incubated overnight at room temperature. The glucose content was then determined by the hexose kinase method as previously described. The difference in glucose concentration between the first two aliquots gives the total glycogen content. In this thesis, one mole of glycogen corresponds to one mole of glycosyl units originating from glycogen.

2.17 Oil red O lipid staining

2.17.1 Reagents

Oil Red O was obtained from Cayman (UK) and isopropanol from Fisher (UK). Mayer's Haematoxylin solution and paraformaldehyde were obtained from Sigma (UK).

2.17.2 Protocol

Cells were grown in a 24-well plate and treated as previously described. After the indicative endpoint, cells were fixed with 4% paraformaldehyde in PBS for 10 min and then stained with 1.8 mg/mL oil Red O in 60% aqueous isopropanol for 15 min at room temperature. This was then rinsed five times with 60% aqueous isopropanol and PBS. Fixed cells were subsequently counterstained with Mayer's haematoxylin solution for 1 minute and viewed under a light microscope at x40 magnification. For quantitative

analysis of cellular lipids, isopropanol was added to each of the stained culture plates. The extracted dye was removed immediately by gentle pipetting and its absorbance was monitored at 495 nm using a microplate reader. Cellular neutral lipid content was normalised with cellular protein concentration. The protein concentration of each cell lysate was measured with BCA protein assay reagent as previously described.

2.18 Periodic Acid Schiff staining for glycogen

2.18.1 Reagents

Periodic Acid-Schiff (PAS) staining was done using the kit (catalogue number: 395B) by Sigma, UK following manufacturer's protocol.

2.18.2 Background

Histochemical determination of glycogen is based upon the periodic acid-Schiff reaction which was originally described by MacManus in 1948 [177]. The PAS reaction involves the oxidation of glycols within polysaccharides (like glycogen) to form dialdehydes which react with the Schiff reagent to form a purple-magenta colour. However, it is not specific to glycogen as it is able to react with mucopolysaccharides and basement membranes.

2.18.3 Protocol

Cells were grown in a 24-well plate and treated as previously described. After the indicative endpoint, cells were fixed for 10 minutes with 4% paraformaldehyde in PBS and stained with periodic acid solution for 5 minutes. After five washes, cells were stained with Schiff's reagent for 15 minutes and counterstained with Mayer's

haematoxylin solution for 1 minute and viewed under a light microscope at x40 magnification. Staining intensity was quantified using ImageJ software.

2.19 Extraction of total ribonucleic acid (RNA)

2.19.1 Reagents

Extraction of total RNA from cells was done using the RNeasy mini extraction kit (Qiagen, UK). Other materials used include sterile RNase-free pipet tips, microcentrifuge (with rotor for 2 ml tubes), 70% ethanol, a sterile syringe with 20-gauge needle (washed prior to use with 0.1M NaOH, 1mM EDTA and rinsed with RNase-free water) and β-mercaptoethanol (β-ME).

2.19.2 Protocol

2 x 10^6 cells were harvested as previously described and washed three times with PBS. The cells were centrifuged at 300g for 5 minutes and the PBS removed. 350µl of RLT (lysis) buffer supplemented with 3µl of β-ME was added and vortexed for 30 seconds. A syringe attached to a 20-gauge needle was used to homogenise the sample. The lysate was then stored at -80˚C until required or extracted immediately. 350µl of 70% ethanol was then added to the homogenised lysate and mixed thoroughly by pipetting up and down several times. 700µl of the sample was then transferred (including any precipitate that may have formed) to an RNeasy spin column placed in a 2 ml collection tube and centrifuged for 15 seconds at ≥8000 x g (≥10,000 rpm). The flow-through was discarded. 700µl of Buffer RW1 was added to the RNeasy spin column and centrifuged for 15 s at ≥8000 x g (≥10,000 rpm) to wash the spin column membrane. After discarding the flow-through, 500µl Buffer RPE was added to

the RNeasy spin column and centrifuged for 15 s at ≥8000 x g (≥10,000 rpm) again to wash the spin column membrane. After discarding the flow-through, the membrane was again washed with Buffer RPE and centrifuged for 2 min at ≥8000 x g (≥10,000 rpm). The long centrifugation dries the spin column membrane, ensuring that no ethanol was carried over during elution of RNA, because residual ethanol may interfere with downstream reactions. The flow-through was discarded and the column placed in a new 2ml collection tube. The column was centrifuged again for 1 min to ensure no residual ethanol is left on the column. The collection tube was then replaced with a new 1.5 ml collection tube and 50µl of RNase-free water was added directly to the spin column membrane. RNA was eluted by centrifuging for 1 min at ≥8000 x g (≥10,000 rpm). The concentration and purity of the extracts were determined using a Nanodrop (diluted in 10 mM Tris·Cl,* pH 7.0 and 10 mM Tris·Cl,* pH 7.5 respectively). The ratio at absorbance 260nm and 280nm (260/280) of 2 was used as a primary measure for RNA purity while a 260/230 absorbance ratio of 2.0-2.2 was used as a secondary measure of nucleic acid purity.

2.20 Reverse transcriptase quantitative polymerase chain reaction (RT-qPCR)

2.20.1 Reagents

All primers were purchased from Thermo Fisher Scientific (UK) except the reference gene, *YWHAZ*, which was obtained from Qiagen (UK). The list of primers sequences can be found in table 2.1. The primer sequence for YWHAZ was not made available by Qiagen. SYBR green PCR master mix (Primer Design, UK), 96 well PCR plates, strip caps, nuclease free water, Quantitect reverse transcription kit (Qiagen, UK), PCR primers, Stratagene mx3000p qPCR thermocycler.

2.20.2 Protocol

Reverse transcription was performed using a high capacity reverse transcription kit purchased from Qiagen, to convert extracted RNA to cDNA. A master mix solution was made from the reverse transcription kit components, consisting of per sample; 4µl reverse transcriptase buffer, 1µl Quantiscript reverse transcriptase and 1µl RT primer mix. The master mix was mixed by vortexing and 10µl added to 200µl PCR tubes. An equal volume of extracted RNA sample (containing 500ng RNA) was added to the PCR tubes. To control for possible genomic DNA contamination, the samples were also incubated with a master mix solution without the addition of the reverse transcriptase enzyme. The converted cDNA was diluted 1 in 10 with nuclease-free water and stored at -20°C until needed. The expression of specific mRNA was measured by RT-qPCR analysis of the diluted cDNA. A qPCR reaction stock solution was made by mixing for each sample: 0.5µl of the forward and reverse primers, 4µl nuclease free water and 10µl SYBR green master mix. To each well on a qPCR plate 15µl of the reaction stock solution was added to 2µl of the diluted cDNA. A negative control was included in the experiment by using 2 µl of nuclease-free water instead of cDNA. The wells were sealed with strip caps and the plate loaded onto a Stratagene mx3000p qPCR thermocycler. The following PCR condition were used: 95º C, 2 minutes hold for 1 cycle; 95º C, 10 sec hold + 60º C, 30 sec hold, for 45 cycles; 1 cycle – 60º C, 30 sec + 95º C, 30 sec. The produced data was analysed using the comparative delta-delta C_T method. In the delta-delta C_T method, the C_T value of the gene of interest is first subtracted from the C_T value of the reference gene to obtain ΔC_T for each experimental sample, then the difference between the ΔC_T values of

each experimental gene and the control gene is determined (this is now called $\Delta\Delta C_T$). Finally, the formula $2^{(-\Delta\Delta C_T)}$ was used to calculate the fold change in the expression of the gene of interest [178]. Therefore, results are normalised as a fold change relative to untreated controls and normalising to the C_T value for the reference gene. Where multiple plates were used, a reference gene, negative control and untreated control was added to each plate for corresponding experimental genes of interest.

Table 2.1: List of primers sequences[1] used for RT-qPCR, including forward (F) and reverse (R) sequences.

Oligo Name	Sequence (5' to 3')
ABCD1 (F)	TACCGGGTCAGCAACATGG
ABCD1 (R)	TGGTCAGGTTGGAGTAGAGGT
ABCD2 (F)	GGATGGAAAAATCGTGAAAAGCA
ABCD2 (R)	ATGGCAATCATAAGCCACTTGA
ABCD3 (F)	GCTGGTGTCTCGAACATATTGT
ABCD3 (R)	ATCTTTCCTGCTACGACCAATG
ACAA2 (F)	CTGCTCCGAGGTGTGTTTGTA

[1] Primer sequence for reference gene not made available by QIAGEN (UK)

Oligo Name	Sequence (5' to 3')
ACAA2 (R)	GGCAGCAAATTCAGACAAGTCA
ACAD10 (F)	GTACGAACCTGGGTTAAGCAG
ACAD10 (R)	CAGCCATTCGATCAGCCTCT
ACADL (R)	CGCAACTACAATCACAACATCAC
ACDL (F)	TGCAATAGCAATGACAGAGCC
ACOX1 (F)	AATCGGGACCCATAAGCCTTT
ACOX1 (R)	GGGAATACGATGGTTGTCCATTT
ACSL1 (F)	CTTATGGGCTTCGGAGCTTTT
ACSL1 (R)	CAAGTAGTGCGGATCTTCGTG
CAT (F)	TGGGATCTCGTTGGAAATAACAC
CAT (R)	TCAGGACGTAGGCTCCAGAAG
CD36 (F)	CTTTGGCTTAATGAGACTGGGAC
CD36 (R)	GCAACAAACATCACCACACCA

Oligo Name	Sequence (5' to 3')
CPT1A (F)	ATCAATCGGACTCTGGAAACGG
CPT1A (R)	TCAGGGAGTAGCGCATGGT
CPT2 (F)	CATACAAGCTACATTTCGGGACC
CPT2 (R)	AGCCCGGAGTGTCTTCAGAA
FABP1 (F)	GTGTCGGAAATCGTGCAGAAT
FABP1 (R)	GACTTTCTCCCCTGTCATTGTC
FASN (F)	AAGGACCTGTCTAGGTTTGATGC
FASN (R)	TGGCTTCATAGGTGACTTCCA
GSK3 (F)	GTGCCCGAGACAGTGTACC
GSK3 (R)	ACACCTTGACATAGAGGATAGGG
KPNA2 (F)	GGCACTGTAAATTGGTCTGTTGA
KPNA2 (R)	CCTGGCAGCTTGAGTAGCTT
KPNB1 (F)	CCACTTTCCTTGTGGAACTGT

Oligo Name	Sequence (5' to 3')
KPNB1 (R)	CTCTGCTGATATTGTGCCTTGA
MLYCD (F)	ACCTAGAACGGGTTACCTGG
MLYCD (R)	CAGGGGTCGAACAGTGAGAA
NCOA1 (F)	AATGAATACGAGCGTCTACAGC
NCOA1 (R)	TTTCGTCGTGTTGCCTCTTGA
PPARA (F)	TTCGCAATCCATCGGCGAG
PPARA (R)	CCACAGGATAAGTCACCGAGG
RXRa (F)	GACGGAGCTTGTGTCCAAGAT
RXRa (R)	AGTCAGGGTTAAAGAGGACGAT
SCD1 (F)	CTCCACTGCTGGACATGAGA
SCD1 (R)	AATGAGTGAAGGGGCACAAC
SCD5 (F)	TGCGACGCCAAGGAAGAAAT
SCD5 (R)	CCTCCAGACGATGTTCTGCC

Oligo Name	Sequence (5' to 3')
SLC25A20 (F)	GACACGGTCAAGGTCCGAC
SLC25A20 (R)	GCAGCCATTCCCCGATATAGC
SLC2A2 (F)	GCCTGGTTCCTATGTATATCGGT
SLC2A2 (R)	GCCACAGATCATAATTGCCCAAG

3 CHAPTER 3: Fatty acid predictors of insulin resistance and methodological optimisations

3.1 INTRODUCTION

The increasing burden of T2DM has been associated with an increase in sedentary lifestyle, an increasingly ageing population and a rise in the prevalence of obesity [179]. The ß-islet cells in the pancreas are responsible for the production and secretion of insulin, the primary regulatory hormone for glucose metabolism. An increase in body-mass index (BMI) and the consequent increase in adiposity contributes to an increase in FFAs in circulation and leads to a selective utilisation of these FFAs for energy, at the expense of glucose. Excess FFAs also suppress ß-islet cell function, as well as activate processes that lead to impaired cellular insulin signalling [180, 181]. Therefore, T2DM is thought to be due to pancreatic dysfunction resulting from a complex interplay of peripheral insulin resistance and reduced insulin secretion, consequently resulting in impaired glucose and FA uptake from the circulation and hyperglycaemia with associated hyperlipidemia [182]. The factors that contribute to the onset and complications of T2DM are complex and include genetic and environmental factors.

Obesity has long been established as a modifiable risk factor for T2DM because most people with T2DM are obese; supported by the fact that the rise in prevalence of obesity has also coincided with a concomitant rise in prevalence of T2DM. Also, patients that have undergone bariatric surgery for obesity and/or modified their weight through diet or increased physical activity have observed an improvement in glycaemic control and reduced diabetic risk [183-188]. Epidemiologic and experimental studies have established an association between T2DM and obesity including complex interactions that involve mitochondrial dysfunction, deranged FA metabolism, pro-

inflammatory cytokines and adipokines, energy overload, peripheral insulin resistance and ectopic fat deposition (especially liver fat and visceral adipose tissue) [189]. Although these interactions are not fully understood, recent studies have expanded further on the nature of adipocytes in T2DM. For instance, visceral adipose tissue (VAT) over subcutaneous adipose (SAT) was considered by some a more significant predictor of insulin resistance [190, 191]. Others suggested that abdominal SAT might be as important [31]. Perhaps this difference might also be explained by a diversity of immune response in these locations. There is evidence to suggest that diets rich in monounsaturated FA (instead of saturated FAs), as is the case with Mediterranean diets, can reduce the risks of T2DM even without changes in weight or physical activity [192-194]. Furthermore, animal studies show expression of anti-inflammatory macrophage phenotypes (M2) in the mesenteric adipose tissue after dietary oleic acid intake [195]. There is also evidence of the anti-atherogenic activity of MUFA but not saturated FA like palmitate, which preferably displays a pro-inflammatory and pro-atherogenic phenotype that promotes insulin resistance [196-198].

It is a well-accepted fact that the concentration of total FFAs in the plasma increases with obesity, T2DM and age. However, knowledge of the distribution of specific FAs according to length and saturation is limited despite the view that structural diversity determines their functions. The cellular FA distribution, mainly found in phospholipids, ceramide and sphingomyelin in membranes, is determined by both dietary FA supply and metabolic enzyme activity, including elongases (encoded by the ELOVL genes) and desaturases [199]. How membrane phospholipids and the total FA lipidome change with age, obesity, insulin resistance, and T2DM is poorly understood.

Nevertheless, membrane FAs act as organisational platforms for insulin receptor signalling and as substrates for synthesis of anti-inflammatory and pro-resolving mediators of inflammation. Furthermore, there is substantial epidemiological evidence from the EPIC study linking the FA profile of erythrocyte membrane phospholipids and activity of desaturase enzymes with the incidence of T2DM [200].

Many obese people do not have T2DM, raising a conundrum about the metabolically healthy obese. A cross-sectional study designed to characterise metabolically healthy obesity in rare pairs of obesity-discordant monozygotic twins revealed the presence of liver fat as the most important predictor of insulin resistance [32]. The ectopic deposition of fat in the liver could be explained by SAT inflammation resulting in local mitochondrial dysfunction and associated failure to metabolise fat in SAT. Further mitochondrial dysfunction in T2DM can also be explained by an increase in reactive oxygen species (ROS) leakage from complex 1, which is usually due to nutrient excess from circulating glucose and FFAs. This results in a vicious negative feedback cycle that includes increased protein oxidation and a down-regulation of glyceraldehyde phosphate dehydrogenase (GADPH) as well as an increase in several pathways, that include but are not limited to increased formation of advanced glycation end-products (AGE); increase in the polyol pathway; increase in the hexosamine pathway; and an increase in activation of protein kinase C (PKC) [189, 201]. Figure 3.1 attempts to simplify the complex interactions that encompass T2DM.

T2DM complications are heavily associated with inflammatory changes, especially in the vasculature. People with T2DM have a higher risk of myocardial infarction, stroke

and other cardiovascular disorders than the general population [202]. Because the treatment options for these complications are limited and sometimes palliative, it has become imperative to identify markers to predict these complications during the early stages of the disease and identify drug targets to help prevent them. Therefore, it will be useful to have a model to predict the onset of T2DM in the general population to aid focused prevention strategies.

Much work has been done in developing risk prediction models for the onset of T2DM. This practice has been encouraged by evidence from different preventive strategies on people with impaired glucose tolerance or impaired fasting glycaemia in different countries [184, 190, 203]. Despite the different widespread use of weak prediction model methods, some risks have appeared consistently as possible predictors of diabetic outcomes [204]. Even though some of these prediction scores are never used in practice because the tests are not available for routine use, it has identified biomarkers and indices for further research. Regarding FA biomarkers, there has been a growing interest in the biological relevance of odd-chain saturated FAs (OCSFA) over the last decade. These FA were initially assumed to be metabolically irrelevant in humans and were therefore used as internal standards in lipid profiling by gas chromatography (GC). However, this narrative has been challenged by growing evidence showing a negative correlation between dairy intake and metabolic disease development, and emerging evidence pointing to an association between OCSFA and dairy intake [205]. Despite ongoing debate regarding the human ability to biosynthesise or indeed metabolise OCSFA, its relationship with T2DM prevention has been buttressed by publications from the European Prospective Investigation (EPIC)

study cohort [200, 206, 207]. However, the relationship between OCSFA and markers of inflammation are still not well characterised.

3.2 AIMS AND HYPOTHESIS

This chapter aims to determine the role of FFAs as predictive biomarkers of fasting blood glucose and inflammation in T2DM with a particular focus on pentadecanoic acid (C15:0), one of the more abundant OCSFA in human plasma. The detection of OCSFAs in plasma samples is challenging because they are less abundant in blood compared to their saturated counterparts. Traditionally, FAs are recovered from plasma samples by a time-consuming two-step method of Folch extraction followed by methylation. This chapter will look at optimising a robust method for efficient plasma lipid extraction and analysis by a direct method. The direct method is less time-consuming and requires less resources and has the potential to accurately quantify the lipid profile of patients with T2DM, with particular emphasis on OCSFAs, with the same efficiency as the two-step method.

3.2.1 Aims

1. To develop a method for reproducible plasma lipid extraction and identification of OCSFAs using gas chromatography
2. To characterise the lipidome in patients with T2DM and age-matched controls
3. To use FA profiles to develop a predictive model for fasting blood glucose and markers of inflammation
4. To evaluate the protein carbonyl content as a marker of oxidative stress for the progression of T2DM.

3.2.1.1 Hypothesis

1. The recovery efficiency of FAs from plasma will not differ between the direct method and two-step method.
2. The concentration of C15:0 will negatively correlate with fasting blood glucose levels
3. Markers of adiposity (leptin and BMI) will correlate positively with FAs
4. FAs will positively correlate with marker of inflammation.

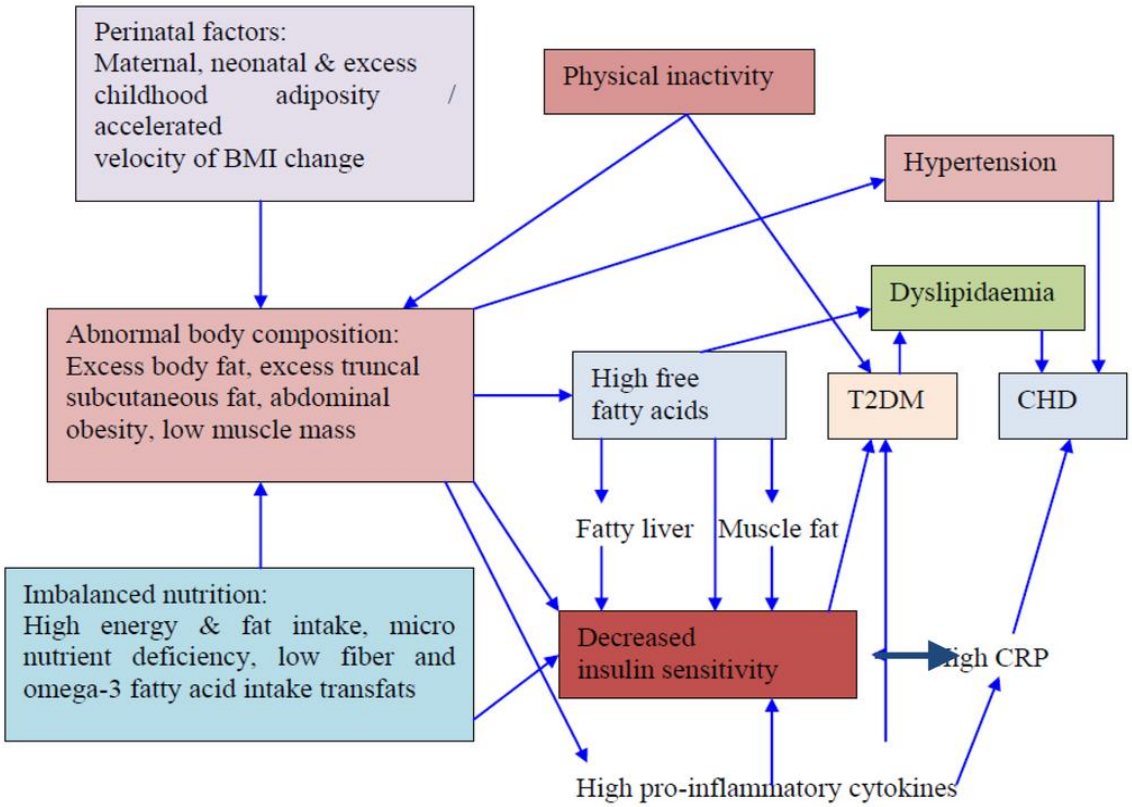

Figure 3.1 : A simplified schematic of the interactions that lead to T2DM. *CHD (Coronary Heart Disease), CRP (C-reactive protein), T2DM (Type 2 diabetes) (Misra and Shrivastava 2013)*

3.3 METHODS

3.3.1 Protein carbonyl ELISA

Protein carbonyls were detected in plasma by an ELISA based assay as described in section 2.11.2

3.3.2 BCA assay

A BCA assay was performed on all the samples to determine their protein concentrations. All reagents used were obtained from Sigma (UK). Briefly, 400 µl of copper (II) sulphate was added into 20 ml of BCA solution. A protein standard was aliquoted into a 96-well plate to correspond to 0, 0.2, 0.4, 0.6, 0.8 and 1.0 mg/ml of protein to generate a standard curve. 10 µl of representative samples were then aliquoted into separate wells in the 96-well plate in triplicates and 200 µl of the BCA solution was then added and left to incubate at 37°C for 30 minutes after which it was read on a microplate reader at a wavelength of 570nm. Protein concentration of samples were then interpolated from the standard curve.

3.3.3 Folch lipid extraction from plasma

A modified Folch method was employed for lipid extraction from plasma samples as described in section 2.10.2.

3.3.4 Methylation of FFA

FAs in plasma were esterified to FA methyl esters (FAMEs) using either BCl_3 or HCl method as described section 2.10.3.2.

3.3.5 Study population

Plasma samples used in this thesis were taken from a cohort of T2DM patients and controls recruited in Birmingham. Ninety-six samples (47 controls and 49 T2DM, NHS ethics study number 11/WM/0288) were sampled randomly from this cohort for analysis. Details of the study population used for this study, the protocol, ethics, inclusion and exclusion criteria, has already been described [208]. Briefly, a random number was generated by excel and paired with each sample. This number was then sorted in ascending order, and the first 50 samples for each cohort were selected for the study. Five samples (3 control and 1 T2DM) were excluded from the analysis because there was no fasting glucose measurement recorded. Standard universal precautions were observed in collecting and extracting plasma samples from whole blood. Blood samples were collected in EDTA bottles and centrifuged at 300g for 10 minutes to extract plasma. All study participants were recruited from the same community in Birmingham. Ethical approval was granted by the Aston University and Staffordshire NHS Research ethical committees.

3.3.6 Statistical analysis

Data were analysed using SPSS version 21 (Armonk, New York, USA). Descriptive analysis of biochemical data was performed for all variables with percentages and mean (standard deviation) as appropriate for normally distributed data, or median (range) for non-normally distributed data. A two-tailed, unpaired student's t-test was used to compare means between two groups of normally distributed data, while a Mann-Whitney test was used in the same scenario for non-normally distributed data.

3.3.6.1 Statistical model

The following steps were undertaken in model development. Missing values were analysed pairwise and data from all participants (controls and T2DM) were included in the regression analysis.

1. Based on the hypothesis, C15:0 was fitted into a multiple linear regression model to predict the independent variable of interest. On the basis that FAs interact biologically, all FAs in our data were also included in the model as interactors and analysed in a backward stepwise method. Variables with a variance inflation factor (VIF) > 10 (to account for multicollinearity) and F statistic > 0.10 were removed from the next step of the model. Statistically significant variables remaining in the final step of the model were considered predictive of the independent variable and added to the next step in the model.
2. Subsequently, a bivariate analysis was performed to determine the variables (baseline characteristics) which correlated significantly with the independent variable of interest. These variables were then used to adjust for the predictor variable of interest.
3. Statistically significant FAs and variables from step 2 were then fitted into a generalised linear regression.

3.3.7 Gas chromatography

Table 3.1: Details of the GC protocol used in the analysis of fatty acid methyl esters (FAME)

Column	**Omegawax 250** **Fused silica** **Bonded; poly(ethylene) phase** **Capillary column** **30m x 0.25mm x 0.25µm** **280°C maximum oven temperature**
Injection volume	1µl
Inlet type	Splitless
Injection port temperature	280°C
Carrier gas velocity	35cm/sec at 40°C
Splitless hold time	1 minute
Start oven temperature	40°C
Oven temperature programme	40°C hold 2 minutes, then ramp 50°C per minute to 260°C, hold 6.6 minutes (13 minutes runtime)
Final oven temperature	260°C
Standard mix used	SUPELCO 37 FAME mix
Instrument	Agilent 7820A
Data analysis software	ChemStation

Table 3.2: GC protocol for SUPELCO (recommended) method

Column	**Omegawax 250** **Fused silica** **Bonded; poly(ethylene) phase** **Capillary column** **30m x 0.25mm x 0.25µm** **280°C maximum oven temperature**
Injection volume	1µl
Inlet type	Splitless
Injection port temperature	250°C
Carrier gas velocity	30cm/sec at 50°C
Splitless hold time	0.75minute
Start oven temperature	50°C
Oven temperature programme	50°C hold 2 minutes, then ramp 4°C per minute to 220°C, hold 15 minutes (59 minutes runtime)
Final oven temperature	220°C
Standard mix used	SUPELCO 37 FAME mix
Instrument	Agilent 7820A
Data analysis software	ChemStation

3.4 RESULTS

3.4.1 Gas chromatography optimisation

The GC optimisation aimed to reduce analysis time, to allow increased sample throughput, without negatively affecting elution pattern, peak identification, resolution, and quantification. The optimised method used for this study was adapted from the protocol recommended by Supelco for use on the Omegawax 250 column for the 37 FAME mix. Details of the protocol for both methods are found in Table 3.1. The first step of the optimisation involved increasing the oven temperature ramp at a rate of 4˚C per run until the maximum ramp rate the machine can handle without lagging was achieved. The outcome measured was the number of resolved peaks identified. It was expected that any optimum condition would resolve 35 peaks as stated on the Supelco FAME mix catalogue. For the Agilent 7820a, 52˚C/minute was the highest oven temperature ramp rate that did not result in oven temperature lag. 50˚C/minute was therefore used as the set ramp rate for this method.

3.4.1.1 Inlet temperature

To determine the optimum inlet temperature, temperatures within a range of +/-50˚C of the recommended injection temperature (250˚C) was tested. The outcome measures were the number of peaks and mean peak areas from each standard injection temperature run. A repeated measure one-way ANOVA was used to analyse the experiment with the 250˚C run set as control (Figure 3.2). All the inlet temperatures yielded 35 peaks; hence, attention was then focused on the mean peak area from each run. The mean peak area increased with increasing inlet temperature as shown in Figure 3.2a ($p < 0.001$). Also, high molecular weight discrimination reduced with

increasing inlet temperature (Figure 3.2b), which is depicted by an increase in the mean peak areas of the last eight peaks (each FAME is represented by a single bar within each temperature run in Figure 3.2b) as temperature increases. Furthermore, the mean peak areas of inlet temperatures of 300˚C and 280˚C were statistically significantly higher than 250˚C ($p < 0.0001$ and 0.04 respectively) as shown in Figure 3.2c.

The decision to stick with 280˚C as the optimal inlet temperature was made based on the fact that there was no thermal degradation of any of the FAMEs. In comparison, several lower molecular weight FAMEs were degraded with the 300˚C run (Figure 3.2: signal overlay of both runs).

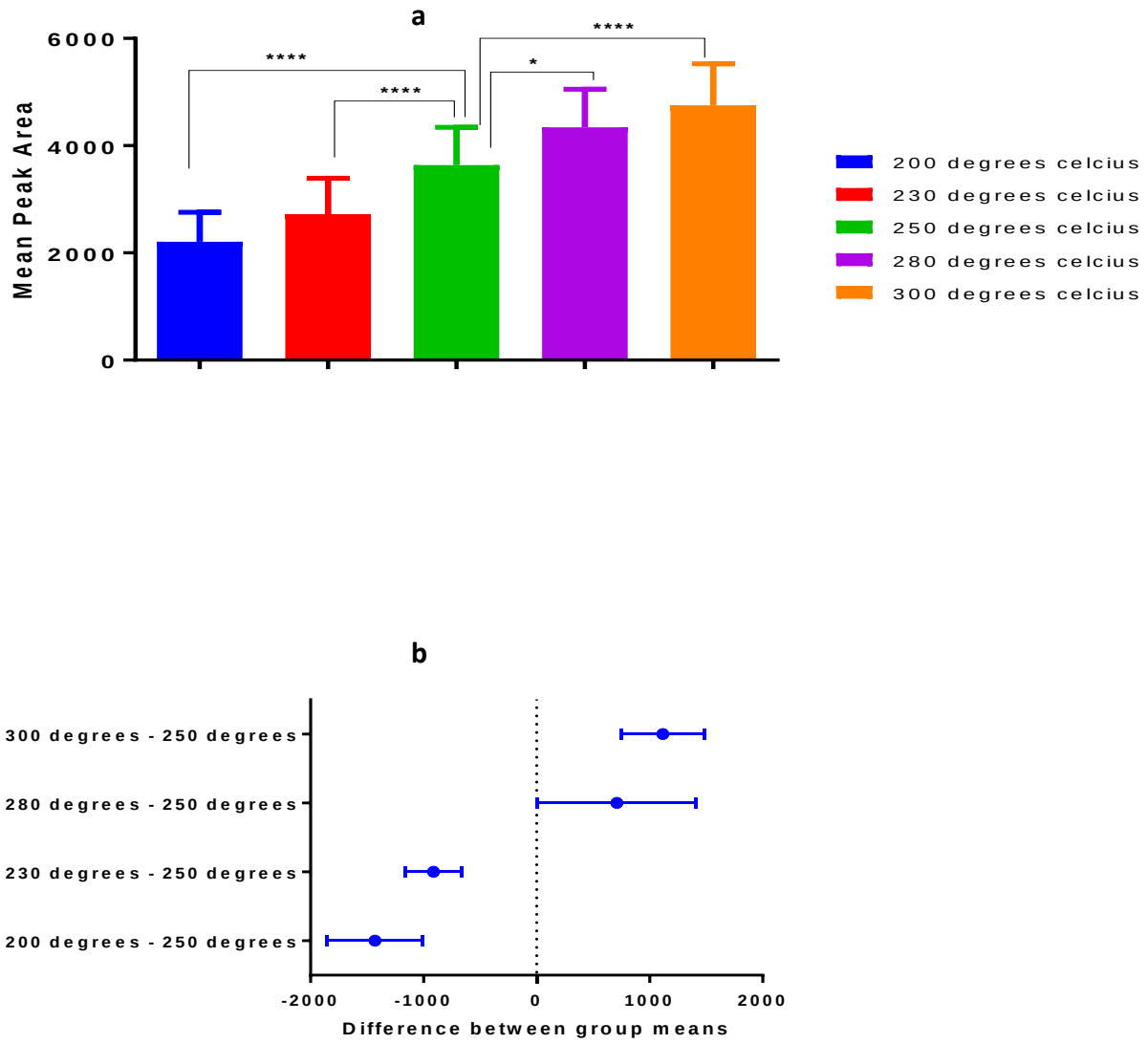

Figure 3.2 : Effect of Inlet temperatures on FAME elution.

*The Supelco FAME 37 mix was run at the recommended Supelco protocol and the inlet temperature was altered for each run. Five separate standard runs were carried out for each set inlet port temperature. The FAMEs were analysed using the resultant peak areas from the GC. (a) The difference in total mean peak areas of each temperature runs. Data presented as Mean and 95% CI. **** represents a $p < 0.00001$, ** represents $p = 0.001$, and * $p < 0.05$ after a repeated measure one-way ANOVA with Geisser Greenhouse correction and Tukey post-test comparison. (b) Shows the mean difference and 95% CI between each inlet temperature run and the control (250˚C).*

3.4.1.2 Splitless Purge Time

In a splitless injection, excess solvent (and sometimes excess sample) in the inlet is purged through the split vent to prevent tailing of the solvent throughout the chromatogram that would otherwise prevent identification of analytes. Because different analytes have different boiling points and migrate at different speeds in the inlet, it is important that the purge time be long enough to capture as much sample as possible and short enough to prevent tailing of the solvent on an analyte. To determine the optimal splitless purge time for the study protocol, different purge times were plotted against mean peak areas of all analytes (Figure 3.3a) and analytes of interest (Figure 3.3b). The 'analytes of interest' were C4:0, C17:0 and C24:0, representing early, middle and late eluting FAMEs. There was a statistically significant linear increase in mean peak areas as split purge time increased from 0.5 minutes to 1.25 minutes. The smallest observed difference in mean peak areas was between 0.75 and 1.0 minute. However, this difference was also statistically significant (mean difference: 451.6; 95% CI: 180-722; $p = 0.0005$). From these data, a splitless purge time of 1.25 minutes looked to be the optimal choice, however, on further analysis of analytes of interest, C4 was observed to co-elute with the solvent when a splitless purge time of 1.25 minutes was applied (Figure 3.3b). Therefore, 1 minute was set as the optimal splitless purge time.

3.4.1.3 Final oven temperature

Final oven temperatures of 200˚C, 220˚C, 240˚C and 260˚C were compared for the number of peak areas that could be identified (maximum oven temperature for column

= 280˚C). Final oven temperatures of 200˚C, 220˚C and 240˚C only eluted 34 peaks compared to the 35 peaks observed in the 260˚C run.

3.4.1.4 Other variables

All other variables like inlet pressure, carrier gas velocity and flow rate were left at the recommendations of SUPELCO for use on the 37 FAME mix (Table 3.2). The FID detector temperature was increased from 260˚C (SUPELCO recommendation) to 300˚C based on the recommendation of the Agilent 7820a GC manual (to set detector temperatures to at least 300˚C to prevent soot collection). A splitless injection was used instead of a split because it was predicted that the samples to be analysed would be in minute quantities.

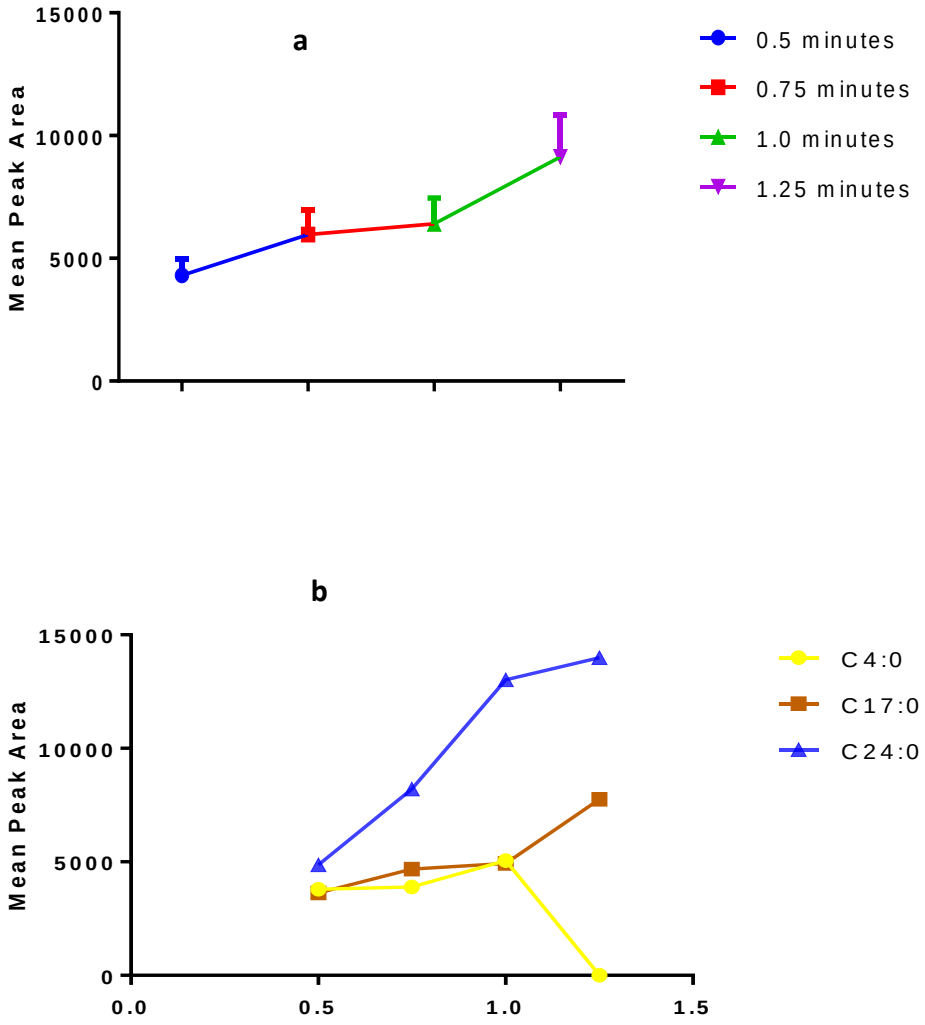

Figure 3.3 : Effect of altering Inlet splitless purge time on FAME elution.
The Supelco FAME 37 mix was run at the recommended Supelco protocol and the splitless purge time was altered for each run. 5 separate standard runs were carried out for each set splitless purge time. The FAMEs were analysed using the resultant peak areas from the GC. (a) Shows the mean peak areas of all 37 FAME analytes between different splitless purge times. b) Shows peak areas for C4, C17 and C24 plotted against different splitless purge times.

3.4.1.5 New protocol vs SUPELCO recommended protocol

The new protocol had a run time of 13 minutes compared to 59 minutes (SUPELCO), saving 46 minutes, which is enough time for just over three runs with the new protocol. To validate the new protocol, its variability and reliability were compared with the recommended protocol. The coefficient of variation (CV) for retention time was calculated for both protocols using data from 20 runs of Supelco FAME 37 mix (5 runs each on Day 1, 2, 8 and 9; to account for inter-run, inter-days and inter-week variation). The CV of the new and old protocol was 1.35% and 0.46% respectively (usually, a CV of 4% or less is an acceptable level of variation/precision for an instrument). To determine the reliability of the new protocol, the Cronbach's alpha internal consistency reliability estimate was calculated. The new protocol was found to be 99.6% reliable.

3.4.1.6 Limit of detection

To determine how sensitive the GC was in identifying small samples, the FAME 37 mix was diluted serially with a factor of 10 until the GC could no longer identify 35 peaks. This limit was reached with a 1:100 dilution which represents 2ng of C17:0.

3.4.1.7 C17:0 standard curve.

To determine how accurately the GC quantifies different concentrations of FAMEs after methylation, a standard curve was generated using C17:0 (internal standard). The peak area was used for quantification and found to be highly correlated to C17:0 amount ($R^2 = 0.99$)

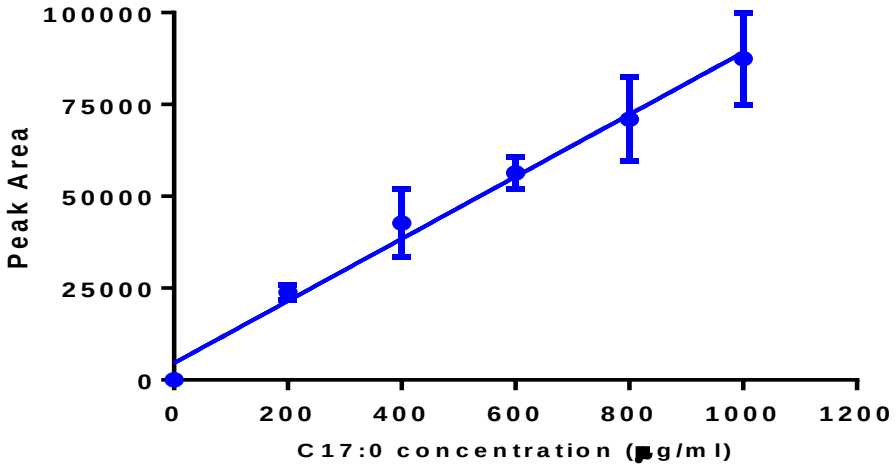

Figure 3.4: Standard curve for C17:0 internal standard.
1mg/ml solution of C17:0 was prepared in chloroform/methanol as previously described. A serial dilution was done to obtain 0.2mg/ml, 0.4mg/ml, 0.6mg/ml and 0.8mg/ml C17:0 solutions. Three 100µl aliquots of each dilution were extracted by the direct method and derivatised using BCl_3 and analysed by GC. The R^2 for the curve was 0.99

3.4.2 Lipid extraction and methylation optimisation

3.4.2.1 Lipid extraction before methylation

FA analysis by GC depends upon the volatility of the different FAs and discrete chromatographic separation of them in the absence of contaminating molecules. Methylation of FA to yield (FAMEs) renders them volatile. The Folch method (modified by adding BHT to prevent FA oxidation) is one of the most widely used and reliable extraction methods for lipids from biological samples, but it is time-consuming. To test the value of pre-extraction before methylation, three independent aliquots from the same pool of plasma sample were analysed directly (without prior extraction), or by a two-step procedure (methylation with prior modified Folch extraction). The aim was to

measure the FFA recovery from both methods as represented by peak areas of FAMEs quantified by the GC. The peak area represents the quantity of FAMEs detected on GC.

To measure the difference between both derivatisation methods, a Wilcoxon matched-pairs test and a two-way ANOVA were applied to test the difference between the total FAME amount detected and the peak areas for individual FAMES respectively (Figure 3.5). The two-step method had a higher average peak area (mean difference: 16.48; 95% CI: -117.5 to 150.6) compared to the direct method, but this was not statistically significant (two-tailed p value = 0.58), even after excluding C17:0 (internal standard) from the analysis (p = 0.79). However, the direct method recovered more internal standard (C17:0) on average than the two-step method (OR: 1.6; p= 0.144) and was expected, therefore, to differ significantly for the amount of FAMEs detected as interpolated by C17:0. However, this was not exactly the case. Although the direct method had a higher FAME recovery (mean difference: 57.4ng, 95% CI: -254.6 to 369.4; median of difference [MoD]: 33.8, 97.85% CI -25 to 86) compared to the two-step method, this was not statistically significant (two-tailed p value = 0.16). Interestingly, the direct method also recovered more C15:0 compared to the two-step method (Figure 3.5a), but this was not statistically significant (mean peak area difference 144.6; 95% CI: -426 to 719).

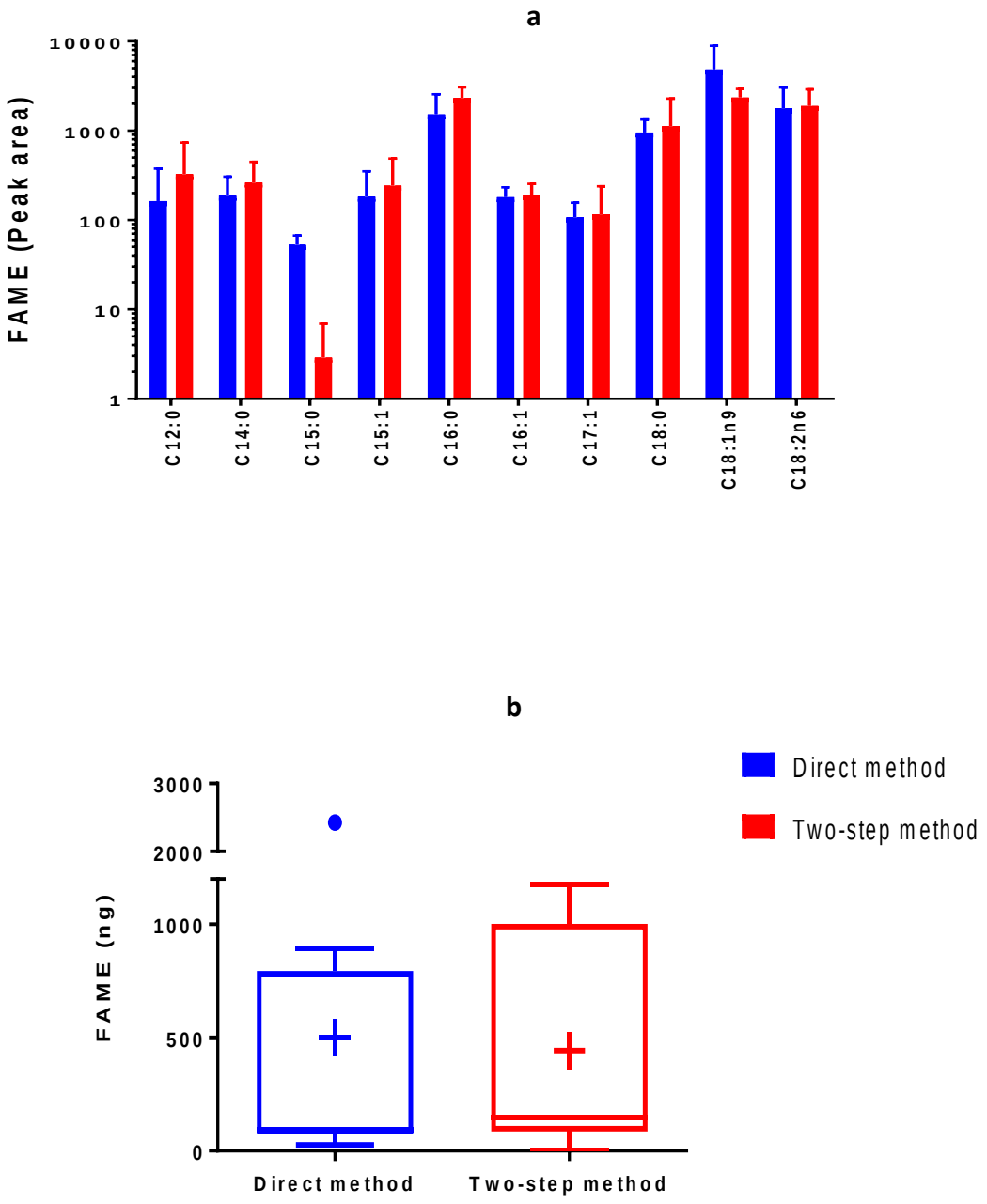

Figure 3.5 : The effect of extraction and derivatisation approach of fatty acid quantification from plasma.
Pooled plasma (500µl) were either derivatised and extracted in one step (Direct method) or extracted by modified Folch method prior to derivatisation (Two-step method). Three independent samples were derivatised with HCl as detailed in methods and analysed for each group. Derivatised lipids were separated by GC and detected as peak areas and compound amount. (a) A comparative recovery of FAMEs between the two methods showing log peak area for selected FFA identified. (b) Total FFA recovered determined against a standard curve of FAMEs and relative to internal standard. A Two-Way Anova with repeated measures was used to test the difference between derivitisation methods and FAME peak areas for (a), and a Wilcoxon matched-pairs sign rank test was used to assess statistical significance for (b).
Key for box and whisker plot: *Vertical line within box represents median, cross within box represents mean, whiskers represent highest and lowest observations, box represents interquartile range, dots outside box represents an outlier.*

3.4.2.2 Methylation methods

To determine which methylation method to employ, two acid-catalysed transmethylation methods were compared. Three 500µl pooled plasma samples were aliquoted, extracted and derivatised separately by the direct method. Each sample was run thrice on the GC with identified FFA recorded as peak areas. C17:0 was added as an internal standard, and FAME amounts were interpolated from the areas of identified peaks on the chromatogram. The recovery amount for the two methods was analysed using a Wilcoxon matched-pairs sign rank test.

After excluding C17:0 recovery from the analysis, the BCl_3 method showed higher amounts of FAMEs compared to the HCl method (Figure 3.6b), with a MoD of 121.1 (97.85% CI: 66.7 to 3047, two-tailed exact $p < 0.001$). The most statistically significant observed differences between both methods in terms of FA recovered were among C18:1n9 and C18:2n6 (two-tailed p value < 0.01 for both observations).

3.4.3 Plasma sample volume

Different volumes of plasma were compared to determine the lowest optimal volume required to identify and quantify FAMEs with no loss of sensitivity. Decreasing plasma volumes (500µl, 100µl and 50µl) were compared and analysed by repeated measure one-way ANOVA using the amount of FAMEs recovered as an outcome. To correct for identification and quantification bias due to dilution, a dilution correction was applied to the final lipid extract volume as follows: final lipid extracts from 500µl, 100µl, and 50µl plasma samples were dried down to 250µl, 50µl, and 25µl respectively.

As shown in Figure 3.7, the amount of FAMEs recovered reduces with increasing volumes of plasma samples used for extraction and methylation. A repeated measures one-way ANOVA analysis showed that there is a 92.57% chance that the differences in the mean FAME amounts observed between the different plasma volume groups in this study is real and not due to chance (p value= 0.015). The most considerable observed mean difference (and only statistically significant difference found) in FAME amount was between the 50µl and 100µl samples (mean difference: 9.912µg/ml; p = 0.03). However, when C17:0 was removed from the analysis, there was no statistically significant difference in the FAME amounts recovered between all groups. The mean differences between 50µl samples compared to 500µl samples was 9.039µg/ml (p = 0.06), and there was no significant difference in FAME concentrations between 500µl and 100µl samples (mean difference: -0.87µg/ml; p = 0.92).

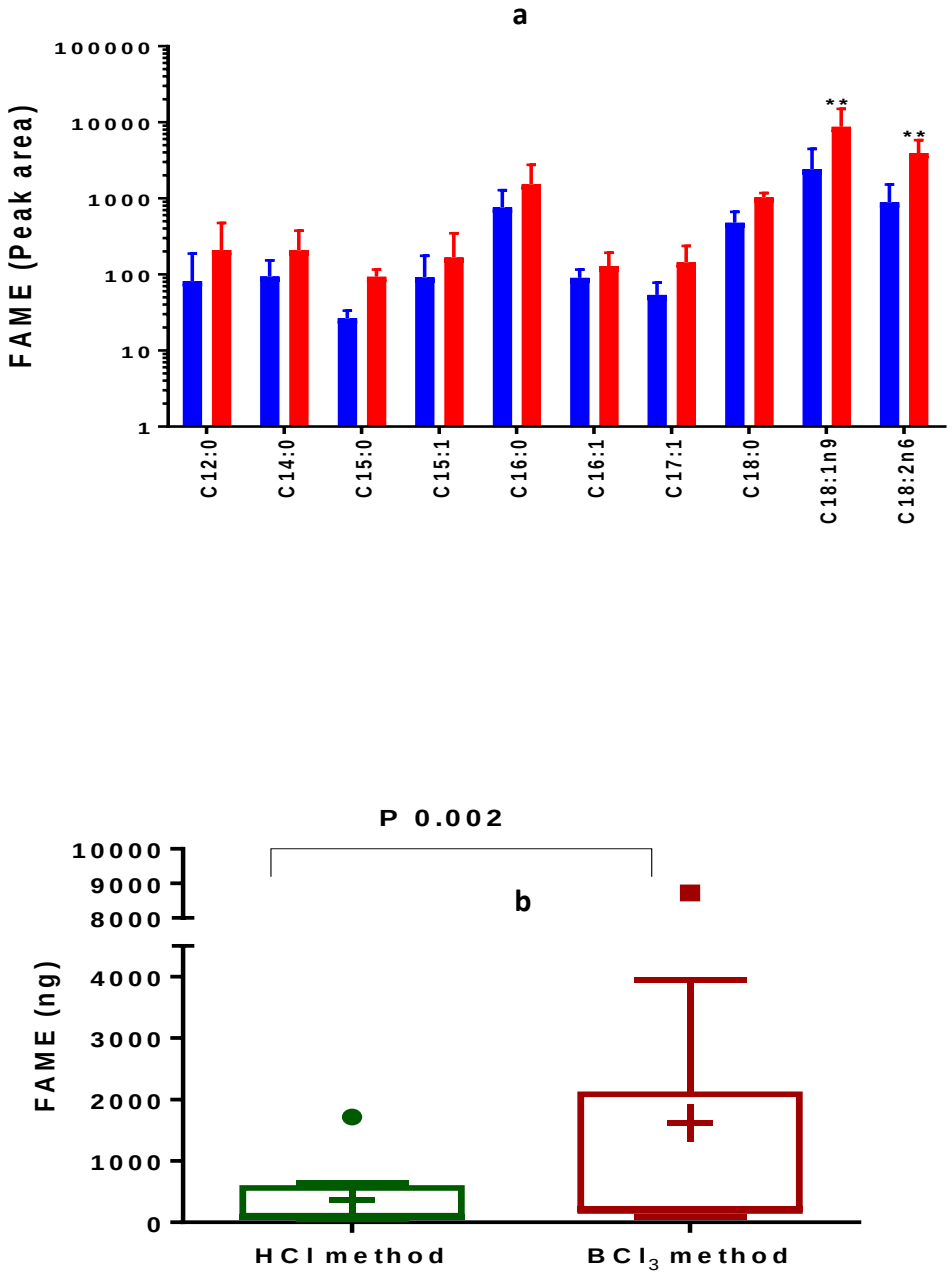

Figure 3.6 : The effect of derivatisation methods on free fatty acid quantification from plasma.
500µl of pooled plasma were either derivatised with HCl or BCl3.Three independent samples were derivatised and analysed for each group. Derivatised lipids were separated by GC and detected as either peak area of selected fatty acids (a) or total fatty acid recovery amount (b). Amount was calculated using a calibration table that measures individual response factors of each FAME based on an external standard run (FAME 37 mix) and the amount of C17:0 internal standard in the sample. A Two-Way Anova with repeated measures was used to test the difference between derivitisation methods and FAME peak areas for (a), and a Wilcoxon matched-pairs sign rank test was used to assess statistical significance for (b).
***Key for box and whisker plot**: Vertical line within box represents median, cross within box represents mean, whiskers represent highest and lowest observations, box represents interquartile range, dots outside box represents an outlier.*

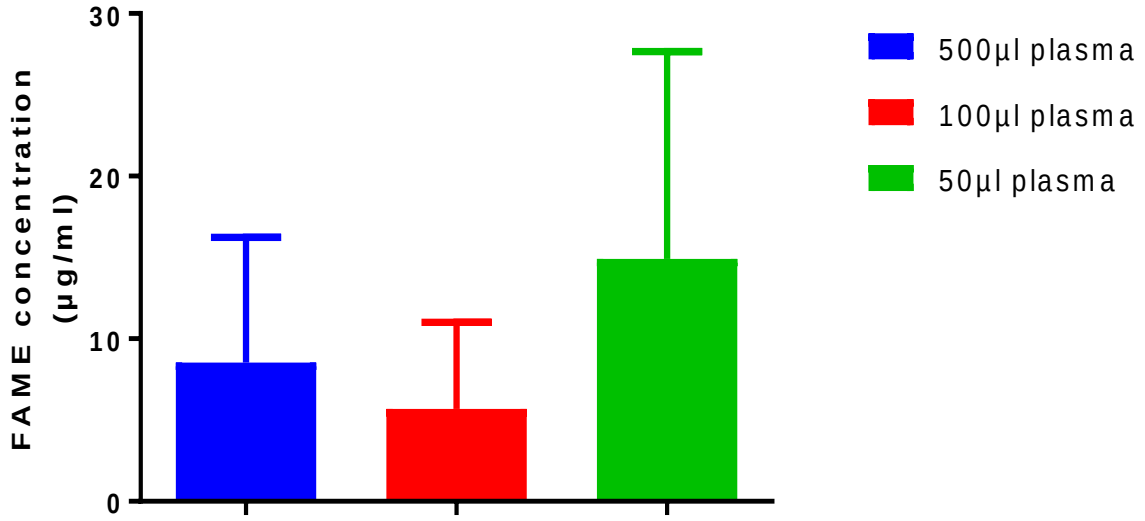

Figure 3.7 : The effect of plasma volume on FFA quantification by GC.
BCl_3 was used to derivatise three volumes of pooled plasma (50µl, 100µl or 500µl). Three independent samples were derivatised and analysed for each group. Derivatised lipids were separated by GC and detected as the compound amount. The amount was calculated using a calibration table that measures individual response factors of each FAME based on an external standard run (FAME 37 mix) and the amount of C17:0 internal standard in the sample. A dilution was applied to avoid identification bias. Dilution calculation resulted in diluting the final concentrations of 500µl and 100µl samples by 10 and two times the final volume of 50µl sample. Data presented as mean and 95% CI. Statistical analysis assessed by One-way ANOVA, applying a Geisser Greenhouse correction, with Tukey's post-test comparison.

3.4.4 Baseline characteristics of study participants

Participants from this study were sampled from an existing cohort of type 2 diabetics (T2DM) and healthy controls as detailed in the method section.

There was no significant difference in the disposition of males or females between control and healthy cohorts. The diabetic cohort was significantly older (mean difference: 17.71years, $p < 0.0001$), with a higher BMI (mean difference: 8.85kg/m^2, $p < 0.0001$), compared to the control cohort. A statistically significant higher difference was also observed with the visceral fat score in the diabetic cohort compared to the control (mean score difference: 6.69, $p< 0.0001$). Fasting plasma glucose, Leptin, soluble E-selectin, soluble thrombomodulin, C-reactive protein and protein carbonyl levels were higher in the diabetic cohort compared to healthy controls (Table 3.3).

To estimate how well protein carbonyl levels and the plasma lipid profile predict T2DM or inflammation, a multiple linear regression model was developed comparing them (predictor variables) to fasting plasma glucose, leptin, BMI and markers of inflammation. The regression models were fit through a backward step method. The variance inflation factor (VIF) was used to detect colinearity, while the R squared values and chi-squared of each variable were used as factors to eliminate variables from the model. Any variable with a VIF > 10 and chi-square > 0.05 was eliminated from the next step of the model. The best fit model was achieved when all the variables left in the model had a VIF <10, a statistically significant ANOVA and chi-square value.

Table 3.3: Baseline characteristics of study participants

Statistically significant differences between control and diabetic cohorts were adjusted for during regression analysis.

	Healthy controls n=47	Type 2 Diabetes group n=49	Total (n=96) Frequency/ Mean difference	p value
Gender -female -male	15 (51.7%) 14 (48.3%)	13 (41.9%) 18 (58.1%)	28 (46.7%) 592 (53.3%)	0.44
Age (years)	42.21 (12.63)	59.48 (14.25)	17.71	<0.0001
Height(cm)	171.38 (1.95)	167.10 (1.76)	4.27	0.10
Weight (Kg)	72.941 (2.65)	85.32 (8.43)	12.37	0.01
BMI (Kg/m^2)	24.45 (0.95)	30.31 (1.10)	5.85	<0.0001
Visceral fat score (1-59)	5.93 (0.63)	12.62 (0.86)	6.69	<0.0001
Leptin ng/ml	8.41 (1.09)	1160 (180)	1151.59	<0.0001
Soluble E-selectin ng/ml	33.28 (4.59)	48.08 (4.7)	14.80	0.01
Fasting plasma glucose (mmol/L)	4.3 (0.13)	9.3 (0.8)	5.03	<0.0001
CRP (µg/ml)	0.85 (0.14)	5.06 (0.75)	0.79	<0.0001
Protein carbonyl (nmol/mg)	2.75 (.08)	3.89 (0.17)	1.14	<0.0001

Table 3.4: Fatty acid concentration in plasma (expressed as a percentage of total FA) from fasting healthy controls and patients with T2DM.

Comparisons between healthy controls and the T2DM group was performed using appropriate statistical tests: chi-squared tests for categorical variables, Student's t-test for normally distributed continuous variables and Mann–Whitney U-test for non-normally distributed continuous variables

FAME (% of total FA)	**Healthy controls** **Median(range)/ Mean (SD)** **n=47**	**Type 2 diabetes group** **Median (range)/ Mean (SD)** **n=49**	**p value**
C14:0[a]	0.95 (6.39)	1.07 (3.43)	0.34
C15:0[a]	0.07 (2.05)	0.00 (0.36)	0.05
C16:0[a]	20.01 (44.81)	21.82 (100.00)	0.33
C16:1	2.13 (1.14)	2.56 (1.36)	0.14
C18:0	5.25 (2.88)	4.98 (2.73)	0.64
C18:1	27.47 (6.70)	29.33 (10.15)	0.32
C18:2n6	33.44 (12.36)	26.51 (12.26)	0.01
C18:3n6[a]	0.06 (56.02)	0.25 (41.22)	0.43
C18:3n3[a]	0.48 (1.48)	0.60 (38.59)	0.25

3.4.5 Predicting fasting plasma glucose

To find out how lipid profile and protein carbonyl level predict fasting plasma glucose, they were fitted into a model comparing them with the most significant predictors of fasting plasma glucose in our data, vis: age, gender and BMI (Table 8.1 in appendix). Pentadecanoic acid (C15:0), palmitic acid (C16:0), stearic acid (C18:0), linoleic acid (C18:2n6) and alpha-linolenic acid (C18:3n3) were found to be the only FA that predicted fasting plasma glucose in our model (Table 3.5). The correlation between fasting plasma glucose and these FAs in the model was 0.54, representing a moderate correlation, and the observations accounted for 22.6% of the variation in fasting plasma glucose after adjusting for chance agreement (R^2 = 0.292, adjusted R^2 = 0.226). C16:0 had the largest predictive effect on fasting plasma glucose (0.843, 95% CI: 0.009 to 0.047), and along with C18:3n3, were the only FAs that predicted a unit increase in fasting plasma glucose. After adjusting for the effects of age, gender and BMI, only C15:0, C18:0 and C18:3n3 were found to be statistically significant predictors of fasting plasma glucose (Table 3.6).

The lipidome and protein carbonyl levels were also tested in a model with leptin. It is not surprising to find that FFA that were negatively correlated with fasting plasma glucose is also positively correlated with plasma leptin (Table 3.7) since leptin correlates negatively with fasting plasma glucose. There was a moderate correlation (R 0.56) between the variables in the model and leptin, and these variables accounted for 26.4% of the variation in the data for leptin after chance adjustment. The model showed a negative correlation between protein carbonyls and leptin levels even after adjusting for age, gender, BMI and fasting plasma glucose (Table 3.8).

There was a strong correlation (R = 0.64) between FAs and BMI as shown in Table 3.8. The FAs in the model accounted for 37.2% of the variability in BMI. The model for BMI showed a positive correlation with cis-13,16-docosadienoic acid (C22:2) and oleic acid (C18:1n9). Only linoleic acid (C18:2n6) showed a negative correlation (Table 3.9). These three FFAs were still statistically significant even after adjusting for age and gender (Table 3.10).

Table 3.5: Predictors of fasting plasma glucose

Variable	Unstandardised coefficients	Standardised coefficients	p value	95% CI
Constant	7.355		< 0.0001	4.508 to 10.202
C15:0	-0.879	-0.491	0.003	-1.453 to – 0.304
C16:0	0.28	0.843	0.005	0.009 to 0.047
C18:0	-0.077	-0.561	0.022	-0.143 to -0.012
C18:2n6	-.006	-0.438	0.016	-0.011 to -0.001
C18:3n3	0.235	0.428	0.010	0.059 to 0.411

Model summary: R = 0.540; R^2 = 0.292; Adjusted R^2 = 0.226; outcome variable = Fasting plasma glucose

Table 3.6: Predictors of Fasting blood glucose. Adjusted for age, gender, and BMI

Variable	Standardised coefficients	p value	95% CI
C15:0	0.454	0.002	0.273-0.754
C18:0	0.938	0.038	0.882-0.996
C18:3n3	1.237	0.013	1.043-1.463
Age	1.037	0.126	0.990-1.086
BMI	1.027	0.674	0.906-1.165
Gender (male)	1.654	0.500	0.383-7.134

Table 3.7: Predictors of Leptin

Variable	Unstandardised coefficients	Standardised coefficients	p value	95% CI
Constant	10.028		0.003	3.534 to 16.522
Protein carbonyl	-2.120	-0.373	0.003	-3.499 to -0.742
C16:0	-0.031	-0.685	0.021	-0.057 to -0.005
C18:0	0.108	0.577	0.015	0.022 to 0.199
C18:2n6	0.007	0.341	0.062	0.000 to 0.014
C18:3n3	0.235	0.428	0.010	0.059 to 0.411

Model summary: R = 0.560; R^2 = 0.314; Adjusted R^2 = 0.264; outcome variable = Leptin

Table 3.8: Predictors of Leptin: Adjusted for fasting plasma glucose, BMI, age gender

Variable	Standardised coefficients	p value	95% CI
Protein carbonyl	0.093	<0.0001	0.25-0.345
Fasting plasma glucose	0.716	0.011	0.553-0.927
Gender (M)	0.046	0.006	0.005-0.405
Age	0.981	0.547	0.920- 1.045
BMI	0.992	0.934	0.828- 1.190
C18:2n6	1.001	0.832	0.995- 1.005
C18:3n3	1.059	0.562	0.572- 1.287

Table 3.9: Predictors of BMI

Variable	Unstandardised coefficients	Standardised coefficients	p value	95% CI
Constant	28.392		< 0.0001	25.527 to 31.257
C15:0	-0.452	-0.182	0.096	-0.986 to 0.082
C18:1n9	0.019	0.746	<0.0001	0.011 to 0.027
C18:2n6	-0.016	-0.818	<0.0001	-0.022 to -0.011
C22:2	0.181	0.225	0.038	0.059 to 0.411

Model summary: R = 0.644; R^2 = 0.414; Adjusted R^2 = 0.372; outcome variable = BMI

Table 3.10: Predictors of BMI after adjusting for age, gender, fasting blood glucose and Leptin

Variable	Standardised coefficients	p value	95% CI
C18:2n6	0.983	<0.0001	0.978-0.989
C18:1n9	1.021	<0.0001	1.013-1.027
C22:2	1.215	<0.0001	1.151-1.281
Age	0.969	0.492	0.886- 1.060
Gender	1.689	0.647	0.179- 15.921
Fasting plasma glucose	1.190	0.142	0.943- 1.501
Leptin	1.025	0.791	0.853- 1.232

3.4.6 Predictors of inflammation

To determine which FFAs predict inflammatory events, FFAs and protein carbonyl levels were tested against three markers of inflammation, vis: C-reactive protein, soluble thrombomodulin and soluble E-selectin.

In one of the models, palmitoleic acid (C16:1) and an ω3 FA, cis-11,14,17-eicosatrienoic acid (C20:3n3) were found to be moderately (R = 0.447) negatively correlated with soluble thrombomodulin (Table 3.11). On the contrary, C18:0 and C18:1n9 were positively correlated even after adjusting for possible confounders (Table 3.12). The FAs in the model accounted for only 14.2% of the variation within soluble thrombomodulin within the data.

Soluble E-selectin was predicted by C15:0, C18:2n6 and C18:3n3. C15:0 and C18:2n6 were negatively correlated with soluble E-selectin (Table 3.13). There was a weak correlation between the FAs in the model and soluble E-selectin (R = 0.43), and the

predictors could only account for 14.2% of the variation in soluble E-selectin. However, when these FFAs were adjusted for other inflammatory markers, the only FFA that predicted soluble E-selectin was C18:2n6 (Table 3.14).

Only protein carbonyl levels and C18:3n3 were found to be correlated significantly with C-reactive protein, both showing positive moderate (R = 0.58) correlations (Table 3.15). However, when adjusted for known predictors of inflammation, leptin also becomes negatively correlated with CRP (Table 3.16).

Table 3.11: Predictors of soluble thrombomodulin

Variable	Unstandardised coefficients	Standardised coefficients	p value	95% CI
Constant	4.609		< 0.0001	2.667 to 6.551
C16:1	-0.056	-0.478	0.024	-0.105 to -0.008
C18:0	0.028	0.320	0.072	-0.003 to 0.059
C18:1n9	0.006	0.472	0.021	0.001 to 0.010
C20:3n3	-0.037	-0.524	0.003	-0.062 to -0.013

Model summary: R = 0.447; R^2 = 0.220; Adjusted R^2 = 0.142; outcome variable = soluble thrombomodulin

Table 3.12: Predictors of Soluble thrombomodulin. Adjusted for age, fasting blood glucose, CRP, soluble E-selectin and BMI

Variable	Standardised coefficients	p value	95% CI
C18:2n6	0.996	0.008	0.993-0.999
C18:1n9	1.003	0.031	1.001-1.015
C16:1	0.933	0.002	0.892-0.975
C18:0	1.022	0.040	1.001-1.044
Fasting blood glucose	1.307	0.008	1.072-1.593
Age	1.006	0.729	0.972- 1.042
BMI	0.989	0.827	0.892- 1.095
Soluble E-selectin	1.017	0.098	0.997- 1.037
CRP	0.817	0.083	0.651- 1.027
Protein carbonyl	0.745	0.330	0.412- 1.348

Table 3.13: Predictors of soluble E-selectin

Variable	Unstandardised coefficients	Standardised coefficients	p value	95% CI
Constant	60.465		< 0.0001	47.219 to 73.712
C15:0	-3.168	-0.302	0.050	-6.338 to 0.001
C18:2n6	-0.037	-0.434	0.002	0.060 to -0.014
C183n3	1.081	0.336	0.048	0.010 to 2.150

Model summary: R = 0.431; R^2 = 0.186; Adjusted R^2 = 0.142; outcome variable = soluble E-selectin

Table 3.14: Predictors of soluble E-selectin: Adjusted for Age, BMI, Fasting plasma glucose, leptin, and CRP

Variable	Standardised coefficients	p value	95% CI
C18:2n6	0.960	0.004	0.934-0.987
Age	0.616	0.004	0.442-0.858
Fasting blood glucose	6.503	<0.0001	2.777-15.228
BMI	1.217	0.740	0.381- 3.893
Leptin	0.595	0.515	0.125- 2.843
CRP	1.189	0.874	0.141- 10.032

Table 3.15: Predictors of C-reactive protein

Variable	Unstandardised coefficients	Standardised coefficients	p value	95% CI
Constant	-3.776		0.01	-0.668 to 0.884
Protein carbonyl	1.718	0.446	<0.0001	0.885 to 2.551
C18:3n3	0.165	0.328	0.004	0.056 to 0.274

Model summary: R = 0.588; R^2 = 0.345; Adjusted R^2 = 0.322; outcome variable = C-reactive protein

Table 3.16: Predictors of CRP. Adjusted for Age, BMI, Fasting plasma glucose, and soluble E-selectin

Variable	Standardised coefficients	p value	95% CI
Protein carbonyl	3.017	0.032	1.101-8.264
C18:3n3	1.179	0.003	1.056-1.316
Leptin	0.851	0.031	0.735-0.985
Age	1.020	0.483	0.966- 1.077
Fasting blood glucose	0.973	0.836	0.751- 1.260
Soluble E-selectin	1.016	0.471	0.973- 1.060

3.5 DISCUSSION

This chapter describes the successful validation and application of reproducible and robust methods for determination of plasma FAs and protein carbonyls in populations of healthy adults and patients with T2DM.

Many direct derivatisation techniques have been developed over the years to eliminate time spent on lipid extraction and potentially cut cost on reagents. Most of these techniques have been modifications of the method by Lepage and Roy (1984). This study compared a direct method, which involved methylation of plasma without prior extraction, with a two-step method that involved prior extraction by the modified Folch method. The direct method recovered more C17:0 standard compared to the two-step method. A logical explanation to this could be that C17:0 is possibly lost during the modified Folch extraction of lipids from plasma since this involves several extraction steps and manipulations (Sattler et al., 1991, Lepage and Roy, 1986). However, Amusquivar et al. (2011) showed that the direct method recovered less internal standard compared to the standard two-step method, leading to an overestimation of quantified FFAs. They explain that the high polarity of most internal standards used (C15:0 and C17:0) means that prior extraction with chloroform/methanol is more favourable, especially with increasing amounts of internal standards added (Amusquivar et al., 2011). Paradoxically, the direct method recovered less FAMEs on average than the two-step method, although this was not statistically significant. C13:0 caused most of the variation between FAME recoveries between both methods. The twentyfold difference in recovery of C13:0 (shown in the appendix) between both methods suggests it is possibly due to an artefact. Artefacts are expected to be

produced with the modified Folch method due to the methylation of BHT (formation of methyl-toluene) that is added to extracting solvent and used to minimise oxidation. However, the artefact for methyl-toluene is usually expected to elute with C16:0 or C16:1 rather than C13:0. It is important to note that there are conflicting reports from literature reviewing both direct and two-step-method (Cavonius et al., 2014, Amusquivar et al., 2011, Castro-Gómez et al., 2014). Most studies comparing the two methods usually use methods partially modified in their labs, making it difficult to standardise or compare directly. However, in this study, both methods did not differ much, and the most likely cause of the variation could be as a result of artefact formation.

The HCl method of FFA methylation offers the advantage of being safer and producing fewer artefacts, compared to the conventional boron trifluoride method (BF_3). The HCl method is the reference method used in our laboratory. However, reports suggest that the BCl_3 method is associated with less unwanted side reactions seen with BF_3 and is as effective (Klopfenstein, 1971). Perhaps the most significant advantage of using either BF_3 or BCl_3 is that less time is required for derivatisation. It takes between 5-10 minutes for full derivatisation of FFA with the BCl_3 method compared to 60 minutes for the HCl method. This study found a statistically significant difference in the mean recoveries of FAMEs between both methods. The BCl_3 method recovered more FAMEs on average than the HCl method, the most prominent difference being with the long chain FFA- especially those with 18 carbon atoms or more. The significant higher recovery of these long-chain FAs is unlikely due to methyl-toluene artefact since both methods were evaluated with the direct method. There is insufficient literature

covering the derivatisation of FFA with BCl_3, although its efficacy has been compared to BF_3 (Klopfenstein, 1971). The most cited limitation of BF_3 is the shelf-life. Left for too long, even when refrigerated, it is notorious for producing artefacts with significant loss of PUFAs. Here, BCl_3 recovery of PUFA was better than that of HCl.

This study showed that there is no difference in FAME recovery when 50µl, 100µl, or 500µl of plasma is derivatised. To correct for detection bias and water content, both 50µl and 100µl samples were diluted to a consistent final volume of 500µl with PBS. Small amounts of water in plasma, glassware, reagents and the atmosphere can interfere with FAME formation, especially PUFAs (Christie, 2011); therefore it was important to account for this in the analysis. Because water is a stronger electron donor than most aliphatic alcohols, the presence of water favours the formation of intermediates and prevents the completion of the reaction.

The second phase of optimisation that is described in this report is in use of instrumentation. In GC, the three most common consequence of an inappropriate inlet temperature is high molecular weight discrimination, sample decomposition and splitless purge time (Klee, 2015). These were the measures considered for optimising the GC protocol for this study. High molecular weight discrimination often occurs when the inlet temperature is too low and high molecular weight analytes fail to vaporise in the inlet; therefore, not adequately reaching the column. During the optimisation of this protocol, it was observed that peak areas towards the last third of the run increased with rising temperature. Another possible cause of high molecular weight discrimination, needle discrimination, was accounted for in this study by using the hot

needle injection technique. Optimal inlet temperature choice for this study also considered sample decomposition. Some low molecular weight highly volatile analytes are thermally labile and decompose at high inlet temperatures, which is usually observed on the chromatogram as several split peaks in the first third of the chromatogram. In this study, the inlet temperature showing the least discrimination was the 300˚C run. However, the 280˚C run was chosen as the optimal temperature because, unlike the former, it did not display any signs of thermal decomposition of any analytes (Restek, 2012).

Finally, inject mode protocol was considered. The splitless purge time is the time between sample introduction and the opening of the split vent in splitless liners. When the split vent is open, the inlet is purged of any excess solvent to prevent solvent tailing throughout the chromatogram. The optimal splitless time is the amount of time required for all or most of the analytes to transfer to the head of the column, particularly high molecular weight analytes. One minute was determined as the optimal splitless purge time for the study protocol because it was just enough time to improve elution of high molecular weight analytes while preventing tailing of the solvent on the first analyte of interest (C4:0).

With the conditions established for optimal separation and identification, the protocol was validated for sensitivity and reproducibility using conventional clinical chemistry approaches. These studies confirmed limits of detection and coefficients of variation that were suitable for subsequent sample analysis to test the hypothesis that specific FFA are predictors of T2DM.

It is accepted and backed by strong evidence, that plasma levels of FFA increases with obesity. This potentially results in insulin resistance, which consequently leads to increased lipolysis in a vicious cycle that explains the process of T2DM. This simplistic view has come under heavy scrutiny in recent times as evidence from several studies shows the relationship between FFA, obesity and T2DM is much more complicated. There are strong suggestions that the association between increased FFA and T2DM might be confounded by other metabolic predictors of T2DM like BMI and gender (Il'yasova et al., 2010). Therefore, here, the associations between FFAs and these metabolic predictors were examined.

This study found a statistically significant positive correlation between C22:2 and C18:1n9 to BMI, while C18:2n6 returned a negative correlation (even after adjusting for age and gender). A systematic review of 43 studies suggests that there is no relationship between FFAs and BMI or body fat mass, and differences observed are mainly due to within-subject day-to-day variations in fasting FFAs (Karpe et al., 2011). An important observation from reviewing literature is that most studies that try to quantify the effect of FFAs on the metabolic predictors of T2DM focus on total FFAs or FFA categories like saturated vs unsaturated FFAs rather than individual effects of FFAs. Perhaps the variation in the effect of total FFAs in these studies can be explained by variations in the individual FFA profile. It is interesting that this study found a positive correlation between docosahexaenoic acid and a negative interaction between linoleic acid with BMI. Lu et al. (2012) found that meal-related increase in docosahexaenoic acid and linoleic acid interacts with a long-chain FA receptor, GPR120, on ghrelin cells to inhibit ghrelin secretion. Ghrelin is a gastric peptide

hormone that regulates appetite and energy homeostasis. Interactions between plasma concentrations of these FAs with ghrelin have not been established; however, going by this evidence, a negative correlation between BMI and linoleic acid would not be surprising. It will be interesting to find out if the positive correlation of docosahexaenoic acid found here is an adaptation of the adipose tissue to increasing BMI (or obesity).

The positive correlation found between alpha-linolenic acid (ALA) and fasting plasma glucose in this study has been considered in other studies. Dietary ALA has been found to be useful in decreasing insulin resistance in several studies (Lee et al., 2014, Hollander et al., 2014), while (Alssema et al., 2014) did not find any significant correlation between ALA and fasting blood glucose. ALA has been shown to reduce pancreatic islet cell damage in rats (Budin et al., 2007) and could be the possible mechanism by which it contributes to reduced fasting plasma glucose in humans. It is possible that the observed increase in ALA with increasing blood glucose levels is an adaptation to improve insulin secretion in those with high fasting blood glucose.

The discovery of a negative correlation between pentadecanoic acid (C15:0) and fasting plasma glucose here (after adjusting for leptin, BMI, age, and gender) is in line with growing evidence from several prospective studies showing negative associations between OCSFA and metabolic disease development [78-80, 209, 210]. Historically, even-chain saturated FAs (SFA) are associated with increased risk of metabolic diseases, and the odd-chain SFA were regarded as physiologically unimportant. Consequently, odd-chain SFAs have been used mostly as internal

standards for lipid research. Following its use as a biomarker for dairy fat consumption [211, 212], evidence began to emerge on the possible beneficial effects of odd chain SFA on various disease states, including T2DM and coronary heart disease. The possible protective effect of OCSFA on T2DM development has been attributed to its dietary sources, like fish and dairy products, which correlate favourably with healthy eating habits and lifestyle [213]. However, there is a reversal in the ratio of C15:0 to C17:0 in these dietary sources (usually 2:1) in human plasma [214, 215], suggesting that there may be other sources of OCSFA, including the possibility of human biosynthesis [216]. In addition to plasma, OCSFAs have been detected in other tissues such as the brain and liver [217], highlighting the possibility of endogenous production and metabolism. In this study, dietary patterns were not analysed and the possible effect it would have on C15:0 levels or its association with insulin resistance cannot be quantified. Future in vivo and in vitro research will likely address the cellular mechanisms underlying the effect of OCSFAs on insulin signalling and glucose homeostasis (Benjamin Jenkins, 2015).

Only age, fasting plasma glucose and protein carbonyl levels predicted leptin in this study. The relationship between protein oxidation (measured as protein carbonyls in this study) and leptin depends on the pathological state. Under normal physiologic conditions, leptin increases thermogenesis by inducing gene expression of *PPARY* co-activator 1-α (Pgc1a) and plays a vital role in energy homeostasis by inducing FA oxidation and lipolysis (Becerril et al., 2012). Furthermore, it stimulates nitric oxide (NO) which induces endothelium-dependent vasorelaxation. However, under pathological conditions, like obesity or diabetes, this vasorelaxation property is

impaired and could induce peroxy-nitrite oxidative stress (Chatterjee et al., 2013, Bełtowski, 2012).

Conflicting reports exist in the literature on the relationship between linoleic acid (C18:2n6) and the pro-inflammatory soluble E-selectin, which is also a marker of vascular endothelial dysfunction. This study found a negative correlation after adjusting for other markers of inflammation. On the contrary, other in-vitro studies have shown that linoleic acid promotes the expression of soluble E-selectin, a cell adhesion molecule that is expressed in endothelial cells and induced by IL-1 and TNF-α (Matesanz et al., 2012, Chiang et al., 2012).

After adjusting for other predictors of inflammation, fasting plasma glucose and four FFAs were significantly correlated with soluble thrombomodulin. Stearic acid (C18:0) and oleic acid (C18:1n9) positively correlated with soluble thrombomodulin, while palmitoleic (C16:1) and linoleic (C18:2n6) were negatively correlated with soluble thrombomodulin. Soluble thrombomodulin is a protein expressed on the surface of endothelial cells where it serves as a co-factor for thrombin-induced activation of protein C. It has been shown to reduce vascular inflammation in chronic kidney disease by downregulating VCAM-1, ICAM-1 and chemokines in TNF-expressing endothelial cells (Rajashekhar et al., 2012). It has also been shown to reduce apoptosis, improve NRF2 activity, and reduce diabetic nephropathy via anti-NF-κB/NLRP3 inflammasome-mediated inflammation (Yang et al., 2014). The anti-inflammatory properties of Oleic acid are well documented (Camell and Smith, 2013), while palmitic acid (C16:0) and Linoleic acid (C18:2n6) have been shown to depress

thrombomodulin activity in a dose-dependent fashion (Wang et al., 2006). Palmitoleic and not palmitic acid was correlated with soluble thrombomodulin in this study. There is no report in the literature showing any relationship between palmitoleic acid or stearic acid and thrombomodulin. It is possible that palmitoleic acid depresses thrombomodulin activity in the same manner as palmitate. Most reports in the literature suggest that stearic acid promotes more pro-inflammatory than anti-inflammatory phenotypes (Anderson et al., 2012, Lavrador et al., 2014, Stryjecki et al., 2012).

In summary, this chapter described a throughput and sensitive method for extracting and analysing lipids from plasma, associated with improved recovery of OCSFAs. Here, we found that the OCSFA, C15:0, predicted plasma glucose level as well as known inflammatory markers leptin and soluble E-selectin in the context of obesity and T2DM.

4 CHAPTER 4: EFFECT OF FATTY ACIDS ON HEPATOCYTE FUNCTION

4.1 INTRODUCTION

The liver is the largest visceral organ in humans with critical metabolic functions including glucose and lipid homeostasis [218]. It is comprised mostly (80%) of parenchymal cells (or hepatocytes), which are the metabolic unit of the liver, and non-parenchymal cells, like kupffer and hepatic stellate cells. Valuable insight into liver activity and pathophysiology have come from both in vivo animal and human models as well as invitro hepatocyte models. Primary hepatocytes are regarded as the gold-standard for gaining mechanistic insights into metabolic and regulatory pathways in cellular models [219-221]. However, cost, inter-donor variability, and the non-proliferative nature of primary hepatocyte raise concerns about its use in vitro [222, 223]. Consequently, hepatocyte cell lines have been developed to mitigate these challenges. Hepatocyte cell lines like HepaRG, HepG2, Hep3b, and Huh 7.0 cells have been used numerous times as invitro substitutes for hepatocyte models. HepG2 cells are the most commonly used hepatocyte cell lines and have been shown to have morphological and physiological differences compared to primary hepatocytes [224-227]. For example, concerning organelle abundance, the mitochondria make up a significantly higher percentage of primary hepatocytes (25%) compared to HepG2 cells (12%), while the reverse is the case for the nucleus in hepatocytes (12%) and HepG2 cells (25%) [228]. Subsequently, mitochondrial proteins are more abundant in hepatocytes; therefore, FA β-oxidation and oxidative phosphorylation are the common metabolic pathways in hepatocytes compared to glycolysis in HepG2 cells. Furthermore, HepG2 cell models are less useful in xenobiotic metabolism research because there is a marked difference in the mRNA expression and protein abundance

of enzymes responsible for drug metabolism (cytochrome P450 enzymes) between hepatocytes and HepG2 cells, with the latter having a deficient expression of these enzymes [225, 229]. It is plausible that these metabolic differences are due in part to the marked difference in age of the source of HepG2 cells (16-year-old) compared to the primary hepatocytes, which are usually sourced from over 65-year-olds. Despite these dissimilarities, HepG2 cells are still the most commonly used hepatic cell line for lipid research mainly because they have been shown to accumulate triglycerides similarly to primary hepatocyte in response to exogenous glucose and FA [230]. Moreover, HepG2 cells can be differentiated using different exogenous chemicals to further resemble primary hepatocytes phenotypically [231-233]. Furthermore, C3A, a clonal derivative of HepG2 cells, has been selected for its ability to become quiescent upon confluency, with increased secretion of albumin, assuming a phenotype more similar to primary hepatocytes compared to its parent cell [234].

HepG2 cells have been used to investigate the mechanisms that underpin saturated FA-induced hepatotoxicity and insulin resistance [235]. While the mechanistic link between FAs, NAFLD, and T2DM is still heavily debated, peroxisome proliferator-activated receptors (PPARs) have been suggested to play a significant role [236-239]. PPAR alpha is highly expressed in the liver and regulates genes involved in enhancing FA transport and mitochondrial β-oxidation [240-243]. Moreover, synthetic PPAR alpha agonists like fenofibrate have been used with varying degree of success for treating hyperlipidaemia [244, 245]. PPAR alpha activation has been shown to prevent intrahepatic lipid accumulation and even reverse the effects of steatohepatitis

(including insulin resistance) in mouse models and clinical studies [246-250]. Physiologically, specific FA, mainly PUFA, act as natural ligands for PPAR alpha [251].

4.2 AIMS AND HYPOTHESIS

Recent studies have shown an inverse relationship between OCSFA and T2DM development. However, the mechanisms underpinning this relationship is still unknown. The liver is heavily involved in glucose homeostasis, and insulin resistance is thought to occur in the liver before appearing peripherally. Furthermore, obesity is causally associated with insulin resistance and the effect of even numbered FAs on hepatic insulin resistance has been extensively studied by using a model of HepG2 cells. Studies have shown that HepG2 cells show genotypic and phenotypic differences compared to primary hepatocytes and various differentiation methods have been applied in literature to mitigate these differences. Therefore, this chapter will aim to examine the differential effects of OCSFA on hepatocyte function and PPAR alpha activation using HepG2 as a model system. Glucose output, glycogen storage, and gene expression profiles for genes involved in lipid metabolism will be used as surrogate markers of hepatocyte function.

4.2.1 Hypothesis

The hypotheses for this study are as follows:

1. HepG2 cells cultured in low serum media will exhibit increased markers of differentiation
2. C16:0 treated cells at indicative concentrations will accumulate more neutral lipids compared to C15:0 treated cells
3. C15:0 treated cells will show no difference in glucose or glycogen content compared to controls
4. The expression of mitochondrial and peroxisomal β-oxidation genes will be upregulated in C15:0 treated hepatocytes
5. C15:0 will increase PPAR alpha transcriptional activity in hepatocytes

4.2.2 AIMS

The purpose of this chapter was to determine the differential effect of OCSFA on hepatocyte function and had the following aims:

1. To determine the effect of OCSFA on glucose homeostasis and inflammation in hepatocytes
2. To determine the effect of OCSFA on FA metabolism in hepatocytes
3. To determine the differential effect of OCSFA on de novo lipogenesis
4. To describe the role of PPAR alpha in OCSFA mediated effect on hepatocyte function

4.3 METHOD

4.3.1 Differentiation of hepatocytes

HepG2/C3A cells were differentiated by growing in low serum as detailed in section 2.2.

4.3.2 Determination of metabolic activity

Following treatment, the metabolic activity of dHepG2 cells was determined by the MTT assay as described in section 2.7.

4.3.3 Determination of Albumin and Urea output

Following differentiation, albumin and urea output were measured using a plate-based assay.

4.3.4 Quantification of cellular growth and viability

Cell growth and viability were measured using the trypan blue exclusion method method with the counting of cells using a haemocytometer as described in section 2.6.

4.3.5 Quantification of intracellular neutral lipids

Following treatment with FAs, the intracellular accumulation of neutral lipids was evaluated by Oil Red O staining as described previously [252] and detailed in section 2.17.

4.3.6 PAS staining for Glycogen

Intracellular glycogen content was determined by PAS stain using a kit from Sigma (Product 395B) according to manufacturer's instructions and as detailed in section 2.18.

4.3.7 Glycogen content quantification

A plate based assay was used to quantify the amount of glycogen stored in hepatocytes after an overnight fast and glucose stimulation as described in section 2.16.

4.3.8 Quantification of cytokines

Following treatment, IL-8 and TNFα were quantified from supernatants by ELISA as described in 2.12.

4.3.9 PPAR alpha transcription factor assay

PPAR alpha activity in the nuclear fraction of cells was measured using a PPAR alpha transcription factor ELISA kit (Abcam, ab133107, UK) as described in section 2.14.

4.3.10 mRNA analysis by RT-qPCR

Following treatment, total RNA was isolated and converted to cDNA and then analysed by RT-qPCR as described in section 2.20. Relative gene expression was calculated using the delta delta ct formula 2-ΔΔCT

4.3.11 Statistical analysis

Data expressed as mean +/- SEM for three independent experiments. Statistical significance was estimated using a repeated measures one way ANOVA with a Geisser-Greenhouse correction to correct for unequal variability of differences, and the Two-stage step-up method of Benjamini, Krieger and Yekutieli [253] for gene expression data (displaying the false discovery rate – FDR), or a Dunnett test for testing significant difference between treatment and control or 300µM C16:0. Data obtained was analysed using GraphPad Prism (v7.0). FDR provides the same degree

of assurance as other multiple comparison methods, like Bonferroni, but are more powerful in detecting individual false positives primary because it does not provide a strong control for familywise error correction [254-256]. In this study, a strict FDR criteria of 1% (or p = 0.01) was set to further reduce the chance of false positives.

4.4 RESULTS

4.4.1 Differentiation of HepG2 cells

HepG2 cells are often used in translational research into the metabolic functions of hepatocytes. However, studies have shown that the metabolic behaviour of HepG2 cells can differ from primary hepatocytes [257]. To improve representativeness in comparison to primary cells, various methods have been used to differentiate HepG2 cells into more quiescent profiles. This includes the use of DMSO, retinoic acid, low serum media, among other methods. Here, HepG2 cells were differentiated with low serum containing media before experimental conditions as described in methods. In order to determine the effect of differentiation, gene expression levels of Albumin and Transferrin were measured (Figure 4.1a and 4.1b). The raw C_T values for albumin and transferrin were lower than 30, showing a high abundance of these genes in the sample. C_T values represent the number of cycles needed for the fluorescent signal to cross the required threshold and is inversely proportional to the amount of target gene in the sample. However, C_T values are not indicative of expression levels or relative abundance; hence the need for ΔC_T calculations which normalises for the amount of loaded sample by factoring in the C_T values of the reference gene. From Table 4.1, it is clear that the ΔC_T value for albumin and transferrin in the differentiated HepG2 cells (dHepG2) are higher compared to control cells (undifferentiated cells), showing that these genes become relatively more abundant with differentiation (Table 4.1). dHepG2 cells showed a fourfold increase in albumin expression compared to control (mean difference 3.27; 95% CI 2.11 – 4.37, $p < 0.001$). Subsequently, albumin production by dHepG2 cells were on average 50% higher compared to control (mean difference 49.9%; 95% CI 37% - 77%, $p < 0.001$). Gene expression of transferrin in dHepG2 cells

was approximately eightfold higher compared to control cells (mean 7.53; 95% CI 6.20 – 8.90), while the amount of urea excreted into the supernatant per cell was 2.5 times higher in dHepG2 cells compared to control (mean 2.53; 95% CI 2.30 – 3.00, $p < 0.001$). Put together, dHepG2 cells showed consistent increases in markers of hepatocyte differentiation compared to controls.

4.4.2 Effect of FAs on cell viability

Following differentiation of HepG2 cells, it was then essential to understand if there was any toxic effect of FA on dHepG2 cells. To determine this, HepG2 cells were treated with varying concentrations of the FAs for 6 and 24 hours to represent acute and long-term effects of FAs on cells. The toxicity of PPAR alpha antagonist and agonist (fenofibrate and GW6471) were also examined at concentrations considered therapeutic according to literature (100µM and 10µM respectively) [258, 259]. Cell viability and cell count were measured by trypan blue exclusion method, while cellular metabolic activity was measured using the MTT assay. Three concentrations of each FA were used to represent the usual range of concentration of C16:0 found in healthy and diseased subjects (50µM, 150µM, and 300µM).

The result shows that cells treated with the odd-chain FA (C15:0) showed an increase in metabolic activity compared to both control and C16:0 treated cells after 6hrs incubation (Figure 4.2a). C15:0 treated cells showed higher formazan reduction compared to control by 24% ($p < 0.01$), 16.5% ($p < 0.001$), and 7.5% ($p < 0.05$) for 50µM, 150µM, and 300µM concentrations respectively. This slight increase in metabolic activity appeared to be short-term as there was no significant difference in metabolic activity between C15:0 treated cells and controls after 24hrs of treatment

(Figure 4.2b). In fact, while metabolic activity increased by 5% in control cells between 6hrs and 24hrs, C15:0 treated cells showed a reduction by 15%, 9%, and 0.5% for 50µM ($p < 0.001$), 150µM ($p < 0.001$), and 300µM ($p > 0.05$) concentrations respectively, between 6hrs and 24hrs. Palmitate (C16:0) at lower concentrations of 50µM and 150µM did not appear to alter MTT reduction compared to controls after 6hrs or 24hrs of treatment. Furthermore, there was a 5% ($p < 0.001$) and 8% ($p < 0.05$) increase in formazan reduction in cells treated with 50µM and 150µM C16:0 respectively between 6hrs and 24hrs incubation. However, C16:0 at higher concentrations, normally found in disease states like T2DM, significantly reduced cellular metabolic activity by 10% ($p < 0.05$) and 11% ($p < 0.001$) after 6hrs and 24hrs respectively compared to control cells, which is reversed by co-incubation with C15:0 (Mean difference 0.3%, $p > 0.05$). There is a 4.4% increase in formazan reduction in 300µM C16:0 treated cells between 6hrs and 24hrs incubation, but this was not statistically significant ($p > 0.05$).

To ensure that changes to metabolic activity were not confounded by the possible toxicity of treatments to cells, cellular viability and cell growth were measured using the trypan blue exclusion method. There were no significant changes to indices of cell death after 24hrs incubation; either by trypan blue exclusion method (Figure 4.3a) or by flow cytometric estimation of propidium iodide intake (Figure 4.3b). Furthermore, FA treatments at different concentrations did not affect cell growth (Figure 4.3c), remaining at a total of five million cells for all treatments. The result also shows that treating cells at therapeutic doses of fenofibrate and GW6471 did not alter indices of cellular viability, metabolic activity or cell growth.

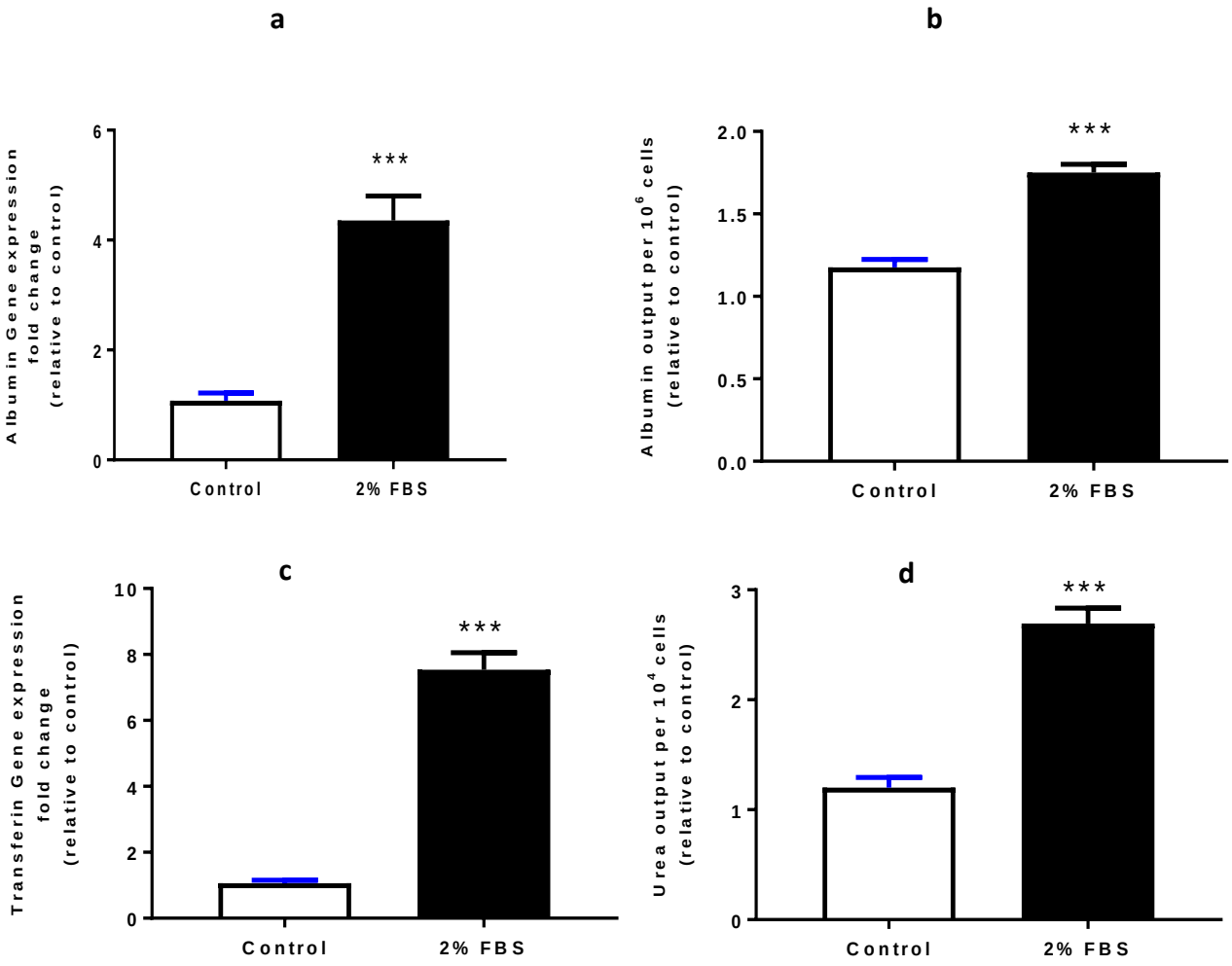

Figure 4.1: Culturing HepG2-3CA clone in low serum media increases markers of differentiation

*HepG2-3CA clones were seeded at 200,000 cells/ml and cultured until 80% confluency as outlined in methods, then cultured in media containing 10% serum or low serum media (2% FBS) for 10 days. The differentiated HepG2 cells (dHepG2) were washed thrice with ice-cold PBS and lysed for total RNA extraction (5 million cells) and RT-qPCR estimation (a and c), or further incubated in serum-free media for 24hrs for quantification of albumin and urea output in media (b and d). (a) Gene expression levels of albumin. (b) Albumin output in media per million cells. (c) Transferrin gene expression levels. (d) Urea output per 10^4 cells. Results are expressed as mean +/- SEM (n=3 independent experiments performed in triplicate). Statistical comparison was done using a paired t test and *** represents a statistically significant difference at a two-tailed P value of <0.001.*

Table 4.1: Raw CT values for a reference gene (YWHAZ) and selected genes of interest (Albumin and Transferrin) in the determination of hepatocyte differentiation.

total RNA was isolated from differentiated and undifferentiated HepG2 cells and converted to cDNA and used to evaluate the levels of Albumin and transferrin genes by RT-qPCR using YWHAZ as reference gene. N represents number of independent experiments

Gene	***YWHAZ***			***Albumin***			***Transferrin***		
	Mean C_T	**SEM**	**N**	**Mean C_T**	**SEM**	**N**	**Mean C_T**	**SEM**	**N**
Undifferentiated	25.6	0.1	3.0	26.8	0.6	3.0	27.7	0.2	3.0
Differentiated	25.2	0.1	3.0	24.2	0.1	3.0	24.4	0.3	3.0

Table 4.2: Raw CT values for a reference gene (YWHAZ) and selected genes of interest (Albumin and Transferrin) in the determination of changes to acute phase proteins by differentiated hepatocytes.

total RNA was isolated from differentiated and undifferentiated HepG2 cells and converted to cDNA and used to evaluate the levels of Albumin and transferrin genes by RT-qPCR using YWHAZ as reference gene. N represents number of independent experiments

Gene	***YWHAZ***			***Albumin***			***Transferrin***		
	Mean C_T	**SEM**	**N**	**Mean C_T**	**SEM**	**N**	**Mean C_T**	**SEM**	**N**
Control (5% BSA)	25.8	0.1	3	21.8	0.2	3	23.4	0.4	3
100μM Fenofibrate	25.4	0.1	3	17.8	0.2	3	21.9	0.4	3
10μM GW6471	25.5	0.1	3	21.7	0.3	3	22.5	0.4	3
50μM C15:0	25.5	0.2	3	17.6	0.2	3	19.1	0.5	3
150μM 15:0	25.8	0.1	3	19.3	0.2	3	20.4	0.3	3
300μM C15:0	25.8	0.1	3	19.7	0.2	3	20.3	0.4	3
50μM C16:0	25.3	0.2	3	19.0	0.1	3	20.9	0.1	3
150μM 16:0	25.2	1.2	3	19.0	0.2	3	20.3	0.2	3
300μM C16:0	25.7	0.3	3	24.8	0.1	3	24.8	0.1	3
150μM 15:0 + 150μM 16:0	25.1	0.1	3	18.8	0.2	3	20.5	0.2	3
200ng/ml LPS	25.4	0.4	3	26.4	0.2	3	26.4	0.3	3

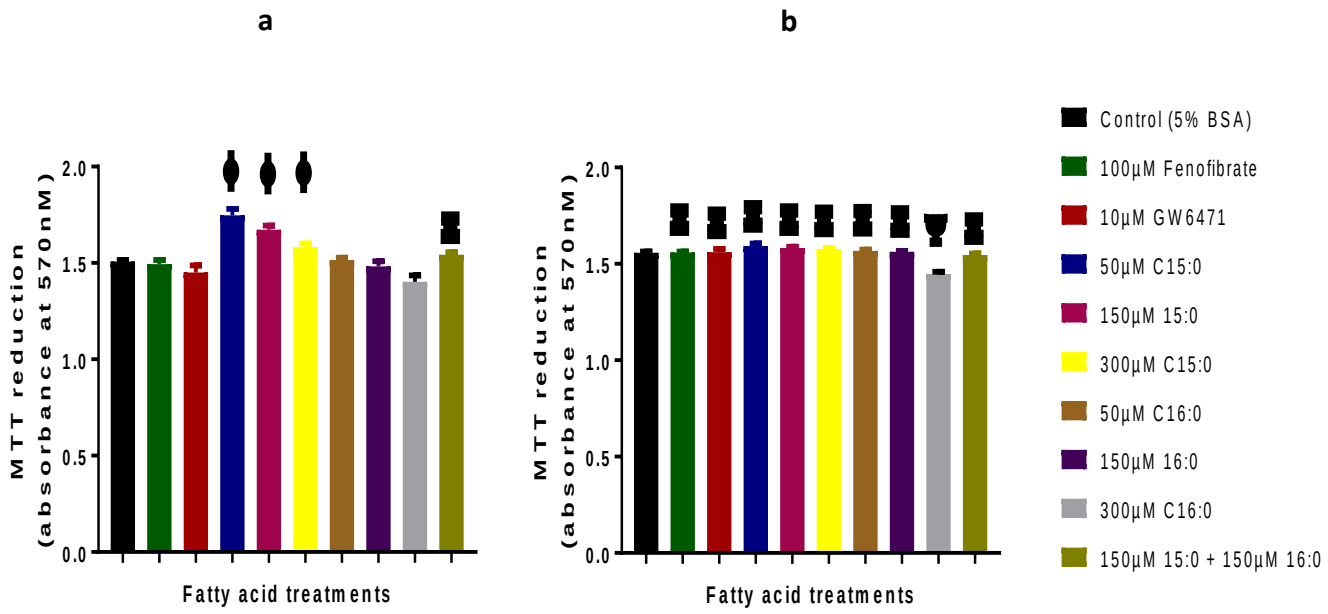

Figure 4.2: C15:0 is only associated with an increase metabolic activity of dHepG2 cells after 6hrs but not after 24hrs of incubation.
dHepG2 cells were treated with fatty acids conjugated to BSA and analysed for metabolic activity using MTT reduction after 6 and 24hrs of exposure. Cells were exposed to varying concentrations of fatty acids conjugated to BSA, or control (5% BSA), and/or a PPARα agonist/antagonist (100µM FB, or 10µM GW6471) as outlined. MTT reagent was added to the media 4 hours prior to the end of the experiment. Cells were then lysed with lysis reagent overnight before analysis under absorbance spectrometry at 570nm. (a) Effect of fatty acid treatments after 6hrs and (b) 24hrs. Results are expressed as mean +/- SEM (n=3 independent experiments performed in triplicate). Statistical significance was determined by a repeated measures one-way ANOVA with Geisser-Greenhouse correction and a Dunnett's post-test comparison. ***Ψ*** *represents a statistical significant difference between treatment versus control,* ***Ξ*** *represents a statistical significant difference between treatment versus 300µM C16:0, and* ***φ*** *represents a statistical significant difference between the treatment versus both control and 300µM C16:0. All symbols represent a statistical significance P value of < 0.05.*

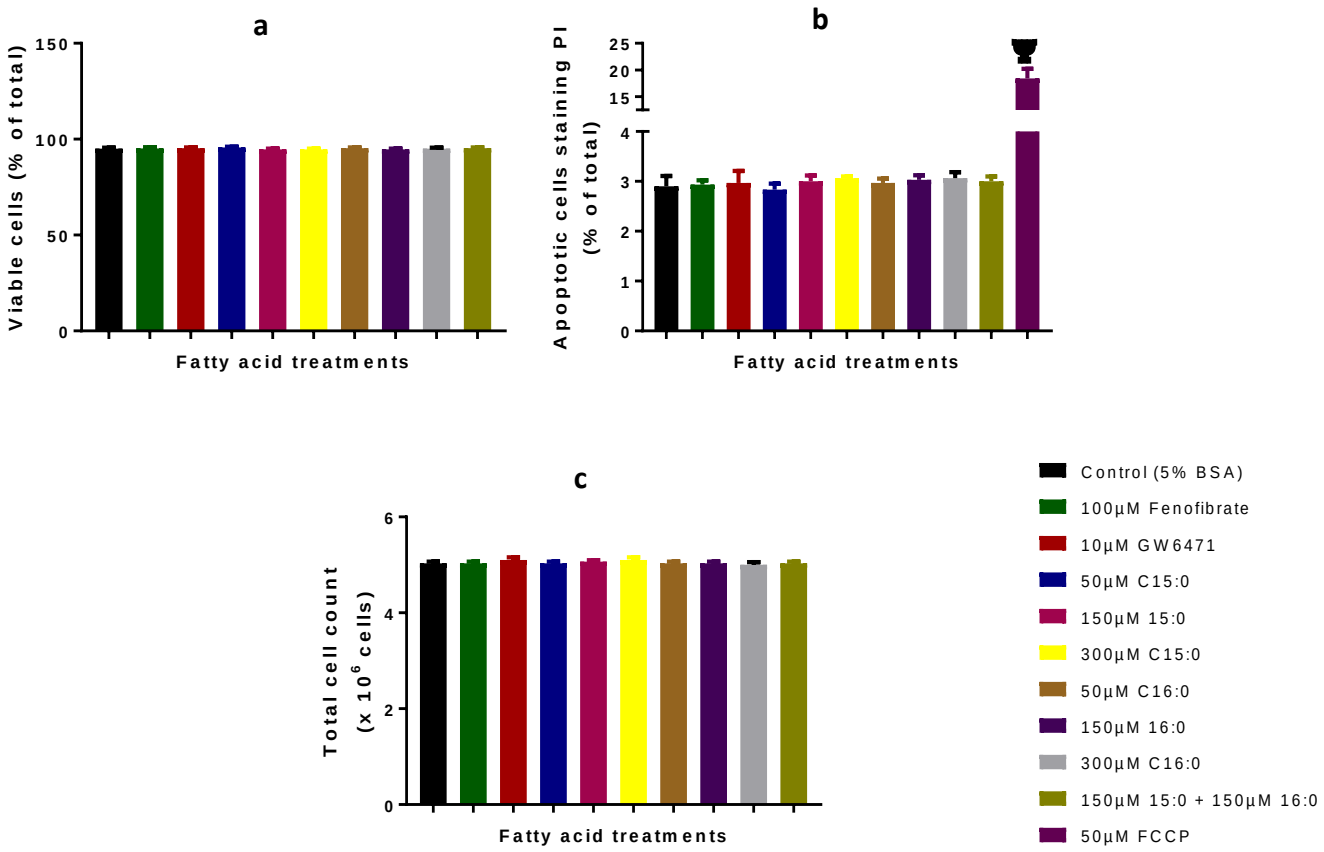

Figure 4.3: Fatty acid treatment at different concentrations do not affect cell viability or growth after 24hrs of exposure.

dHepG2 cells were treated with fatty acids conjugated to BSA and analysed for viability, apoptosis, and cell number after 24hrs incubation. Cells were exposed to varying concentrations of fatty acids conjugated to BSA, or control (5% BSA), and/or a PPARα agonist/antagonist (100µM FB, or 10µM GW6471) as outlined. At the end of the experiment, cells were washed thrice with PBS and trypsinised. (a) To assess viability, cells were mixed 1:1 with Trypan blue before counting on a haemocytometer as outlined in methods. Data is expressed as percentage viable cells. (b) To estimate early apoptotis, cells at a concentration of 500, 000cells/ml were incubated with a hypo-osmotic flourochrome solution containing 50µg/ml of propidium iodide (PI) at 4˚C overnight then washed thrice with PBS and analysed by flow cytometry with FL3. The percentage of apoptosis was quantified by measuring the number of hypoploid nuclei detected after 50,000 events on flow cytometry. Data is expressed as mean percentage of apoptotic cells. 50µM FCCP was used as a positive control. (c) Cells were counted after experiments with a haemocytometer to determine if FA treatments had any effect of cell growth. Results are expressed as mean +/- SEM (n=3 independent experiments performed in triplicate).

Statistical significance was determined by a repeated measures one-way ANOVA with Geisser-Greenhouse correction and a Dunnett's post-test comparison. ***Ψ*** *represents a statistical significant difference between treatments versus control (P value < 0.05).*

4.4.3 C15:0 attenuates the palmitate-induced increase in markers of inflammation

Accumulation of SFA in the liver is known to promote a pro-inflammatory environment with detrimental long-term consequences. The liver reacts to noxious stimuli by altering the levels of so-called acute phase proteins. These proteins are either produced in increased amounts (like pro-inflammatory cytokines), or become diminished (like albumin and, transferrin). So far, the results have shown that palmitate in high concentrations can limit cellular metabolic activity without necessarily affecting cell growth or apoptosis.To determine the immunological response of hepatocytes to FA, dHepG2 cells were incubated with varying concentrations of FAs conjugated to BSA for 24hrs, measuring levels of four acute phase reactants.

As expected, dHepG2 cells treated with 200ng/ml LPS showed a classical acute phase reaction characterised by a threefold increase in the production of pro-inflammatory cytokines TNF-α and IL-8 (p value <0.001) with a similar reduction in gene expression for albumin and transferrin (Figure 4.4 and Table 4.2). Similarly, dHepG2 cells cultured with high concentrations of C16:0 showed a twofold increase in TNF-α and IL-8 output (p value <0.001) as well as a sixfold and threefold reduction in gene expression of albumin and transferrin respectively (p value < 0.01). There was no difference in gene expression levels or cytokine production when dHepG2 cells were incubated with varying concentrations of C15:0, or with low concentrations of C16:0 (50μM and 150μM). Interestingly, co-incubating cells with both odd and even chain FAs showed no significant difference in the production of acute phase proteins compared to control.

4.4.4 C15:0 ameliorates palmitate-induced glucose dysfunction

The liver plays a pivotal role in glucose homeostasis by prioritising glucose production during fasting and glycogen production from excess glucose in the fed state. To determine how FAs affect the ability of hepatocytes to maintain optimal glucose levels, dHepG2 cells were cultured with varying concentrations of C16:0 and C15:0 at different glucose concentrations simulating fasting and fed states as described in method. A plate based assay was used to measure glucose output and glycogen content as described previously. Cells treated with high concentrations of C16:0 (300µM) showed a 54% increase in glucose output (Figure 4.5a) compared to control cells (% difference 54.5%; 95% CI 39.6% - 69.4%, $p < 0.001$). Conversely, there was no significant difference between cells treated with a similar concentration of C15:0 (300µM) compared to control. In fact, there was no significant increase in glucose output in cells treated with 50µM and 150µM C15:0. In comparison with C15:0 treated cells, those incubated with 300µM C16:0 had a statistically significant higher glucose output by 64.0%, 53.5%, and 44.0% for 50µM, 150µM and 300µM C15:0 respectively ($p < 0.001$). Furthermore, when cells are co-incubated with both C15:0 and C16:0 up to a concentration of 300µM, there was no significant difference in glucose output compared to controls.

dHepG2 cells treated with palmitate showed a reduction in glycogen content by 37.5% (Figure 4.5b and Figure 4.6) compared to controls (% difference 37.5%, 95% CI 13.8% - 61.2%, $p < 0.01$) in a fed state. On the other hand, there was a slight average increase in glycogen content in cells treated with different concentrations of C15:0 compared to controls; however, this was not statistically significant. C15:0 treated cells

at concentrations of 300μM showed a statistically significant increase in glycogen content by 41.5% compared to cells treated with similar concentrations of C16:0 (% difference 41.5%, 95% CI 1.9% - 81.1%, $p < 0.05$) and co-incubating cells with both C16:0 and C15:0 up to a concentration of 300μM had similar glycogen contents compared to control.

RNA expression levels of glucose transporter 2 (GLUT2) and glycogen synthase kinase 3β (GSK3β) were measured to test the upstream effect of FAs on glucose transport and glycogen production/regulation (Figure 4.5c and 4.5d). The overall gene expression of GLUT2 was deficient in dHepG2 cells irrespective of treatment, compared to the reference gene (Raw C_T values are shown in Table 4.3). However, dHepG2 cells had very high expression levels of GSK3β. Both C16:0 and C15:0 treated cells upregulated the expression of GLUT2 compared to controls irrespective of concentration (False discovery rate -FDR- of <1%). GLUT2 transports glucose across the cell membrane in a bi-directional manner; therefore, it is difficult to interpret the results of this gene expression data in isolation without referencing the results of the glucose output assay detailed above. Both C15:0 and C16:0 at low concentrations (50μM and 150μM) downregulated GSK3β expression by up to twofold (FDR <1%), whereas FA treatment at 300μM concentrations showed an upregulation of GSK3β (FDR < 0.01%). Cells treated with 300μM C16:0 showed a 98% increase in gene expression of GSK3β compared to controls (FDR <0.01%), while those treated with 300μM C15:0, although showing a 45% upregulation of GSK3β, did not meet statistical significance (FDR 1.6%). Cells treated with 300μM C16:0 had a 52% higher expression of GSK3β compared to cells treated with 300μM C15:0 (FDR < 0.001%).

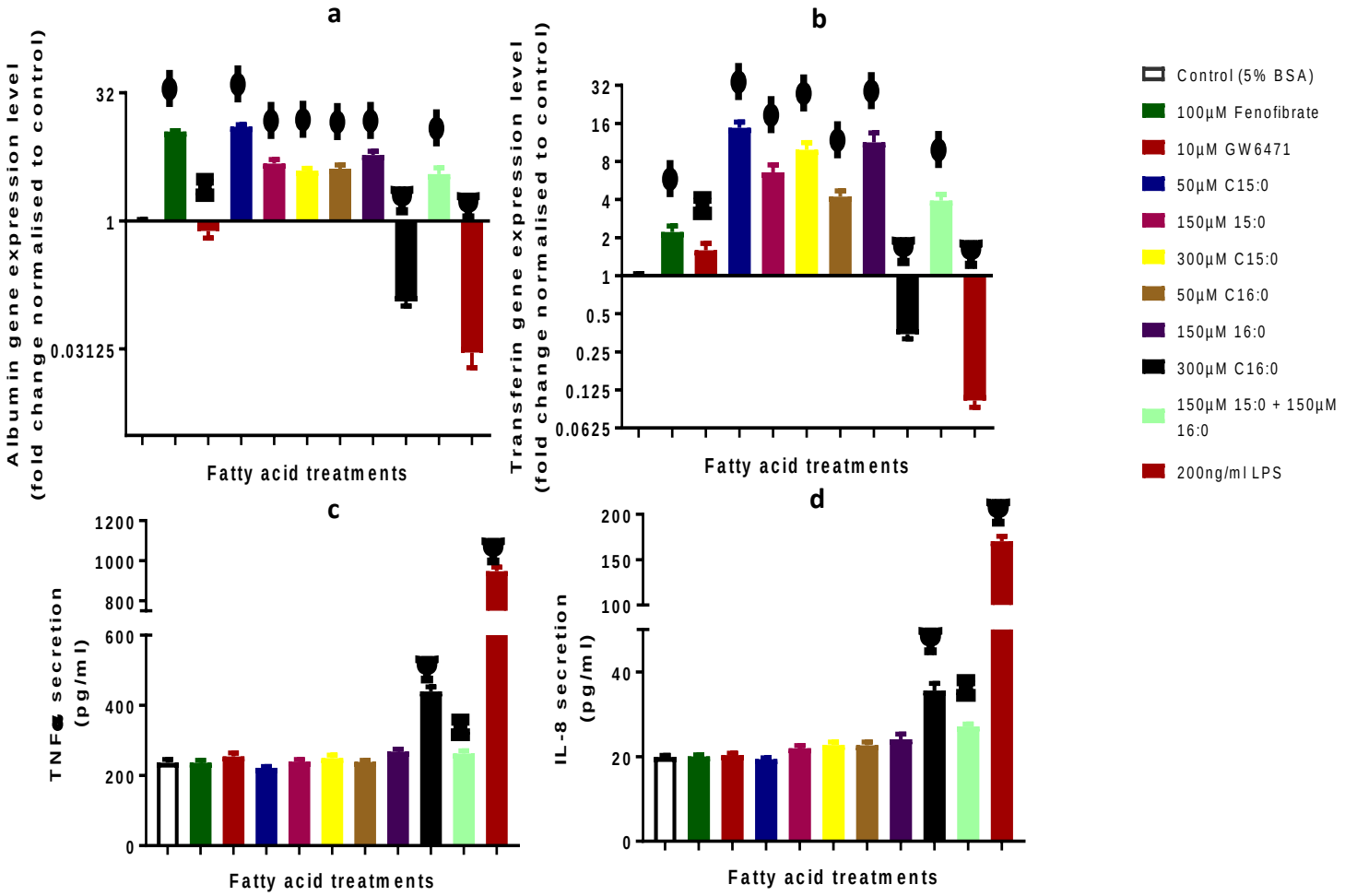

Figure 4.4 : C15:0 attenuates palmitate-induced increase in markers of acute inflammation.

dHepG2 cells were treated with fatty acids conjugated to BSA for 24hrs and analysed for markers of early inflammation. Gene expression levels of albumin and transferrin were used to determine negative acute phase proteins, while positive acute phase response was measured by expression of IL-8 and TNFα levels. Cells were exposed to varying concentrations of fatty acids conjugated to BSA, or control (5% BSA), and/or a PPARα agonist/antagonist (100µM FB, or 10µM GW6471) as outlined. At the end of the experiment, cells were either (a) washed thrice with ice-cold PBS then lysed for total RNA extraction (5 million cells) and RT-qPCR estimation, or (b) the supernatant is extracted for quantification of IL-8 and TNFα by ELISA as outlined. Results are expressed as mean +/- SEM (n=3 independent experiments performed in duplicate for a and b, or triplicate in c and d).

*Statistical significance was determined by a repeated measures one-way ANOVA with Geisser-Greenhouse correction and a Dunnett's post-test comparison test (figure c and d), or the Two-stage step-up method of Benjamini, Krieger and Yekutieli (figure a and b). **Ψ** represents a statistical significant difference between treatment and control, Ξ represents a statistical significant difference between treatment and 300µM C16:0, and **φ** represents a statistical significant difference between the treatment versus both control and 300µM C16:0. All symbols represent a statistical significance q value (adjusted false discovery rate -FDR) of <1% for the two-stage step-up method of Benjamini, Krieger and Yekutieli, or a statistical significance P value of < 0.05 for Dunnett's test.*

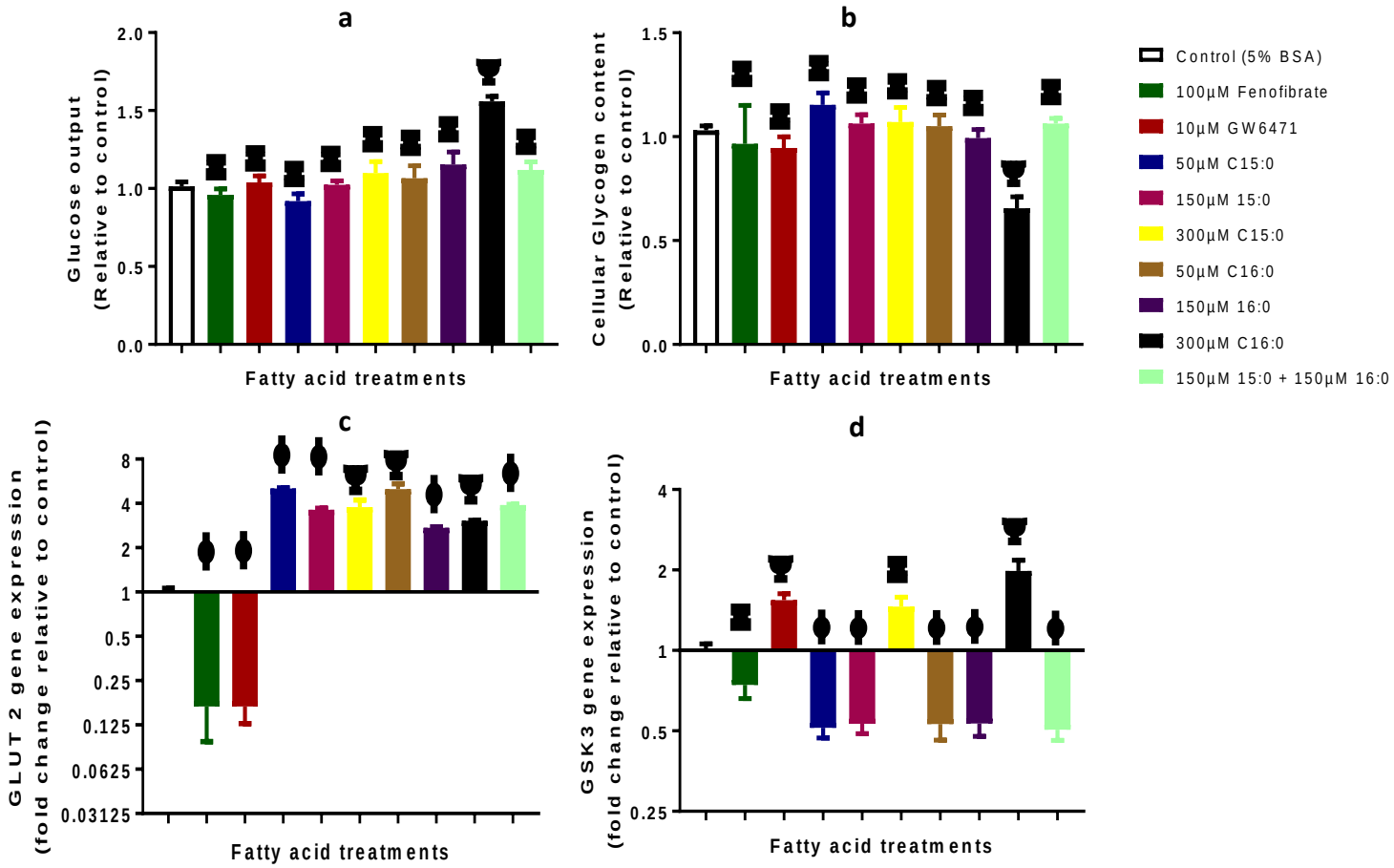

Figure 4.5: C15:0 ameliorates palmitate-induced glucose dysfunction

*dHepG2 cells were treated with fatty acids conjugated to BSA for 24hrs and analysed for markers of glucose homeostasis.(a) After 24 hours of FA exposure, cells were washed three times with PBS to remove any residual glucose in the media and then incubated for 16 hours in glucose production medium as outlined in methods. Insulin (100nmol/l; Sigma) was added during the last hour of incubation. A quantity of the medium was sampled for measurement of glucose concentration using a glucose hexose kinase assay kit (Sigma). Glucose concentration was normalized with cellular protein concentration. (n=3 independent experiments in duplicate, results expressed as mean +/- SEM). (b) After FA exposure for 24hrs, cells were glucose-starved overnight in serum and glucose free RPMI media to deplete intracellular glycogen stores and exposed to RPMI media containing 11mmol/l glucose for 48hrs with 100nmol/l insulin in the final hour of incubation. Cells were washed and harvested using ice-cold 30mmol/l HCL for the glycogen assay as outlined in method (n=3 independent experiments in duplicate, results expressed as mean +/- SEM). (c) and (d) Cells were washed thrice with ice-cold PBS then lysed for total RNA extraction (5 million cells) and RT-qPCR estimation of the gene expression levels of Glut2 and GSK3 respectively as upstream markers of glucose homeostasis (Results are expressed as mean +/- SEM for n=3 independent experiments performed in duplicate). Statistical significance was determined by a repeated measures one-way ANOVA with Geisser-Greenhouse correction and a Tukey's post-test comparison test (figure a and b), or the Two-stage step-up method of Benjamini, Krieger and Yekutieli (figure c and d). **Ψ** represents a statistical significant difference between treatment and control, **Ξ** represents a statistical significant difference between treatment and 300µM C16:0, and **φ** represents a statistical significant difference between the treatment versus both control and 300µM C16:0. All symbols represent a statistical significance q value (adjusted false discovery rate -FDR) of <1% for the two-stage step-up method of Benjamini, Krieger and Yekutieli, or a statistical significance P value of < 0.05 for Dunnett's test.*

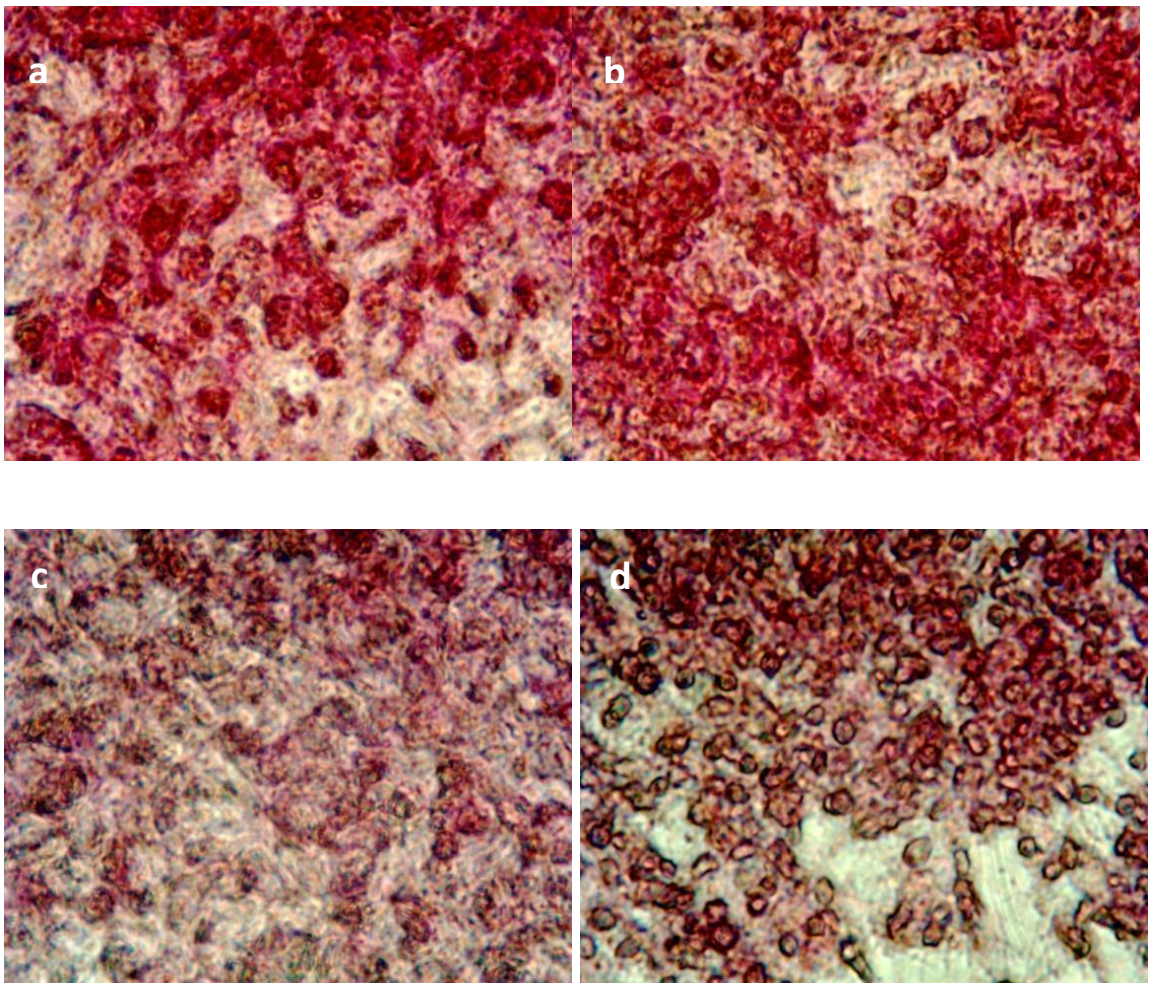

Figure 4.6: C15:0 increases intracellular glycogen content in C16:0 exposed cells.
PAS staining of differentiated HepG2 cells exposed to FAs showing intracellular glycogen accumulation (pink). Control and C15:0 (a and b respectively) exposed cells show increased glycogen content compared to C16:0 exposed cells (c). Cells exposed to both C16:0 and C15:0 (d) Show higher glycogen content compared to cells exposed to C16:0 alone.

Table 4.3: Raw CT values for a reference gene (YWHAZ) and selected genes of interest (GSK3 and GLUT2) for determining the effect of FA on glucose and glycogen homeostasis in dHepG2 cells.

total RNA was isolated from d HepG2 cells and converted to cDNA and used to evaluate the levels of GSK3 and GLUT2 genes by RT-qPCR using YWHAZ as reference gene. N represents number of independent experiments. Reference values for each gene presented independently because experiments were performed on a separate plate.

Gene	***YWHAZ (GSK3)***			***GSK3***			***YWHAZ (GLUT2)***			***GLUT2***		
	Mean C_T	**SEM**	**N**	**Mean C_T**	**SEM**	**N**	**Mean C_T**	**SEM**	**N**	**Mean C_T**	**SEM**	**N**
Control (5% BSA)	25.3	0.3	3	21.8	0.2	3	25.3	1.1	3	29.7	0.7	3
100μM Fenofibrate	25.7	0.2	3	17.8	0.2	3	25.4	0.3	3	32.6	1.2	3
10μM GW6471	25.9	0.0	3	21.7	0.3	3	25.6	0.3	3	32.6	1.0	3
50μM C15:0	25.5	0.3	3	17.6	0.2	3	25.7	0.1	3	27.7	0.1	3
150μM 15:0	25.6	0.2	3	19.3	0.2	3	25.5	0.4	3	28.0	0.4	3
300μM C15:0	25.2	0.2	3	19.7	0.2	3	25.6	0.2	3	28.0	0.1	3
50μM C16:0	25.6	0.5	3	19.0	0.1	3	25.5	0.1	3	27.5	0.2	3
150μM 16:0	25.4	0.1	3	19.0	0.2	3	25.3	0.1	3	28.2	0.0	3
300μM C16:0	25.6	0.0	3	24.8	0.1	3	25.3	0.1	3	28.0	0.1	3
150μM 15:0 + 150μM 16:0	25.5	0.3	3	18.8	0.2	3	25.2	0.1	3	27.6	0.1	3

Table 4.4: Raw CT values for a reference gene (YWHAZ) and selected genes of interest (L-FABP and CD36) for determining the effect of FA on lipid transport in dHepG2 cells.

total RNA was isolated from d HepG2 cells and converted to cDNA and used to evaluate the levels of L-FABP and CD36 genes by RT-qPCR using YWHAZ as reference gene. N represents number of independent experiments. Reference values for each gene presented independently because experiments were performed on a separate plate

Gene	***YWHAZ (L-FABP)***			***L-FABP***			***YWHAZ (CD36)***			***CD36***		
	Mean C_T	**SEM**	**N**	**Mean C_T**	**SEM**	**N**	**Mean C_T**	**SEM**	**N**	**Mean C_T**	**SEM**	**N**
Control (5% BSA)	25.8	0.1	3	25.8	0.1	3	25.7	0.2	3	29.0	0.3	3
100μM Fenofibrate	25.6	0.4	3	23.3	0.2	3	25.8	0.1	3	25.2	0.3	3
10μM GW6471	25.7	0.1	3	25.8	0.2	3	25.8	0.1	3	29.1	0.2	3
50μM C15:0	25.6	0.2	3	24.2	0.4	3	25.8	0.2	3	28.6	0.3	3
150μM 15:0	25.5	0.1	3	24.3	0.5	3	25.1	0.2	3	26.8	0.1	3
300μM C15:0	25.2	0.2	3	20.7	0.3	3	25.9	0.1	3	27.6	0.2	3
50μM C16:0	25.6	0.5	3	23.1	1.0	3	25.1	0.0	3	27.3	0.1	3
150μM 16:0	25.4	0.1	3	23.0	0.1	3	25.3	0.1	3	27.9	0.2	3
300μM C16:0	25.6	0.0	3	23.3	0.2	3	25.6	0.2	3	25.2	0.2	3
150μM 15:0 + 150μM 16:0	25.5	0.3	3	23.2	0.7	3	25.3	0.3	3	27.6	0.3	3

4.4.5 Palmitate is associated with higher intracellular lipid uptake and accumulation compared to C15:0

The accumulation of neutral lipids is a standard physiological response to excess energy. However, extreme and prolonged accumulation has been linked with metabolic diseases like T2DM. To determine the degree of lipid accumulation within cells, an Oil Red O stain was adapted to a plate-based assay. Furthermore, gene expression of CD36 and liver-specific FA binding protein (L-FABP) were measured as markers of cellular FA trafficking.

Both FA increased accumulation of neutral lipids compared to control irrespective of concentration (Figure 4.7). C15:0 treated cells saw an increase in oil red o stain absorbance by 7% (Pp < 0.05), 17% ($p < 0.01$), and 23% ($p < 0.001$) compared to control cells for 50µM, 150µM, and 300µM respectively. Similarly, there was an increase by 12%, 23% and 50% for cells treated with 50µM ($p < 0.01$), 150µM ($p < 0.001$), and 300µM ($p < 0.001$) C16:0 respectively compared to control. For lower concentrations of treatment (50µM and 150µM), C16:0 treated cells showed slightly higher accumulation of neutral lipids compared to C15:0 treated cells (4.8% and 5.6% higher in C16:0 compared to C15:0 for 50µM and 150µM respectively), but this was not statistically significant. However, there was a statistically significant increase in neutral lipids in cells treated with 300µM C16:0 compared to 300µM C15:0 (26.2%, 95% CI 18.5% - 34.0%, $p < 0.001$).

CD36 (FA translocase) modulates the rate of FA uptake by hepatocytes and contributes to the development of fatty liver. Both C16:0 and C15:0 upregulate CD36 expression (Figure 4.8a). C15:0 increases CD36 gene expression levels in a dose-

dependent manner compared to controls (62.1%, 183.2%, and 207.8% for 50µM, 150µM, and 300µM C15:0 respectively, FDR < 0.001%). Furthermore, incubating cells with 300µM C16:0 dramatically increased CD36 gene expression up to 8 times more compared to control (FDR < 0.001%) and up to 4 times more compared to 300µM C15:0 (FDR < 0.001%). L-FABP promotes intracellular trafficking of FAs into cellular organelles. Similar to CD36 gene expression profile, all FA concentrations used upregulated L-FABP gene expression (Figure 4.8b), especially cells treated with 300µM C15:0, which showed a sixteenfold increase compared to controls (FDR < 0.001%) and a fourfold increase relative to 300µM C16:0 treated cells (FDR < 0.001%). Both CD36 and L-FABP genes are relatively abundant in dHepG2 cells as shown in Table 4.4.

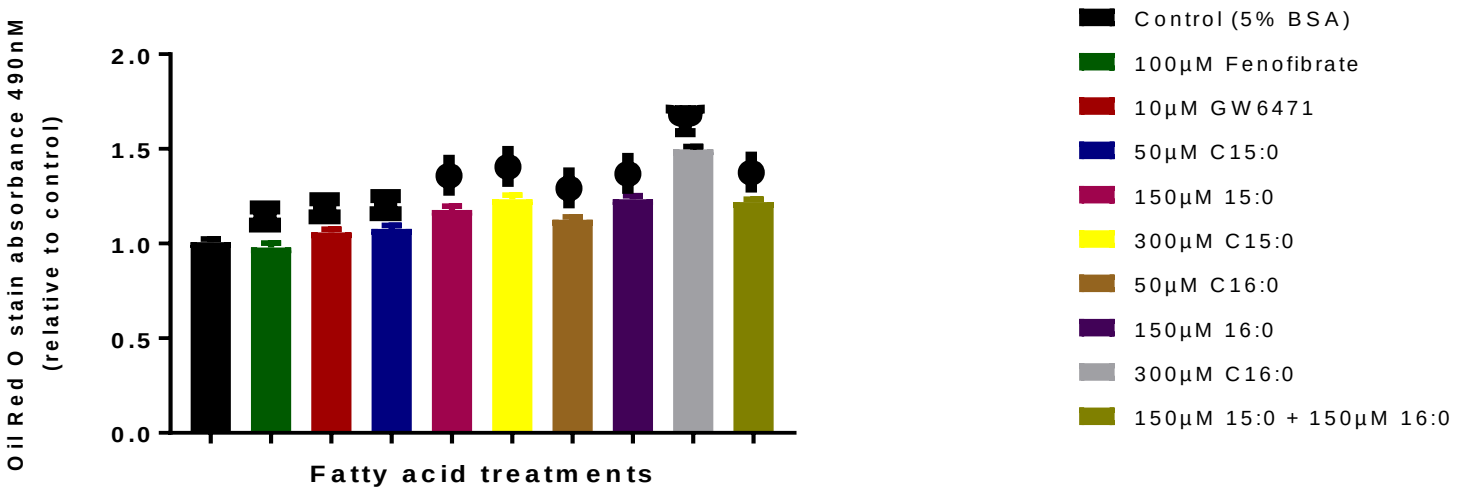

Figure 4.7: Formation of neutral lipids is greater in the presence of C16:0 compared to C15:0.

dHepG2 cells were treated with fatty acids conjugated to BSA for 24hrs and analysed for neutral lipid formation using the Oil Red O stain. Cells were washed three times with PBS after 24hrs incubation and then fixed with 1% paraformaldehyde at room temperature for 30 min prior to adding 60% isopropanol for 5 min. Oil red O stain was then added for 5 minutes prior to washing in isopropanol before analysis under absorbance spectrometry at 490nm. Results are expressed as mean +/- SEM (n=3 independent experiments performed in triplicate).

Statistical significance was determined by a repeated measures one-way ANOVA with Geisser-Greenhouse correction and a Dunnett's post-test comparison. ***Ψ*** *represents a statistical significant difference between treatment versus control, Ξ represents a statistical significant difference between treatment versus 300µM C16:0, and* ***φ*** *represents a statistical significant difference between the treatment versus both control and 300µM C16:0. All symbols represent a statistical significance P value of < 0.05.*

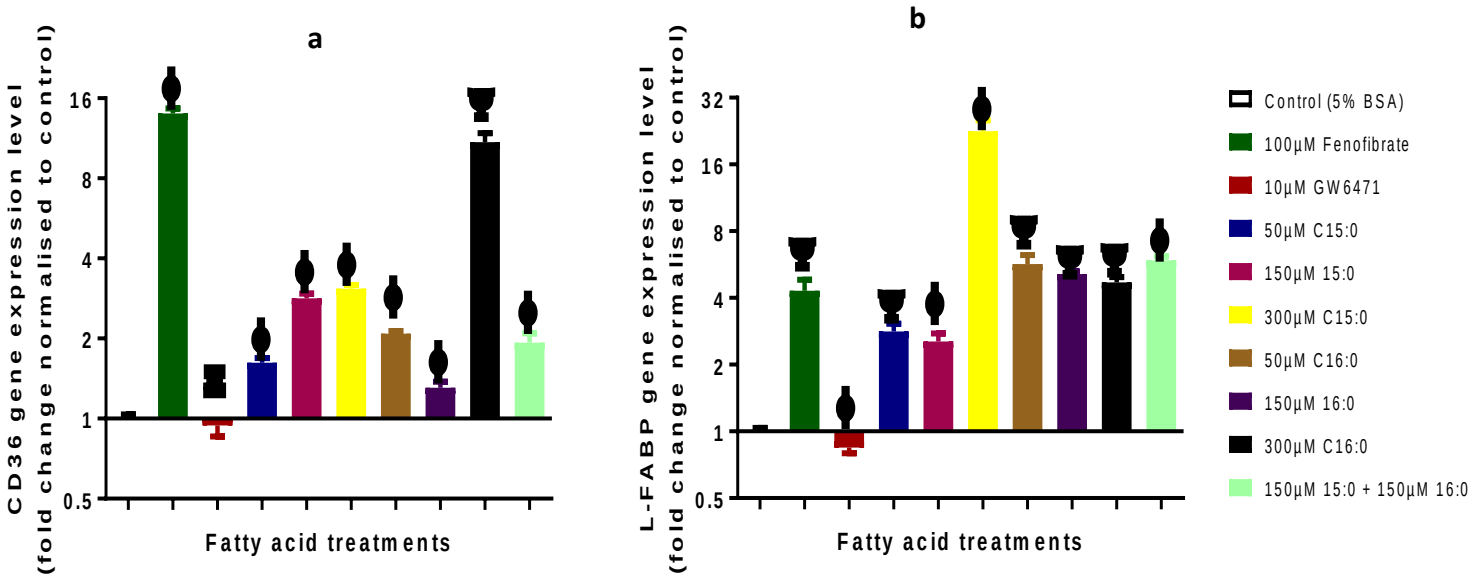

Figure 4.8: Both C15:0 and C15:0 promote intracellular uptake and trafficking of lipids.

dHepG2 cells were treated with fatty acids conjugated to BSA for 24hrs and analysed for markers of intracellular uptake and traffic of FA by looking at the total RNA expression of proteins responsible for intracellular uptake of FA (CD36) and cytoplasmic trafficking of FA into organelles (L-FABP). After 24hrs incubation, cells were washed thrice with ice-cold PBS and lysed for total RNA extraction (5 million cells) and RT-qPCR estimation of (a) CD36, or (b) L-FABP. Results are expressed as mean +/- SEM (n=3 independent experiments performed in duplicate).

Statistical significance was determined by a repeated measures one-way ANOVA with Geisser-Greenhouse correction and the two-stage step-up method of Benjamini, Krieger and Yekutieli (figure c and d). ***Ψ*** *represents a statistical significant difference between treatment and control,* ***Ξ*** *represents a statistical significant difference between treatment and 300µM C16:0, and* ***φ*** *represents a statistical significant difference between the treatment versus both control and 300µM C16:0. All symbols represent a statistical significance q value (adjusted false discovery rate -FDR) of <1%.*

4.4.6 C15:0 potentiates mitochondrial and peroxisomal beta-oxidation of FAs

Intracellular FA have different metabolic fates. In most cases, FFA are catabolised in the liver to release energy mostly driven by mitochondrial beta-oxidation. Alternatively, FFA could be diverted towards triglyceride/neutral lipid formation and storage. In order to determine if a dysfunction in the catabolic pathway contributes to the increased accumulation of neutral lipids as seen previously, the gene expression levels of proteins involved in mitochondrial and peroxisomal beta-oxidation pathways were measured.

All the FAs at varying concentrations increased gene expression of long-chain fatty acid co-ligase 1 (ACSL1) by as much as fourfold (Figure 4.9a) when treated with higher concentrations (300μM) of C15:0 and C16:0 (FDR <0.001%), or more than twofold when treated with lower concentrations (50μM or 150μM) of FA (FDR <0.001%). ACSL1 encodes the enzyme responsible for converting free long-chain FA to Acyl-CoA esters, a step required for intra-mitochondrial trafficking of FA. Carnitine palmitoyltransferase 1 and 2 (CPT1 and CPT2) provide a shuttle system for the transfer of acyl-CoA esters of FA into the mitochondrial matrix. Gene expression levels of both CPT1 (Figure 4.9b) and CPT2 (Figure 4.9c) were upregulated by lower concentrations (50μM or 150μM) of C15:0 and C16:0 FA compared to controls (FDR < 0.001%). Cells treated with 50μM or 150μM C15:0 upregulated both CPT1 and CPT2 by twofold higher than C16:0 cells treated with similar concentrations (FDR < 0.001%). There was no difference in gene expression levels of CPT1 and CPT2 between control cells and those treated with 300μM C16:0. Furthermore, cells treated with 300μM C15:0 showed a sevenfold and fourfold increase in CPT1 and CPT2 gene expression

level respectively compared with cells treated with 300µM C16:0 (FDR < 0.001% for both comparisons). CPT1 and CPT2 gene expression levels were restored with co-incubation of C15:0 and C16:0 (fourfold and twofold increases for CPT1 and CPT2 respectively, FDR < 0.001%). After establishing the effect of FAs on the gene expression levels of mitochondrial transport proteins responsible for trafficking FAs, the gene expression levels of enzymes involved in the final steps of mitochondrial beta-oxidation were examined: ACADL (long-chain acyl-CoA dehydrogenase), ACAD10 (acyl-CoA dehydrogenase family, member 10), and ACAA2 (Acetyl-Coenzyme A acyltransferase 2). C15:0 treatment is associated with an upregulation of ACADL (Figure 4.10a) compared to controls (threefold, eightfold, and sixfold increase with 50µM, 150µM, and 300µM respectively; FDR < 0.001% for all comparisons). Lower concentrations of C16:0 (50µM and 150µM) were also associated with increases in gene expression for ACADL (Figure 4.10a) and ACAD10 (Figure 4.10b). However, there was no significant difference in gene expression levels of ACADL, ACAD10 and ACAA2 (Figure 4.10c) between cells treated with 300µM C16:0 and controls. Even though C15:0 treatments upregulated gene expression levels of ACAD10 and ACAA2, there appears to be a negative correlation between FA concentration and level of gene expression (Figure 4.10b and 4.10c). Co-treating cells with C15:0 and C16:0 upregulated ACAD10 and ACADL gene expression levels.

Peroxisomal beta-oxidation acts as a secondary pathway for FA catabolism especially for very long chain and odd chain FAs and was assessed similarly to mitochondrial beta-oxidation above. Firstly, peroxisomal FA transporters were examined (Figure 4.11a, 4.11b, and 4.11c). ATP Binding Cassette Subfamily D Member 1-3 (ABCD1,

ABCD2, ABCD3) gene expression levels were measured to assess the effect of FAs on peroxisomal very long chain FA transporters. Only C15:0, irrespective of concentration used, upregulated ABCD1 activity compared to controls Figure 4.11a). The addition of 300μM C16:0 downregulated ABCD2 and ABCD3 transporters compared to controls (eightfold and 45% reduction respectively, FDR < 0.001%). Whereas, all C15:0 treatments as well as lower concentrations of C16:0 treatments significantly upregulated gene expression of ABCD2 and ABCD3 in comparison to control. The first reaction in peroxisomal beta-oxidation is catalysed by Peroxisomal acyl-coenzyme oxidase 1, encoded by the gene ACOX1. All FA treatments upregulated ACOX1 gene expression (Figure 4.11d) compared to control apart from 300μM C16:0. There was no correlation between the concentration of C15:0 with gene expression levels. During peroxisomal oxidation, catalase (encoded by the gene CAT) is usually produced to mop up hydrogen peroxide. All FA treatments resulted in an upregulation of CAT (Figure 4.11e), except 300μM C16:0.

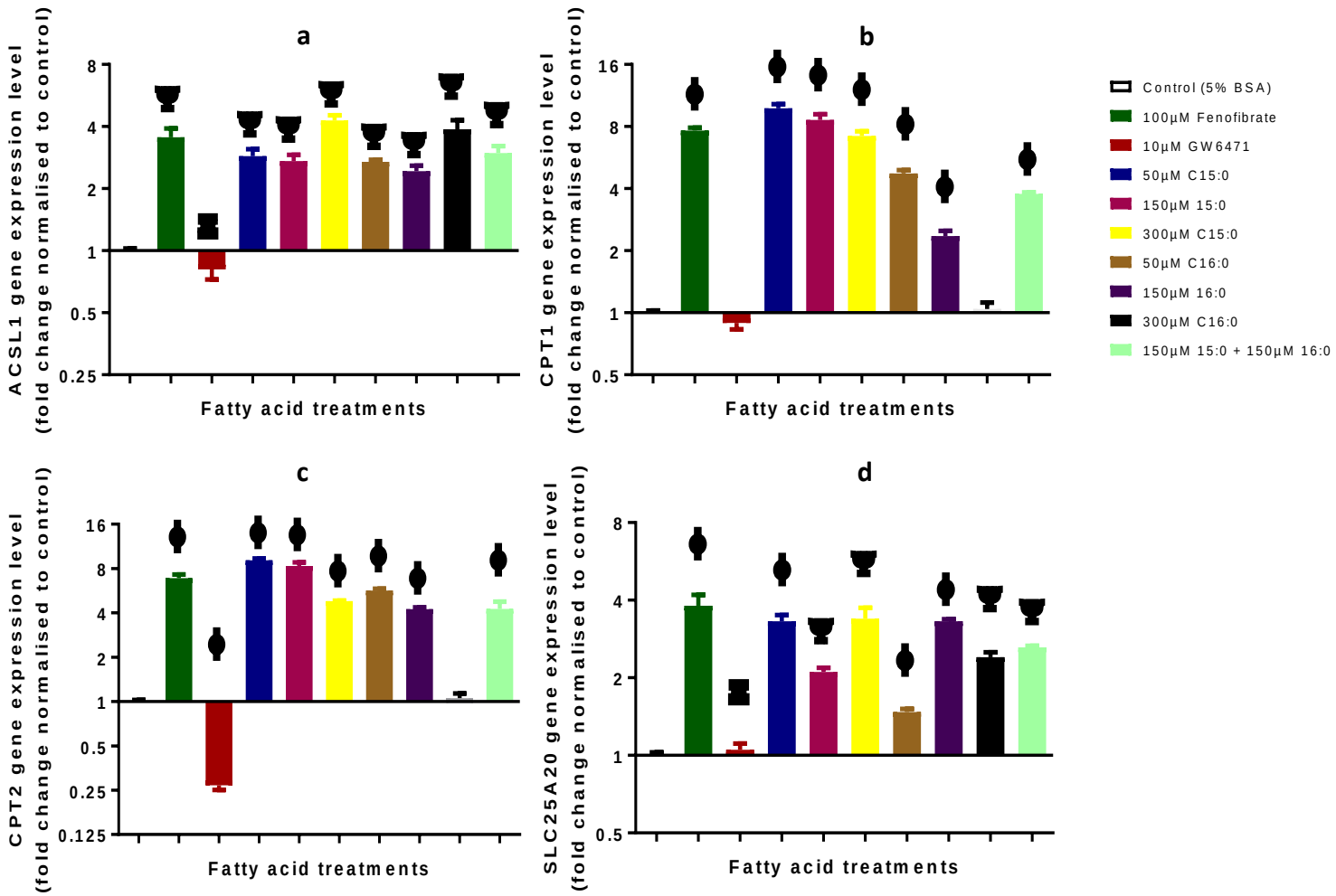

Figure 4.9: C15:0 reverses palmitate induced reduction in mitochondrial uptake of fatty acids.

dHepG2 cells were treated with fatty acids conjugated to BSA for 24hrs and analysed for gene expression markers of FA activation and transport within the mitochondria. After 24hrs incubation, cells were washed thrice with ice-cold PBS and lysed for total RNA extraction (5 million cells) and RT-qPCR estimation of (a) ACSL1- responsible for activating FA for beta-oxidation by converting FA to fatty acyl-COA esters, or (b) CPT1 and (c) CPT2 both responsible for intra-mitochondrial transport of fatty acyl-COA esters, and (d) SLC25A20- responsible for facilitating intra-mitochondrial fatty acyl transport by trafficking both carnitine-FA complexes and carnitine across the inner mitochondrial membrane. Results are expressed as mean +/- SEM (n=3 independent experiments performed in duplicate).

*Statistical significance was determined by a repeated measures one-way ANOVA with Geisser-Greenhouse correction and the two-stage step-up method of Benjamini, Krieger and Yekutieli . **Ψ** represents a statistical significant difference between treatment and control, **Ξ** represents a statistical significant difference between treatment and 300µM C16:0, and **φ** represents a statistical significant difference between the treatment versus both control and 300µM C16:0. All symbols represent a statistical significance q value (adjusted false discovery rate -FDR) of <1%.*

Table 4.5: Raw CT values for a reference gene (YWHAZ) and selected genes of interest for determining the effect of FA on lipid metabolism in dHepG2 cells.
total RNA was isolated from d HepG2 cells and converted to cDNA and used to evaluate the levels of CPT1, CPT2, SCD5, SCD1 and FASN genes by RT-qPCR using YWHAZ as reference gene. N represents number of independent experiments.

Gene	***YWHAZ***			***CPT1***			***CPT2***			***SCD5***			***SCD1***			***FASN***		
	Mean C_T	**SEM**	**N**	**Mean C_T**	**SEM**	**N**	**Mean C_T**	**SEM**	**N**	**Mean C_T**	**SEM**	**N**	**Mean C_T**	**SEM**	**N**	**Mean C_T**	**SEM**	**N**
Control (5% BSA)	25.1	0.1	3	30.3	0.2	3	31.1	0.3	3	29.8	0.0	3	25.9	0.1	3	25.5	0.1	3
100μM Fenofibrate	25.4	0.1	3	27.6	0.3	3	28.6	0.4	3	27.6	0.3	3	25.8	0.3	3	25.4	0.3	3
10μM GW6471	25.5	0.0	3	30.8	0.3	3	33.6	0.1	3	30.0	0.4	3	26.3	0.2	3	26.0	0.3	3
50μM C15:0	25.6	0.4	3	27.5	0.3	3	28.4	0.3	3	28.2	0.2	3	25.7	0.5	3	25.9	0.2	3
150μM 15:0	25.7	0.2	3	27.8	0.1	3	28.7	0.5	3	27.2	0.3	3	26.1	0.3	3	25.3	0.3	3
300μM C15:0	25.6	0.1	3	27.8	0.3	3	29.3	0.1	3	28.6	0.2	3	26.1	0.4	3	25.2	0.2	3
50μM C16:0	25.4	0.2	3	28.4	0.2	3	28.9	0.1	3	28.5	0.4	3	26.2	0.1	3	24.8	0.5	3
150μM 16:0	25.1	0.1	3	29.1	0.2	3	29.0	0.1	3	27.9	0.2	3	25.9	0.3	3	23.9	0.2	3
300μM C16:0	25.6	0.1	3	30.8	0.2	3	31.5	0.4	3	31.7	0.2	3	26.3	0.3	3	24.4	0.2	3
150μM 15:0 + 150μM 16:0	25.5	0.2	3	28.8	0.4	3	29.4	0.7	3	28.2	0.5	3	26.3	0.5	3	25.9	0.6	3

Table 4.6: Raw CT values for a reference gene (YWHAZ) and selected genes of interest for determining the effect of FA on lipid metabolism in dHepG2 cells.
total RNA was isolated from d HepG2 cells and converted to cDNA and used to evaluate the levels of ACSL1, ACADL, ACAD10, MYLCD genes by RT-qPCR using YWHAZ as reference gene. N represents number of independent experiments.

Gene	***YWHAZ***			***ACSL1***			***ACADL***			***ACAD10***			***MYLCD***		
	Mean C_T	**SEM**	**N**	**Mean C_T**	**SEM**	**N**	**Mean C_T**	**SEM**	**N**	**Mean C_T**	**SEM**	**N**	**Mean C_T**	**SEM**	**N**
Control (5% BSA)	25.4	0.2	3	30.1	0.2	3	29.2	0.6	3	27.1	0.2	3	31.2	0.4	3
100μM Fenofibrate	25.8	0.1	3	28.8	0.5	3	28.6	0.3	3	26.1	0.7	3	31.3	0.3	3
10μM GW6471	25.5	0.4	3	30.7	0.5	3	29.2	0.5	3	27.2	0.5	3	31.2	0.5	3
50μM C15:0	25.6	0.2	3	28.8	0.3	3	27.7	0.2	3	25.6	0.2	3	31.2	0.6	3
150μM 15:0	25.4	0.2	3	28.6	0.5	3	25.9	0.6	3	25.9	0.0	3	30.3	0.4	3
300μM C15:0	25.2	0.2	3	27.8	0.3	3	26.5	0.6	3	25.9	0.4	3	30.3	0.3	3
50μM C16:0	25.4	0.1	3	28.7	0.1	3	27.1	0.3	3	26.8	0.1	3	27.0	0.2	3
150μM 16:0	25.5	0.4	3	29.0	0.4	3	27.5	0.0	3	26.3	0.8	3	31.1	0.7	3
300μM C16:0	25.8	0.1	3	28.5	0.7	3	29.6	0.8	3	27.4	0.1	3	32.0	0.2	3
150μM 15:0 + 150μM 16:0	25.7	0.2	3	28.9	0.2	3	26.4	0.5	3	26.8	0.1	3	31.5	0.3	3

Table 4.7: Raw CT values for a reference gene (YWHAZ) and selected genes of interest for determining the effect of FA on lipid metabolism in dHepG2 cells.
total RNA was isolated from d HepG2 cells and converted to cDNA and used to evaluate the levels of ACAA2, SLC25A20, CAT genes by RT-qPCR using YWHAZ as reference gene. N represents number of independent experiments. YWHAZ represents the reference gene C_T values for ACAA2 and SLC25A20.

Gene	***$YWHAZ_1$***			***ACAA2***			***SLC25A20***			***YWHAZ (CAT)***			***CAT***		
	Mean C_T	**SEM**	**N**	**Mean C_T**	**SEM**	**N**	**Mean C_T**	**SEM**	**N**	**Mean C_T**	**SEM**	**N**	**Mean C_T**	**SEM**	**N**
Control (5% BSA)	25.3	1.1	3	26.0	0.0	3	25.7	0.1	3	25.6	0.2	3	33.2	0.1	3
100μM Fenofibrate	25.4	0.3	3	25.2	0.3	3	23.9	0.6	3	25.4	0.3	3	29.6	0.3	3
10μM GW6471	25.6	0.3	3	26.4	0.7	3	25.8	0.5	3	25.3	0.1	3	27.9	0.2	3
50μM C15:0	25.7	0.1	3	25.7	0.2	3	24.4	0.1	3	25.8	0.2	3	30.0	0.1	3
150μM 15:0	25.5	0.4	3	25.7	0.4	3	24.9	0.5	3	25.6	0.1	3	30.7	0.2	3
300μM C15:0	25.6	0.2	3	25.9	0.3	3	24.3	0.3	3	25.6	0.0	3	30.7	0.1	3
50μM C16:0	25.5	0.1	3	26.0	0.2	3	25.2	0.2	3	25.6	0.1	3	30.9	0.2	3
150μM 16:0	25.3	0.1	3	26.2	0.1	3	23.9	0.0	3	25.4	0.5	3	30.8	0.6	3
300μM C16:0	25.3	0.1	3	26.2	0.0	3	24.3	0.0	3	25.5	0.2	3	33.2	0.1	3
150μM 15:0 + 150μM 16:0	25.2	0.1	3	26.1	0.0	3	24.2	0.0	3	25.5	0.3	3	30.3	0.6	3

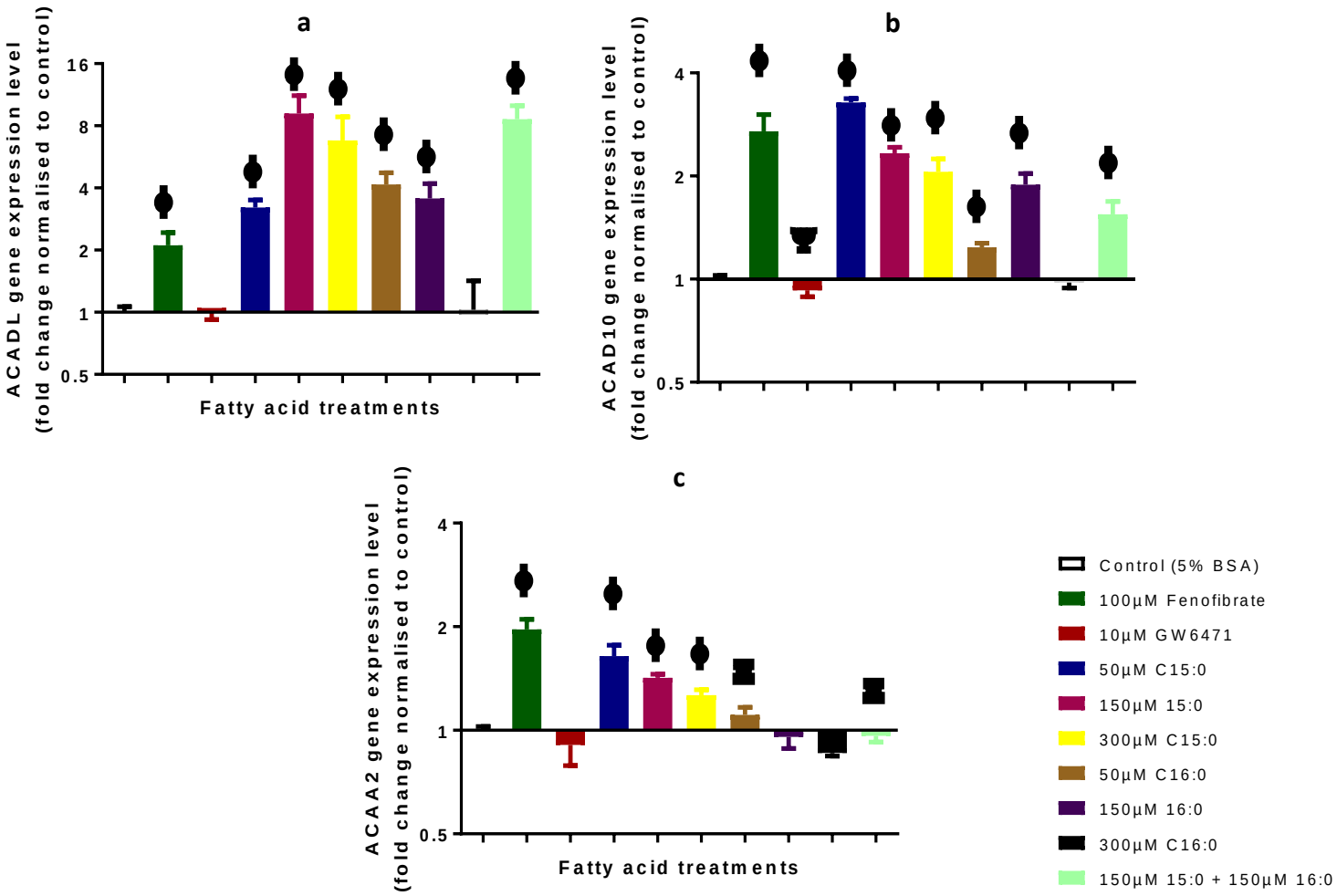

Figure 4.10: C15:0 reverses palmitate induced reduction in fatty acid beta-oxidation.

dHepG2 cells were treated with fatty acids conjugated to BSA for 24hrs and analysed for gene expressionof enzymes in the mitochondria beta-oxidation pathway. After 24hrs incubation, cells were washed thrice with ice-cold PBS and lysed for total RNA extraction (5 million cells) and RT-qPCR estimation of (a) ACSL1- responsible for activating FA for beta-oxidation by converting FA to fatty acyl-COA esters, or (b) CPT1 and (c) CPT2 both responsible for intra-mitochondrial transport of fatty acyl-COA esters, and (d) SLC25A20- responsible for facilitating intra-mitochondrial fatty acyl transport by trafficking both carnitine-FA complexes and carnitine across the inner mitochondrial membrane. Results are expressed as mean +/- SEM (n=3 independent experiments performed in duplicate).

*Statistical significance was determined by a repeated measures one-way ANOVA with Geisser-Greenhouse correction and the two-stage step-up method of Benjamini, Krieger and Yekutieli . **Ψ** represents a statistical significant difference between treatment and control, **Ξ** represents a statistical significant difference between treatment and 300µM C16:0, and **φ** represents a statistical significant difference between the treatment versus both control and 300µM C16:0. All symbols represent a statistical significance q value (adjusted false discovery rate -FDR) of <1%.*

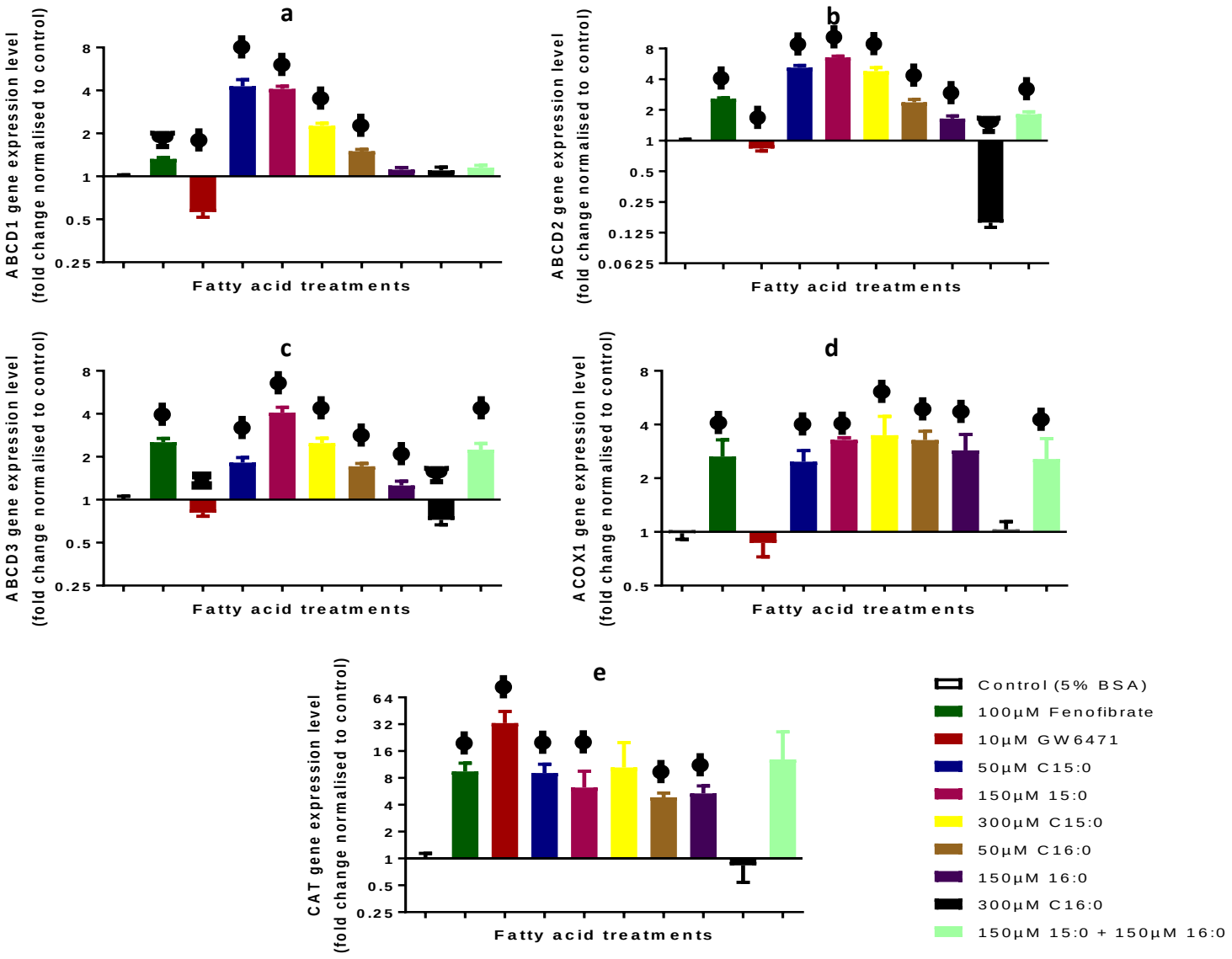

Figure 4.11: C15:0 potentiates peroxisomal oxidation of fatty acids

dHepG2 cells were treated with fatty acids conjugated to BSA for 24hrs and analysed for gene expression markers for peroxisomal FA oxidation. After 24hrs incubation, cells were washed thrice with ice-cold PBS and lysed for total RNA extraction (5 million cells) and RT-qPCR estimation of (a) ABCD1, (b) ABCD2, (c) ABCD3 - responsible for FA transport across the peroxisomal membrane, or (d) ACOX1,the first enzyme in the peroxisomal beta oxidation pathway, and (d) CAT, an enzyme responsible for mopping up hydrogen peroxide formed in the process of peroxisomal beta oxidation. Results are expressed as mean +/- SEM (n=3 independent experiments performed in duplicate).

*Statistical significance was determined by a repeated measures one-way ANOVA with Geisser-Greenhouse correction and the two-stage step-up method of Benjamini, Krieger and Yekutieli . **Ψ** represents a statistical significant difference between treatment and control, **Ξ** represents a statistical significant difference between treatment and 300µM C16:0, and **φ** represents a statistical significant difference between the treatment versus both control and 300µM C16:0. All symbols represent a statistical significance q value (adjusted false discovery rate -FDR) of <1%.*

4.4.7 C15:0 favours MUFA and ω-3 production

De novo lipogenesis and the biosynthesis of PUFA are integral functional aspects of hepatocytes. Gene expression levels of key enzymes involved in de novo lipogenesis, FA desaturation and PUFA biosynthesis were measured to understand the mechanistic role of FAs in de novo pathways.

De novo biosynthesis of FAs from acetyl-CoA is catalysed primarily by the enzyme fatty acid synthase (encoded by the gene FASN). Cells treated with C16:0 appear to upregulate FASN gene expression level compared to control in greater magnitude than cells treated with similar concentrations of C15:0 (Figure 4.12a). For example, cells treated with 300μM C16:0 increase FASN expression levels by up to two times more than cells treated with 300μM C15:0 (FDR < 0.001%). In fact, there was no statistically significant difference in FASN gene expression between cells treated with 50μM C15:0 and controls (5.5% difference, FDR 31.2%). Conversely, cells treated with C15:0 upregulated MLYCD (malonyl CoA decarboxylase) gene expression levels more than C16:0 treated cells with similar concentrations (Figure 4.12b). Low concentrations of C16:0 (50μM and 150μM) did not affect MLYCD gene expression, while 300μM C16:0 downregulated MLYCD gene expression (FDR < 0.001%). The levels of stearoyl-CoA desaturase 1 and 5 (SCD1 and SCD5) gene expression levels were measured as a marker of MUFA production. Only 50μM and 150μM C15:0 upregulated SCD1 gene expression levels (Figure 4.12c) compared to controls (by 170% and 120% respectively, FDR < 0.01% for both comparisons). With SCD5 (Figure 4.12d), 300μM C16:0 downregulated gene expression levels compared to control, while all other FA treatment upregulated SCD5 gene expression levels. To confirm the

effect of C15:0 on MUFA production, cells were washed and extracted for FA analysis using gas chromatography. There was a statistically significant increase in MUFA content in C15:0 treated cells compared to both controls and cells treated with 300µM C16:0 (Table 4.12). There was a mean increase in MUFA concentration of 3.35µM, 4.24µM, and 2.05µM compared to control for 50µM, 150µM, 300µM C15:0 treated cells ($p < 0.05$). Similarly, There was a statistically significant higher MUFA production (difference of 3.24µM) in 300µM C15:0 cells compared to cells treated with a similar concentration of C16:0.

Gene expression levels of fatty acid desaturase 1 and 2 (FADS1 and FADS2), as well as those of ELOVL2 and ELOVL5 (elongation of very long-chain fatty acid protein 2 and 5), were measured to assess the effect of free FA treatments on PUFA production (Figure 4.13a and 4.13b). Only C15:0 treatment significantly affected FADS1 and FADS2 gene expression by upregulation, and the maximum effect was seen in cells having 150µM C15:0. Adding C15:0 to C16:0 treated cells also resulted in upregulation of both FADS1 and FADS2. Cells treated with 300µM of C16:0 downregulated ELOVL5 gene expression by 14% (FDR < 0.01%), but had no significant impact on ELOVL2 gene expression levels (Figure 4.13c and 4.13d respectively). C15:0 showed differential expression of ELOVL5 and ELOVL2. While it upregulated ELOVL5 (Figure 4.13c), it was found to downregulate ELOVL2 (Figure 4.13d). Similarly, cells co-incubated with C15:0 and C16:0 slightly upregulated ELOVL5 and downregulated ELOVL2 gene expression levels. To confirm the effect of the FA on the production PUFA, FA were extracted and analysed from cells as outlined in methods. While there was no statistical significance difference in the level of total PUFA within treatments,

C15:0 treated cells showed a statistically significant higher production of total ω-3 FAs compared to both controls (increased by 1.4μM, 1.34μM, and 2.32μM for 50μM, 150μM, and 300μM C15:0 respectively, $p < 0.05$) and cells treated with 300μM C16:0. Furthermore, total levels of C22:6n3 were higher in C15:0 treated cells compared to controls and C16:0 treated cells. On the other hand, C15:0 treated cells were shown to produce significantly lower levels of total ω-6 FA compared to cells treated with 300μM C16:0 (mean reduction by 1.21μM, 1.21μM. and 0.89μM for 50μM, 150μM, and 300μM C15:0 respectively, $p < 0.05$).

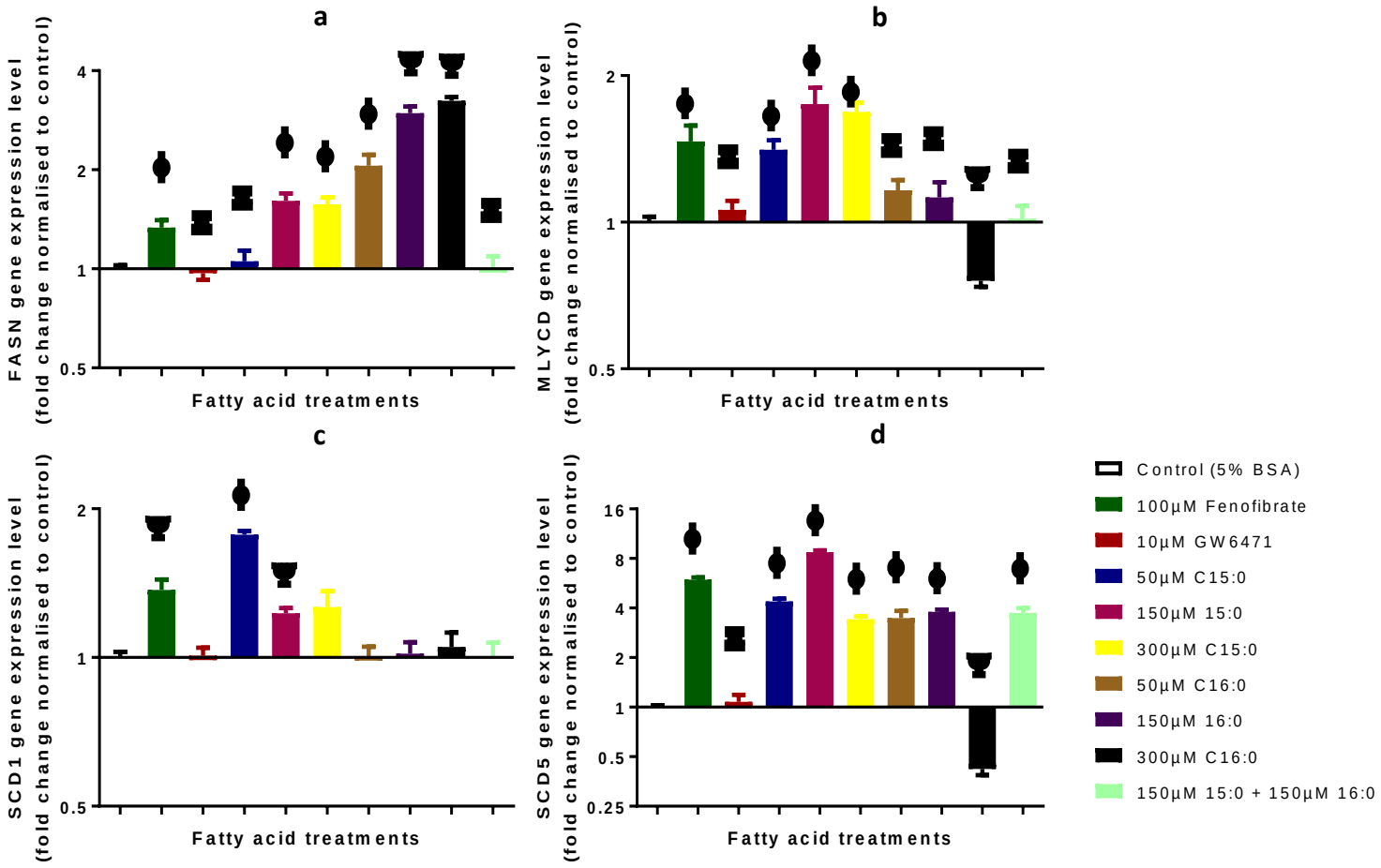

Figure 4.12: C15:0 favours desaturation of fatty acids to MUFA in the de novo lipogenesis pathway

dHepG2 cells were treated with fatty acids conjugated to BSA for 24hrs and analysed for gene expression markers for enzymes in the de novo lipogenesis pathway. After 24hrs incubation, cells were washed thrice with ice-cold PBS and lysed for total RNA extraction (5 million cells) and RT-qPCR estimation of (a) FASN, a multi-enzyme protein responsible for FA synthesis, (b) MLYCD, an enzyme involved in the synthesis of Acetyl-CoA, (c) SCD1 and (d) SCD5 are isoforms of the enzyme catalysing the rate-limiting step of MUFA production. Results are expressed as mean +/- SEM (n=3 independent experiments performed in duplicate).

Statistical significance was determined by a repeated measures one-way ANOVA with Geisser-Greenhouse correction and the two-stage step-up method of Benjamini, Krieger and Yekutieli . Ψ represents a statistical significant difference between treatment and control, Ξ represents a statistical significant difference between treatment and 300µM C16:0, and φ represents a statistical significant difference between the treatment versus both control and 300µM C16:0. All symbols represent a statistical significance q value (adjusted false discovery rate -FDR) of <1%.

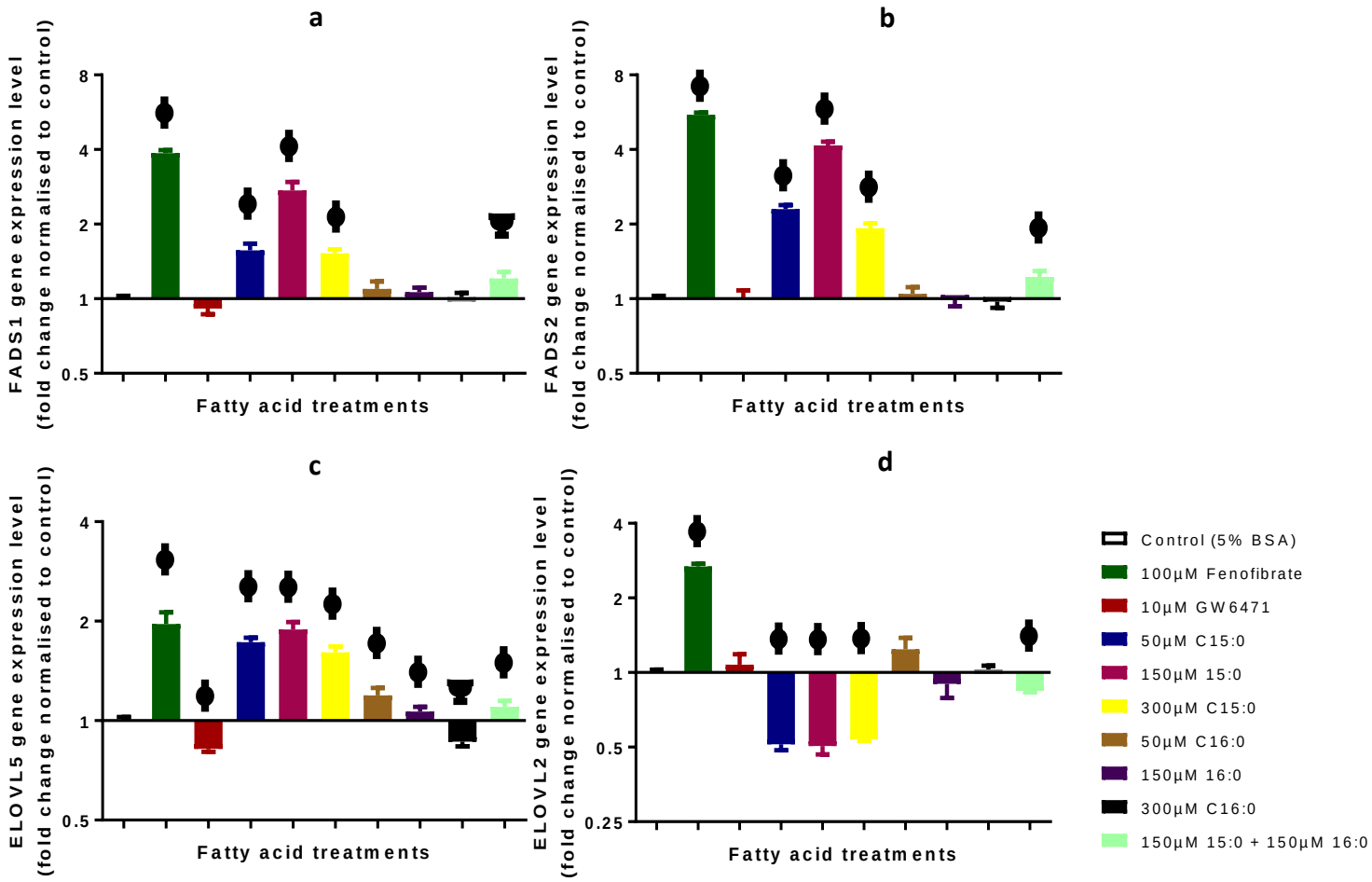

Figure 4.13: C15:0 favours further desaturation of dietary essential fatty acids to PUFA

dHepG2 cells were treated with fatty acids conjugated to BSA for 24hrs and analysed for gene expression markers for enzymes in the de novo lipogenesis pathway. After 24hrs incubation, cells were washed thrice with ice-cold PBS and lysed for total RNA extraction (5 million cells) and RT-qPCR estimation of (a) FADS1, (b) FADS2, (c) ELOVL2 and (d) ELOVL5, enzymes responsible for desaturation and elongation of ω-3 and ω-6 fatty acids. Results are expressed as mean +/- SEM (n=3 independent experiments performed in duplicate).

Statistical significance was determined by a repeated measures one-way ANOVA with Geisser-Greenhouse correction and the two-stage step-up method of Benjamini, Krieger and Yekutieli. Ψ represents a statistical significant difference between treatment and control and φ represents a statistical significant difference between the treatment versus both control and 300µM C16:0. All symbols represent a statistical significance q value (adjusted false discovery rate -FDR) of <1%.

Table 4.8: Raw CT values for a reference gene (YWHAZ) and selected genes of interest for determining the effect of FA on peroxisomal oxidation of lipids in dHepG2 cells.

total RNA was isolated from d HepG2 cells and converted to cDNA and used to evaluate the levels of ACAA2, SLC25A20, CAT genes by RT-qPCR using YWHAZ as reference gene. N represents number of independent experiments. $YWHAZ_1$ represents the reference gene C_T values for ABCD1, ABCD2 and ABCD3.

Gene	***YWHAZ***			***ACOX1***			***$YWHAZ_1$***			***ABCD1***			***ABCD2***			***ABCD3***		
	Mean C_T	**SEM**	**N**	**Mean C_T**	**SEM**	**N**	**Mean C_T**	**SEM**	**N**	**Mean C_T**	**SEM**	**N**	**Mean C_T**	**SEM**	**N**	**Mean C_T**	**SEM**	**N**
Control (5% BSA)	25.3	0.3	3	29.7	0.3	3	25.6	0.2	3	29.2	0.4	3	29.4	0.3	3	28.2	0.2	3
100µM Fenofibrate	25.7	0.2	3	28.4	0.3	3	25.4	0.3	3	28.5	0.4	3	27.7	0.4	3	26.7	0.6	3
10µM GW6471	25.9	0.0	3	26.0	0.3	3	25.3	0.1	3	29.8	0.3	3	29.3	0.3	3	28.2	0.4	3
50µM C15:0	25.5	0.3	3	27.5	0.1	3	25.8	0.2	3	27.2	0.6	3	27.1	0.4	3	27.5	0.5	3
150µM 15:0	25.6	0.2	3	27.4	0.4	3	25.6	0.1	3	27.1	0.2	3	26.6	0.1	3	26.3	0.4	3
300µM C15:0	25.2	0.2	3	28.4	0.4	3	25.6	0.0	3	28.0	0.2	3	27.2	0.5	3	26.9	0.5	3
50µM C16:0	25.6	0.5	3	27.1	0.2	3	25.6	0.1	3	28.6	0.2	3	28.3	0.3	3	27.4	0.2	3
150µM 16:0	25.4	0.1	3	26.3	0.4	3	25.4	0.5	3	28.8	0.5	3	28.4	0.6	3	28.6	0.5	3
300µM C16:0	25.6	0.0	3	28.1	0.2	3	25.5	0.2	3	28.9	0.2	3	32.0	0.3	3	27.7	0.5	3
150µM 15:0 + 150µM 16:0	25.5	0.3	3	26.2	0.5	3	25.5	0.3	3	29.0	0.3	3	28.4	0.2	3	26.8	0.3	3

Table 4.9: Raw CT values for a reference gene (YWHAZ) and selected genes of interest for determining the effect of FA on PUFA synthesis in dHepG2 cells.

total RNA was isolated from d HepG2 cells and converted to cDNA and used to evaluate the levels of ELOVL2, ELOVL5, FADS1, and FADS2 genes by RT-qPCR using YWHAZ as reference gene. N represents number of independent experiments. $YWHAZ_1$ represents the reference gene C_T values for FADS1 and FADS2, while $YWHAZ_0$ represents reference values for the ELOVL genes.

Gene	***$YWHAZ_0$***			***ELOVL2***			***ELOVL5***			***$YHWAZ_1$***			***FADS1***			***FADS2***		
	Mean C_T	**SEM**	**N**	**Mean C_T**	**SEM**	**N**	**Mean C_T**	**SEM**	**N**	**Mean C_T**	**SEM**	**N**	**Mean C_T**	**SEM**	**N**	**Mean C_T**	**SEM**	**N**
Control (5% BSA)	25.8	0.0	3	27.8	0.0	3	26.4	0.4	3	25.2	0.2	3	24.6	0.0	3	27.3	0.0	3
100µM Fenofibrate	25.5	0.1	3	26.2	0.3	3	25.4	0.5	3	25.7	0.2	3	23.1	0.3	3	25.3	0.1	3
10µM GW6471	25.9	0.0	3	27.7	0.5	3	26.7	0.1	3	25.2	0.1	3	24.7	0.3	3	27.3	0.4	3
50µM C15:0	25.6	0.1	3	28.7	0.1	3	25.4	0.0	3	25.5	0.1	3	24.2	0.3	3	26.4	0.3	3
150µM 15:0	25.4	0.4	3	28.3	0.5	3	25.1	0.6	3	25.8	0.1	3	23.6	0.1	3	25.7	0.1	3
300µM C15:0	25.8	0.0	3	28.7	0.1	3	25.7	0.2	3	25.6	0.0	3	24.4	0.2	3	26.6	0.2	3
50µM C16:0	25.1	0.1	3	26.8	0.5	3	25.5	0.3	3	25.3	0.1	3	24.6	0.2	3	27.4	0.5	3
150µM 16:0	25.6	0.1	3	27.7	0.6	3	26.1	0.2	3	25.3	0.1	3	24.7	0.2	3	27.4	0.3	3
300µM C16:0	25.1	0.1	3	27.1	0.2	3	26.0	0.1	3	25.7	0.1	3	25.0	0.2	3	27.9	0.1	3
150µM 15:0 + 150µM 16:0	25.3	0.1	3	27.5	0.0	3	25.7	0.2	3	25.7	0.1	3	24.9	0.0	3	27.4	0.3	3

Table 4.10: Raw CT values for a reference gene (YWHAZ) and selected genes of interest for determining the effect of FA on PPARa activity in dHepG2 cells.
total RNA was isolated from d HepG2 cells and converted to cDNA and used to evaluate the levels of PPARa and RxRa genes by RT-qPCR using YWHAZ as reference gene. N represents number of independent experiments

Gene	***YWHAZ***			***PPARa***			***RxRa***		
	Mean C_T	**SEM**	**N**	**Mean C_T**	**SEM**	**N**	**Mean C_T**	**SEM**	**N**
Control (5% BSA)	25.7	0.2	3	27.5	0.3	3	28.5	0.2	3
100μM Fenofibrate	25.8	0.1	3	24.6	0.0	3	28.6	0.2	3
10μM GW6471	25.8	0.1	3	28.0	0.4	3	28.8	0.3	3
50μM C15:0	25.8	0.2	3	26.6	0.3	3	28.2	0.4	3
150μM 15:0	25.1	0.2	3	26.0	0.2	3	27.3	0.6	3
300μM C15:0	25.9	0.1	3	27.2	0.1	3	28.5	0.2	3
50μM C16:0	25.1	0.0	3	26.7	0.1	3	26.6	0.2	3
150μM 16:0	25.6	0.2	3	27.9	0.1	3	28.3	0.5	3
300μM C16:0	25.3	0.1	3	26.9	0.1	3	28.7	0.0	3
150μM 15:0 + 150μM 16:0	25.3	0.3	3	27.1	0.2	3	27.2	0.5	3

Table 4.11: Raw CT values for a reference gene (YWHAZ) and selected genes of interest for determining the effect of FA on PPARa activity in dHepG2 cells.
total RNA was isolated from d HepG2 cells and converted to cDNA and used to evaluate the levels of KPNA2, KPNB1 and NCOA2 genes by RT-qPCR using YWHAZ as reference gene. N represents number of independent experiments

Gene	***YWHAZ***			***KPNA2***			***KPNB1***			***NCOA2***		
	Mean C_T	**SEM**	**N**	**Mean C_T**	**SEM**	**N**	**Mean C_T**	**SEM**	**N**	**Mean C_T**	**SEM**	**N**
Control (5% BSA)	25.3	0.3	3	24.5	0.1	3	29.8	0.1	3	30.4	0.7	3
100μM Fenofibrate	25.5	0.2	3	23.9	0.1	3	27.7	0.3	3	29.9	0.1	3
10μM GW6471	25.5	0.1	3	25.1	0.2	3	29.9	0.2	3	31.4	0.3	3
50μM C15:0	25.4	0.3	3	24.2	0.7	3	26.1	0.7	3	28.7	0.1	3
150μM 15:0	25.3	0.4	3	24.0	0.5	3	26.0	0.4	3	29.0	0.5	3
300μM C15:0	25.4	0.1	3	24.1	0.1	3	27.0	0.3	3	29.7	0.3	3
50μM C16:0	25.4	0.3	3	24.3	0.5	3	25.0	0.5	3	30.4	0.2	3
150μM 16:0	25.5	0.3	3	24.6	0.8	3	27.7	0.1	3	30.0	0.5	3
300μM C16:0	25.4	0.3	3	25.0	0.3	3	29.9	0.3	3	30.4	0.5	3
150μM 15:0 + 150μM 16:0	25.1	0.2	3	24.2	0.5	3	26.0	0.7	3	29.6	0.1	3

4.4.8 The metabolic activity of C15:0 is related to PPAR alpha

PPARs, especially PPAR alpha, have been shown to be heavily involved in lipid homeostasis in the liver and other organs. To determine if the general effect of C15:0 is mediated via PPAR alpha, cells were treated with corresponding concentrations of FAs in comparison to a PPAR alpha agonist (100µM Fenofibrate/FB) and antagonist (10µM GW6471). Firstly, PPAR alpha gene expression levels were measured (Figure 4.14a). The agonist increased PPAR alpha gene expression levels by up to eightfold compared to control (FDR < 0.0001%), while the antagonist reduced gene expression by 9.5%, albeit not meeting statistical significance levels (FDR 15.8%). Cells treated with C15:0 upregulated PPAR alpha gene expression levels by up to 100% compared to controls, with the highest stimulation from 50µM C15:0. There was no significant change in gene expression of PPAR alpha between lower concentrations of C16:0 and controls. However, treating cells with 300µM C16:0 downregulated PPAR alpha expression by 32.3% (FDR 0.03%) compared to controls, which was even higher than the antagonist. The retinoid x receptor alpha (RxRa) and nuclear receptor coactivator 2 (NCOA2) gene expression levels were measured to investigate if FA stimulation was exclusive to PPAR alpha,or extends to co-activators. PPAR alpha agonist and antagonist did not have any effect on RxRa gene expression levels (Figure 4.14b). Cells treated with 300µM C16:0 showed downregulation of RxRa by almost twofold (FDR < 0.01%), whereas cells treated with lower concentrations of C16:0 (50µM) showed a twofold upregulation of RxRa (FDR < 0.01%). On the other hand, both high and low concentrations of C15:0 elicited a statistically significant upregulation of RxRa of up to 80% compared to control. The function of PPAR alpha is dependent upon

translocation into the nucleus. Therefore, the gene expression levels of two nuclear shuttling proteins, karyopherin subunit alpha 2 (KPNA2) and karyopherin subunit beta 1 (KPNB1), were measured. As expected, the PPAR alpha agonist increased both KPNA2 (Figure 4.14c) and KPNB1 (Figure 4.14d) gene expression levels by 80% and fourfold respectively (FDR < 0.001%). Similarly, C15:0 treated cells significantly increased both KPNA2 and KPNB1 gene expression levels irrespective of concentrations used, even as high as twofold more than the PPAR alpha agonist with KPNB1. Low concentrations of C16:0 (50μM) was associated with an upregulation of both KPNA2 and KPNB1 expression levels. However, C16:0 at 300μM resulted in a downregulation of both KPNA2 and KPNB1 similar to the PPAR alpha antagonist. NCOA2 is recruited by nuclear receptors to promote downstream upregulation of their target genes. Here, the three concentrations of C15:0 used to treat the cells upregulated NCOA2 gene expression by more than twofold (FDR < 0.01% for all comparisons), similar to 100μM fenofibrate which showed a 40% increase (FDR< 0.001%) in NCOA2 gene expression levels compared to control (Figure 4.14e). Incubating cells with 300μM C16:0 did not affect NCOA2 gene expression levels compared to control. Co-incubating cells with C15:0 and C16:0 increased NCOA2 gene expression levels by 18% (FDR 0.01%). A PPAR alpha transcription assay was performed (Figure 4.15) which confirmed a downstream response to PPAR alpha similar to the gene expression data. Both FB and C15:0 increased PPAR alpha activity by approximately 20% ($p < 0.05$), while GW6471 and C16:0 reduced activity by 23% and 43% respectively ($p < 0.01$ for both observations). Addition of FB or C15:0 to

C16:0 treated cells partially ameliorated the downregulatory effect of palmitate by 6% ($p > 0.05$) and 15% ($p < 0.05$) respectively.

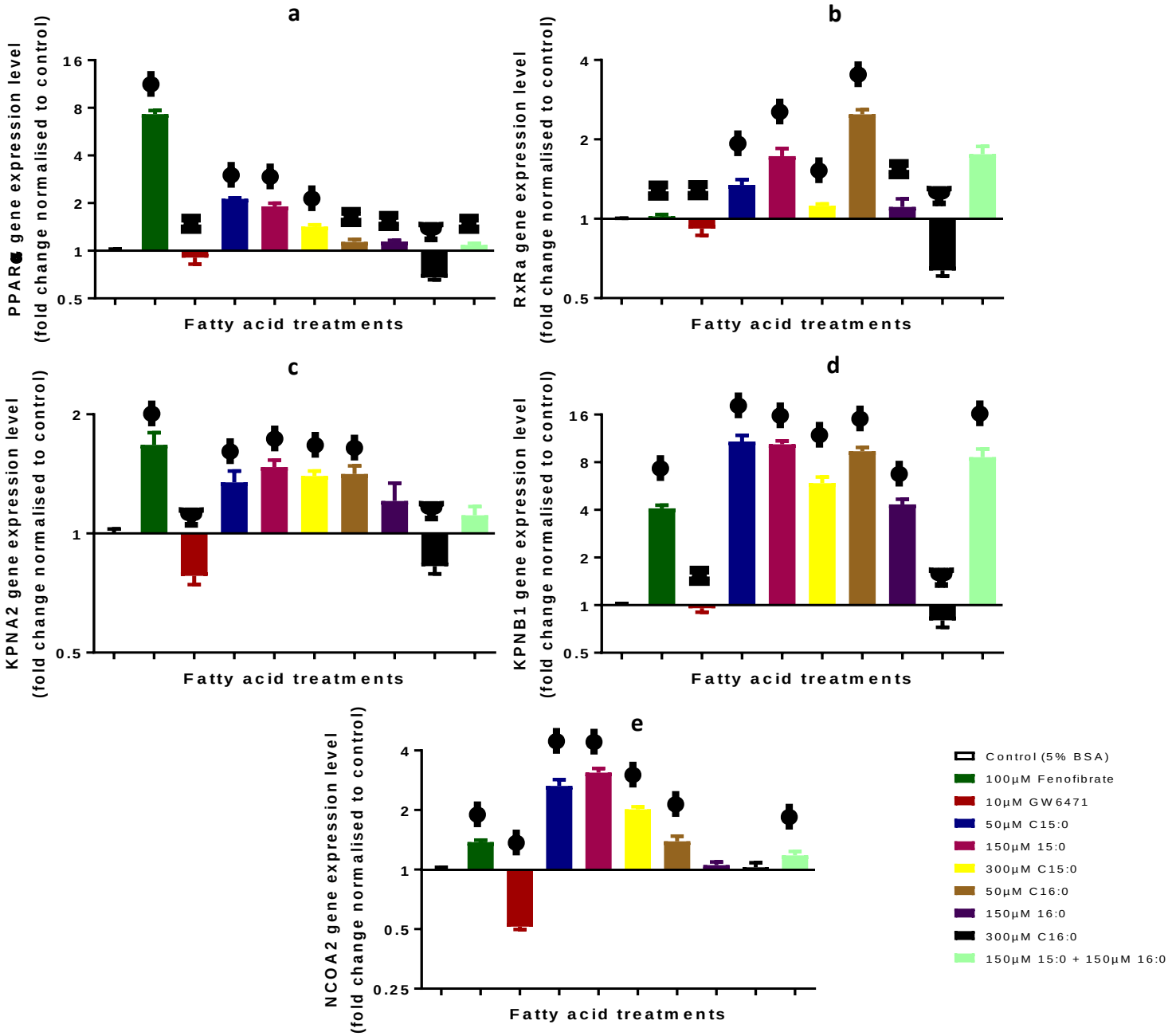

Figure 4.14: C15:0 ameliorates the downregualtory effect of C16:0 on PPARα nuclear transport and expression

dHepG2 cells were treated with fatty acids conjugated to BSA for 24hrs and analysed for gene expression markers for PPARα expressionand regulation. After 24hrs incubation, cells were washed thrice with ice-cold PBS and lysed for total RNA extraction (5 million cells) and RT-qPCR estimation of (a) PPARα, a ligand activated transcription factor responsible for the catabolism of lipids, (b) RxRa, a nuclear receptor that facilitates PPARα transcriptional activity, (c) KPNA2 and (d) KPNB1 are nucleorcytoplasmic proteins responsible for nuclear import of PPARα, (e) NCOA2 a PPARαtranscriptional protein coregulatory. Results are expressed as mean +/- SEM (n=3 independent experiments performed in duplicate).

*Statistical significance was determined by a repeated measures one-way ANOVA with Geisser-Greenhouse correction and the two-stage step-up method of Benjamini, Krieger and Yekutieli . **Ψ** represents a statistical significant difference between treatment and control, **Ξ** represents a statistical significant difference between treatment and 300µM C16:0, and **φ** represents a statistical significant difference between the treatment versus both control and 300µM C16:0. All symbols represent a statistical significance q value (adjusted false discovery rate -FDR) of <1%.*

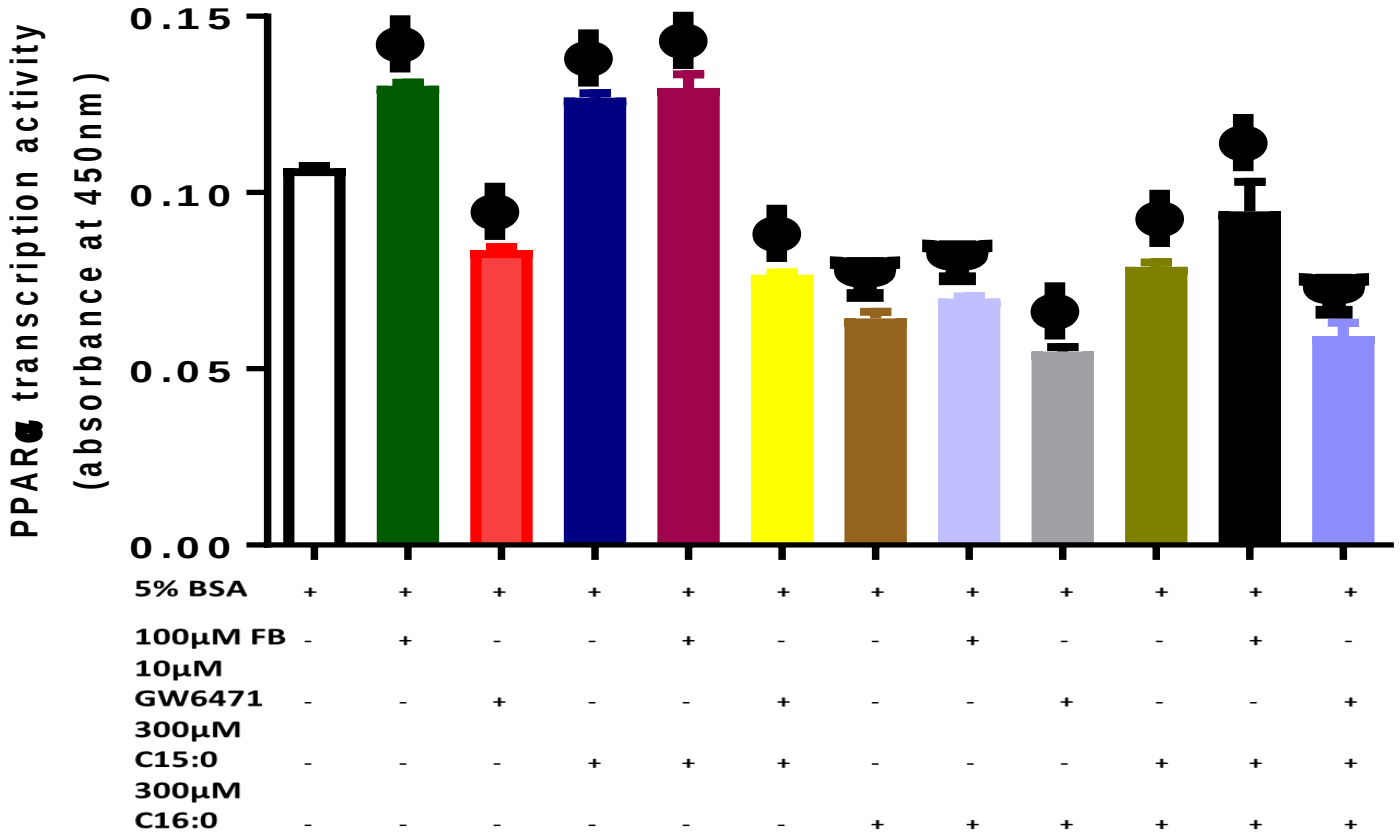

Figure 4.15: C15:0 improves palmitate inhibition of PPARα activity but does not completely ameliorate this effect.

dHepG2 cells were treated with fatty acids conjugated to BSA for 24hrs and analysed for PPARα transcription activity. Cells were washed three times with PBS after 24hrs incubation followed by nuclear extraction as detailed in methods. PPARα transcription activity was measured by a plate-based assay as described with analysis under absorbance spectrometry at 450nm. Results are expressed as mean +/- SEM (n=3 independent experiments performed in triplicate).

Statistical significance was determined by a repeated measures one-way ANOVA with Geisser-Greenhouse correction and a Dunnett's post-test comparison. ***Ψ*** *represents a statistical significant difference between treatment versus control, Ξ represents a statistical significant difference between treatment versus 300µM C16:0, and* ***φ*** *represents a statistical significant difference between the treatment versus both control and 300µM C16:0. All symbols represent a statistical significance P value of < 0.05.*

Table 4.12: FAME profile of dHepG2 cells treated with FAs

FAMEs were isolated from dHepG2 cells and measured using GC. FAME data presented as percentage of total FA identified (mean + SD for three independent samples).

Fatty acid (% of total FA) Mean ± SD	Control (5% BSA)	100μM Fenofibrate	10μM GW6471	50μM C15:0	150μM 15:0	300μM C15:0	50μM C16:0	150μM 16:0	300μM C16:0	150μM 15:0 + 150μM 16:0
C14:0	0.30 ± 0.01	0.32 ± 0.02	0.28 ± 0.03	0.31 ± 0.01	0.32 ± 0.02	0.31 ± 0.02	0.32 ± 0.02	0.32 ± 0.03	0.31 ± 0.02	0.30 ± 0.01
C15:0	0.24 ± 0.02	0.25 ± 0.02	0.23 ± 0.01	0.38 ± 0.02	0.40 ± 0.01	0.24 ± 0.02	0.40 ± 0.01	0.26 ± 0.01	0.27 ± 0.01	0.30 ± 0.01
C15:1	0.05 ± 0.01	0.06 ± 0.01	0.06 ± 0.01	0.19 ± 0.01	0.17 ± 0.01	0.05 ± 0.01	0.17 ± 0.01	0.06 ± 0.02	0.06 ± 0.02	0.12 ± 0.01
C16:0	**32.03 ± 0.55§**	**30.00 ± 0.29†§**	**32.71 ± 0.63†§**	**28.51 ± 0.16†§**	**28.13 ± 0.94†§**	**32.00 ± 0.85†§**	**28.13 ± 0.94§**	**31.93 ± 0.33§**	**33.83 ± 0.24†**	**31.06 ± 0.12†§**
C16:1	**4.62 ± 0.55§**	**5.23 ± 0.49§**	**4.63 ± 0.41§**	**5.16 ± 0.32§**	**5.36 ± 0.18†§**	**5.08 ± 0.23†§**	5.36 ± 0.18	**5.34 ± 0.25†**	**6.00 ± 0.21†**	**5.10 ± 0.14§**
C17:0	0.48 ± 0.03	0.49 ± 0.02	0.53 ± 0.08	0.72 ± 0.02	0.78 ± 0.01	0.47 ± 0.02	0.78 ± 0.01	0.53 ± 0.04	0.41 ± 0.02	0.65 ± 0.02
C17:1	0.11 ± 0.01	0.11 ± 0.01	0.08 ± 0.01	0.24 ± 0.02	0.31 ± 0.02	0.10 ± 0.01	0.31 ± 0.02	0.09 ± 0.01	0.07 ± 0.01	0.16 ± 0.01
C18:0	12.00 ± 0.85	11.6 ± 0.45	**12.72 ± 0.46†§**	**10.99 ± 0.23†§**	**10.56 ± 0.16†§**	**10.50 ± 1.02†§**	**10.56 ± 0.16†§**	**10.70 ± 0.16†§**	11.86 ± 0.24	**10.23 ± 0.33†§**
C18:1n9	**37.27 ± 1.26§**	**39.78 ± 0.22†§**	**36.16 ± 0.24†§**	**39.80 ± 0.21†§**	**40.4 ± 0.57†§**	**38.86 ± 0.54†§**	**40.40 ± 0.57†§**	**38.10 ± 0.16†§**	**34.73 ± 0.38†**	**38.10 ± 0.32†§**
C18:2n6	2.12 ± 0.13	2.16 ± 0.13	2.05 ± 0.13	2.17 ± 0.26	2.08 ± 0.3	2.23 ± 0.09	2.08 ± 0.30	2.25 ± 0.14	2.33 ± 0.20	2.33 ± 0.20
C18:3n6	0.34 ± 0.02	0.33 ± 0.01	0.37 ± 0.04	0.34 ± 0.01	0.35 ± 0.01	0.33 ± 0.02	0.35 ± 0.01	0.32 ± 0.01	0.35 ± 0.05	0.38 ± 0.01
C18:3n3	0.46 ± 0.02	0.46 ± 0.01	0.46 ± 0.01	0.46 ± 0.02	0.45 ± 0.01	0.42 ± 0.01	0.45 ± 0.01	0.44 ± 0.02	0.42 ± 0.02	0.43 ± 0.01
C20:3n6	0.68 ± 0.02	0.67 ± 0.02	0.68 ± 0.02	0.66 ± 0.03	0.68 ± 0.01	0.63 ± 0.02	0.68 ± 0.01	0.66 ± 0.01	0.64 ± 0.01	0.62 ± 0.01
C20:3n3	0.26 ± 0.04	0.29 ± 0.01	0.22 ± 0.01	0.55 ± 0.02	0.54 ± 0.03	0.27 ± 0.02	0.54 ± 0.03	0.28 ± 0.02	0.24 ± 0.03	0.34 ± 0.02

Fatty acid (% of total FA) Mean ± SD	Control (5% BSA)	100μM Fenofibrate	10μM GW6471	50μM C15:0	150μM 15:0	300μM C15:0	50μM C16:0	150μM 16:0	300μM C16:0	150μM 15:0 + 150μM 16:0
C20:4n6	4.20 ± 0.29	4.03 ± 0.24	4.33 ± 0.2	**3.60± 0.16§**	**3.66 ± 0.12†§**	**3.90 ± 0.16§**	**3.66 ± 0.12§**	4.33 ± 0.20	4.66 ± 0.12	4.50 ± 0.16
C20:5n3	0.42 ± 0.04	0.44 ± 0.05	0.41 ± 0.03	0.66 ± 0.01	0.65 ± 0.01	0.40 ± 0.06	0.65 ± 0.01	0.46 ± 0.09	0.36 ± 0.06	0.48 ± 0.11
C22:1n9	0.05 ± 0.01	0.05 ± 0.01	0.08 ± 0.02	0.06 ± 0.01	0.10 ± 0.01	0.05 ± 0.01	0.10 ± 0.01	0.05 ± 0.02	0.05 ± 0.01	0.07 ± 0.02
C22:6n3	3.63 ± 0.24	3.36 ± 0.16	3.35 ± 0.12	**4.50 ± 0.16†§**	**4.46 ± 0.16†§**	**3.63 ± 0.20†§**	4.46 ± 0.16	3.50 ± 0.32	3.00 ± 0.08	**4.20 ± 0.21§**
Total SFA	**45.06 ± 1.38§**	**42.67 ± 0.68†**	**46.49 ± 0.13†§**	**40.93 ± 0.29†§**	**40.21 ± 1.04†§**	**43.53 ± 0.68†§**	**40.21 ± 1.04†§**	**43.75 ± 0.22†§**	**46.7 ± 0.05†**	**42.55 ± 0.27†§**
Total MUFA	**42.11 ± 1.70§**	**45.24 ± 0.73†§**	41.03 ± 0.31	**45.46 ± 0.21†§**	**46.35 ± 0.72†§**	**44.16 ± 0.67†§**	**46.35 ± 0.72†§**	**43.64 ± 0.30†§**	**40.92 ± 0.15†**	**43.56 ± 0.37†§**
Total PUFA	12.14 ± 0.05	11.77 ± 0.2	11.90 ± 0.18	12.96 ± 0.25	12.90 ± 0.38	11.83 ± 0.38	12.90 ± 0.38	12.26 ± 0.34	12.02 ± 0.18	13.3 ± 0.14
Total ω-3	4.78 ± 0.33	4.56 ± 0.24	4.45 ± 0.13	**6.18 ± 0.15†§**	**6.12 ± 0.20†§**	**4.73 ± 0.30†§**	6.12 ± 0.20	4.69 ± 0.41	4.02 ± 0.16	**5.45 ± 0.31§**
Total ω-6	7.35 ± 0.34	7.21 ± 0.35	7.44 ± 0.06	**6.78 ± 0.28§**	**6.78 ± 0.34§**	**7.10 ± 0.12§**	6.78 ± 0.34	7.57 ± 0.33	7.99 ± 0.29	7.84 ± 0.16
OCSFA	0.72 ± 0.05	0.74 ± 0.03	0.76 ± 0.08	1.10 ± 0.01	1.19 ± 0.01	0.72 ± 0.01	1.19 ± 0.01	0.79 ± 0.05	0.68 ± 0.03	0.95 ± 0.02
ECSFA	**44.33 ± 1.41§**	**41.92 ± 0.64†§**	**45.72 ± 0.15†**	**39.82 ± 0.30†§**	**39.02 ± 1.04†§**	**42.81 ± 0.67†§**	**39.02 ± 1.04†§**	**42.95 ± 0.28†§**	**46.01 ± 0.02†§**	**41.6 ± 0.24†§**
C16:1/C16:0	0.14 ± 0.01	0.17 ± 0.01	0.14 ± 0.01	0.18 ± 0.01	0.19 ± 0.01	0.15 ± 0.01	0.19 ± 0.01	0.16 ± 0.01	0.17 ± 0.01	0.16 ± 0.01
C18:1n9/C18:0	3.12 ± 0.3	3.43 ± 0.15	2.84 ± 0.12	3.62 ± 0.07	3.82 ± 0.09	3.73 ± 0.37	3.82 ± 0.09	3.56 ± 0.03	2.92 ± 0.08	3.72 ± 0.15
C17:0/C17:1	0.23 ± 0.04	0.22 ± 0.03	0.16 ± 0.02	0.33 ± 0.04	0.39 ± 0.02	0.21 ± 0.02	0.39 ± 0.02	0.16 ± 0.01	0.17 ± 0.03	0.25 ± 0.01

† Represents a statistical significance of P< 0.05 for treatments vs control, while § represents a significant difference between treatment and C16:0

4.5 DISCUSSION

The previous chapter described a negative correlation between C15:0 and plasma glucose in fasting blood samples, which is in keeping with an emerging theme in several large-scale longitudinal studies [200, 206, 207]. However, the cellular mechanisms by which C15:0 exert any metabolic effect remains unknown. This chapter aimed to identify a mechanistic pathway to explain the protective effect of OCSFA through changes to glucose and FA metabolism in the liver. The results show that C15:0 significantly ameliorated C16:0 induced insulin resistance in vitro, by increasing glycogen production and reducing gluconeogenesis; both mechanisms that contribute significantly to increased plasma glucose in T2DM [260-262]. Furthermore, C15:0 reduced TNFα and IL-8 secretion by C16:0 treated hepatocytes. Also, C15:0 differentially modulates hepatocyte metabolic activity, favouring increased mitochondrial and peroxisomal oxidation of FA, which appears to be mediated via PPAR alpha.

To understand the effect of FAs on hepatocyte function, HepG2 cells needed to be differentiated to closely resemble primary hepatocytes, which are more quiescent and are characterised by increased expression of markers such as albumin, urea, as well as phase I and phase II enzymes [41]. Here, we found that growing the cells in low serum media induced hepatocyte differentiation with an increase in markers of differentiation, including albumin, transferrin, and urea, with no effect on cellular viability. Traditionally, retinoic acid (RA) and its derivatives are more commonly used to induce cell cycle arrest and cellular differentiation [263-266], by various mechanisms, which include the regulation of cyclin-dependent kinases, p53, p21,

retinoic-X receptor (RXR) amongst others, leading to cell cycle arrest predominantly in the G0/G1 phase. However, low serum has been shown to be as effective resulting in less toxicity to cells [267, 268] as RA also induces apoptosis, especially at high concentrations. The other justification for using low serum to induce quiescence in this study is that RA interferes with lipid metabolism by transactivating the PPAR alpha/RxRα heterodimer [269], which would have confounded the determination of FA effect on PPAR alpha transcription.

Chronic low-grade inflammation has been suggested as a link between the progression from NAFLD to a state of insulin resistance. Mature hepatocytes can alter the expression of specific proteins including cytokines, independent of resident macrophages, in response to inflammatory and stress stimuli [270, 271]. Here, we find that palmitate-treated cells induce an acute phase reaction similar to LPS without inducing apoptosis or affecting cellular viability. Several studies have shown palmitate-induced inflammation in hepatocytes mediated by several mechanisms including upregulation of NFƘB -by inducing oxidative stress [272], or toll-like receptors [273, 274]- upregulation of NOD-like receptor protein 4 (NLRC4) and caspase-1 activation mediated maturation of cytokines [275], amongst others. Others suggest that the toxic effect of palmitate can be explained by the intracellular accumulation of saturated phospholipids and intermediates (like ceramides) resulting in cellular dysfunction, especially in the mitochondria, due to an insufficient capacity to dispose of SFA by mitochondrial beta-oxidation, [276-278]. On the other hand, C15:0 treated cells increased metabolic activity, at least in the first six hours of treatment, corresponding to an increased mitochondrial succinate dehydrogenase activity (responsible for

reducing MTT), which may represent an increase in mitochondrial function- as evidenced by improved mitochondrial β-oxidation (Figure 4.10). Co-treating cells with C15:0 removed the toxic effect of C16:0. These toxic effects are absent in cells treated with oleate, a MUFA, despite significant lipid accumulation[63]. In fact, oleate protects C16:0 treated cells from insulin resistance and metabolic dysfunction via several mechanisms in different cell lines [279, 280], suggesting a differential effect of FA on cellular metabolic activity and viability. It was therefore interesting that the results in this chapter showed an increase in oleate production and an increase in the MUFA/SFA ratio in C15:0 treated cells (Table 4.12). Therefore, it is plausible that the protective effect of C15:0 in our study could be partially due to the mobilisation of C16:0 produced de novo, or acquired otherwise, into the less harmful MUFA, especially oleate. There is conflicting evidence from clinical studies on the benefits of a high MUFA/SFA ratio[281-284] mainly because these studies fail to distinguish between FAs from diet and de novo lipogenesis[285], and also mostly look at C16:0/C16:1 ratio as an indication for desaturase enzyme activity. However, clear benefits exist when diets high on MUFA are consumed in preference to high carbohydrate diets [286-289].

After establishing the presence of inflammation in C16:0 treated cells, which is ameliorated by C15:0, it was essential to ascertain if this had any impact on glucose homeostasis vis-à-vis insulin resistance. The results revealed that C15:0 significantly ameliorated C16:0 induced decrease in glycogen production and increase in glucose output; both mechanisms that contribute significantly to increased plasma glucose in T2DM [260-262]. A reduction in glycogen content in cells treated with high

concentrations of C16:0 was associated with an upregulation of GSK3β. GSK3β is known to inactivate glycogen synthase by phosphorylation, therefore, preventing glycogen production. In animal studies where hepatic steatosis is induced by high-fat diet, insulin resistance develops when there is a failure to inactivate GSKβ by impairment of insulin-stimulated tyrosine phosphorylation of IRS-1 and IRS-2, in a process likely to involve PKC activation of JNK [290]. The importance of GSK3β in palmitate-induced insulin resistance is buttressed by studies which show an improvement in insulin sensitivity, glucose homeostasis and cellular viability by the knockdown, silencing or inhibition of GSK3β [291, 292]. Interestingly, the data also showed upregulation of GSK3β by cells treated with high concentrations of C15:0 without affecting cellular glycogen content. The production of glycogen by an alternate pathway, possibly involving an insulin-dependent activation of glycogen synthase via glucose-6-phosphate, in C15:0 treated cells cannot be ruled out [293]. The data also showed upregulation of GLUT2 mRNA and gene expression by all FA treatments. However, only 300μM C16:0 treated cells showed a significant increase in glucose output in the supernatant. The upregulation of GLUT2 is an unreliable indicator for increased gluconeogenesis because the glucose transporter is bi-directional and non-specific for glucose[294] and very likely to reflect any movement of glucose across the cell membrane irrespective of FA treatments or concentration. It is also plausible that the upregulation of GLUT2 seen here reflects the acute insulin-mediated uptake of glucose by FAs [295]. However, as shown in some studies, GLUT2 is indispensable for glucose uptake [296] and alternative mechanisms exist for glucose output [297,

298]. Therefore, it is difficult to interpret the results of the GLUT2 data with respect to insulin resistance.

So far, we have seen that C15:0 reduced IL-8 and TNFα secretion by C16:0 treated hepatocytes. Previous studies have shown that lipid accumulation following C16:0 treatment induces an immune-mediated metabolic dysregulation [252] with reduced insulin-stimulated glucose uptake mediated via PI3-kinase signalling [196]. Moreover, Lee, Jin-young and colleagues observed insulin resistance in C16:0 treated HepG2 cells without significant lipid accumulation [299]. However, lipid accumulation features prominently in the pathway connecting inflammation and insulin resistance. Here, C16:0-induced increase in glucose output and reduced glycogen storage was associated with both raised inflammatory markers and lipid accumulation. It was important to understand the mechanisms that led to lipid accumulation in hepatocytes following FA treatment.

Hepatic lipid accumulation is thought to arise as a result of an interplay between excess uptake, defective FA oxidation, de novo lipogenesis, and VLDL export [300]. In this chapter, the first three factors have been studied using gene expression data. To examine the differential effect of FA on lipid uptake, gene expression of CD36 and liver-specific fatty acid binding protein (FABP) were examined. There was a high basal expression of CD36 in dHepG2 cells (similar mRNA content as relatively abundant reference gene), which is in keeping with hepatocyte maturity and differentiation. Unsurprisingly, all FA treatments upregulated CD36 gene expression, but to different degrees, with cells treated with 300μM C16:0 appearing to exert to most effect.

Several factors are known to increase the expression of CD36 including age, a high-fat diet, and insulin [301-303]. More specifically, SFA [304], MUFA [305], and PUFA [306] are all known to stimulate CD36 expression, to aid their cellular intake; however, there has been no report of differential sensing of FA by CD36 in the liver, despite limited evidence supporting this occurrence in other cells [307]. Similarly, all FA treatments in this study upregulated L-FABP. L-FABP plays an important role in trafficking cytoplasmic FAs into organelles, including the mitochondria and peroxisomes for β-oxidation, and the nuclei, where these FA could act as ligands for transcription factors [308]. In addition to FA, hypolipidaemic drugs like statins regulate L-FABP by interacting with PPAR alpha [309]. Therefore, it is possible that the differential upregulation of L-FABP by FA may be related to their individual ability to stimulate PPAR. It is difficult to predict the phenotypic expression and function of these FA transporters by their gene expression data. However, going by the data presented so far, high concentrations of C16:0 is associated with massive influx of FAs mediated by CD36 upregulation, which is not matched by a similar rise in L-FABP, leaving the possibility of cytoplasmic lipid accumulation leading to the formation of neutral lipid droplets and/or lipid intermediates such as ceramides, diacylglycerol, and lysophosphatidylcholine (LPC). Considerable but distinct upregulation of both CD36 and L-FABP may partly explain the increased lipid accumulation noted in cells treated with high concentrations of C16:0, but does not explain why other FA treated cells, which similarly upregulated both CD36 and L-FABP, show comparable amounts of neutral lipid accumulation with control cells. Therefore, FA oxidation was explored to explain any differences in mitochondrial or peroxisomal metabolism in FA stimulated

cells. Here, cells treated with high concentrations of C16:0 show similar gene expression levels CPT1 and CPT2 as controls, which is disproportionate to the level of CD36 and L-FABP as seen earlier. CPT1 is usually considered the rate-limiting step for mitochondrial FA oxidation, and along with CPT2, is responsible for the transport of fatty acid acyl esters across the mitochondrial membrane, in a process involving the incorporation of carnitine to fatty acyl esters [310-312]. The importance of CPT1 to FA oxidation is reinforced by mice knockout studies where the deficiency of CPT1 results in lipid accumulation secondary to reduced mitochondrial FA oxidation [313], and in studies where in vitro inhibition of CPT1 by etomoxir produces the same outcome [314]. Palmitate usually stimulates CPT1 & CPT2, especially in lower concentrations. In fact, there is only limited direct evidence in support of a downregulatory effect at concentrations as high as 750µM resulting in dysfunctional FA oxidation [315]. Here, the effect of palmitate is disproportionally equivocal to control suggesting a reduction in FA oxidation in these cells. However, in in vitro and mice models of palmitate-induced insulin resistance, lipid accumulation is usually associated with generalised mitochondrial dysfunction and consequently reduced FA oxidation, ameliorated by MUFA and PPAR alpha [310, 316-319]. The results from this chapter also show that co-incubating cells with C15:0 and C16:0 ameliorates palmitate-induced dysfunction in genes involved in mitochondrial and peroxisomal β-oxidation, in a process that might be similar to how MUFA protect cells from palmitate-induced dysfunction. Additionally, the results suggest that C16:0 treated cells probably favour de novo lipogenesis by upregulating FASN gene expression. Put together, cells treated with high concentrations of C16:0 potentiate intracellular lipid traffic but show disproportionate

β-oxidation functionality, which in addition to increase de novo lipogenesis could explain increased intracellular lipid accumulation as observed. Conversely, C15:0 treated cells appear to maintain normal levels of neutral lipids by increasing FA oxidation to account for the influx of FA and likely slight increase in de novo lipogenesis.

The protective effect of C15:0 on palmitate-induced hepatocyte dysfunction has so far mirrored that of MUFA in literature. In this chapter, the result shows that C15:0 increased the expression of both SCD1 and SCD5, suggesting that some of the protective effect of C15:0 may be the consequence of MUFA production. This is confirmed by a higher MUFA/SFA ratio in these cells compared to palmitate-treated cells. Interestingly, only C15:0 treated cells upregulated SCD1, which is more highly expressed in dHpG2 cells. Furthermore, an examination of ELOVL1, FADS1 and FADS2 show that C15:0 treated cells show a preference for the biosynthesis of ω-3 PUFA as opposed to ω-6 PUFA, which are preferentially produced by C16:0 treated cells. Again, PUFA shows a comparable protective effect as MUFA in literature in the context of palmitate-induced hepatocyte dysfunction. Therefore, the ability of C15:0 to promote the production of MUFA and PUFA may underpin its overall effect on hepatocytes metabolically.

The apparent hypolipidaemic effect of C15:0, especially in the context of increased FA oxidation (especially in the peroxisomes) raises the suspicion of PPAR involvement. Pararasa et al. (2013) have previously shown that the effect of FA on macrophage differentiation and phenotype was related to PPARγ [252]. It was therefore pertinent

to identify any associations between C15:0 and PPAR alpha, which is more predominantly involved with FA oxidation than other PPARs in the liver. As seen in the results, C15:0 treated cells appear to upregulate PPAR alpha upstream similar to the fenofibrate, a known PPAR alpha agonist, associated with a rise in RxRα expression, which is required to form the PPAR alpha/RxRα heterodimer prerequisite for transcriptional activity. Moreover, C15:0 at all concentrations upregulate KPNA2 and KPNB1, necessary for nuclear translocation of ligands and proteins. Importantly, C15:0 and fenofibrate exclusively increase gene expression levels of NCOA2, which amplifies the downstream transcriptional activity of target genes by histone acetylation [320, 321]. To verify the gene expression data, a transcription activity assay was performed which shows that C15:0 significantly increased PPAR alpha activity compared to control, similar to fenofibrate.The fact that PPAR alpha transcriptional activity was similar between C15:0 treated and fenofibrate treated cells suggested that the protective effect of C15:0 vis-a-vis the increase in MUFA content could be mediated via a PPAR alpha pathway. Moreover, C15:0 increased PPAR alpha activity in C16:0 treated cells more than fenofibrate and the addition of a PPAR alpha antagonist eliminated this effect. PPAR alpha activation has been shown to increase FA catabolism, β-oxidation, improve insulin resistance and reduce liver steatosis and inflammation in mouse models[322-324]. However, these effects were seldom observed in humans until recently when the use of a dual PPAR alpha/δ agonist (GFT505) showed a liver-specific reduction in insulin resistance[325]. Once activated, PPAR alpha regulates several genes to promote lipid metabolism. This study found many of these genes (CPT1, CPT2, SCD1, NCOA2, FADS1, FADS2) to be highly

upregulated with C15:0 treatment alone, or with C15:0 and C16:0. An upregulation of SCD1 is in keeping with our finding of an increased level of MUFA in C15:0 treated cells. Some PUFA acts as natural ligands for PPAR alpha [251] and would make sense if the PPAR alpha activation noted with C15:0 is partly due to the increased PUFA production elicited by C15:0. There is a suggestion from our results that C15:0 may be acting as a ligand for PPAR alpha. We cannot exclude effects on other PPARs due to their overlapping regulatory effects and redundancy.

Gene expression for de novo lipogenesis pathway was marginally upregulated with C15:0 treatment in our study. This is in line with a recent study that identified de novo lipogenesis as an essential player in the generation of an endogenous ligand for PPAR alpha, 1-palmitoyl-2-oleoyl-*sn*-glycerol-3-phosphocholine (16:0/18:1-GPC). Taking this evidence together, it is plausible that in addition to PUFA production, C15:0 either acts directly as a ligand for PPAR alpha or induces the process of producing an endogenous PPAR alpha ligand, subsequently leading to PPAR alpha transcription and downstream target gene expression.

This study is limited by relying on gene expression data to demonstrate metabolic mechanisms underpinning lipid metabolism. Gene expression by RT-qPCR provides information on the relative abundance of mRNA and is no way indicative of gene/protein function. Moreover, there are several other complex processes involved in gene regulation and function such as post-transcriptional and post-translational changes, that determine the physiologic and functional end-product of genes. These processes were not accounted for in this study. Consequently, fold change gene

expression data does not account for downstream production of target proteins or their activation and inhibition. Therefore, the degree of regulation at gene expression level does not necessarily reflect target protein expression or function.

This study did not qualify or quantify the enzymes involved in lipid metabolism in hepatocytes or attempt to identify their phosphorylated product as a measure of regulation. Therefore, the results from this study are physiologically redundant and at best, provides a useful suggestion for future studies.

In conclusion, this study attempted to demonstrate a cellular metabolic mechanism to explain the effect of OCSFA on palmitate-induced cellular dysfunction in a model of insulin-resistant hepatocytes. C15:0 treated cells showed a different metabolic outcome compared to its even chain counterpart (C16:0) in terms of glucose production, glycogen storage, and intracellular accumulation of neutral lipids. Furthermore, results from RT-qPCR suggest a differential gene expression profile between C15:0 and C16:0 in lipid metabolism. However, further studies are required to shed more light on the physiologic importance of these differences and to validate the mechanisms underpinning the effect of OCSFA on hepatocyte function.

5 CHAPTER 5: EFFECT OF FATTY ACIDS ON MONOCYTE FUNCTION

5.1 INTRODUCTION

The mechanisms linking inflammation and insulin resistance are complex and mostly still held as hypotheses. Many factors have been identified as either inducers or modifiers of the inflammatory process leading to metabolic disorders, and monocytes and macrophages have been acknowledged as key players in this inflammatory process [326, 327].

The circulation of excess FFA is usually causally linked to the development of the chronic low-grade inflammation associated with T2DM and other metabolic syndromes [328-331]. A few clinical studies have shown a positive correlation between obesity indices, such as elevated FFA, and raised inflammatory markers like CRP [332-334]. Although the exact mechanism by which FAs induce and maintain inflammation is still mostly unknown, much work has been done in recent times to explore the mechanistic effect of FA on innate immunity. SFA have been shown to activate Toll-like receptors (TLRs), especially TLR2 and TLR4, both of which are implicated with LPS-induced pro-inflammatory changes [335, 336]. TLRs mediate the expression of IL-6 and TNFα [337-339], which have become useful biomarkers of inflammation in lipid research. Interestingly, UFA inhibit TLR mediated expression and signalling of pro-inflammatory activity [340-342] and it is still unknown if OCSFA will behave differently compared to the more abundant even chain SFAs like palmitate. TLRs and their associated cytokines are highly expressed in monocytes, making this peripheral immune cells an essential target for lipid research.

Monocyte diversity and macrophage polarisation are becoming increasingly important in the discussion around the immune induction of metabolic diseases [143, 343-348]. Monocyte and macrophage phenotypes are functionally distinct in innate-immune driven processes; therefore, a careful understanding of the different classes of monocytes and macrophages, their phenotypic differences, and the different factors that modulate these phenotypes can shed light on the occurrence of a low-grade inflammatory state prevalent in metabolic diseases. Monocytes are classified as classical, intermediate, or non-classical; depending on the expression of CD14 and CD16 on the cell surface [349, 350]. The classical monocyte subset represents 80% of circulating monocytes and expresses high levels of CD14 and very low levels of CD16 (otherwise denoted $CD14^{++}/CD16^{-}$ population) [351, 352]. This subpopulation of monocytes express less TNFα and more IL-10 cytokines after LPS stimulation and are thought to be anti-inflammatory, with high phagocytic function, but quick resolution post-inflammation. Intermediate monocyte subsets are characterised by high levels of CD14, and higher levels of CD16 compared to classical monocytes (denoted as $CD14^{+}/CD16^{+}$ monocytes) and have been denoted to be pro-inflammatory in more recent studies. Along with intermediate monocytes, the non-classical monocytes (or $CD14^{-}/CD16^{++}$ sub-population) are associated with increased production of pro-inflammatory cytokines and are increased in infectious diseases as well as chronic metabolic disorders [349, 353]. Similarly, monocytes differentiate into distinct classes of macrophages depending on the stimuli. M1 macrophages, like intermediate and non-classical monocytes, are associated with elevated levels of pro-inflammatory cytokines like IL-6 and TNFα [354, 355]. Whereas, M2 macrophages, induced in vivo

by T helper 2 cells, express an anti-inflammatory or pro-resolution phenotype, associated with increased secretion of IL-10 [354, 355].. There is a complex relationship between FAs and monocyte/macrophage differentiation, and there is a dearth of studies exploring the mechanisms by which FAs influence the diversity of monocytes and macrophages. Pararasa (2013) showed that palmitate cause differential alteration of macrophages by inducing a pro-inflammatory environment, resulting in the production of M1 macrophage, compared to oleate, an UFA, which tends towards M2 induction; highlighting the importance of FA class/type in immune modulation [356]. However, there has been no study looking at the possible difference in monocyte/macrophage induction or differentiation among OCSFAs in comparison with even chain SFAs.

5.2 AIMS AND HYPOTHESIS

There is a growing recognition of the contribution of monocyte phenotypes in normal healthy physiology and disease states. Recent studies have shown that FA classes may have different effect on monocytes and macrophages. Many of these studies have concentrated on the more abundant even chain FAs. However, with growing evidence in support of a protective effect of OCSFA on diseases like T2DM known to be associated with chronic inflammatory states, it has become imperative to elucidate the effect of OCSFA on monocyte function. The harmful effect of FAs on immune cells as shown in literature is usually mediated via disturbances in metabolic activity and an expression of a pro-inflammatory phenotype. However, work from several studies have shown that PPAR alpha antagonists induce an anti-inflammatory response in

immune cells. Subsequently, results from section 4.4.8 show that C15:0 increases transcriptional activity of PPAR alpha in hepatocytes. Therefore, this chapter aims to show the differential effect of OCSFA compared to palmitate on monocyte phenotype and function by exploring their influence on LPS stimulated monocytes.

5.2.1 Hypothesis

The Hypotheses for this study are as follows:

1. C15:0 will increase metabolic activity in THP-1 cells
2. C15:0 and C16:0 will show differential alteration in cell surface markers corresponding to different monocyte subsets
3. C15:0 will ameliorate pro-inflammatory response to LPS in THP-1 cells

5.3 METHOD

5.3.1 Determination of metabolic activity

Following treatment, the metabolic activity of THP-1 monocytes was determined by the MTT assay as described in section 2.7.

5.3.2 Quantification of cellular growth and viability

Cell growth and viability were measured using the trypan blue exclusion method with the counting of cells using a haemocytometer as described in section 2.6.

5.3.3 DNA cell cycle analysis by Flow Cytometry

Following treatment, cell cycle analysis was performed following the method described by Phillips et al. (2003) as detailed in section 2.4 [357]

5.3.4 Flow cytometry analysis of surface antigen expression

Flow cytometry was used to quantify surface expression of CD14, CD16, and CD36 as described in section 2.5.

5.3.5 Differentiation of monocyte

Following priming with FAs, THP-1 monocytes were differentiated to macrophages by stimulating with PMA as detailed in section 2.3.

5.3.6 Quantification of cytokines

Following treatment, IL-6, IL-10, and TNFα were quantified from supernatants by ELISA as described in section 2.12.

5.3.7 Statistical analysis

Data expressed as mean +/- SEM for three independent experiments. FACS data expressed as median fluorescence intensity to account for the non-normally

distributed flow intensity data. Statistical significance was estimated using repeated measures one way ANOVA with a Geisser-Greenhouse correction to correct for the unequal variability of differences, and a Dunnett's post-test for multiple comparisons. FACS data were analysed by a Friedman's test with Dunn's post-test for multiple comparisons. Data obtained was analysed using GraphPad Prism (v7.0)

5.4 RESULTS

5.4.1 C15:0 increases metabolic activity

THP-1 monocytes were cultured at 500,000 cells/ml with indicative concentrations of FA or control for 6hrs and 24hrs, to determine cellular metabolic activity. The result shows that C15:0 is associated with an increase in metabolic activity (Figure 5.1a) by 13% ($p < 0.001$), 12% ($p < 0.001$), and 10% ($p < 0.001$) compared to control for 50μM, 150μM, and 300μM C15:0 respectively after 6hrs of incubation. In comparison to cells treated with 300μM C16:0, this represents an increase in metabolic activity by 30% ($p < 0.001$), 27% ($p < 0.001$), and 24% ($p < 0.001$) for 50μM, 150μM, and 300μM C15:0 respectively. Treating cells with C16:0 showed the opposite effect compared to C15:0 treated cells. C16:0 decreased metabolic activity in THP-1 cells corresponding to a 1.6% ($p < 0.05$), 2.7% ($p < 0.01$), and 11% ($p < 0.001$) decrease in metabolic activity after 6hrs compared to control for 50μM, 150μM, and 300μM C16:0 concentrations respectively. Interestingly, the decrease in metabolic activity with C16:0 is abolished when co-treated with C15:0. Over 24hrs, there was no statistically significant difference in metabolic activity between all C15:0 treated cells and controls (Figure 5.1b). However, cells treated with C16:0 still showed a significant reduction in metabolic activity compared to control by 1.8% ($p < 0.05$), 1.9% ($p < 0.01$), 11.6% ($p < 0.001$) for 50μM, 150μM, and 300μM C16:0 concentrations respectively. Again, this effect is abolished by co-treating with C15:0. Furthermore, as seen in figure 5.2, high concentrations of C16:0 reduces total cell count in monocytes as early as 6hrs after treatment.

5.4.2 C16:0 is associated with markers of cell death

THP-1 cells were assessed for cell viability to exclude any toxic effect of FAs. As seen in previous results, C15:0 increases metabolic activity, while C16:0 decreases activity. To determine if this effect is confounded by the toxicity of FA to cells, propidium iodide was used to assess cellular viability. Viable cells with intact membranes usually exclude dyes such as trypan blue and propidium iodide; therefore, providing a means of checking viability. The ability of the fluorescent dye, propidium iodide, to intercalate with DNA, provides a useful means to measure the proportion of dead cells in any given sample. Apoptotic cells have reduced DNA content. It is evident from the results that cells treated with C16:0 show significantly increased levels of apoptotic nuclei in a dose-dependent manner (Figure 5.3a). There was a 9.3% ($p < 0.05$), 15.2% ($p < 0.001$), and 22.4% ($p < 0.01$) increase in apoptotic nuclei found in cells treated with 50µM, 150µM, and 300µM C16:0 respectively compared to control cells. There was an excellent linear correlation between treatment concentration of C16:0 and percentage increase in apoptotic nuclei (R^2 0.99). In contrast, cells treated with varying concentrations of C15:0 had less apoptotic cells compared to controls. There was a 44.2%, 52%, and 41% decrease in the number of apoptotic cells compared to controls in cells treated with 50µM, 150µM, and 300µM C15:0 respectively (all p values < 0.001).

5.4.3 FAs alter cell cycle dynamics of monocytes

It is clear from the results shown so far that C16:0 inhibits metabolic activity and impacts negatively upon cell growth, probably by inducing apoptosis, whereas, C15:0 appears to improve these indices. Therefore, it was important to investigate the effect

of these FAs on cell cycle dynamics (Figure 5.3). Generally, for C15:0 treated cells, there were more cells found in the G0/G1 phase with a reciprocal decrease in cells found in the S-phase. C15:0 treatment increased the proportion of cells found in the G0/G1 phase by 13% ($p < 0.01$), 16% ($p < 0.001$), and 13% ($p < 0.001$) for 50µM, 150µM, and 300µM C15:0 respectively compared to control cells. In contrast, there were less cells found in the S-phase compared to control by 10% ($p > 0.05$), 13% ($p < 0.05$), 13% ($p < 0.05$) for 50µM, 150µM, and 300µM C16:0 respectively. Only 150µM C15:0 treated cells accounted for statistically significant fewer cells in the G2/M phase compared to controls among C15:0 treated cells (13% reduction, $p < 0.05$). There was no statistically significant difference in the proportion of cells in the G1/G0 or S-phase in C16:0 treated cells compared to controls. However, there was a dose-dependent decrease in the proportion of cells in the G2/M phase for C16:0 treated cells compared to control; 3.4% ($p < 0.05$), 11.4% ($p < 0.01$), 16% ($p < 0.01$) decrease for 50µM, 150µM, and 300µM C16:0 respectively.

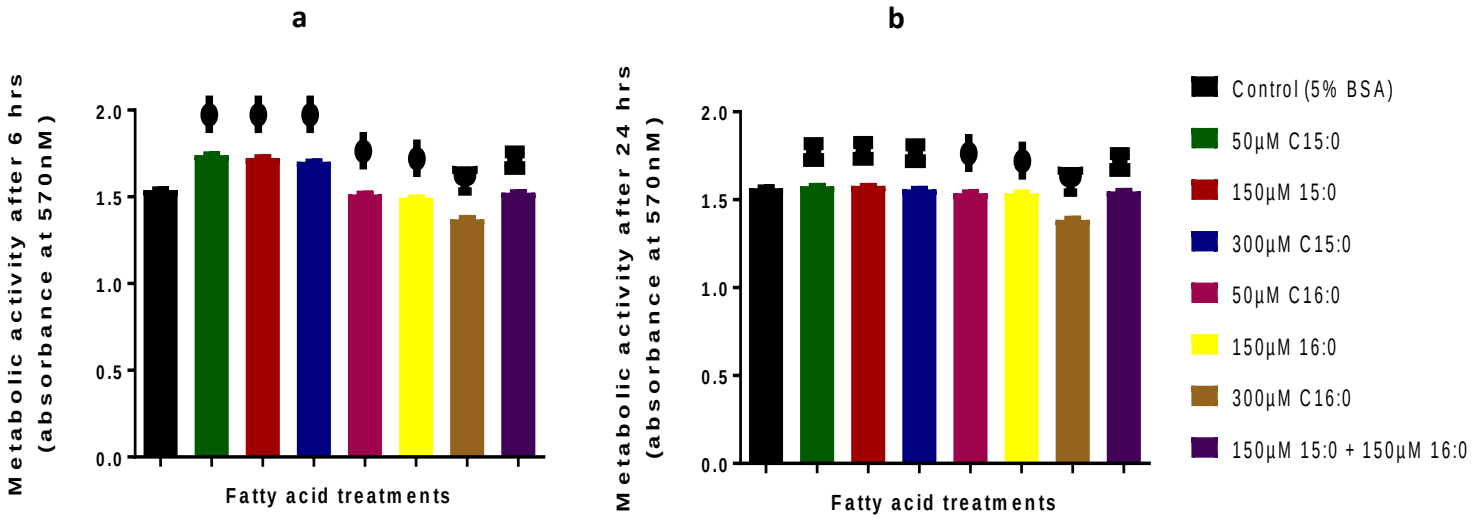

Figure 5.15.1: C15:0 is associated with a short-lived increase in metabolic activity in monocytes.

THP1 monocytes at a density of 5 x 10^5 cells were treated with fatty acids conjugated to BSA and analysed for metabolic activity using MTT reduction after 6 and 24hrs of exposure. Cells were exposed to varying concentrations of fatty acids, or control (5% BSA) as outlined. MTT reagent was added to the media 4 hours prior to the end of the experiment. Cells were then lysed with lysis reagent overnight before analysis under absorbance spectrometry at 570nm. (a) Effect of fatty acid treatments after 6hrs and (b) 24hrs. Results are expressed as mean +/- SEM (n=3 independent experiments). Statistical significance was determined by a repeated measures one-way ANOVA with Geisser-Greenhouse correction and a Dunnett's post-test comparison. ***Ψ*** *represents a statistical significant difference between treatment versus control, Ξ represents a statistical significant difference between treatment versus 300µM C16:0, and* ***φ*** *represents a statistical significant difference between the treatment versus both control and 300µM C16:0. All symbols represent a statistical significance P value of < 0.05.*

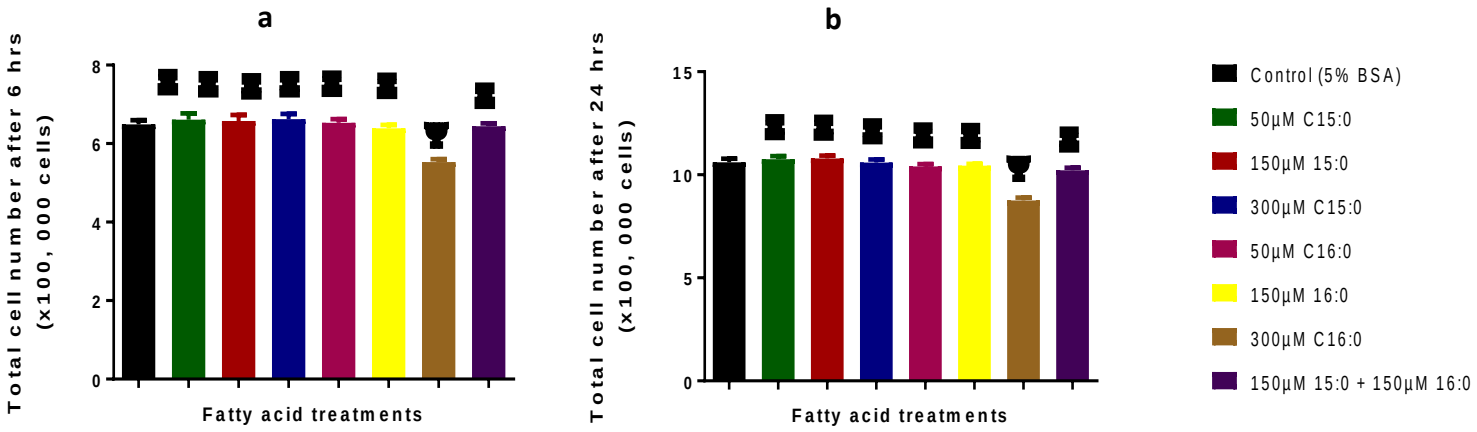

Figure 5.2: High concentrations of C16:0 causes Monocyte growth arrest

THP1 monocytes at a density of 5 x 10^5 cells were treated with fatty acids conjugated to BSA and analysed for cell growth after 6 and 24hrs of exposure. Cells were exposed to varying concentrations of fatty acids, or control (5% BSA) as outlined. To assess cell growth, THP1 cells were counted with a haemocytometer after (a) 6hrs or (b) 24hrs of fatty acid treatment. Results are expressed as mean +/- SEM (n=3 independent experiments). Statistical significance was determined by a repeated measures one-way ANOVA with Geisser-Greenhouse correction and a Dunnett's post-test comparison. ***Ψ*** *represents a statistical significant difference between treatment versus control, Ξ represents a statistical significant difference between treatment versus 300µM C16:0, and* ***φ*** *represents a statistical significant difference between the treatment versus both control and 300µM C16:0. All symbols represent a statistical significance P value of < 0.05.*

5.4.4 C15:0 and C16:0 show differential alteration of cell surface antigen expression in THP-1 monocytes

FA have been shown to induce phenotypic changes on monocytes, including antigen cell surface expression. It has already been shown from results above that OCSFA differs in its interaction with monocytes regarding cellular viability and metabolic activity. To determine if there was a distinction between C15:0 and C16:0 on monocyte cell surface expression, the levels of CD14, CD16, and CD36 were measured (Figure 5.4) by FACS. High concentrations (300μM) of both FA significantly reduced CD14 cell surface expression, but C16:0 ($p < 0.001$) by up to twofold more than C15:0 ($p < 0.01$). There was no significant difference in the cell surface expression of CD14 between control and the lower concentrations of C15:0 treated cells, or with cells treated with 50μM C16:0. However, there was a significant decrease in CD14 expression in cells treated with 150μM C16:0 ($p < 0.05$). Furthermore, there was a negative linear correlation between the concentration of C16:0 and CD14 cell surface expression (R^2 0.99). FA treatment did not affect CD16 cell surface expression (Figure 5.4b) irrespective of chain length or concentration. High concentrations of C16:0 (300μM) significantly increased the cell surface expression of CD36 (Rank sum difference 21, $p < 0.05$) compared to control (Figure 5.4c), and there was a positive linear correlation between the concentration of C16:0 and CD36 surface expression (R^2 0.98). In contrast, there was no statistically significant change in CD36 expression for THP-1 cells treated with varying concentrations of C15:0.

5.4.5 Palmitate but not C15:0 increases pro-inflammatory cytokine production

We have already seen from previous results that FA may modify monocyte phenotype by altering cell surface expression of CD14. Here, we determine if FA induce a pro-inflammatory or anti-inflammatory environment by measuring the levels of cytokine production via ELISA as outlined in methods. THP-1 monocytes were incubated with varying concentrations of FA for 24hrs, after which the supernatant was extracted and measured for production of IL-6, IL-10, and TNFα (Figure 5.5). There was a definite linear correlation between FA concentration and TNFα production (R^2 0.98 for C15:0 and R^2 0.94 for C16:0). 50μM C15:0 was associated with a 17% reduction in TNFα production compared to control ($p < 0.05$). There was no statistically significant difference in TNFα production between control and cells treated with 150μM and 300μM C15:0, or any concentration of C16:0. LPS, used as a positive control, was associated with a fourfold increase in TNFα production ($p < 0.001$). IL-6 production followed a similar trend to TNFα (Figure 5.5b). Among all FA treatments, only 300μM C16:0 showed a significant difference in IL-6 production compared to controls (27% increase, $p < 0.05$). Furthermore, no FA treatment, irrespective of concentration, altered the production of the anti-inflammatory cytokine IL-10.

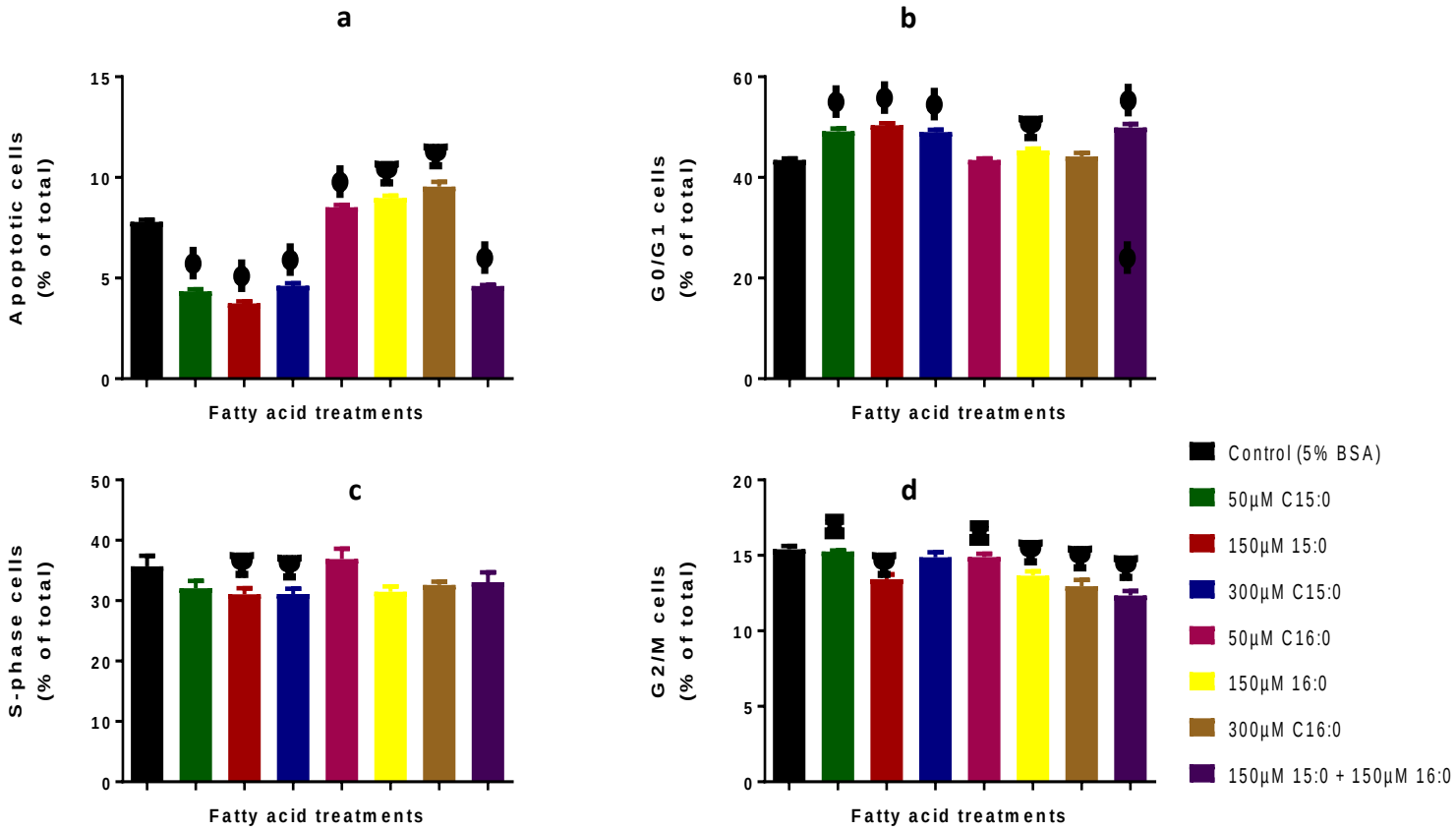

Figure 5.3: C15:0 causes cell cycle arrest at G0 phase and protects THP1 monocytes from palmitate induced apoptosis.

THP1 monocytes at a density of 5 x 10^5 cells were treated with fatty acids conjugated to BSA and analysed using flow cytometry for cell cycle arrest as outlined in methods. Cells were exposed to varying concentrations of fatty acids, or control (5% BSA) as outlined. (a) Apoptosis (b) G0/G1 phase (c) S-phase (d) G2/M phase. Results are expressed as mean +/- SEM (n=3 independent experiments).

Statistical significance was determined by a repeated measures one-way ANOVA with Geisser-Greenhouse correction and a Dunnett's post-test comparison. ***Ψ*** *represents a statistical significant difference between treatment versus control, Ξ represents a statistical significant difference between treatment versus 300µM C16:0, and* ***φ*** *represents a statistical significant difference between the treatment versus both control and 300µM C16:0. All symbols represent a statistical significance P value of < 0.05.*

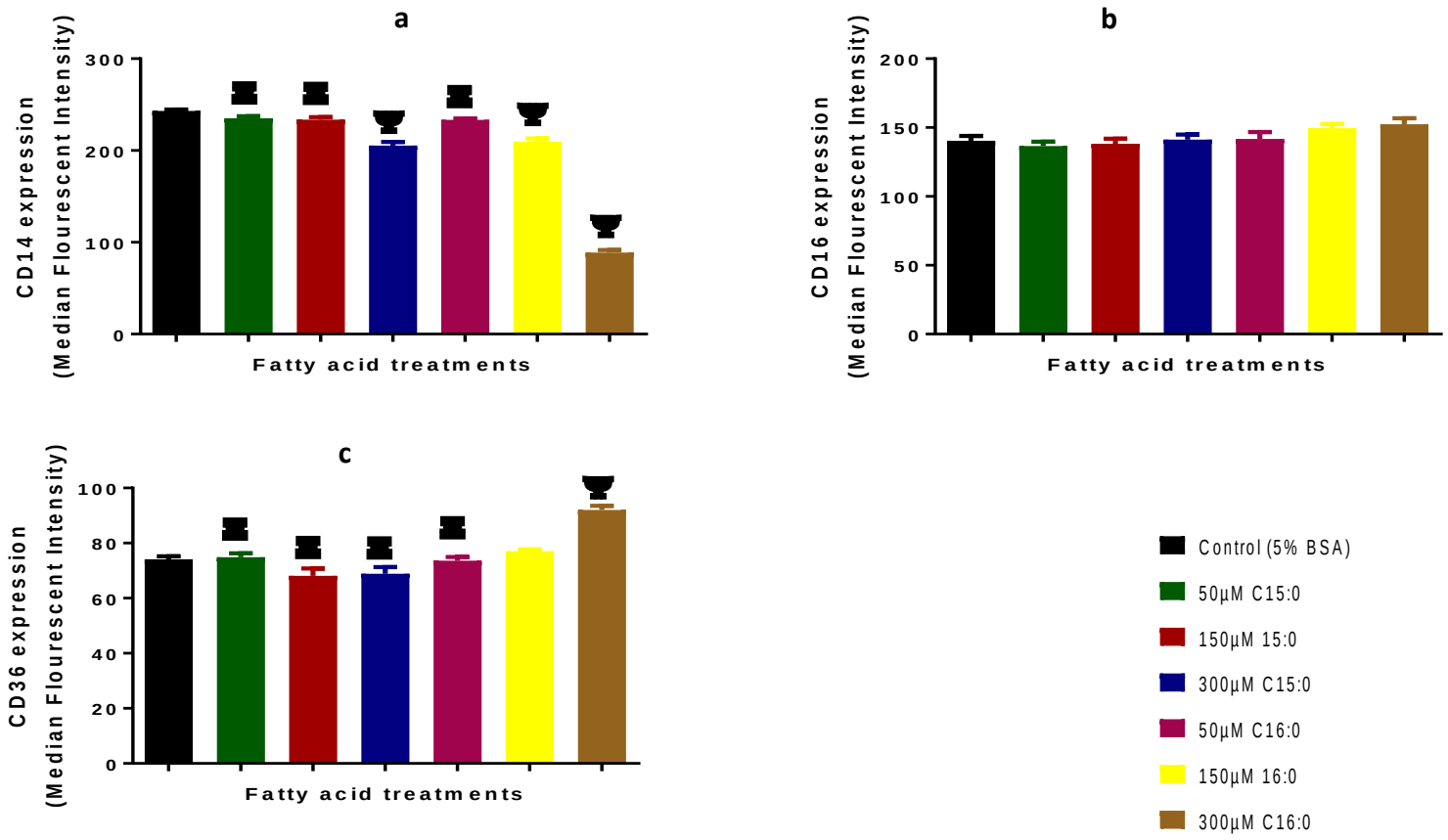

Figure 5.4: Effect of fatty acids on the cell surface expression of CD14, CD16 and CD36.

THP1 monocytes at a density of 5 x 10^5 cells were treated with fatty acids conjugated to BSA and analysed using flow cytometry for cell surface expression of CD14, CD16 and CD36 as outlined in methods. Briefly, cells were exposed to varying concentrations of fatty acids, or control (5% BSA) and then incubated with anti-CD14, andti-CD16, and anti-CD36 antibodies. (a)MFI for CD14 (b) MFI for CD16 (c) MFI for CD36. Results presented for 3 independent experiments).
Statistical significance was determined by a Friedman's test and a Dunn's post-test comparison. Ψ represents a statistical significant difference between treatment versus control, Ξ represents a statistical significant difference between treatment versus 300µM C16:0. All symbols represent a statistical significance P value of < 0.05.

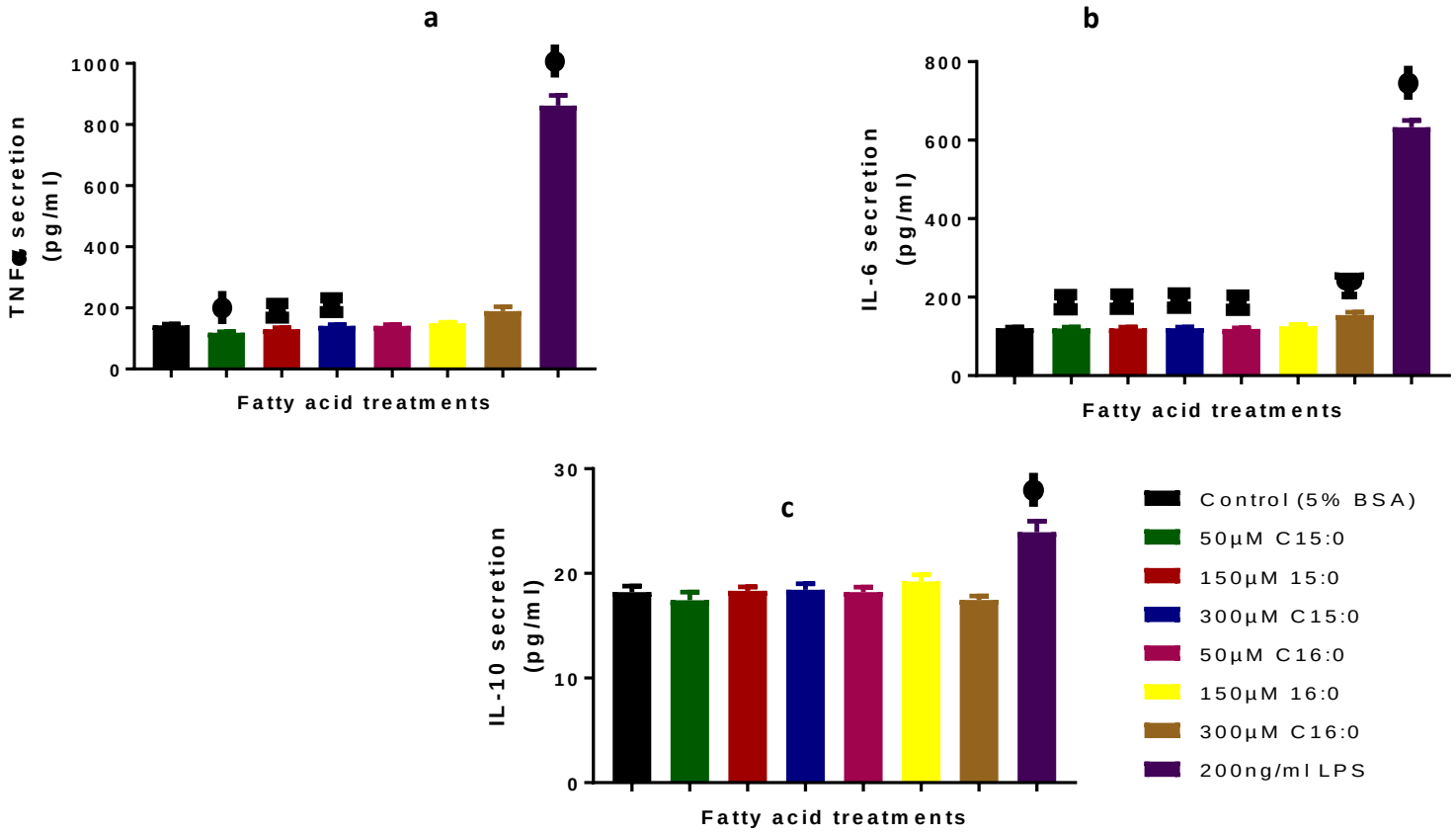

Figure 5.5: C16:0 at high concentrations is associated with an increase in pro-inflammatory cytokines in THP1 monocytes.

THP1 monocytes at a density of 5 x 10^5 cells were treated with fatty acids conjugated to BSA or 200ng/ml of LPS. Supernatants were extracted after 24hrs of incubation and analysed for cytokines by ELISA. (a) TNFα secretion (b) IL-6 secretion (c)IL-10 secretion. Results are expressed as mean +/- SEM (n=3 independent experiments).

Statistical significance was determined by a repeated measures one-way ANOVA with Geisser-Greenhouse correction and a Dunnett's post-test comparison. ***Ψ*** *represents a statistical significant difference between treatment versus control, Ξ represents a statistical significant difference between treatment versus 300µM C16:0, and* ***φ*** *represents a statistical significant difference between the treatment versus both control and 300µM C16:0. All symbols represent a statistical significance P value of < 0.05.*

5.4.6 Pre-treatment with C15:0 ameliorates pro-inflammatory response to LPS

Previous reports have shown that C16:0 is associated with a pro-inflammatory response in monocytes and prior results in this chapter have shown that the C15:0 treated cells show a different monocyte phenotype compared to C16:0 treated THP-1 cells. To further understand how FA affect monocytes in a pro-inflammatory environment, THP-1 cells were pre-treated with FA for 6hrs then with LPS for 18hrs (total treatment time of 24hrs), followed by analysis of the supernatant for pro-inflammatory cytokines TNFα and IL-6 (Figure 5.6). There was a sixfold increase in TNFα production with monocytes treated with LPS vs baseline control cells ($p < 0.001$). Although cells treated with C15:0 + LPS showed higher levels of TNFα compared to controls (5% BSA no LPS), the levels of TNFα were significantly reduced compared to positive controls [5% BSA + LPS] (72%, 70%, and 65% reduction for 50μM, 150μM and 300μM C15:0 respectively; $p < 0.01$). Whereas, C16:0 treated cells did not alter TNFα secretion compared to positive control. In fact, there was a slightly higher but statistically insignificant increase in TNFα secretion in cells treated with 300μM C16:0 compared to positive control (6.5% increase, $p > 0.05$). The same trend was noted with IL-6 secretion (Figure 5.6b); C15:0 treated cells significantly reduced IL-6 secretion compared to positive control cells ($p < 0.001$), while there was no significant difference in IL-6 output between C16:0 treated cells and positive control.

5.4.7 C15:0 prime macrophages display an anti-inflammatory phenotype.

THP-1 monocytes can differentiate into classical (M1), or alternative (M2) macrophages, broadly corresponding to a pro-inflammatory or anti-inflammatory phenotype respectively. THP-1 cells primed with FA for 6hrs were differentiated to macrophages with PMA for 48hrs. Cytokine analysis was performed on the macrophages to determine the phenotype. Cells primed with LPS was used as positive control for pro-inflammatory macrophage differentiation. TNFα secretion was increased by more than three folds in LPS primed macrophages (Figure 5.7a) compared to controls (5% BSA). Priming with C16:0 was associated with an increase in TNFα secretion compared to control cells primed with 5% BSA, corresponding to a pro-inflammatory phenotype- 21.6% ($p > 0.05$), 36.2% ($p < 0.05$), 68% ($p < 0.001$) increase for 50µM, 150µM and 300µM C16:0 respectively. There was no statistically significant difference in TNFα secretion between control and C15:0 primed macrophages. On the other hand, C15:0 primed macrophages appear to display an anti-inflammatory phenotype by increasing IL-10 secretion by 70% ($p < 0.01$), 54% ($p < 0.05$), and 65% ($p < 0.001$) for 50µM, 150µM and 300µM C15:0 respectively. There were no significant differences between control and C16:0 primed macrophages

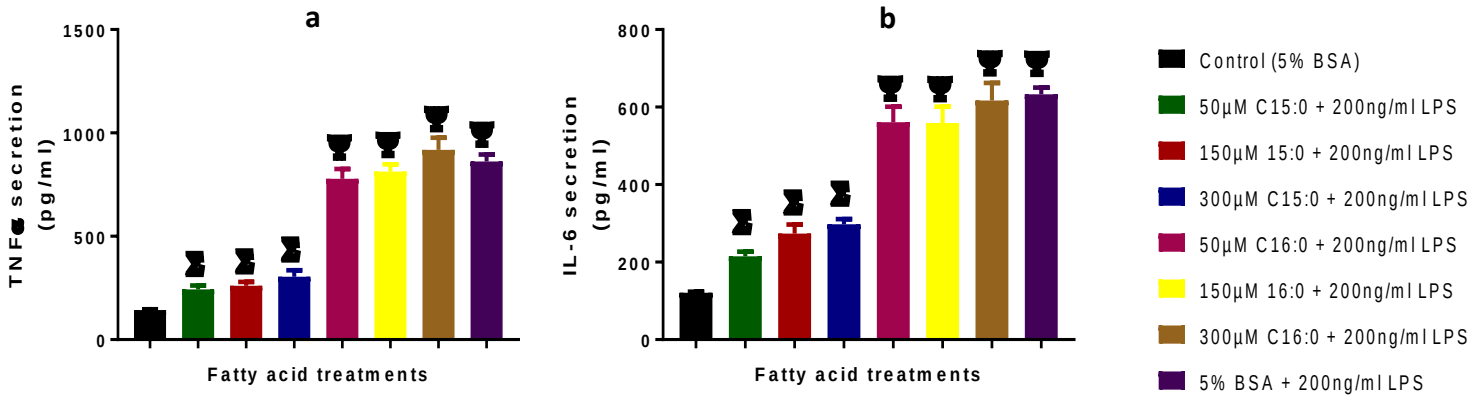

Figure 5.6: C15:0 ameliorates LPS induced increase in pro-inflammatory cytokines

THP1 monocytes at a density of 5 x 10^5 cells were treated with fatty acids conjugated to BSA or control (5% BSA) for 6hrs then with 200ng/ml LPS to make up a total of24hrs. Supernatants were extracted after 24hrs of incubation and analysed for cytokines by ELISA. (a) TNFα secretion (b) IL-6 secretion. Results are expressed as mean +/- SEM (n=3 independent experiments).

Statistical significance was determined by a repeated measures one-way ANOVA with Geisser-Greenhouse correction and a Dunnett's post-test comparison. ***Ψ*** *represents a statistical significant difference between treatment versus control,* ***Ξ*** *represents a statistical significant difference between treatment versus 300µM C16:0,* ***φ*** *represents a statistical significant difference between the treatment versus both control and 300µM C16:0, and Σ represents a statistical significant difference between the treatment versus control, 300µM C16:0 and 200ng/ml LPS. All symbols represent a statistical significance P value of < 0.05.*

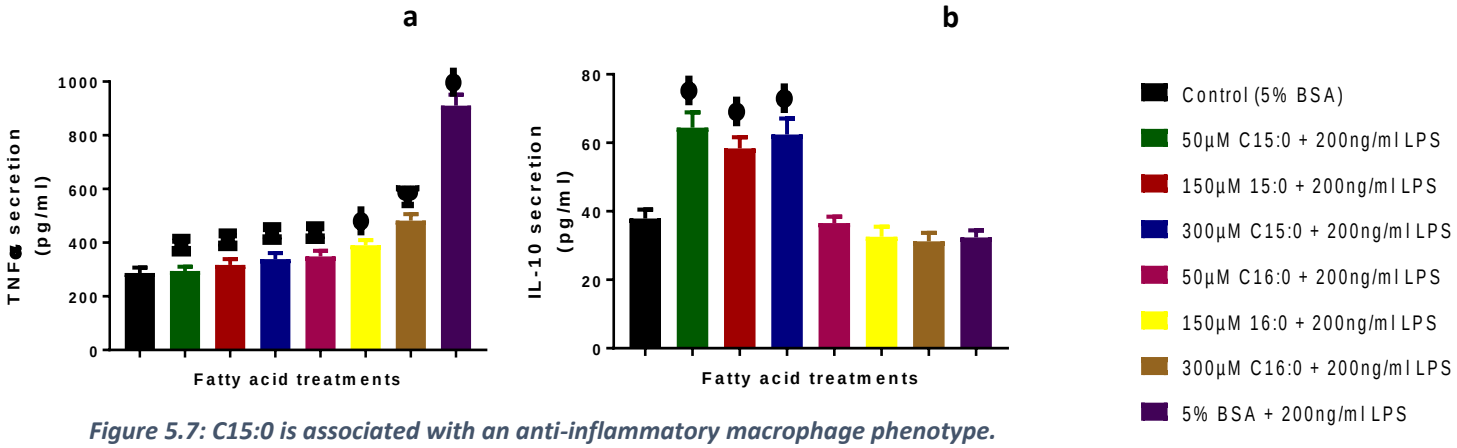

Figure 5.7: C15:0 is associated with an anti-inflammatory macrophage phenotype.

THP1 cells were pre-incubated with fatty acids or control conditions (5% BSA) for 6hrs then treated with PMA for 72hrs to induce macrophage differentiation as outlined in methods. LPS pre-treated cells were used as positive control. Supernatants were extracted after 24hrs of incubation and analysed for cytokines by ELISA. (a) TNFα secretion (b) IL-10 secretion. Results are expressed as mean +/- SEM (n=3 independent experiments).

Statistical significance was determined by a repeated measures one-way ANOVA with Geisser-Greenhouse correction and a Dunnett's post-test comparison. ***Ψ*** *represents a statistical significant difference between treatment versus control, Ξ represents a statistical significant difference between treatment versus 300µM C16:0,* ***φ*** *represents a statistical significant difference between the treatment versus both control and 300µM C16:0. All symbols represent a statistical significance P value of < 0.05.*

5.5 Discussion

Monocytes and macrophages play a critical role in innate immunity and are influential in the development and sustenance of several diseases [358, 359]. The onset of T2DM is likely to be multifactorial, involving complex mechanisms; however, the presence of chronic low-grade inflammation, induced by elevated levels of FA, has been continually observed and implicated as a possible bridge between those with borderline hyperglycaemia and full-blown diabetes [331, 360, 361]. There has been a surge in the study of monocytes and macrophages (clinical and in vitro studies) as chief players in innate immunity and the differential response to inflammatory stimuli in healthy individuals compared to people with metabolic disorders. In vitro experiments of monocytes have been performed using immortalised cell lines, the most popular being THP-1 cells. Several studies have reported glaring differences between primary monocytes and THP-1 cells while others have shown it to very closely replicate primary monocytes by phenotype and function [362-365]. The THP-1 cells used in these studies will vary according to age, batch, passage numbers, among other factors, which may explain the disparity within results. However, THP-1 cells are accepted as good monocyte models within lipid research. In this chapter, THP-1 cells have been used as a model to determine the effect of two classes of FAs on monocyte phenotype and function in the context of cell surface expression, macrophage differentiation and cytokine production.

In general, the results show that cells treated with OCSFA maintain the same level of expression of CD14, CD16 and CD36 as controls, whereas palmitate-treated cells appear to have depleted CD14 expression, concurrently increasing CD16 and CD36

expression. There also appeared to be an effect of nutrient overload on CD14 expression, evident by a reduction in CD14 surface expression with high concentrations of both FA, even though this effect was more pronounced in palmitate-treated cells compared to its odd chain counterpart. As previously discussed, the cell surface expression of CD14 and CD16 determine monocyte phenotype regarding its overall ability to be pro/anti-inflammatory, which is in contrast to the previously misleading method of classifying monocytes by morphology alone. There has been an increased interest in monocyte classification over the last decade. Continuous attempts to better qualify monocyte populations has been warranted by their role in disease states. For example, the intermediate sub-population of monocytes and non-classical monocytes are increased in bacterial and viral infections, stress, as well as in metabolic and inflammatory conditions such as rheumatoid arthritis, cardiovascular diseases, and chronic kidney disease [349, 353].

The CD14 expression in this study did not change with low concentrations of FA (50µM); however, a differential effect is noticed as the concentration of FA begin to increase. At 150µM, palmitate-treated cells begin to show a reduction in CD14 expression, trending even further downwards as concentrations reached 300µM. This is in contrast to C15:0 treated cells that only show a reduction in CD14 expression at 300µM. CD14 expression reduces as monocytes move between the spectrum from classical to non-classical monocytes. CD14 is an important co-receptor for the detection of pathogens, with LPS being its principal ligand [366, 367]. Saresella et al. (2017) showed that “Western diet” characterised by high SFA content, is associated with a reduction in CD14 expression in monocytes [368], indicating that high energy

load is negatively correlated with CD14 expression. Conversely, Sun-Mi Kim et al. (2015) showed that consumption of a high cholesterol diet increases expression of CD14 [369]. There are many reasons why these and many other studies looking at the effect of diet on cell surface expression are not directly comparable, explaining the disparity in results, including differences in sample population and intervention used. More importantly, these studies differ in the methods used to quantify CD14 expression; the anti-CD14 antibodies used, the gating strategy, and most importantly, the use of isotype controls (the former applies isotype controls, and the latter does not). The use of isotype control for FACS analysis divides opinions [370-373]. In this study, an isotype control, gate compensation and the use of blocking agent were employed for each analysis to minimise background signal and reduce the chance of false positives. Frey and De Maio (2007) provide further evidence in support of the fact that high energy load could lead to lower CD14 expression. They showed that treating macrophages with lovastatin to lower cholesterol increases membrane-bound CD14 expression [374]. Energy overload may partly explain why the CD14 expression is lower in palmitate-treated cells compared to C15:0 with higher concentrations of treatment. It is plausible that higher concentrations of C15:0 is required to overwhelm monocytes compared to palmitate as seen with hepatocytes in the previous chapter. The CD36 expression lends credence to this. Palmitate treated at high concentrations have a significantly higher CD36 expression compared to control and C15:0 treated cells at a similar concentration. CD36 interacts with oxidised low-density lipoproteins to increase the influx of lipids. Therefore, palmitate-treated cells are more likely to accumulate lipids leading to energy overload.

Neither C16:0 nor C15:0 affected CD16 expression in this study. The finding is similar to studies performed by Pararasa et al. (2013) in vitro, and Alshahrani et al. (2017) in vivo that showed no effect of SFA on CD16 surface expression [356, 375]. There is insufficient evidence from literature showing a direct link between diet or FA on CD16 expression. However, many studies have shown that CD16+ cells express high levels of TLRs which is the primary driver of its pro-inflammatory phenotype [376, 377]. This is important to note because several studies have shown a direct association between saturated FAs and increased TLRs expression [378-381].

Put together; one may suggest that OCSFA induce a phenotype at least close to the classical monocyte sub-population, while palmitate at high concentrations influences a more intermediate or non-classical phenotype. However, there are several limitations to this interpretation.

Firstly, this study was not designed to measure both CD14 and CD16 surface expression simultaneously. Traditionally, both surface antigens are measured at once using fluorescent dyes at distinct wavelengths (for example, FITC and APC). Three gates can then be set to quantify classical, intermediate, and non-classical populations. However, this is not without considerable challenge, and it is often difficult to optimise. Gating is very subjective and is likely subject to much variabilities, making standardisations difficult [382, 383]. More so, dye spillover may occur, especially when one dye is much brighter than the other (e.g. FITC and APC). In this study, appropriate compensation techniques were applied to mitigate dye spill over; however,

compensation is not standerdised across studies, making pooled analysis and interpretation across studies difficult.

Secondly, the effect of the distinction in cellular viability on CD16 or CD14 cell surface expression cannot be ignored. Heidenreich (1999) showed that a reduction in CD14 surface expression precedes apoptosis induced by IL-4 in monocytes [384]. Additionally, work by Fingerle-Rowson et al. (1998) and Ziegler-Heitbrock (2015) allude to the fact that glucocorticoid-induced stress prompts selective apoptosis in non-classical monocytes [385, 386]. Here, palmitate induces apoptosis and reduces CD14 expression at concentrations more than 150µM. Moreover, cells treated with high concentrations of palmitate begin to show reduced cell proliferation and growth (measured by cell count relative to control) even as early as 6hrs with no associated cell cycle arrest. Many studies confirm the cytotoxic effect of palmitate on THP-1 cells and even show that MUFA can protect THP-1's from palmitate-induced toxicity. No previous study has demonstrated the effect of OCSFA on THP-1 viability or metabolic activity. Palmitate induces cell death by several mechanisms including activation of various caspases (3/4/5), increased MMP-9 expression, inhibition of Sirt1, an increase in mitochondrial ROS, and p53 pathway; all of which can be mediated by TLR4 signalling [387-392].

Put together; it is difficult to interpret these results as representative of monocyte sub-population differentiation by cell surface markers. However, an examination of the functional ability to produce cytokines remains a viable indication for monocyte phenotype. Cytokine production was measured in monocytes and macrophages to

determine their functional phenotype after FA stimulation. The role of cytokines in the development of T2DM and its complications is well defined in the literature. There is a vicious cycle comprised of elevated metabolites, like glucose and FA, and increased adipokines that activate monocytes, leading to a rise in pro-inflammatory cytokines, which potentially instigates and enhances insulin resistance by various mechanisms. Kim and coworkers (2012) were able to show that hyperglycaemia triggers the acetylation of p65 and inhibition of histone deacetylase (HDAC) by activating histone acetylases (HAT) resulting in NF-ƙB activation, consequently leading to IL-6 and TNFα expression [393]. Subsequently, Kang et al. (2016) showed a strong correlation between TNFα in adipose tissue and HOMA-IR in obese people with prediabetes, with no macrophage infiltration or change in macrophage phenotype, suggesting that alterations in cytokine production precede any monocyte/macrophage phenotypic modifications [394]. The results from this chapter demonstrate an alteration in the baseline pro-inflammatory cytokine profile in cells treated with high concentrations of palmitate for 24hrs, which is consistent with the hypothesis of a low-grade inflammatory state stimulated by elevated FA. However, cells treated with similar concentrations of C15:0 did not show an elevation of pro-inflammatory cytokines, indicating that the inflammatory process triggered by palmitate is not entirely explained by a high energy state. There is evidence to suggest that cells have different cytotoxicity thresholds for different classes of FA, but the differences are usually more divergent, for example, there is a considerable difference between palmitate, MUFA and PUFA because of the double bonds linking the carbon atoms. On the other hand, the only distinguishing feature between palmitate and C15:0 is a single carbon atom.

This subtle difference has already been discussed in the previous chapter, and the observable difference in the inflammatory profile may be related to signalling ability or the distinction in the metabolic pathway as discussed. In addition to having a higher baseline level of pro-inflammatory cytokines, THP-1 cells primed with palmitate display a pro-inflammatory cytokine profile resembling an M1 phenotype [395], while PUFA priming show M2 anti-inflammatory phenotype. This is in keeping with what is seen in this chapter with palmitate showing an M1 phenotype; with an increase in TNFα secretion and no change in IL-10 secretion. Like PUFAs, C15:0 primed macrophages displayed an anti-inflammatory M2 phenotype, with raised IL-10 secretion. This discrepancy has not been elucidated previously. This interaction is likely to be more complicated in vivo as it is still unknown to what extent in vitro experiments in immortalised cells represent in vivo environments; however, this research presents a novel perspective regarding saturated FAs as a whole, as indeed, C15:0 is a SFA.

After establishing that palmitate and C15:0 show differential effect on baseline cytokine levels and plausibly macrophage differentiation, it was pertinent to elucidate the effect of FA on monocytes in the event of ongoing inflammation. THP-1 cells were primed with FA

for 6hrs then treated with LPS to simulate an ongoing inflammatory response. Interestingly, but in keeping with previous results in the chapter, C15:0 primed cells exhibited an anti-inflammatory response contrasting with C16:0 treated cells. LPS is the main ligand for CD14 and stimulates an inflammatory response by triggering TLRs. Palmitate is known to stimulate TLRs with or without LPS (also known as sterile

inflammation); therefore the results were not surprising [396, 397]. The study failed to expound the exact mechanism that C15:0 mediates an anti-inflammatory response in LPS induced monocytes. There is a good reason to think that it is plausible it does so in similar fashion to ω3-PUFAs, which acts as regulators of inflammation. One of the ways ω3-PUFA regulates inflammation is by acting as a competitive substrate for ω6-PUFA metabolism. ω6-PUFAs act as substrates for prostaglandins and leukotrienes and are therefore naturally pro-inflammatory. It is plausible that OCSFA acts competitively against its even chain counterpart to regulate inflammation. We saw from the hepatocyte chapter that palmitate-treated cells favour ω6-PUFA production, while C15:0 cells showed preferential production of ω3-PUFA. Perhaps the regulatory properties of C15:0 is mediated via ω3-PUFA production associated with all its downstream effects, including, but not limited to increased resolving lipids, competitive activation of GPR120, or downregulation of NF-ƙB via TLR4.

Taken together, the results in this chapter indicates an exciting prospect for OCSFA as anti-inflammatory agents. Further research is required to elucidate the mechanisms that underpin this process and explore the role of gut microbiota in the metabolism and function of OCSFA in the context of the immune system.

6 CHAPTER 6: CONCLUDING REMARKS

6.1 General discussion

The major aim of this study was to identify a relationship between FA and fasting plasma glucose, with particular focus on OCSFAs, and to explain the mechanistic link between energy excess, inflammation and insulin resistance.

The contribution of FA to the development and maintenance of T2DM has been heavily studied in the past and continues to divide opinions. Recent improvement in GC and mass spectrometry technologies has amplified the search for FA biomarkers for diseases. In this study, a GC detection technique was optimised to allow for optimal detection of OCSFAs in small quantities of plasma. Furthermore, a multiple linear regression analysis was carried out to identify FA predictive of insulin resistance.

In this study, elevated levels of ECSFA, like palmitate and stearate, were more likely to predict a unit rise in fasting plasma glucose in a multiple linear regression model despite no significant difference in absolute levels between control and T2DM cohorts. Hyperglycaemia is one of the consequences of insulin resistance, which is a state characterised by an inability to drive glucose into tissues. ECFA are known to correlate positively with insulin resistance in the literature. In fact, the most commonly held opinions on SFA and insulin resistance is influenced by palmitate, which is the most abundant SFA. Animal knockdown studies along with in vitro cellular models of insulin resistance have highlighted the association between elevated palmitate levels and the development of ER stress, mitochondrial dysfunction, direct inhibition of insulin signalling, as part of many ways in which elevated palmitate levels results in the development of insulin resistance in tissues. Therefore, the relationship between

palmitate and insulin resistance is well established from a mechanistic point of view. However, in human studies, this distinct relationship is usually much more difficult to ascertain for various reasons, and the presence of metabolic disease, or even obesity, does not always translate to higher circulating levels (absolute) of palmitate, as seen in this study. There are a few reasons for this. Firstly, the circulating levels of FAs are amendable to diet and physical exercise and this is (at least the former) difficult to accurately quantify in large scale studies. Also, daily variations in plasma FA levels exist and the effect of age, stress, gender on FA levels cannot be ignored. Some authors have tried to mitigate these confounders by presenting and analysing results as percentage of total FA (%wt). However, this method is likely error prone because currently available lipid extraction and analysis methods are not robust enough to detect every FA in a given sample. Here, a multiple linear regression method was instead used to adjust for known confounders.

The GC optimisation was targeted specifically to increase recovery of OCSFA to good effect. This meant that the OCSFA, C15:0, was more accurately assessed in our study. The concentration of C15:0 detected in this study is slightly higher than plasma levels found in previous other larger scale cross-sectional studies [80, 206], reinforcing the importance of the lipid extraction and FAME detection optimisation. Here, the concentration of C15:0 as a proportion of FAs measured was higher in controls compared to individuals with T2DM, which is consistent with other studies which show higher levels of C15:0 in healthy individuals compared to different disease states. For example, a nested case control design within the EPIC study looking at more than two thousand incident cases of coronary heart disease (CHD), found an inverse

relationship between plasma C15:0 levels and the development of CHD [398]. Subsequently, a multi-ethnic US cohort of just under three thousand participants found a 19% reduction in atherosclerotic risk with every unit increase in C15:0, which was found in higher concentration among controls [78]. In terms of epidemiologic evidence for the relationship between C15:0 and diabetes, three Australian studies found a negative correlation between C15:0 and indices of insulin resistance similar to the results in this study [79, 81, 399]. Furthermore, studies have reported gender and age-specific differences in C15:0 plasma concentrations [400]. Interestingly, people who report healthy lifestyles, including non-smoking, moderate alcohol intake, and increased physical activity, usually have significantly higher levels of plasma C15:0 [398]. The direct interpolation of C15:0 plasma concentration between health and disease is therefore likely to be confounded by lifestyle choices and modifications. Consequently, it was important to employ a multiple linear regression model to test the relationship between C15:0 and fasting plasma glucose, adjusting for age, gender, and BMI. Plasma glucose correlated negatively with C15:0 in this study, in line with many other longitudinal studies. Despite a clear correlation, it is difficult to pinpoint if this finding is a cause or consequence of plasma glucose levels.

This study was a nested case control design within an already existing cohort that was not designed for FA analysis. Therefore, there was no dietary assessment in this study. It is impossible to comment on the likely impact of dietary habits on the FA profile of individuals within this study. Indeed, C15:0 levels have been correlated with dietary habits in previous studies [85]. However, diet alone is unlikely to fully explain the beneficial effect of C15:0 regarding T2DM prevention. An interesting observation

from literature regarding diet and OCSFA is the similarity in the dietary sources of ALA (an ω-3 PUFA) and OCSFA [401], both being abundant in dairy products and fish oil.

To summarise, the clinical data from this study although limited by low sample size and a lack of dietary assessment, provides data in support of a correlation between C15:0 and fasting blood glucose, similar to other large cross-sectional and longitudinal studies. The close relationship between diet and C15:0 and the similarity between the dietary source of PUFA and C15:0 provides an explanation for the possible mechanism by which C15:0 is prevents T2DM in the absence of in vitro or animal studies to explain the mechanistic link between C15:0 and glucose homeostasis.

There is substantial evidence suggesting a disparity in cellular metabolic response to SFA in comparison to their unsaturated counterparts. The metabolic switch in response to different classes of FA has been put forward as a possible reason for the differential effect of saturates in terms of insulin resistance. A distinction in metabolic activity was observed between OCSFA and palmitate in this study, including differences in the biosynthesis and catabolism of FA, as well as differences in PPAR alpha signalling.

In this study, C15:0 induced an acute increase in metabolic activity, which is observed to normalise within 24hrs, in both hepatocyte and monocyte cell lines. The reduction of MTT to purple formazan is influenced by several factors including cell proliferation, availability of reduced products (like reduced glutathione), and increased mitochondrial number and function. In rapidly proliferating cells, like immortalised cancer cells, MTT reduction has long been correlated with cellular proliferation and

multiplication. However, there are a few reasons why the increase in MTT reduction found in this study is less likely to reflect proliferation. Firstly, MTT reduction in C15:0 treated cells did not correspond to an increase in number of cells compared to control in both monocyte and hepatocyte cell lines. Furthermore, in hepatocytes, C16:0 elicited a decrease in MTT reduction compared to control and C15:0 treated cells despite no significant changes in cell count after 6hrs or 24hrs. In addition, in THP-1, the observable reduction in cell count as a reflection of cellular proliferation, did not correlate with the magnitude of MTT reduction in C16:0 treated cells. The other possible explanation for the difference in MTT reduction is the presence of reducing enzymes. This study did not measure glutathione levels; therefore, it is impossible to comment on the likely effect of C15:0 on glutathione synthesis. However, previous studies have showed that oleate and palmitate are able to affect the levels of glutathione differently in THP-1 monocytes (Pararasa, 2013), while some authors have observed a direct association between glutathione synthesis/depletion with MTT reduction [402]. The use of MTT as a measure of cellular proliferation and viability relies on the assumption that mitochondrial activity is constant for all viable cells [403]. However, researchers have shown that mitochondrial activity is modulated by FA. Dietary PUFA has been shown to alter mitochondrial bioenergetics by several mechanisms, including modification of mitochondrial membrane composition and function, changes to mitochondrial redox state, as well as altering mitochondrial enzymes [404-408]. MUFA are also known to favourably alter mitochondrial function [409, 410], while palmitate induce mitochondrial dysfunction [411-413]. It is plausible that improved mitochondrial β-oxidation in C15:0 treated cells, as seen in this study,

is partially responsible for increases in metabolic activity. It is also plausible that C15:0 increased metabolic activity by increasing the production of propionyl Co-A, an anaplerotic intermediate for the citric acid cycle [414, 415].

Normally, the liver reacts to excess FA by increasing lipid catabolism and reducing de novo lipogenesis. However, more energy demands lead to formation and accumulation of triglycerides, in a vicious cycle that ultimately results in inflammation and insulin resistance. In NAFLD, a condition that is common in people with T2DM, cellular lipid and glucose homeostasis is impaired, worsening on disease progression. Many studies have been able to directly correlate an impairment of FA oxidation with the development of fatty liver in animal and in vitro models of high fat diet and FA induced NAFLD. In chapter 4, the result show a difference in the gene expression of FA oxidation between C15:0 and C16:0 in hepatocytes; and considering the limitations of the methodology, it provides a limited understanding of the differences between OCSFA and its even chain counterpart, partly explaining why OCSFA may be protective with T2DM disease development or progression. Cells treated with high concentrations of palmitate showed marked lipid accumulation which can be partially explained by key differences between C16:0 and C15:0 treated cells in gene expression of β-oxidation enzymes. Here, cells treated with high concentrations of C16:0 show disproportionate expression of CPT1 and CPT2 genes. These two genes are typically overexpressed during fasting and other conditions that prompt increased FA oxidation. Bazhan and colleagues showed an age-related deficiency of CTP1 in adult C57B1 mice, which was not improved by fasting [416]; this deficiency resulted in age-related obesity and subsequently impaired glucose homeostasis. Similarly,

Fujiwara and colleagues showed that a downregulation of CPT2 is associated with steatohepatitis in mice fed a high fat diet [417]. CPT1 and CPT2 are integral components of the carnitine palmitoyltransferase system, which mediates the transfer of activated FA across the mitochondrial membrane for β-oxidation. Therefore, their upregulation, as seen with cells treated with C15:0 would be the expected response in high fat environments, to shift intracellular FAs towards mitochondrial β-oxidation. The same pattern of expression was observed for C15:0 and C16:0 treated cells with respect to gene expression of the enzymes that catalyse the final steps of mitochondrial FA β-oxidation. Again, C16:0 at high concentrations show equivocal expression of ACADL and ACAD10, and a downregulation of ACAA2. This correlates with the data showing reduced CPT1 and CPT2 expression and suggests a deficient β-oxidation, which would explain increased lipid accumulation. The ability of C15:0 to drive β-oxidation would explain why the clinical data in chapter 3 shows a statistically significant negative correlation between the concentrations of C15:0 and C16:0 and provides a reasonable explanation to why increase in dairy intake is associated with C16:0 levels in cross-sectional studies. Further robust in vivo studies would be required to fully explain a causal relationship between C15:0 and C16:0 levels. The alternate explanation for a negative correlation between C15:0 and C16:0 levels in studies would be the possibility of α-oxidation. Alpha oxidation involves a series of steps where FA are hydroxylated at the α-carbon after activation, requiring Iron and α-keto-glutarate as co-factors, then followed by the removal of the terminal carboxyl group in a process involving thymine pyrophosphate and magnesium ions. The product of these steps is able to undergo normal β-oxidation. Alpha oxidation has been

proven to occur in humans but was previously thought to be confined to peroxisomes and the oxidation of phytanic acid. However, recent evidence suggests that SFA can undergo α-oxidation and the mitochondria is also heavily involved in this process; C16:0 and C18:0 can be converted to C15:0 and C17:0 as an endogenous source of OCSFA. However, the trigger for this event is unknown, but the gut microbiome has been implicated. An increase in α-oxidation as a consequence of C15:0 treatment may explain why mitochondrial activity (evidenced by increased FA oxidation and high MTT reduction) and peroxisome transport (ABCD genes) is upregulated in this study. Although, this is difficult to prove, it is plausible that the induction of an extra oxidative pathway amplifies FA oxidation, consequently leading to less lipid accumulation. Taken together, C15:0 may be acting as an activator of the α-oxidation pathway which amplifies β-oxidation, ultimately promoting the endogenous conversion of C16:0 to C15:0. This hypothesis is limited by the ratio of C16:0 to C15:0 (approximately 150:1) in plasma, even in healthy individuals. This shows that the intracellular relationship between C15:0 and C16:0 is likely to be complex and tightly regulated. The difference between C15:0 and C16:0 observed in this study only seem to appear at palmitate concentrations of 300μM. One limitation of this study is that it was not designed to explain the metabolic switch that occurred across different concentrations of C16:0. In fact, there is a dearth of published evidence in support of a metabolic switch induced by FA, but this is usually thought to be secondary to energy overload. Therefore, it was interesting that this switch only occurred with C16:0. C15:0 is only found in small quantities in plasma; however, this study employed concentrations as high as 300μM to eliminate the possibility that energy overload is responsible for the differential effects

of C16:0. This finding highly suggests that the differential effect found between C15:0 and C16:0 is likely to be related to a difference in signalling pathway. PPAR alpha is heavily implicated in diet induced metabolic switch from glucose to FA energy dependence. PPAR alpha transcription mediates FA oxidation by enhancing genes involved with β-oxidation and mitochondrial function. It was therefore logical that PPAR alpha activity is explored as a possible mechanism by which C15:0 exerts its differential effect. Here, all concentrations of C15:0 induced PPAR alpha activity at gene expression and transcription level, which translated to PPAR alpha target gene expression. Conversely, C16:0 inhibited PPAR alpha transcription activity similar to the antagonist GW6471. Natural PPAR alpha ligands have been reported to include PUFA (like DHA and EPA), as well as palmitoylethanolamide (PEA). It is possible that C15:0 acts as a natural ligand, or as seen in this study, may induce PPAR alpha by increasing production of PUFA. Taken together, the differential effect of C15:0 and C16:0 can be explained by their stimulation of PPAR alpha. The “excess energy” environment created by C15:0 leads to effective sensing of PPAR alpha resulting in energy burning mediated via increased FA oxidation, while an improper PPAR alpha sensing by C16:0 results in defective FA oxidation, lipotoxicity, lipid accumulation, and eventually insulin resistance. Therefore, the potential impact of OCSFA on PPAR alpha as a mechanism that underpins anti-inflammatory process cannot be ruled out. In this study, palmitate-induced pro-inflammatory responses were abrogated by C15:0 in hepatocytes, while LPS-induced inflammation was ameliorated by C15:0 in monocytes. Furthermore, C15:0 played a role in the differentiation of M2 macrophage phenotype. All these effects have been replicated in studies using PPAR alpha

agonists, suggesting a possible role of PPAR alpha in the anti-inflammatory phenotype observed with C15:0. PPAR alpha mediated inhibition of pro-inflammatory cytokines has been shown to be PPRE independent. Upon activation by a ligand, PPAR alpha binds to either p65 or the N-terminus JNK-responsive part of cJun, preventing them from binding to NF-ƙB response element, consequently leading to inhibition of TNFα and IL-6 expression [418]. Alternatively, a suppression of TNFα-induced IL-6 transcriptional activity can be achieved by ligand-activated PPAR alpha-GR (glucocorticoid receptor) interaction coupled to p65 and p50 [419]. In addition, the anti-inflammatory properties of C15:0 could be driven via increased PUFA, specifically ω-3 PUFA, which also acts as natural ligands for PPAR alpha.

The effect of propionate, a likely end-product of alpha-oxidation of OCSFA, merits discussion. Propionate has been shown to induce satiety and anti-inflammation in adipocytes by stimulating leptin [420] and GPR41/GPR43 receptors [421, 422]. It has also been shown to reduce fatty liver in a six month dietary intervention study of people with NAFLD [423]. In monocytes, it has been shown to reduce TNFα secretion induced via TLR1/2 as well as IL-6 induced via TLR4, but not LPS stimulated TNFα via TLR4 [424]; showing that propionate production does not wholly explain the anti-inflammatory properties of C15:0 (at least in monocytes). It is important to mention briefly the role of the gut microbiota, which produces propionate and other SCFA derivatives as a possible source or consequence of C15:0 mediated anti-inflammatory properties. Propionate is produced by the gut microbiome by several mechanisms including fermentation of fibres and it is directly correlated with C15:0 production. In an animal dietary intervention study where C3H/HeOuJ mice diets were supplemented

with propionate, C15:0 production increased after 22 weeks supplementation, associated with an attenuation of insulin resistance and fatty liver [425]. Consequently, neonates with propionic acidaemia have high circulating levels of C15:0, re-enforcing the link between C15:0 and propionate [77]. Moreover, emerging evidence shows that propionate upregulates PPAR alpha by ERK phosphorylation.

6.2 Conclusion

Taken together, the results obtained here suggest that the anti-inflammatory properties of C15:0 and its protection of hepatocytes from palmitate-induced consequence of insulin resistance is likely mediated via PPAR alpha and although there were observable differences in the abundance of MUFA and ω-3 PUFA between samples, the study was not designed to measure their metabolic impact. This study has also shown that C15:0 predicts fasting blood glucose in a healthy and T2DM cohort. Individuals with T2DM have significantly highly markers of inflammation, which can also be predicted by FAs.

6.3 Future work

Several studies will be required to supplement the work in this thesis. The link between OCSFA and T2DM is becoming well-established in literature. However, many of these studies have been conducted in small groups or as part of a nested cohort. Considering the relatively low abundance of OCSFA in plasma, and their variability, large samples are required to adequately power studies to detect significant associations with markers of inflammation and indices of glucose homeostasis. Moreover, sub-set analyses are challenging and limited by sample sizes. Therefore, a

meta-analysis of current data will be informative in providing a broader view of the associations especially within sub-sets, like people with prediabetes, or with poorly-controlled T2DM with or without complications. In chapter 3, FAME profiles were measured with an optimised GC protocol. GC has been a useful tool in measuring FAME profiles for decades; however, mass spectrometry (MS) is a more sensitive approach for measuring FAME profiles especially with OCSFA and other FAs displaying low abundance. Future work will involve the optimisation of a GC-MS protocol for optimal identification and quantification of OCSFAs. Furthermore, a GC-MS technique will allow quantification of isomers of C15:0 with specific focus on anteiso-C15:0, to differentiate between different sources of C15:0 (diet, de novo lipogenesis, and gut microbiome).

In chapter 4, an attempt was made to identify cellular mechanisms underpinning the differential effects of C15:0 and C16:0 in hepatocytes. Future work will rely on a model of primary hepatocytes owing to the limitations of HepG2 cells as discussed. Furthermore, more robust methodology will be used to measure glucose and lipid homeostasis. The primary aim of the future work on hepatocytes will be to identify the metabolic fate of glucose and FAs after treatment with C15:0. A radioisotope study will be used to determine the metabolic fate of glucose and FAs in primary hepatocyte treated with C15:0. Subsequently, Western blot and MS techniques will be optimised to measure protein concentrations of enzymes identified in gene expression data to confirm downstream regulation and physiologic function. This thesis did not explore the potential modulation of cell surface receptors in hepatocytes by C15:0. Future work will aim to develop western blot and immunoprecipitation techniques to identify key

differences in insulin signalling in cells treated with C15:0, with particular focus on IRS-1/AKT kinase-mediated insulin signalling.

In chapter 5, this study showed that C15:0 displayed some anti-inflammatory properties in LPS stimulated THP-1 cells. Future work should focus on optimising techniques for isolating monocytes from plasma of healthy controls and T2DM to determine the effect of C15:0 on inflammation in both sub-sets. Specifically, the FACs protocol will be optimised to measure CD14 and CD16 expression simultaneously, to determine M1 and M2 monocyte sub-sets. The major focus of future work on monocytes will cover the downstream effect of the competitive activation of GPR120, or downregulation of NF-ƙB via TLRs by C15:0.

7 REFERENCES

1. Menke, A., et al., *Prevalence of and trends in diabetes among adults in the United States, 1988-2012.* Jama, 2015. **314**(10): p. 1021-1029.

2. NCD-RiSC, *Worldwide trends in diabetes since 1980: a pooled analysis of 751 population-based studies with 4·4 million participants.* The Lancet, 2016. **387**(10027): p. 1513-1530.

3. Holden, S.E., et al., *Prevalence, glucose control and relative survival of people with Type 2 diabetes in the UK from 1991 to 2013.* Diabetic Medicine, 2017. **34**(6): p. 770-780.

4. UK, D. *Diabetes in the UK; facts and figure*. 2018 [cited 2018 20/01/2018]; Available from: https://www.diabetes.org.uk/Professionals/Position-statements-reports/Statistics?gclid=Cj0KCQjwnfLVBRCxARIsAPvl82HEXUAZ21WqdFBFs4tQ_0Uzil1Z9Wz5FjObbQ97yEUEq4LgjSwsXR8aAkf5EALw_wcB.

5. Tao, Z., A. Shi, and J. Zhao, *Epidemiological perspectives of diabetes.* Cell biochemistry and biophysics, 2015. **73**(1): p. 181-185.

6. Hex, N., et al., *Estimating the current and future costs of Type 1 and Type 2 diabetes in the UK, including direct health costs and indirect societal and productivity costs.* Diabetic Medicine, 2012. **29**(7): p. 855-862.

7. Inzucchi, S.E., et al., *Management of hyperglycaemia in type 2 diabetes: a patient-centered approach. Position statement of the American Diabetes Association (ADA) and the European Association for the Study of Diabetes (EASD).* Diabetologia, 2012. **55**(6): p. 1577-1596.

8. Association, A.D., *Economic costs of diabetes in the US in 2012.* Diabetes care, 2013. **36**(4): p. 1033-1046.

9. UK, D. *WHAT CAUSES DIABETES?* 2017 1804/2017]; Available from: https://www.diabetes.org.uk/Guide-to-diabetes/Teens/What-is-diabetes/.

10. Pedersen, J.L.M., *Adverse Psychosocial, socioeconomic, and developmental processes and risk of inflammation and type 2 diabetes mellitus in later life*. 2015, Faculty of Health and Medical Sciences, University of Copenhagen.

11. !!! INVALID CITATION !!! [11-17].

12. Fogarty, M.P., et al., *Identification of a regulatory variant that binds FOXA1 and FOXA2 at the CDC123/CAMK1D type 2 diabetes GWAS locus.* PLoS genetics, 2014. **10**(9): p. e1004633.

13. !!! INVALID CITATION !!! [13-15].

14. Ahlqvist, E., et al., *Novel subgroups of adult-onset diabetes and their association with outcomes: a data-driven cluster analysis of six variables.* The Lancet Diabetes & Endocrinology, 2018.

15. !!! INVALID CITATION !!! [15-18].

16. Hruby, A. and F.B. Hu, *The Epidemiology of Obesity: A Big Picture.* PharmacoEconomics, 2015. **33**(7): p. 673-689.

17. Deurenberg, P., M. Yap, and W.A. van Staveren, *Body mass index and percent body fat: a meta analysis among different ethnic groups.* International Journal Of Obesity, 1998. **22**: p. 1164.

18. !!! INVALID CITATION !!! [18-21].

19. NCD-RiSC, *Trends in adult body-mass index in 200 countries from 1975 to 2014: a pooled analysis of 1698 population-based measurement studies with 19·2 million participants.* The Lancet, 2016. **387**(10026): p. 1377-1396.

20. Kelly, T., et al., *Global burden of obesity in 2005 and projections to 2030.* International Journal Of Obesity, 2008. **32**: p. 1431.

21. Wang, Y., et al., *Will All Americans Become Overweight or Obese? Estimating the Progression and Cost of the US Obesity Epidemic.* Obesity, 2008. **16**(10): p. 2323-2330.

22. FAO, *The state of food and agriculture*. 2013.

23. Hawkes, C., *Uneven dietary development: linking the policies and processes of globalization with the nutrition transition, obesity and diet-related chronic diseases.* Globalization and health, 2006. **2**(1): p. 4.

24. Gregg, E.W. and J.E. Shaw, *Global health effects of overweight and obesity*. 2017, Mass Medical Soc.

25. !!! INVALID CITATION !!! [24-28].

26. Colditz, G.A., et al., *Weight gain as a risk factor for clinical diabetes mellitus in women.* Annals of internal medicine, 1995. **122**(7): p. 481-486.

27. !!! INVALID CITATION !!! [27-30].

28. Jung, C.H., W.J. Lee, and K.-H. Song, *Metabolically healthy obesity: a friend or foe?* The Korean Journal of Internal Medicine, 2017. **32**(4): p. 611-621.

29. Gallagher, D., et al., *Adipose tissue distribution is different in type 2 diabetes.* The American Journal of Clinical Nutrition, 2009. **89**(3): p. 807-814.

30. Demerath, E.W., et al., *Visceral adiposity and its anatomical distribution as predictors of the metabolic syndrome and cardiometabolic risk factor levels.* The American journal of clinical nutrition, 2008. **88**(5): p. 1263-1271.

31. Koska, J., et al., *Increased fat accumulation in liver may link insulin resistance with subcutaneous abdominal adipocyte enlargement, visceral adiposity, and hypoadiponectinemia in obese individuals–.* The American Journal of Clinical Nutrition, 2008. **87**(2): p. 295-302.

32. Naukkarinen, J., et al., *Characterising metabolically healthy obesity in weight-discordant monozygotic twins.* Diabetologia, 2014. **57**(1): p. 167-176.

33. Jackson, R., et al., *Impact of glucose ingestion on hepatic and peripheral glucose metabolism in man: an analysis based on simultaneous use of the forearm and double isotope techniques.* The Journal of Clinical Endocrinology & Metabolism, 1986. **63**(3): p. 541-549.

34. Taylor, R., et al., *Direct assessment of liver glycogen storage by 13C nuclear magnetic resonance spectroscopy and regulation of glucose homeostasis after a mixed meal in normal subjects.* The Journal of clinical investigation, 1996. **97**(1): p. 126-132.

35. Thiebaud, D., et al., *The effect of graded doses of insulin on total glucose uptake, glucose oxidation, and glucose storage in man.* Diabetes, 1982. **31**(11): p. 957-963.

36. Kowalski, G.M. and C.R. Bruce, *The regulation of glucose metabolism: implications and considerations for the assessment of glucose homeostasis in rodents.* American Journal of Physiology-Endocrinology and Metabolism, 2014. **307**(10): p. E859-E871.

37. Cherrington, A.D., *Control of glucose uptake and release by the liver in vivo.* Diabetes, 1999. **48**(5): p. 1198.

38. Lim, E.L., et al., *Reversal of type 2 diabetes: normalisation of beta cell function in association with decreased pancreas and liver triacylglycerol.* Diabetologia, 2011. **54**(10): p. 2506-2514.

39. Brøns, C., et al., *Impact of short-term high-fat feeding on glucose and insulin metabolism in young healthy men.* The Journal of Physiology, 2009. **587**(10): p. 2387-2397.

40. Cornier, M.-A., B.C. Bergman, and D.H. Bessesen, *The effects of short-term overfeeding on insulin action in lean and reduced-obese individuals.* Metabolism-Clinical and Experimental, 2006. **55**(9): p. 1207-1214.

41. Berasain, C. and M.A. Avila, *Regulation of hepatocyte identity and quiescence.* Cellular and Molecular Life Sciences, 2015. **72**(20): p. 3831-3851.

42. Yanger, K., et al., *Adult Hepatocytes Are Generated by Self-Duplication Rather than Stem Cell Differentiation.* Cell Stem Cell, 2014. **15**(3): p. 340-349.

43. Chalasani, N., et al., *The diagnosis and management of non-alcoholic fatty liver disease: Practice Guideline by the American Association for the Study of Liver Diseases, American College of Gastroenterology, and the American Gastroenterological Association.* Hepatology, 2012. **55**(6): p. 2005-2023.

44. Masuoka, H.C. and N. Chalasani, *Nonalcoholic fatty liver disease: an emerging threat to obese and diabetic individuals.* Annals of the new York Academy of Sciences, 2013. **1281**(1): p. 106-122.

45. Paschos, P. and K. Paletas, *Non alcoholic fatty liver disease and metabolic syndrome.* Hippokratia, 2009. **13**(1): p. 9.

46. Hamaguchi, M., et al., *The metabolic syndrome as a predictor of nonalcoholic fatty liver disease.* Annals of internal medicine, 2005. **143**(10): p. 722-728.

47. Giorda, C., et al., *Occurrence over time and regression of nonalcoholic fatty liver disease in type 2 diabetes.* Diabetes/metabolism research and reviews, 2017. **33**(4).

48. Marchesini, G., et al., *Nonalcoholic fatty liver, steatohepatitis, and the metabolic syndrome.* Hepatology, 2003. **37**(4): p. 917-923.

49. Yamazaki, H., et al., *Independent association between improvement of nonalcoholic fatty liver disease and reduced incidence of type 2 diabetes.* Diabetes Care, 2015. **38**(9): p. 1673-1679.

50. Portillo-Sanchez, P., et al., *High prevalence of nonalcoholic fatty liver disease in patients with type 2 diabetes mellitus and normal plasma aminotransferase levels.* The Journal of Clinical Endocrinology & Metabolism, 2015. **100**(6): p. 2231-2238.

51. Kasturiratne, A., et al., *Influence of non-alcoholic fatty liver disease on the development of diabetes mellitus.* Journal of gastroenterology and hepatology, 2013. **28**(1): p. 142-147.

52. Gaggini, M., et al., *Non-alcoholic fatty liver disease (NAFLD) and its connection with insulin resistance, dyslipidemia, atherosclerosis and coronary heart disease.* Nutrients, 2013. **5**(5): p. 1544-1560.

53. Bae, J.C., et al., *Combined effect of nonalcoholic fatty liver disease and impaired fasting glucose on the development of type 2 diabetes: a 4-year retrospective longitudinal study.* Diabetes Care, 2011. **34**(3): p. 727-729.

54. Younossi, Z.M., et al., *Global epidemiology of nonalcoholic fatty liver disease—Meta-analytic assessment of prevalence, incidence, and outcomes.* Hepatology, 2016. **64**(1): p. 73-84.

55. Gunn, N.T. and M.L. Shiffman, *The Use of Liver Biopsy in Nonalcoholic Fatty Liver Disease: When to Biopsy and in Whom.* Clinics in liver disease, 2018. **22**(1): p. 109-119.

56. Dai, W., et al., *Prevalence of nonalcoholic fatty liver disease in patients with type 2 diabetes mellitus: A meta-analysis.* Medicine, 2017. **96**(39): p. e8179.

57. Holt, R.I.G., *Diagnosis, epidemiology and pathogenesis of diabetes mellitus: An update for psychiatrists.* British Journal of Psychiatry, 2004. **184**(S47): p. s55-s63.

58. Ginsberg, H.N., *Is the slippery slope from steatosis to steatohepatitis paved with triglyceride or cholesterol?* Cell metabolism, 2006. **4**(3): p. 179-181.

59. Donnelly, K.L., et al., *Sources of fatty acids stored in liver and secreted via lipoproteins in patients with nonalcoholic fatty liver disease.* The Journal of clinical investigation, 2005. **115**(5): p. 1343-1351.

60. Mei, S., et al., *Differential roles of unsaturated and saturated fatty acids on autophagy and apoptosis in hepatocytes.* Journal of Pharmacology and Experimental Therapeutics, 2011. **339**(2): p. 487-498.

61. Borradaile, N.M., et al., *Disruption of endoplasmic reticulum structure and integrity in lipotoxic cell death.* Journal of lipid research, 2006. **47**(12): p. 2726-2737.

62. Deguil, J., et al., *Modulation of Lipid-Induced ER Stress by Fatty Acid Shape.* Traffic, 2011. **12**(3): p. 349-362.

63. Nakamura, S., et al., *Palmitate induces insulin resistance in H4IIEC3 hepatocytes through reactive oxygen species produced by mitochondria.* Journal of Biological Chemistry, 2009. **284**(22): p. 14809-14818.

64. Poulos, A., et al., *Cerebro-hepato-renal (Zellweger) syndrome, adrenoleukodystrophy, and Refsum's disease: plasma changes and skin fibroblast phytanic acid oxidase.* Human genetics, 1985. **70**(2): p. 172-177.

65. Keys, A., J.T. Anderson, and F. Grande, *Serum cholesterol response to changes in the diet: IV. Particular saturated fatty acids in the diet.* Metabolism-Clinical and Experimental, 1965. **14**(7): p. 776-787.

66. Keys, A., J.T. Anderson, and F. Grande, *Prediction of serum-cholesterol responses of man to changes in fats in the diet.* Lancet, 1957. **273**: p. 959-966.

67. Mensink, R.P., et al., *Effects of dietary fatty acids and carbohydrates on the ratio of serum total to HDL cholesterol and on serum lipids and apolipoproteins: a meta-analysis of 60 controlled trials.* The American journal of clinical nutrition, 2003. **77**(5): p. 1146-1155.

68. Ramsden, C.E., et al., *Re-evaluation of the traditional diet-heart hypothesis: analysis of recovered data from Minnesota Coronary Experiment (1968-73).* BMJ, 2016. **353**.

69. Dresner, A., et al., *Effects of free fatty acids on glucose transport and IRS-1-associated phosphatidylinositol 3-kinase activity.* J Clin Invest, 1999. **103**(2): p. 253-9.

70. Reynoso, R., L.M. Salgado, and V. Calderón, *High levels of palmitic acid lead to insulin resistance due to changes in the level of phosphorylation of the insulin receptor and insulin receptor substrate-1*, in *Vascular Biochemistry*. 2003, Springer. p. 155-162.

71. Schenk, S., M. Saberi, and J.M. Olefsky, *Insulin sensitivity: modulation by nutrients and inflammation.* The Journal of clinical investigation, 2008. **118**(9): p. 2992-3002.

72. Gao, D., et al., *The effects of palmitate on hepatic insulin resistance are mediated by NADPH Oxidase 3-derived reactive oxygen species through JNK and p38MAPK pathways.* Journal of Biological Chemistry, 2010. **285**(39): p. 29965-29973.

73. Laliotis, G.P., I. Bizelis, and E. Rogdakis, *Comparative Approach of the de novo Fatty Acid Synthesis (Lipogenesis) between Ruminant and Non Ruminant Mammalian Species: From Biochemical Level to the Main Regulatory Lipogenic Genes.* Current Genomics, 2010. **11**(3): p. 168-183.

74. Mannaerts, G.P., et al., *Peroxisomal lipid degradation via β-and α-oxidation in mammals.* 2000. **32**(1-3): p. 73-87.

75. Wanders, R.J., et al., *Phytanic acid alpha-oxidation, new insights into an old problem: a review.* 2003. **1631**(2): p. 119-135.

76. Forouhi, N.G., et al., *Differences in the prospective association between individual plasma phospholipid saturated fatty acids and incident type 2 diabetes: the EPIC-InterAct case-cohort study.* 2014. **2**(10): p. 810-818.

77. Coker, M., et al., *Plasma total odd-chain fatty acids in the monitoring of disorders of propionate, methylmalonate and biotin metabolism.* Journal of inherited metabolic disease, 1996. **19**(6): p. 743-751.

78. de Oliveira Otto, M.C., et al., *Biomarkers of dairy fatty acids and risk of cardiovascular disease in the multi-ethnic study of atherosclerosis.* Journal of the American Heart Association, 2013. **2**(4): p. e000092.

79. Hodge, A.M., et al., *Plasma phospholipid and dietary fatty acids as predictors of type 2 diabetes: interpreting the role of linoleic acid–.* The American journal of clinical nutrition, 2007. **86**(1): p. 189-197.

80. Khaw, K.-T., et al., *Plasma Phospholipid Fatty Acid Concentration and Incident Coronary Heart Disease in Men and Women: The EPIC-Norfolk Prospective Study.* PLoS Medicine, 2012. **9**(7): p. e1001255.

81. Meikle, P.J., et al., *Plasma lipid profiling shows similar associations with prediabetes and type 2 diabetes.* PloS one, 2013. **8**(9): p. e74341.

82. Mock, D.M., S.B. Johnson, and R.T. Holman, *Effects of biotin deficiency on serum fatty acid composition: evidence for abnormalities in humans.* The Journal of nutrition, 1988. **118**(3): p. 342-348.

83. Moser, H.W., et al., *Adrenoleukodystrophy.* Neurology, 1981. **31**(10): p. 1241.

84. Holman, R.T., et al., *Patients with anorexia nervosa demonstrate deficiencies of selected essential fatty acids, compensatory changes in nonessential fatty acids and decreased fluidity of plasma lipids.* The Journal of nutrition, 1995. **125**(4): p. 901-907.

85. Jenkins, B.J., et al., *Odd Chain Fatty Acids; New Insights of the Relationship Between the Gut Microbiota, Dietary Intake, Biosynthesis and Glucose Intolerance.* Scientific Reports, 2017. **7**: p. 44845.

86. Frayn, K.N., P. Arner, and H.J.E.i.b. Yki-Järvinen, *Fatty acid metabolism in adipose tissue, muscle and liver in health and disease.* 2006. **42**: p. 89-103.

87. Harwood, J.L.J.A.R.o.P.P. and P.M. Biology, *Fatty acid metabolism.* 1988. **39**(1): p. 101-138.

88. Veerkamp, J. and H. Van Moerkerk, *Fatty acid-binding protein and its relation to fatty acid oxidation*, in *Cellular Fatty Acid-Binding Proteins II*. 1993, Springer. p. 101-106.

89. Kerner, J., C.J.B.e.B.A.-M. Hoppel, and C.B.o. Lipids, *Fatty acid import into mitochondria.* 2000. **1486**(1): p. 1-17.

90. Wanders, R.J., J. Komen, and S.J.T.F.j. Kemp, *Fatty acid omega-oxidation as a rescue pathway for fatty acid oxidation disorders in humans.* 2011. **278**(2): p. 182-194.

91. Wanders, R., et al., *Peroxisomal fatty acid α-and β-oxidation in humans: enzymology, peroxisomal metabolite transporters and peroxisomal diseases*. 2001, Portland Press Limited.

92. Guillou, H., et al., *The key roles of elongases and desaturases in mammalian fatty acid metabolism: Insights from transgenic mice.* 2010. **49**(2): p. 186-199.

93. Blasiole, D.A., R.A. Davis, and A.D.J.M.b. Attie, *The physiological and molecular regulation of lipoprotein assembly and secretion.* 2007. **3**(9): p. 608-619.

94. Byrne, C.D. and G.J.J.o.h. Targher, *NAFLD: a multisystem disease.* 2015. **62**(1): p. S47-S64.

95. Schwarz, J.-M., et al., *Short-term alterations in carbohydrate energy intake in humans. Striking effects on hepatic glucose production, de novo lipogenesis, lipolysis, and whole-body fuel selection.* 1995. **96**(6): p. 2735-2743.

96. Ameer, F., et al., *De novo lipogenesis in health and disease.* 2014. **63**(7): p. 895-902.

97. Acheson, K., et al., *Glycogen storage capacity and de novo lipogenesis during massive carbohydrate overfeeding in man.* 1988. **48**(2): p. 240-247.

98. Chong, M.F., et al., *Parallel activation of de novo lipogenesis and stearoyl-CoA desaturase activity after 3 d of high-carbohydrate feeding.* 2008. **87**(4): p. 817-823.

99. Marques-Lopes, I., et al., *Postprandial de novo lipogenesis and metabolic changes induced by a high-carbohydrate, low-fat meal in lean and overweight men.* 2001. **73**(2): p. 253-261.

100. Hellerstein, M.K., J.-M. Schwarz, and R.A.J.A.r.o.n. Neese, *Regulation of hepatic de novo lipogenesis in humans.* 1996. **16**(1): p. 523-557.

101. Schreurs, M., F. Kuipers, and F.J.o.r. Van Der Leij, *Regulatory enzymes of mitochondrial β-oxidation as targets for treatment of the metabolic syndrome.* 2010. **11**(5): p. 380-388.

102. Kohjima, M., et al., *SREBP-1c, regulated by the insulin and AMPK signaling pathways, plays a role in nonalcoholic fatty liver disease.* 2008. **21**(4): p. 507-511.

103. Lewis, G.F., et al., *Disordered fat storage and mobilization in the pathogenesis of insulin resistance and type 2 diabetes.* Endocrine reviews, 2002. **23**(2): p. 201-229.

104. Jeong, Y.-S., et al., *Integrated Expression Profiling and Genome-Wide Analysis of ChREBP Targets Reveals the Dual Role for ChREBP in Glucose-Regulated Gene Expression*. Vol. 6. 2011. e22544.

105. Lee, Y.S., J. Wollam, and J.M. Olefsky, *An Integrated View of Immunometabolism.* Cell, 2018. **172**(1): p. 22-40.

106. Williamson, R.T., *On the Treatment of Glycosuria and Diabetes Mellitus with Sodium Salicylate.* British Medical Journal, 1901. **1**(2100): p. 760-762.

107. Reid, J., A.I. Macdougall, and M.M. Andrews, *Aspirin and Diabetes Mellitus.* British Medical Journal, 1957. **2**(5053): p. 1071-1074.

108. Yuan, M., et al., *Reversal of Obesity- and Diet-Induced Insulin Resistance with Salicylates or Targeted Disruption of Ikkβ.* Science, 2001. **293**(5535): p. 1673-1677.

109. Arkan, M.C., et al., *IKK-β links inflammation to obesity-induced insulin resistance.* Nature Medicine, 2005. **11**: p. 191.

110. Baron, S.H., *Salicylates as hypoglycemic agents.* Diabetes Care, 1982. **5**(1): p. 64-71.

111. Wasko, M.C., et al., *Diabetes mellitus and insulin resistance in patients with rheumatoid arthritis: Risk reduction in a chronic inflammatory disease.* Arthritis Care & Research, 2011. **63**(4): p. 512-521.

112. Asterholm, I.W., et al., *Adipocyte Inflammation is Essential for Healthy Adipose Tissue Expansion and Remodeling.* Cell metabolism, 2014. **20**(1): p. 103-118.

113. Hotamisligil, G.S., N.S. Shargill, and B.M. Spiegelman, *Adipose expression of tumor necrosis factor-alpha: direct role in obesity-linked insulin resistance.* Science, 1993. **259**(5091): p. 87-91.

114. Uysal, K.T., et al., *Protection from obesity-induced insulin resistance in mice lacking TNF-α function.* Nature, 1997. **389**(6651): p. 610.

115. de La Serre, C.B., G. de Lartigue, and H.E. Raybould, *Chronic exposure to Low dose bacterial lipopolysaccharide inhibits leptin signaling in vagal afferent neurons().* Physiology & behavior, 2015. **139**: p. 188-194.

116. Münzberg, H., J.S. Flier, and C. Bjørbæk, *Region-Specific Leptin Resistance within the Hypothalamus of Diet-Induced Obese Mice.* Endocrinology, 2004. **145**(11): p. 4880-4889.

117. Schmidt, M.I., et al., *Markers of inflammation and prediction of diabetes mellitus in adults (Atherosclerosis Risk in Communities study): a cohort study.* The Lancet, 1999. **353**(9165): p. 1649-1652.

118. Duncan, B.B., et al., *Low-Grade Systemic Inflammation and the Development of Type 2 Diabetes.* The Atherosclerosis Risk in Communities Study, 2003. **52**(7): p. 1799-1805.

119. Pradhan, A.D., et al., *C-reactive protein, interleukin 6, and risk of developing type 2 diabetes mellitus.* JAMA, 2001. **286**(3): p. 327-334.

120. Festa, A., et al., *Elevated Levels of Acute-Phase Proteins and Plasminogen Activator Inhibitor-1 Predict the Development of Type 2 Diabetes.* The Insulin Resistance Atherosclerosis Study, 2002. **51**(4): p. 1131-1137.

121. Freeman, D.J., et al., *C-Reactive Protein Is an Independent Predictor of Risk for the Development of Diabetes in the West of Scotland Coronary Prevention Study.* Diabetes, 2002. **51**(5): p. 1596-1600.

122. Paz, K., et al., *A molecular basis for insulin resistance elevated serine/threonine phosphorylation of irs-1 and irs-2 inhibits their binding to the juxtamembrane region of the insulin receptor and impairs their ability to undergo insulin-induced tyrosine phosphorylation.* Journal of Biological Chemistry, 1997. **272**(47): p. 29911-29918.

123. Aguirre, V., et al., *Phosphorylation of Ser307 in insulin receptor substrate-1 blocks interactions with the insulin receptor and inhibits insulin action.* Journal of Biological Chemistry, 2002. **277**(2): p. 1531-1537.

124. Aguirre, V., et al., *The c-Jun NH2-terminal kinase promotes insulin resistance during association with insulin receptor substrate-1 and phosphorylation of Ser307.* Journal of Biological Chemistry, 2000. **275**(12): p. 9047-9054.

125. Hotamisligil, G.S., et al., *IRS-1-mediated inhibition of insulin receptor tyrosine kinase activity in TNF-α-and obesity-induced insulin resistance.* Science, 1996. **271**(5249): p. 665-670.

126. Gao, Z., et al., *Inhibition of insulin sensitivity by free fatty acids requires activation of multiple serine kinases in 3T3-L1 adipocytes.* Molecular endocrinology, 2004. **18**(8): p. 2024-2034.

127. Nakatani, Y., et al., *Modulation of the JNK pathway in liver affects insulin resistance status.* Journal of Biological Chemistry, 2004. **279**(44): p. 45803-45809.

128. Hirosumi, J., et al., *A central role for JNK in obesity and insulin resistance.* Nature, 2002. **420**(6913): p. 333.

129. Pérez, S., et al., *Age-dependent regulation of antioxidant genes by p38α MAPK in the liver.* Redox Biology, 2018. **16**: p. 276-284.

130. Shoelson, S.E., J. Lee, and A.B. Goldfine, *Inflammation and insulin resistance.* Journal of Clinical Investigation, 2006. **116**(7): p. 1793-1801.

131. Parisi, L., et al., *Macrophage polarization in chronic inflammatory diseases: Killers or builders?* 2018. **2018**.

132. Xue, W., et al., *The chemokine system and its role in obesity.* 2019. **234**(4): p. 3336-3346.

133. Patel, P.S., E.D. Buras, and A.J.J.o.o. Balasubramanyam, *The role of the immune system in obesity and insulin resistance.* 2013. **2013**.

134. Grage-Griebenow, E., H.D. Flad, and M.J.J.o.l.b. Ernst, *Heterogeneity of human peripheral blood monocyte subsets.* 2001. **69**(1): p. 11-20.

135. Skrzeczyńska-Moncznik, J., et al., *Peripheral blood CD14high CD16+ monocytes are main producers of IL-10.* 2008. **67**(2): p. 152-159.

136. Fadini, G., et al., *An unbalanced monocyte polarisation in peripheral blood and bone marrow of patients with type 2 diabetes has an impact on microangiopathy.* 2013. **56**(8): p. 1856-1866.

137. Stew, S.S., et al., *Differential expression of monocyte surface markers among TB patients with diabetes co-morbidity.* 2013. **93**: p. S78-S82.

138. Verschoor, C.P., et al., *Alterations to the frequency and function of peripheral blood monocytes and associations with chronic disease in the advanced-age, frail elderly.* 2014. **9**(8): p. e104522.

139. Mukherjee, R., et al., *Non-classical monocytes display inflammatory features: validation in sepsis and systemic lupus erythematous.* 2015. **5**: p. 13886.

140. Italiani, P. and D.J.F.i.i. Boraschi, *From monocytes to M1/M2 macrophages: phenotypical vs. functional differentiation.* 2014. **5**: p. 514.

141. Mantovani, A., et al., *The chemokine system in diverse forms of macrophage activation and polarization.* 2004. **25**(12): p. 677-686.

142. Rőszer, T.J.M.o.i., *Understanding the mysterious M2 macrophage through activation markers and effector mechanisms.* 2015. **2015**.

143. Lumeng, C.N., J.L. Bodzin, and A.R. Saltiel, *Obesity induces a phenotypic switch in adipose tissue macrophage polarization.* The Journal of clinical investigation, 2007. **117**(1): p. 175-184.

144. Lumeng, C.N., et al., *Phenotypic Switching of Adipose Tissue Macrophages With Obesity Is Generated by Spatiotemporal Differences in Macrophage Subtypes.* Diabetes, 2008. **57**(12): p. 3239-3246.

145. Fujisaka, S., et al., *Regulatory Mechanisms for Adipose Tissue M1 and M2 Macrophages in Diet-Induced Obese Mice.* Diabetes, 2009. **58**(11): p. 2574-2582.

146. Patsouris, D., et al., *Ablation of CD11c-Positive Cells Normalizes Insulin Sensitivity in Obese Insulin Resistant Animals.* Cell Metabolism. **8**(4): p. 301-309.

147. Weisberg, S.P., et al., *Obesity is associated with macrophage accumulation in adipose tissue.* The Journal of Clinical Investigation, 2003. **112**(12): p. 1796-1808.

148. Klöting, N., et al., *Insulin-sensitive obesity.* American Journal of Physiology-Endocrinology and Metabolism, 2010. **299**(3): p. E506-E515.

149. Zeyda, M., et al., *Human adipose tissue macrophages are of an anti-inflammatory phenotype but capable of excessive pro-inflammatory mediator production.* International journal of obesity, 2007. **31**(9): p. 1420.

150. Tordjman, J., et al., *Association between omental adipose tissue macrophages and liver histopathology in morbid obesity: Influence of glycemic status.* Journal of Hepatology. **51**(2): p. 354-362.

151. Fjeldborg, K., et al., *Human adipose tissue macrophages are enhanced but changed to an anti-inflammatory profile in obesity.* Journal of immunology research, 2014. **2014**.

152. Berger, J. and D.E.J.A.r.o.m. Moller, *The mechanisms of action of PPARs.* 2002. **53**(1): p. 409-435.

153. Haluzik, M. and M.J.P.r. Haluzik, *PPAR-alpha and insulin sensitivity.* 2006. **55**(2): p. 115.

154. Fruchart, J.-C., P. Duriez, and B.J.C.o.i.l. Staels, *Peroxisome proliferator-activated receptor-alpha activators regulate genes governing lipoprotein metabolism, vascular inflammation and atherosclerosis.* 1999. **10**(3): p. 245-257.

155. Grygiel-Górniak, B.J.N.j., *Peroxisome proliferator-activated receptors and their ligands: nutritional and clinical implications-a review.* 2014. **13**(1): p. 17.

156. Elisaf, M.J.C.m.r. and opinion, *Effects of fibrates on serum metabolic parameters.* 2002. **18**(5): p. 269-276.

157. Zhou, Y.-C. and D.J. Waxman, *STAT5b Down-regulates peroxisome proliferator-activated receptor α transcription by inhibition of ligand-independent activation function region-1trans-activation domain.* Journal of Biological Chemistry, 1999. **274**(42): p. 29874-29882.

158. Patel, H., et al., *Activity and subcellular compartmentalization of peroxisome proliferator-activated receptor α are altered by the centrosome-associated protein CAP350.* J Cell Sci, 2005. **118**(1): p. 175-186.

159. McMullen, P.D., et al., *A map of the PPARα transcription regulatory network for primary human hepatocytes.* Chemico-biological interactions, 2014. **209**: p. 14-24.

160. George, C.L., S.L. Lightman, and S.C. Biddie, *Transcription factor interactions in genomic nuclear receptor function.* Epigenomics, 2011. **3**(4): p. 471-485.

161. Burns, K.A., J.P.V.J.B.e.B.A.-M. Heuvel, and C.B.o. Lipids, *Modulation of PPAR activity via phosphorylation.* 2007. **1771**(8): p. 952-960.

162. Wadosky, K.M., M.S.J.A.J.o.P.-H. Willis, and C. Physiology, *The story so far: post-translational regulation of peroxisome proliferator-activated receptors by ubiquitination and SUMOylation.* 2011. **302**(3): p. H515-H526.

163. Patel, H., et al., *Activity and subcellular compartmentalization of peroxisome proliferator-activated receptor α are altered by the centrosome-associated protein CAP350.* 2005. **118**(1): p. 175-186.

164. Chinetti, G., et al., *Activation of proliferator-activated receptors α and γ induces apoptosis of human monocyte-derived macrophages.* Journal of Biological Chemistry, 1998. **273**(40): p. 25573-25580.

165. Bishop-Bailey, D. and T. Hla, *Endothelial cell apoptosis induced by the peroxisome proliferator-activated receptor (PPAR) ligand 15-deoxy-Δ12, 14-prostaglandin J2.* Journal of Biological Chemistry, 1999. **274**(24): p. 17042-17048.

166. Iwamoto, F., et al., *Nuclear transport of peroxisome-proliferator activated receptor α.* 2010. **149**(3): p. 311-319.

167. Umemoto, T. and Y.J.G.t.C. Fujiki, *Ligand-dependent nucleo-cytoplasmic shuttling of peroxisome proliferator-activated receptors, PPARα and PPARγ.* 2012. **17**(7): p. 576-596.

168. Vitale, S.G., et al., *Peroxisome Proliferator-Activated Receptor Modulation during Metabolic Diseases and Cancers: Master and Minions.* PPAR Research, 2016. **2016**: p. 6517313.

169. Yoon, M., *The role of PPARα in lipid metabolism and obesity: Focusing on the effects of estrogen on PPARα actions.* Pharmacological Research, 2009. **60**(3): p. 151-159.

170. More, V.R., et al., *PPAR-α, a lipid-sensing transcription factor, regulates blood–brain barrier efflux transporter expression.* Journal of Cerebral Blood Flow & Metabolism, 2017. **37**(4): p. 1199-1212.

171. Nikolic, D., et al., *PPAR agonists, atherogenic dyslipidemia and cardiovascular risk.* Current pharmaceutical design, 2017. **23**(6): p. 894-902.

172. Ferri, N., et al., *PPAR-α agonists are still on the rise: an update on clinical and experimental findings.* Expert opinion on investigational drugs, 2017. **26**(5): p. 593-602.

173. Feng, X., et al., *PPAR-α agonist fenofibrate decreased RANTES levels in type 2 diabetes patients with hypertriglyceridemia.* Medical science monitor: international medical journal of experimental and clinical research, 2016. **22**: p. 743.

174. Feng, X., et al., *PPAR-α agonist fenofibrate decreased serum irisin levels in type 2 diabetes patients with hypertriglyceridemia.* PPAR research, 2015. **2015**.

175. Derosa, G., A. Sahebkar, and P. Maffioli, *The role of various peroxisome proliferator-activated receptors and their ligands in clinical practice.* Journal of cellular physiology, 2018. **233**(1): p. 153-161.

176. Alisi, A., et al., *Retinoic acid modulates the cell-cycle in fetal rat hepatocytes and HepG2 cells by regulating cyclin-cdk activities.* 2003. **23**(3): p. 179-186.

177. Schaart, G., et al., *A modified PAS stain combined with immunofluorescence for quantitative analyses of glycogen in muscle sections.* 2004. **122**(2): p. 161-169.

178. Livak, K.J. and T.D.J.m. Schmittgen, *Analysis of relative gene expression data using real-time quantitative PCR and the 2− ΔΔCT method.* 2001. **25**(4): p. 402-408.

179. Bertoglia, M.P., et al., *The population impact of obesity, sedentary lifestyle, and tobacco and alcohol consumption on the prevalence of type 2 diabetes: Analysis of a health population survey in Chile, 2010.* PLoS One, 2017. **12**(5): p. e0178092.

180. Kizilgul, M., et al., *Effect of Intrapancreatic Fat on Diabetes Outcomes After Total Pancreatectomy with Islet Autotransplantation.* Journal of diabetes, 2017.

181. Lee, S.-H., et al., *High-throughput screening and bioinformatic analysis to ascertain compounds that prevent saturated fatty acid-induced β-cell apoptosis.* Biochemical pharmacology, 2017. **138**: p. 140-149.

182. Kahn, S., *The relative contributions of insulin resistance and beta-cell dysfunction to the pathophysiology of type 2 diabetes.* Diabetologia, 2003. **46**(1): p. 3-19.

183. Group, D.P.P.R., *Reduction in the incidence of type 2 diabetes with lifestyle intervention or metformin.* New England journal of medicine, 2002. **346**(6): p. 393-403.

184. Pan, X.-R., et al., *Effects of diet and exercise in preventing NIDDM in people with impaired glucose tolerance: the Da Qing IGT and Diabetes Study.* Diabetes care, 1997. **20**(4): p. 537-544.

185. Kashyap, S.R., et al., *Metabolic effects of bariatric surgery in patients with moderate obesity and type 2 diabetes: analysis of a randomized control trial comparing surgery with intensive medical treatment.* Diabetes care, 2013. **36**(8): p. 2175-2182.

186. Mingrone, G., et al., *Bariatric surgery versus conventional medical therapy for type 2 diabetes.* New England Journal of Medicine, 2012. **366**(17): p. 1577-1585.

187. Courcoulas, A.P., et al., *Surgical vs medical treatments for type 2 diabetes mellitus: a randomized clinical trial.* JAMA surgery, 2014. **149**(7): p. 707-715.

188. Sjöström, L., et al., *Association of bariatric surgery with long-term remission of type 2 diabetes and with microvascular and macrovascular complications.* Jama, 2014. **311**(22): p. 2297-2304.

189. Teodoro, J.S., et al., *Uncovering the beginning of diabetes: the cellular redox status and oxidative stress as starting players in hyperglycemic damage.* Molecular and cellular biochemistry, 2013. **376**(1-2): p. 103-110.

190. Xavier Heshka Stanley, M.A.S.G.o.t.L.A.R.G.G.D.d.c.e.K.D.E.Y.J.-E.S.N.A.J.B.L.P.-S.F., *Adipose tissue distribution is different in type 2 diabetes–.* The American journal of clinical nutrition, 2009. **89**(3): p. 807-814.

191. Demerath, E.W., et al., *Visceral adiposity and its anatomical distribution as predictors of the metabolic syndrome and cardiometabolic risk factor levels–.* The American journal of clinical nutrition, 2008. **88**(5): p. 1263-1271.

192. Esposito, K., et al., *The effects of a Mediterranean diet on the need for diabetes drugs and remission of newly diagnosed type 2 diabetes: follow-up of a randomized trial.* Diabetes care, 2014. **37**(7): p. 1824-1830.

193. Chiva-Blanch, G., L. Badimon, and R. Estruch, *Latest evidence of the effects of the Mediterranean diet in prevention of cardiovascular disease.* Current atherosclerosis reports, 2014. **16**(10): p. 446.

194. Salas-Salvadó, J., et al., *Reduction in the incidence of type 2 diabetes with the Mediterranean diet: results of the PREDIMED-Reus nutrition intervention randomized trial.* Diabetes care, 2011. **34**(1): p. 14-19.

195. Camell, C. and C.W. Smith, *Dietary oleic acid increases m2 macrophages in the mesenteric adipose tissue.* PloS one, 2013. **8**(9): p. e75147.

196. Gao, D., H.R. Griffiths, and C.J. Bailey, *Oleate protects against palmitate-induced insulin resistance in L6 myotubes.* British journal of nutrition, 2009. **102**(11): p. 1557-1563.

197. Gao, D., et al., *Palmitate promotes monocyte atherogenicity via de novo ceramide synthesis.* Free radical biology and medicine, 2012. **53**(4): p. 796-806.

198. Namgaladze, D., et al., *AICAR inhibits PPARγ during monocyte differentiation to attenuate inflammatory responses to atherogenic lipids.* Cardiovascular research, 2013. **98**(3): p. 479-487.

199. Guillou, H., et al., *The key roles of elongases and desaturases in mammalian fatty acid metabolism: Insights from transgenic mice.* Progress in lipid research, 2010. **49**(2): p. 186-199.

200. Kröger, J., et al., *Erythrocyte membrane phospholipid fatty acids, desaturase activity, and dietary fatty acids in relation to risk of type 2 diabetes in the European Prospective Investigation into Cancer and Nutrition (EPIC)–Potsdam Study–.* The American journal of clinical nutrition, 2010. **93**(1): p. 127-142.

201. Henriksen, E.J., M.K. Diamond-Stanic, and E.M. Marchionne, *Oxidative stress and the etiology of insulin resistance and type 2 diabetes.* Free Radical Biology and Medicine, 2011. **51**(5): p. 993-999.

202. Forbes, J.M. and M.E. Cooper, *Mechanisms of diabetic complications.* Physiological reviews, 2013. **93**(1): p. 137-188.

203. Tuomilehto, J. and J. Lindström, *The major diabetes prevention trials.* Current Diabetes Reports, 2003. **3**(2): p. 115-122.

204. Noble, D., et al., *Risk models and scores for type 2 diabetes: systematic review.* Bmj, 2011. **343**: p. d7163.

205. Jenkins, B., J.A. West, and A. Koulman, *A review of odd-chain fatty acid metabolism and the role of pentadecanoic acid (C15: 0) and heptadecanoic acid (C17: 0) in health and disease.* Molecules, 2015. **20**(2): p. 2425-2444.

206. Forouhi, N.G., et al., *Differences in the prospective association between individual plasma phospholipid saturated fatty acids and incident type 2 diabetes: the EPIC-InterAct case-cohort study.* The Lancet. Diabetes & Endocrinology, 2014. **2**(10): p. 810-818.

207. De Souza, R.J., et al., *Intake of saturated and trans unsaturated fatty acids and risk of all cause mortality, cardiovascular disease, and type 2 diabetes: systematic review and meta-analysis of observational studies.* Bmj, 2015. **351**: p. h3978.

208. Rana, K.S., et al., *Plasma irisin is elevated in type 2 diabetes and is associated with increased E-selectin levels.* Cardiovascular diabetology, 2017. **16**(1): p. 147.

209. Zheng, J.-S., et al., *Change in plasma phospholipid fatty acids over 13 years and determinants of change: EPIC-Norfolk Study.* The FASEB Journal, 2017. **31**(1 Supplement): p. 646.28-646.28.

210. Dijkstra, J., et al., *Relationships between methane production and milk fatty acid profiles in dairy cattle.* Animal Feed Science and Technology, 2011. **166**: p. 590-595.

211. Weitkunat, K., et al., *Odd-chain fatty acids as a biomarker for dietary fiber intake: a novel pathway for endogenous production from propionate, 2.* The American journal of clinical nutrition, 2017. **105**(6): p. 1544-1551.

212. Venäläinen, T.M., M.A. Lankinen, and U.S. Schwab, *Odd-chain fatty acids as dietary biomarkers for fiber and fish intake.* The American journal of clinical nutrition, 2017. **106**(3): p. 954-954.

213. Gijsbers, L., et al., *Consumption of dairy foods and diabetes incidence: a dose-response meta-analysis of observational studies, 2.* The American journal of clinical nutrition, 2016. **103**(4): p. 1111-1124.

214. Dewhurst, R., et al., *Apparent recovery of duodenal odd-and branched-chain fatty acids in milk of dairy cows.* Journal of dairy science, 2007. **90**(4): p. 1775-1780.

215. Fievez, V., et al., *Milk odd-and branched-chain fatty acids as biomarkers of rumen function—An update.* Animal Feed Science and Technology, 2012. **172**(1-2): p. 51-65.

216. Roberts, L.D., et al., *Metabolic phenotyping of a model of adipocyte differentiation.* Physiological genomics, 2009. **39**(2): p. 109-119.

217. Hodson, L., et al., *Plasma and Erythrocyte Fatty Acids Reflect Intakes of Saturated and n–6 PUFA within a Similar Time Frame–3.* The Journal of nutrition, 2013. **144**(1): p. 33-41.

218. Bechmann, L.P., et al., *The interaction of hepatic lipid and glucose metabolism in liver diseases.* Journal of hepatology, 2012. **56**(4): p. 952-964.

219. LeCluyse, E.L. and E. Alexandre, *Isolation and culture of primary hepatocytes from resected human liver tissue*, in *Hepatocytes*. 2010, Springer. p. 57-82.

220. Li, A.P., *Human hepatocytes: isolation, cryopreservation and applications in drug development.* Chemico-biological interactions, 2007. **168**(1): p. 16-29.

221. Soldatow, V.Y., et al., *In vitro models for liver toxicity testing.* Toxicology research, 2013. **2**(1): p. 23-39.

222. Leffert, H., et al., *Growth state-dependent phenotypes of adult hepatocytes in primary monolayer culture.* Proceedings of the National Academy of Sciences, 1978. **75**(4): p. 1834-1838.

223. Rogue, A., et al., *Inter-individual variability in gene expression profiles in human hepatocytes and comparison with HepaRG cells.* Drug Metabolism and Disposition, 2011: p. dmd. 111.042028.

224. Wilkening, S., F. Stahl, and A. Bader, *Comparison of primary human hepatocytes and hepatoma cell line Hepg2 with regard to their biotransformation properties.* Drug metabolism and disposition, 2003. **31**(8): p. 1035-1042.

225. Westerink, W.M. and W.G. Schoonen, *Phase II enzyme levels in HepG2 cells and cryopreserved primary human hepatocytes and their induction in HepG2 cells.* Toxicology in vitro, 2007. **21**(8): p. 1592-1602.

226. Ikehara, T., et al., *Different responses of primary normal human hepatocytes and human hepatoma cells toward cyanobacterial hepatotoxin microcystin-LR.* Toxicon, 2015. **105**: p. 4-9.

227. Sison-Young, R.L., et al., *A multicenter assessment of single-cell models aligned to standard measures of cell health for prediction of acute hepatotoxicity.* Archives of toxicology, 2017. **91**(3): p. 1385-1400.

228. Wiśniewski, J.R., et al., *In-depth quantitative analysis and comparison of the human hepatocyte and hepatoma cell line HepG2 proteomes.* Journal of proteomics, 2016. **136**: p. 234-247.

229. Rodriguez-Antona, C., et al., *Cytochrome P450 expression in human hepatocytes and hepatoma cell lines: molecular mechanisms that determine lower expression in cultured cells.* Xenobiotica, 2002. **32**(6): p. 505-520.

230. Green, C.J., et al., *From whole body to cellular models of hepatic triglyceride metabolism: man has got to know his limitations.* American Journal of Physiology - Endocrinology and Metabolism, 2015. **308**(1): p. E1-E20.

231. Nikolaou, N., et al., *Optimizing human hepatocyte models for metabolic phenotype and function: effects of treatment with dimethyl sulfoxide (DMSO).* Physiological Reports, 2016. **4**(21): p. e12944.

232. Burley, M.R. and C.M. Roth, *Effects of Retinoic Acid on Proliferation and Differentiation of HepG2 Cells.* The Open Biotechnology Journal, 2007. **1**(1).

233. Nakanishi, M., et al., *Identification of transcriptional regulatory cascades in retinoic acid-induced growth arrest of HepG2 cells.* Nucleic Acids Research, 2008. **36**(10): p. 3443-3454.

234. Kelly, J.H., *Permanent human hepatocyte cell line and its use in a liver assist device (LAD)*, U. Patent, Editor. 1994: US.

235. Kim, D.-S., et al., *Metformin regulates palmitate-induced apoptosis and ER stress response in HepG2 liver cells.* Immunopharmacology and immunotoxicology, 2010. **32**(2): p. 251-257.

236. Tailleux, A., K. Wouters, and B. Staels, *Roles of PPARs in NAFLD: potential therapeutic targets.* Biochimica et Biophysica Acta (BBA)-Molecular and Cell Biology of Lipids, 2012. **1821**(5): p. 809-818.

237. Gross, B., et al., *PPARs in obesity-induced T2DM, dyslipidaemia and NAFLD.* Nature Reviews Endocrinology, 2017. **13**(1): p. 36.

238. Liss, K.H. and B.N. Finck, *PPARs and nonalcoholic fatty liver disease.* Biochimie, 2017. **136**: p. 65-74.

239. Wang, N., et al., *Peroxisome Proliferator-Activated Receptors Associated with Nonalcoholic Fatty Liver Disease.* PPAR Research, 2017. **2017**.

240. Pineda, I.T., P. Gervois, and B. Staels, *Peroxisome proliferator-activated receptor alpha in metabolic disease, inflammation, atherosclerosis and aging.* Current opinion in lipidology, 1999. **10**(2): p. 151-159.

241. Kota, B.P., T.H.-W. Huang, and B.D. Roufogalis, *An overview on biological mechanisms of PPARs.* Pharmacological Research, 2005. **51**(2): p. 85-94.

242. Martin, G., et al., *Coordinate regulation of the expression of the fatty acid transport protein and acyl-CoA synthetase genes by PPARα and PPARγ activators.* Journal of Biological Chemistry, 1997. **272**(45): p. 28210-28217.

243. Stahl, A., *A current review of fatty acid transport proteins (SLC27).* Pflügers Archiv, 2004. **447**(5): p. 722-727.

244. Guérin, M., et al., *Fenofibrate reduces plasma cholesteryl ester transfer from HDL to VLDL and normalizes the atherogenic, dense LDL profile in combined hyperlipidemia.* Arteriosclerosis, thrombosis, and vascular biology, 1996. **16**(6): p. 763-772.

245. Nakaya, N. and Y. Goto, *A retrospective meta-analysis of the efficacy and tolerability of fenofibrate 300 mg/d on high-density lipoprotein cholesterol levels in randomized, double-blind, comparative studies conducted in Japan().* Current Therapeutic Research, Clinical and Experimental, 2003. **64**(8): p. 634-644.

246. Ip, E., et al., *Administration of the potent PPARα agonist, Wy-14,643, reverses nutritional fibrosis and steatohepatitis in mice.* Hepatology, 2004. **39**(5): p. 1286-1296.

247. Beraza, N., et al., *Pharmacological IKK2 inhibition blocks liver steatosis and initiation of non-alcoholic steatohepatitis.* Gut, 2008. **57**(5): p. 655-663.

248. Jeong, S. and M. Yoon, *Fenofibrate inhibits adipocyte hypertrophy and insulin resistance by activating adipose PPARα in high fat diet-induced obese mice.* Experimental & molecular medicine, 2009. **41**(6): p. 397.

249. Idzior-Waluś, B., *Fibrate influence on lipids and insulin resistance in patients with metabolic syndrome.* Przeglad lekarski, 2001. **58**(10): p. 924-927.

250. Rizos, E., et al., *Effect of ciprofibrate on C-reactive protein and fibrinogen levels.* Angiology, 2002. **53**(3): p. 273-277.

251. Grygiel-Górniak, B., *Peroxisome proliferator-activated receptors and their ligands: nutritional and clinical implications–a review.* Nutrition journal, 2014. **13**(1): p. 1.

252. Pararasa, C., et al., *Age-associated changes in long-chain fatty acid profile during healthy aging promote pro-inflammatory monocyte polarization via PPARγ.* Aging Cell, 2016. **15**(1): p. 128-139.

253. Benjamini, Y. and D.J.T.a.o.s. Yekutieli, *The control of the false discovery rate in multiple testing under dependency.* 2001. **29**(4): p. 1165-1188.

254. Clarke, S. and P.J.T.A.o.S. Hall, *Robustness of multiple testing procedures against dependence.* 2009. **37**(1): p. 332-358.

255. Farcomeni, A.J.S.m.i.m.r., *A review of modern multiple hypothesis testing, with particular attention to the false discovery proportion.* 2008. **17**(4): p. 347-388.

256. Groppe, D.M., T.P. Urbach, and M.J.P. Kutas, *Mass univariate analysis of event-related brain potentials/fields I: A critical tutorial review.* 2011. **48**(12): p. 1711-1725.

257. Gerets, H., et al., *Characterization of primary human hepatocytes, HepG2 cells, and HepaRG cells at the mRNA level and CYP activity in response to inducers and their predictivity for the detection of human hepatotoxins.* Cell biology and toxicology, 2012. **28**(2): p. 69-87.

258. Mukherjee, R., et al., *Assay for PPAR ligand dependent gene modulation*. 2004, Google Patents.

259. Gao, Y., et al., *Upregulation of hepatic VLDLR via PPARα is required for the triglyceride-lowering effect of fenofibrate.* 2014. **55**(8): p. 1622-1633.

260. Chung, S.T., et al., *Increased gluconeogenesis in youth with newly diagnosed type 2 diabetes.* Diabetologia, 2015. **58**(3): p. 596-603.

261. Nurjhan, N., A. Consoli, and J. Gerich, *Increased lipolysis and its consequences on gluconeogenesis in non-insulin-dependent diabetes mellitus.* Journal of Clinical Investigation, 1992. **89**(1): p. 169.

262. Boden, G. and X. Chen, *Effects of fat on glucose uptake and utilization in patients with non-insulin-dependent diabetes.* Journal of Clinical Investigation, 1995. **96**(3): p. 1261.

263. Alisi, A., et al., *Retinoic acid modulates the cell-cycle in fetal rat hepatocytes and HepG2 cells by regulating cyclin-cdk activities.* Liver international, 2003. **23**(3): p. 179-186.

264. Suzui, M., et al., *Acyclic retinoid activates retinoic acid receptor β and induces transcriptional activation of p21CIP1 in HepG2 human hepatoma cells.* Molecular cancer therapeutics, 2004. **3**(3): p. 309-316.

265. Zhu, X., et al., *All-trans retinoic acid-induced deficiency of the Wnt/β-catenin pathway enhances hepatic carcinoma stem cell differentiation.* PloS one, 2015. **10**(11): p. e0143255.

266. Liu, H., et al., *A novel all-trans retinoic acid derivative 4-amino-2-trifluoromethyl-phenyl retinate inhibits the proliferation of human hepatocellular carcinoma HepG2 cells by inducing G0/G1 cell cycle arrest and apoptosis via upregulation of p53 and ASPP1 and downregulation of iASPP.* Oncology reports, 2016. **36**(1): p. 333-341.

267. He, Y., et al., *Low serum concentration facilitates the differentiation of hepatic progenitor cells.* Saudi medical journal, 2011. **32**(2): p. 128-134.

268. Pramfalk, C., et al., *Culturing of HepG2 cells with human serum improve their functionality and suitability in studies of lipid metabolism.* Biochimica et Biophysica Acta (BBA)-Molecular and Cell Biology of Lipids, 2016. **1861**(1): p. 51-59.

269. Amengual, J., et al., *Induction of carnitine palmitoyl transferase 1 and fatty acid oxidation by retinoic acid in HepG2 cells.* The International Journal of Biochemistry & Cell Biology, 2012. **44**(11): p. 2019-2027.

270. Gomez-Quiroz, L., et al., *Interleukin 8 response and oxidative stress in HepG2 cells treated with ethanol, acetaldehyde or lipopolysaccharide.* Hepatology research, 2003. **26**(2): p. 134-141.

271. Gutierrez-Ruiz, M., et al., *Cytokine response and oxidative stress produced by ethanol, acetaldehyde and endotoxin treatment in HepG2 cells.* The Israel Medical Association journal: IMAJ, 2001. **3**(2): p. 131-136.

272. Yang, H.-C., et al., *Glucose 6-phosphate dehydrogenase knockdown enhances IL-8 expression in HepG2 cells via oxidative stress and NF-κB signaling pathway.* Journal of Inflammation, 2015. **12**(1): p. 34.

273. Shi, H., et al., *TLR4 links innate immunity and fatty acid–induced insulin resistance.* The Journal of clinical investigation, 2006. **116**(11): p. 3015-3025.

274. Szabo, G., et al., *Modulation of Non-Alcoholic Steatohepatitis by Pattern Recognition Receptors in Mice: The Role of Toll-Like Receptors 2 and 4.* Alcoholism: Clinical and Experimental Research, 2005. **29**(s2).

275. Luo, X., et al., *Docosahexaenoic acid ameliorates palmitate-induced lipid accumulation and inflammation through repressing NLRC4 inflammasome activation in HepG2 cells.* Nutrition & metabolism, 2012. **9**(1): p. 34.

276. Paumen, M.B., et al., *Inhibition of carnitine palmitoyltransferase I augments sphingolipid synthesis and palmitate-induced apoptosis.* Journal of Biological Chemistry, 1997. **272**(6): p. 3324-3329.

277. Day, C.P. and O.F. James, *Steatohepatitis: a tale of two "hits"?* Gastroenterology, 1998. **114**(4): p. 842-845.

278. Schaffer, J.E., *Lipotoxicity: when tissues overeat.* Current opinion in lipidology, 2003. **14**(3): p. 281-287.

279. Coll, T., et al., *Oleate reverses palmitate-induced insulin resistance and inflammation in skeletal muscle cells.* Journal of biological chemistry, 2008. **283**(17): p. 11107-11116.

280. Peng, G., et al., *Oleate blocks palmitate-induced abnormal lipid distribution, endoplasmic reticulum expansion and stress, and insulin resistance in skeletal muscle.* Endocrinology, 2011. **152**(6): p. 2206-2218.

281. Mahendran, Y., et al., *Association of erythrocyte membrane fatty acids with changes in glycemia and risk of type 2 diabetes.* The American journal of clinical nutrition, 2014: p. ajcn. 069740.

282. Kröger, J., et al., *Erythrocyte membrane phospholipid fatty acids, desaturase activity, and dietary fatty acids in relation to risk of type 2 diabetes in the European Prospective Investigation into Cancer and Nutrition–Potsdam Study.* The American journal of clinical nutrition, 2010: p. ajcn. 005447.

283. Krachler, B., et al., *Fatty acid profile of the erythrocyte membrane preceding development of Type 2 diabetes mellitus.* Nutrition, Metabolism and Cardiovascular Diseases, 2008. **18**(7): p. 503-510.

284. Faas, F., et al., *Red blood cell and plasma fatty acid composition in diabetes mellitus.* Metabolism, 1988. **37**(8): p. 711-713.

285. Ma, W., et al., *Prospective association of fatty acids in the de novo lipogenesis pathway with risk of type 2 diabetes: the Cardiovascular Health Study.* The American journal of clinical nutrition, 2015. **101**(1): p. 153-163.

286. Lee, H.-J., et al., *The dietary monounsaturated to saturated fatty acid ratio modulates the genetic effects of GCKR on serum lipid levels in children.* Clinica Chimica Acta, 2015. **450**: p. 155-161.

287. Duarte-Salles, T., et al., *Dietary fat, fat subtypes and hepatocellular carcinoma in a large European cohort.* International Journal of Cancer, 2015. **137**(11): p. 2715-2728.

288. O'Reilly, M., et al., *High-Density Lipoprotein Proteomic Composition, and not Efflux Capacity, Reflects Differential Modulation of Reverse Cholesterol Transport by Saturated and Monounsaturated Fat Diets.* Circulation, 2016. **133**(19): p. 1838-1850.

289. Li, Y., et al., *Saturated fats compared with unsaturated fats and sources of carbohydrates in relation to risk of coronary heart disease: a prospective cohort study.* Journal of the American College of Cardiology, 2015. **66**(14): p. 1538-1548.

290. Samuel, V.T., et al., *Mechanism of hepatic insulin resistance in non-alcoholic fatty liver disease.* Journal of Biological Chemistry, 2004. **279**(31): p. 32345-32353.

291. Ibrahim, S.H., et al., *Glycogen synthase kinase-3 (GSK-3) inhibition attenuates hepatocyte lipoapoptosis.* Journal of hepatology, 2011. **54**(4): p. 765-772.

292. Cao, J., et al., *Saturated free fatty acid sodium palmitate-induced lipoapoptosis by targeting glycogen synthase kinase-3β activation in human liver cells.* Digestive diseases and sciences, 2014. **59**(2): p. 346-357.

293. Bouskila, M., et al., *Insulin promotes glycogen synthesis in the absence of GSK3 phosphorylation in skeletal muscle.* American Journal of Physiology-Endocrinology and Metabolism, 2008. **294**(1): p. E28-E35.

294. Postic, C., et al., *Evidence for a transient inhibitory effect of insulin on GLUT2 expression in the liver: studies in vivo and in vitro.* Biochemical Journal, 1993. **293**(Pt 1): p. 119.

295. Pu, J., et al., *Palmitic acid acutely stimulates glucose uptake via activation of Akt and ERK1/2 in skeletal muscle cells.* Journal of lipid research, 2011. **52**(7): p. 1319-1327.

296. Abraham, P., et al., *Increased hepatic gluconeogenesis and decreased glucose uptake, and increased hepatic de novo lipogenesis in rat model of maternal diabetes.* Biomedical Research, 2016. **27**(3).

297. Guillam, M.-T., R. Burcelin, and B. Thorens, *Normal hepatic glucose production in the absence of GLUT2 reveals an alternative pathway for glucose release from hepatocytes.* Proceedings of the National Academy of Sciences, 1998. **95**(21): p. 12317-12321.

298. Strable, M.S. and J.M. Ntambi, *Genetic control of de novo lipogenesis: role in diet-induced obesity.* Critical reviews in biochemistry and molecular biology, 2010. **45**(3): p. 199-214.

299. Lee, J.-y., H.-K. Cho, and Y.H. Kwon, *Palmitate induces insulin resistance without significant intracellular triglyceride accumulation in HepG2 cells.* Metabolism, 2010. **59**(7): p. 927-934.

300. Ress, C. and S. Kaser, *Mechanisms of intrahepatic triglyceride accumulation.* World journal of gastroenterology, 2016. **22**(4): p. 1664.

301. Wilson, C.G., et al., *Hepatocyte-specific disruption of CD36 attenuates fatty liver and improves insulin sensitivity in HFD-fed mice.* Endocrinology, 2015. **157**(2): p. 570-585.

302. Koonen, D.P., et al., *Increased hepatic CD36 expression contributes to dyslipidemia associated with diet-induced obesity.* Diabetes, 2007. **56**(12): p. 2863-2871.

303. Steneberg, P., et al., *Hyperinsulinemia enhances hepatic expression of the fatty acid transporter Cd36 and provokes hepatosteatosis and hepatic insulin resistance.* Journal of Biological Chemistry, 2015. **290**(31): p. 19034-19043.

304. Bonen, A., et al., *Regulation of fatty acid transport by fatty acid translocase/CD36.* Proceedings of the Nutrition Society, 2004. **63**(2): p. 245-249.

305. Krammer, J., et al., *Overexpression of CD36 and acyl-CoA synthetases FATP2, FATP4 and ACSL1 increases fatty acid uptake in human hepatoma cells.* International journal of medical sciences, 2011. **8**(7): p. 599.

306. Aguilera, A.A., et al., *Induction of Cd36 expression elicited by fish oil PUFA in spontaneously hypertensive rats.* The Journal of nutritional biochemistry, 2006. **17**(11): p. 760-765.

307. Chen, C.S.-Y., et al., *Preference for linoleic acid in obesity-prone and obesity-resistant rats is attenuated by the reduction of CD36 on the tongue.* American Journal of Physiology-Regulatory, Integrative and Comparative Physiology, 2013. **305**(11): p. R1346-R1355.

308. Hostetler, H.A., et al., *L-FABP directly interacts with PPARα in cultured primary hepatocytes.* Journal of lipid research, 2009. **50**(8): p. 1663-1675.

309. Wolfrum, C., et al., *Fatty acids and hypolipidemic drugs regulate peroxisome proliferator-activated receptors α- and γ-mediated gene expression via liver fatty acid binding protein: A signaling path to the nucleus.* Proceedings of the National Academy of Sciences, 2001. **98**(5): p. 2323-2328.

310. Bruce, C.R., et al., *Overexpression of carnitine palmitoyltransferase-1 in skeletal muscle is sufficient to enhance fatty acid oxidation and improve high-fat diet–induced insulin resistance.* Diabetes, 2009. **58**(3): p. 550-558.

311. Malandrino, M.I., et al., *Enhanced fatty acid oxidation in adipocytes and macrophages reduces lipid-induced triglyceride accumulation and inflammation.* American Journal of Physiology-Endocrinology and Metabolism, 2015. **308**(9): p. E756-E769.

312. Bonnefont, J.-P., et al., *Carnitine palmitoyltransferases 1 and 2: biochemical, molecular and medical aspects.* Molecular aspects of medicine, 2004. **25**(5-6): p. 495-520.

313. Wicks, S.E., et al., *Impaired mitochondrial fat oxidation induces adaptive remodeling of muscle metabolism.* Proceedings of the National Academy of Sciences, 2015. **112**(25): p. E3300-E3309.

314. Dzamko, N., et al., *AMPK-independent pathways regulate skeletal muscle fatty acid oxidation.* The Journal of physiology, 2008. **586**(23): p. 5819-5831.

315. Bhattacharjee, S., et al., *Fenofibrate reverses palmitate induced impairment in glucose uptake in skeletal muscle cells by preventing cytosolic ceramide accumulation.* Cellular Physiology and Biochemistry, 2015. **37**(4): p. 1315-1328.

316. Hellemans, K., et al., *Peroxisome proliferator-activated receptor α–retinoid X receptor agonists induce beta-cell protection against palmitate toxicity.* The FEBS journal, 2007. **274**(23): p. 6094-6105.

317. Bergouignan, A., et al., *Physical inactivity differentially alters dietary oleate and palmitate trafficking.* Diabetes, 2009. **58**(2): p. 367-376.

318. Thörn, K. and P. Bergsten, *Fatty acid-induced oxidation and triglyceride formation is higher in insulin-producing MIN6 cells exposed to oleate compared to palmitate.* Journal of cellular biochemistry, 2010. **111**(2): p. 497-507.

319. Louet, J., et al., *Long-chain fatty acids regulate liver carnitine palmitoyltransferase I gene (L-CPT I) expression through a peroxisome-proliferator-activated receptor alpha (PPARalpha)-independent pathway.* Biochemical Journal, 2001. **354**(Pt 1): p. 189.

320. Voegel, J.J., et al., *TIF2, a 160 kDa transcriptional mediator for the ligand-dependent activation function AF-2 of nuclear receptors.* The EMBO journal, 1996. **15**(14): p. 3667-3675.

321. Beischlag, T.V., et al., *Recruitment of the NCoA/SRC-1/p160 family of transcriptional coactivators by the aryl hydrocarbon receptor/aryl hydrocarbon receptor nuclear translocator complex.* Molecular and cellular biology, 2002. **22**(12): p. 4319-4333.

322. Chou, C.J., et al., *WY14, 643, a peroxisome proliferator-activated receptor α (PPARα) agonist, improves hepatic and muscle steatosis and reverses insulin resistance in lipoatrophic A-ZIP/F-1 mice.* Journal of Biological Chemistry, 2002. **277**(27): p. 24484-24489.

323. Guerre-Millo, M., et al., *Peroxisome proliferator-activated receptor α activators improve insulin sensitivity and reduce adiposity.* Journal of Biological Chemistry, 2000. **275**(22): p. 16638-16642.

324. Staels, B., et al., *Mechanism of action of fibrates on lipid and lipoprotein metabolism.* Circulation, 1998. **98**(19): p. 2088-2093.

325. Massaro, M., et al., *Therapeutic potential of the dual peroxisome proliferator activated receptor (PPAR) α/γ agonist aleglitazar in attenuating TNF-α-mediated inflammation and insulin resistance in human adipocytes.* Pharmacological research, 2016. **107**: p. 125-136.

326. Baker, R.G., M.S. Hayden, and S. Ghosh, *NF-κB, inflammation, and metabolic disease.* Cell metabolism, 2011. **13**(1): p. 11-22.

327. Chawla, A., K.D. Nguyen, and Y.S. Goh, *Macrophage-mediated inflammation in metabolic disease.* Nature Reviews Immunology, 2011. **11**(11): p. 738.

328. Kahn, S.E., R.L. Hull, and K.M. Utzschneider, *Mechanisms linking obesity to insulin resistance and type 2 diabetes.* Nature, 2006. **444**(7121): p. 840.

329. Donath, M.Y. and S.E. Shoelson, *Type 2 diabetes as an inflammatory disease.* Nature Reviews Immunology, 2011. **11**(2): p. 98.

330. Xu, H., et al., *Chronic inflammation in fat plays a crucial role in the development of obesity-related insulin resistance.* The Journal of clinical investigation, 2003. **112**(12): p. 1821-1830.

331. Esser, N., et al., *Inflammation as a link between obesity, metabolic syndrome and type 2 diabetes.* Diabetes research and clinical practice, 2014. **105**(2): p. 141-150.

332. Wilkins, J., et al., *Systemic Inflammation Mediates the Relationship between Obesity and Health Related Quality of Life.* bioRxiv, 2017: p. 231720.

333. Visser, M., et al., *Elevated C-reactive protein levels in overweight and obese adults.* Jama, 1999. **282**(22): p. 2131-2135.

334. Suri, S.R., A.R.O. Siddiqui, and M. Manikanta, *Assessment of inflammatory markers and lipid profile levels in normotensive, primary hypertensive and secondary hypertensive male obese individuals.* Journal of Evolution of Medical and Dental Sciences, 2015. **4**(98): p. 16337-16341.

335. Nicholas, D.A., et al., *Palmitic acid is a toll-like receptor 4 ligand that induces human dendritic cell secretion of IL-1β.* PloS one, 2017. **12**(5): p. e0176793.

336. Garibotto, G., et al., *Toll-like receptor-4 signaling mediates inflammation and tissue injury in diabetic nephropathy.* Journal of nephrology, 2017. **30**(6): p. 719-727.

337. Akira, S. and K. Takeda, *Toll-like receptor signalling.* Nature reviews immunology, 2004. **4**(7): p. 499.

338. Tang, M., et al., *Toll-like receptor 2 activation promotes tumor dendritic cell dysfunction by regulating IL-6 and IL-10 receptor signaling.* Cell reports, 2015. **13**(12): p. 2851-2864.

339. Jiménez-Dalmaroni, M.J., M.E. Gerswhin, and I.E. Adamopoulos, *The critical role of toll-like receptors—from microbial recognition to autoimmunity: a comprehensive review.* Autoimmunity reviews, 2016. **15**(1): p. 1-8.

340. Hwang, D.H., J.-A. Kim, and J.Y. Lee, *Mechanisms for the activation of Toll-like receptor 2/4 by saturated fatty acids and inhibition by docosahexaenoic acid.* European journal of pharmacology, 2016. **785**: p. 24-35.

341. Takashima, A., et al., *N-3 Polyunsaturated Fatty Acids Inhibit Inflammatory Responses in Macrophages by the Reduction of Toll-like Receptor 4 Expression in Lipid Rafts, Leading to the Suppression of Atherogenesis in Apolipoprotein E Deficient Mice*. 2015, Am Heart Assoc.

342. Honda, K.L., et al., *EPA and DHA Exposure Alters the Inflammatory Response but not the Surface Expression of Toll-like Receptor 4 in Macrophages.* Lipids, 2015. **50**(2): p. 121-129.

343. Yang, J., et al., *Monocyte and macrophage differentiation: circulation inflammatory monocyte as biomarker for inflammatory diseases.* Biomarker research, 2014. **2**(1): p. 1.

344. Wang, Y., et al., *A nonclassical monocyte phenotype in peripheral blood is associated with nonalcoholic fatty liver disease: a report from an EMIL subcohort.* 2015.

345. Connaughton, E.P., et al., *Phenotypic and functional heterogeneity of human intermediate monocytes based on HLA-DR expression.* Immunology & Cell Biology, 2018.

346. Bhattacharya, S. and S. Mukherjee, *Lipid links inflammation, immunity and insulin resistance to cause epidemic diabetes.* Current Science, 2016. **110**(10): p. 1922.

347. Kraakman, M.J., et al., *Macrophage polarization in obesity and type 2 diabetes: weighing down our understanding of macrophage function?* Frontiers in immunology, 2014. **5**: p. 470.

348. Ohashi, K., et al., *Adiponectin promotes macrophage polarization toward an anti-inflammatory phenotype.* Journal of Biological Chemistry, 2010. **285**(9): p. 6153-6160.

349. Ziegler-Heitbrock, L., et al., *Nomenclature of monocytes and dendritic cells in blood.* Blood, 2010. **116**(16): p. e74-e80.

350. Ong, S.-M., et al., *The pro-inflammatory phenotype of the human non-classical monocyte subset is attributed to senescence.* Cell death & disease, 2018. **9**(3): p. 266.

351. Chimen, M., et al., *Monocyte subsets co-regulate inflammatory responses by integrated signalling through TNF and IL-6 at the endothelial cell interface.* Journal of immunology (Baltimore, Md. : 1950), 2017. **198**(7): p. 2834-2843.

352. Boyette, L.B., et al., *Phenotype, function, and differentiation potential of human monocyte subsets.* PLoS ONE, 2017. **12**(4): p. e0176460.

353. Poitou, C., et al., *CD14dimCD16+ and CD14+ CD16+ monocytes in obesity and during weight loss: relationships with fat mass and subclinical atherosclerosis.* Arteriosclerosis, thrombosis, and vascular biology, 2011. **31**(10): p. 2322-2330.

354. Martinez, F.O., et al., *Macrophage activation and polarization.* Frontiers in bioscience: a journal and virtual library, 2008. **13**: p. 453-461.

355. Jetten, N., et al., *Anti-inflammatory M2, but not pro-inflammatory M1 macrophages promote angiogenesis in vivo.* Angiogenesis, 2014. **17**(1): p. 109-118.

356. Pararasa, C., *Fatty acids, monocytes and ageing*. 2013, Aston University.

357. Phillips, D.C., K.J. Woollard, and H.R. Griffiths, *The anti-inflammatory actions of methotrexate are critically dependent upon the production of reactive oxygen species.* British journal of pharmacology, 2003. **138**(3): p. 501-511.

358. Taylor, P.R. and S. Gordon, *Monocyte heterogeneity and innate immunity.* Immunity, 2003. **19**(1): p. 2-4.

359. Mantovani, A. and A. Sica, *Macrophages, innate immunity and cancer: balance, tolerance, and diversity.* Current opinion in immunology, 2010. **22**(2): p. 231-237.

360. Akash, M.S.H., K. Rehman, and S. Chen, *Role of inflammatory mechanisms in pathogenesis of type 2 diabetes mellitus.* Journal of cellular biochemistry, 2013. **114**(3): p. 525-531.

361. Herder, C., et al., *Low-grade inflammation, obesity, and insulin resistance in adolescents.* The Journal of Clinical Endocrinology & Metabolism, 2007. **92**(12): p. 4569-4574.

362. Qin, Z., *The use of THP-1 cells as a model for mimicking the function and regulation of monocytes and macrophages in the vasculature.* Atherosclerosis, 2012. **221**(1): p. 2-11.

363. Chanput, W., J.J. Mes, and H.J. Wichers, *THP-1 cell line: an in vitro cell model for immune modulation approach.* International immunopharmacology, 2014. **23**(1): p. 37-45.

364. Heil, T., et al., *Human peripheral blood monocytes versus THP-1 monocytes for in vitro biocompatibility testing of dental material components.* Journal of oral rehabilitation, 2002. **29**(5): p. 401-407.

365. Schildberger, A., et al., *Monocytes, peripheral blood mononuclear cells, and THP-1 cells exhibit different cytokine expression patterns following stimulation with lipopolysaccharide.* Mediators of inflammation, 2013. **2013**.

366. Park, B.S. and J.-O. Lee, *Recognition of lipopolysaccharide pattern by TLR4 complexes.* Experimental & molecular medicine, 2013. **45**(12): p. e66.

367. Borzęcka, K., et al., *CD14 mediates binding of high doses of LPS but is dispensable for TNF-α production.* Mediators of inflammation, 2013. **2013**.

368. Saresella, M., et al., *Immunological and Clinical Effect of Diet Modulation of the Gut Microbiome in Multiple Sclerosis Patients: A Pilot Study.* Frontiers in Immunology, 2017. **8**: p. 1391.

369. Kim, S.-M., et al., *27-Hydroxycholesterol up-regulates CD14 and predisposes monocytic cells to superproduction of CCL2 in response to lipopolysaccharide.* Biochimica et Biophysica Acta (BBA)-Molecular Basis of Disease, 2015. **1852**(3): p. 442-450.

370. Keeney, M., et al., *Isotype controls in the analysis of lymphocytes and CD34+ stem and progenitor cells by flow cytometry—time to let go?* Cytometry Part A, 1998. **34**(6): p. 280-283.

371. Maecker, H.T. and J. Trotter, *Flow cytometry controls, instrument setup, and the determination of positivity.* Cytometry Part A, 2006. **69**(9): p. 1037-1042.

372. Hulspas, R., et al., *Considerations for the control of background fluorescence in clinical flow cytometry.* Cytometry Part B: Clinical Cytometry, 2009. **76**(6): p. 355-364.

373. Andersen, M.N., et al., *Elimination of erroneous results in flow cytometry caused by antibody binding to Fc receptors on human monocytes and macrophages.* Cytometry Part A, 2016. **89**(11): p. 1001-1009.

374. Frey, T. and A. De Maio, *Increased expression of CD14 in macrophages after inhibition of the cholesterol biosynthetic pathway by lovastatin.* Molecular Medicine, 2007. **13**(11-12): p. 592.

375. Alshahrani, A., et al., *Phenotypic Characterization of Human Monocytes following Macronutrient Intake in Healthy Humans.* Frontiers in Immunology, 2017. **8**: p. 1293.

376. Belge, K.-U., et al., *The proinflammatory CD14+ CD16+ DR++ monocytes are a major source of TNF.* The Journal of Immunology, 2002. **168**(7): p. 3536-3542.

377. Skinner, N., et al., *Regulation of Toll-like receptor (TLR) 2 and TLR4 on CD14dimCD16+ monocytes in response to sepsis-related antigens.* Clinical & Experimental Immunology, 2005. **141**(2): p. 270-278.

378. Zezina, E., et al., *Mitochondrial fragmentation in human macrophages attenuates palmitate-induced inflammatory responses.* Biochimica et Biophysica Acta (BBA)-Molecular and Cell Biology of Lipids, 2018. **1863**(4): p. 433-446.

379. Ann, S.-j., et al., *Palmitate and minimally-modified low-density lipoprotein cooperatively promote inflammatory responses in macrophages.* PloS one, 2018. **13**(3): p. e0193649.

380. Yin, J., et al., *Toll-like receptor 2/4 links to free fatty acid-induced inflammation and β-cell dysfunction.* Journal of leukocyte biology, 2014. **95**(1): p. 47-52.

381. Sindhu, S., et al., *Palmitate-induced MMP-9 expression in the human monocytic cells is mediated through the TLR4-MyD88 dependent mechanism.* Cellular Physiology and Biochemistry, 2016. **39**(3): p. 889-900.

382. Givan, A.L., *Flow cytometry: first principles*. 2013: John Wiley & Sons.

383. Maecker, H.T., et al., *A model for harmonizing flow cytometry in clinical trials.* Nature immunology, 2010. **11**(11): p. 975.

384. Heidenreich, S., *Monocyte CD14: a multifunctional receptor engaged in apoptosis from both sides.* Journal of leukocyte biology, 1999. **65**(6): p. 737-743.

385. Fingerle-Rowson, G., et al., *Down-regulation of surface monocyte lipopolysaccharide-receptor CD14 in patients on cardiopulmonary bypass undergoing aorta-coronary bypass operation.* The Journal of thoracic and cardiovascular surgery, 1998. **115**(5): p. 1172-1178.

386. Ziegler-Heitbrock, L., *Blood monocytes and their subsets: established features and open questions.* Frontiers in immunology, 2015. **6**: p. 423.

387. Liu, J., et al., *Palmitate promotes autophagy and apoptosis through ROS-dependent JNK and p38 MAPK.* Biochemical and biophysical research communications, 2015. **463**(3): p. 262-267.

388. Sadeghi, A., et al., *Resveratrol Ameliorates Palmitate-Induced Inflammation in Skeletal Muscle Cells by Attenuating Oxidative Stress and JNK/NF-κB Pathway in a SIRT1-Independent Mechanism.* Journal of cellular biochemistry, 2017. **118**(9): p. 2654-2663.

389. Seeßle, J., et al., *Palmitate activation by fatty acid transport protein 4 as a model system for hepatocellular apoptosis and steatosis.* Biochimica et Biophysica Acta (BBA)-Molecular and Cell Biology of Lipids, 2015. **1851**(5): p. 549-565.

390. Machado, M., et al., *Caspase-2 promotes obesity, the metabolic syndrome and nonalcoholic fatty liver disease.* Cell death & disease, 2017. **7**(2): p. e2096.

391. Listenberger, L.L., D.S. Ory, and J.E. Schaffer, *Palmitate-induced apoptosis can occur through a ceramide-independent pathway.* Journal of Biological Chemistry, 2001. **276**(18): p. 14890-14895.

392. De Pablo, M., et al., *Palmitate induces apoptosis via a direct effect on mitochondria.* Apoptosis, 1999. **4**(2): p. 81-87.

393. Kim, H.J., S.H. Kim, and J.-M. Yun, *Fisetin inhibits hyperglycemia-induced proinflammatory cytokine production by epigenetic mechanisms.* Evidence-Based Complementary and Alternative Medicine, 2012. **2012**.

394. Kang, Y.E., et al., *The roles of adipokines, proinflammatory cytokines, and adipose tissue macrophages in obesity-associated insulin resistance in modest obesity and early metabolic dysfunction.* PloS one, 2016. **11**(4): p. e0154003.

395. Lyons, C.L., E.B. Kennedy, and H.M. Roche, *Metabolic inflammation-differential modulation by dietary constituents.* Nutrients, 2016. **8**(5): p. 247.

396. Davis, J.E., et al., *Tlr-4 deficiency selectively protects against obesity induced by diets high in saturated fat.* Obesity, 2008. **16**(6): p. 1248-1255.

397. Youssef-Elabd, E.M., et al., *Acute and chronic saturated fatty acid treatment as a key instigator of the TLR-mediated inflammatory response in human adipose tissue, in vitro.* The Journal of nutritional biochemistry, 2012. **23**(1): p. 39-50.

398. Khaw, K.-T., et al., *Plasma phospholipid fatty acid concentration and incident coronary heart disease in men and women: the EPIC-Norfolk prospective study.* PLoS Med, 2012. **9**(7): p. e1001255.

399. Nestel, P.J., et al., *Specific plasma lipid classes and phospholipid fatty acids indicative of dairy food consumption associate with insulin sensitivity.* The American Journal of Clinical Nutrition, 2014. **99**(1): p. 46-53.

400. Kurotani, K., et al., *Even- and odd-chain saturated fatty acids in serum phospholipids are differentially associated with adipokines.* PLoS ONE, 2017. **12**(5): p. e0178192.

401. Abedi, E. and M.A. Sahari, *Long-chain polyunsaturated fatty acid sources and evaluation of their nutritional and functional properties.* Food science & nutrition, 2014. **2**(5): p. 443-463.

402. Makarov, P., et al., *Consumption of redox energy by glutathione metabolism contributes to hypoxia/reoxygenation-induced injury in astrocytes.* Molecular and cellular biochemistry, 2006. **286**(1-2): p. 95-101.

403. van Meerloo, J., G.J. Kaspers, and J. Cloos, *Cell sensitivity assays: the MTT assay*, in *Cancer cell culture*. 2011, Springer. p. 237-245.

404. Chapkin, R.S., et al., *Dietary n− 3 PUFA alter colonocyte mitochondrial membrane composition and function.* Lipids, 2002. **37**(2): p. 193.

405. Garrel, C., et al., *Omega-3 fatty acids enhance mitochondrial superoxide dismutase activity in rat organs during post-natal development.* The international journal of biochemistry & cell biology, 2012. **44**(1): p. 123-131.

406. Marei, W.F., D.C. Wathes, and A.A. Fouladi-Nashta, *Differential effects of linoleic and alpha-linolenic fatty acids on spatial and temporal mitochondrial distribution and activity in bovine oocytes.* Reproduction, Fertility and Development, 2012. **24**(5): p. 679-690.

407. Song, B.-J., et al., *Prevention of alcoholic fatty liver and mitochondrial dysfunction in the rat by long-chain polyunsaturated fatty acids.* Journal of hepatology, 2008. **49**(2): p. 262-273.

408. Ochoa, J.J., et al., *Coenzyme Q10 protects from aging-related oxidative stress and improves mitochondrial function in heart of rats fed a polyunsaturated fatty acid (PUFA)-rich diet.* The Journals of Gerontology Series A: Biological Sciences and Medical Sciences, 2005. **60**(8): p. 970-975.

409. Quiles, J.L., et al., *Ageing-related tissue-specific alterations in mitochondrial composition and function are modulated by dietary fat type in the rat.* Journal of bioenergetics and biomembranes, 2002. **34**(6): p. 517-524.

410. Battino, M. and M.S. Ferreiro, *Ageing and the Mediterranean diet: a review of the role of dietary fats.* Public health nutrition, 2004. **7**(7): p. 953-958.

411. Yuzefovych, L.V., et al., *Protection from palmitate-induced mitochondrial DNA damage prevents from mitochondrial oxidative stress, mitochondrial dysfunction, apoptosis, and impaired insulin signaling in rat L6 skeletal muscle cells.* Endocrinology, 2012. **153**(1): p. 92-100.

412. Egnatchik, R.A., et al., *ER calcium release promotes mitochondrial dysfunction and hepatic cell lipotoxicity in response to palmitate overload.* Molecular metabolism, 2014. **3**(5): p. 544-553.

413. Bonnard, C., et al., *Mitochondrial dysfunction results from oxidative stress in the skeletal muscle of diet-induced insulin-resistant mice.* The Journal of clinical investigation, 2008. **118**(2): p. 789-800.

414. Pfeuffer, M. and A. Jaudszus, *Pentadecanoic and heptadecanoic acids: multifaceted odd-chain fatty acids.* Advances in Nutrition, 2016. **7**(4): p. 730-734.

415. Park, M.J., et al., *Anaplerotic triheptanoin diet enhances mitochondrial substrate use to remodel the metabolome and improve lifespan, motor function, and sociability in MeCP2-null mice.* PLoS One, 2014. **9**(10): p. e109527.

416. Bazhan, N.M., et al., *Expression of genes involved in carbohydrate-lipid metabolism in muscle and fat tissues in the initial stage of adult-age obesity in fed and fasted mice.* Physiological Reports, 2017. **5**(19): p. e13445.

417. Fujiwara, N., et al., *CPT2 downregulation adapts HCC to lipid-rich environment and promotes carcinogenesis via acylcarnitine accumulation in obesity.* Gut, 2018.

418. Bougarne, N., et al., *PPARα blocks glucocorticoid receptor α-mediated transactivation but cooperates with the activated glucocorticoid receptor α for transrepression on NF-κB.* Proceedings of the National Academy of Sciences, 2009. **106**(18): p. 7397-7402.

419. Delerive, P., et al., *Peroxisome proliferator-activated receptor α negatively regulates the vascular inflammatory gene response by negative cross-talk with transcription factors NF-κB and AP-1.* Journal of Biological Chemistry, 1999. **274**(45): p. 32048-32054.

420. Roelofsen, H., M. Priebe, and R. Vonk, *The interaction of short-chain fatty acids with adipose tissue: relevance for prevention of type 2 diabetes.* Beneficial microbes, 2010. **1**(4): p. 433-437.

421. Ang, Z. and J.L. Ding, *GPR41 and GPR43 in Obesity and Inflammation – Protective or Causative?* Frontiers in Immunology, 2016. **7**: p. 28.

422. Inoue, D., G. Tsujimoto, and I. Kimura, *Regulation of Energy Homeostasis by GPR41.* Frontiers in Endocrinology, 2014. **5**: p. 81.

423. Edward Chambers, D., et al., *Effects of Elevating Colonic Propionate on Liver Fat Content in Adults with Non-Alcoholic Fatty Liver Disease.* The FASEB Journal, 2015. **29**(1_supplement): p. 385.2.

424. Ciarlo, E., et al., *Impact of the microbial derived short chain fatty acid propionate on host susceptibility to bacterial and fungal infections in vivo.* Scientific Reports, 2016. **6**: p. 37944.

425. Weitkunat, K., et al., *Importance of propionate for the repression of hepatic lipogenesis and improvement of insulin sensitivity in high-fat diet-induced obesity.* Molecular Nutrition & Food Research, 2016. **60**(12): p. 2611-2621.

8 APPENDICES

Table 8.8.1: Correlation matrix

		Age	BMI	Visc Fat score	FASTING BLOOD Glucose	sol thrombomodulin ng/ml	E-selectin ng/ml	CRP ug/ml	Protein Carbonyl	Leptin
Age	Pearson Correlation	1	0.216	.755**	.298*	0.065	-0.126	.287*	.348**	.348**
	Sig. (2-tailed)		0.100	0.000	0.021	0.620	0.336	0.026	0.006	0.007
		96	95	94	96	96	96	96	96	95
BMI	Pearson Correlation	0.216	1	.722**	0.246	0.051	0.231	.291*	.290*	.276*
	Sig. (2-tailed)	0.100		0.000	0.060	0.703	0.079	0.026	0.026	0.036
		95	95	94	95	95	95	95	94	94
Visc Fat score	Pearson Correlation	.755**	.722**	1	.407**	0.179	-0.004	.332*	.348**	.434**
	Sig. (2-tailed)	0.000	0.000		0.002	0.178	0.977	0.011	0.007	0.001
		96	95	94	96	96	96	96	96	95
FASTING BLOOD Glucose	Pearson Correlation	.298*	0.246	.407**	1	.417**	.318*	0.229	0.220	.630**
	Sig. (2-tailed)	0.021	0.060	0.002		0.001	0.013	0.078	0.091	0.000
		96	95	94	96	96	96	96	96	95

		Age	BMI	Visc Fat score	FASTING BLOOD Glucose	sol thrombomodulin ng/ml	E-selectin ng/ml	CRP ug/ml	Protein Carbonyl	Leptin
sol thrombomodulin ng/ml	Pearson Correlation	0.065	0.051	0.179	.417**	1	0.240	-0.230	-0.112	.560**
	Sig. (2-tailed)	0.620	0.703	0.178	0.001		0.065	0.077	0.392	0.000
		96	95	94	96	96	96	96	96	95
E-selectin ng/ml	Pearson Correlation	-0.126	0.231	-0.004	.318*	0.240	1	0.070	0.063	0.205
	Sig. (2-tailed)	0.336	0.079	0.977	0.013	0.065		0.595	0.632	0.119
		96	95	94	96	96	96	96	96	95
CRP ug/ml	Pearson Correlation	.287*	.291*	.332*	0.229	-0.230	0.070	1	.489**	0.143
	Sig. (2-tailed)	0.026	0.026	0.011	0.078	0.077	0.595		0.000	0.280
		96	95	94	96	96	96	96	96	95
Protein Carbonyl	Pearson Correlation	.348**	.290*	.348**	0.220	-0.112	0.063	.489**	1	.274*
	Sig. (2-tailed)	0.006	0.026	0.007	0.091	0.392	0.632	0.000		0.035
		96	95	94	96	96	96	96	96	95
Leptin	Pearson Correlation	.348**	.276*	.434**	.630**	.560**	0.205	0.143	.274*	1

	Age	BMI	Visc Fat score	FASTING BLOOD Glucose	sol thrombomodulin ng/ml	E-selectin ng/ml	CRP ug/ml	Protein Carbonyl	Leptin
Sig. (2-tailed)	0.007	0.036	0.001	0.000	0.000	0.119	0.280	0.035	
	95	94	93	95	95	95	95	95	95

Table 8.8.2: Parameter estimates for CRP

Parameter Estimates											
Parameter	B	Std. Error	95% Wald Confidence Interval		Hypothesis Test			Exp(B)	95% Wald Confidence Interval for Exp(B)		
			Lower	Upper	Wald Chi-Square	df	Sig.		Lower	Upper	
(Intercept)	-7.381	3.0434	-13.346	-1.416	5.881	1	0.015	0.001	1.600E-06	0.243	
C182n6ct_1	0.003	0.0025	-0.002	0.008	1.474	1	0.225	1.003	0.998	1.008	
Age	0.020	0.0278	-0.035	0.074	0.492	1	0.483	1.020	0.966	1.077	
FASTINGBLOODGlucose_1	-0.027	0.1319	-0.286	0.231	0.043	1	0.836	0.973	0.751	1.260	
BMI_1	0.068	0.0610	-0.052	0.188	1.246	1	0.264	1.071	0.950	1.207	
ProteinCarbonyl_1	1.544	0.5774	0.412	2.676	7.149	1	0.007	4.683	1.510	14.520	
LEPTINNgml	-0.128	0.0820	-0.288	0.033	2.418	1	0.120	0.880	0.750	1.034	
Eselectinngml	0.016	0.0219	-0.027	0.059	0.519	1	0.471	1.016	0.973	1.060	
C222_1	0.066	0.0233	0.020	0.112	7.949	1	0.005	1.068	1.020	1.118	
C181n9ct_1	0.002	0.0028	-0.004	0.007	0.386	1	0.535	1.002	0.996	1.007	
(Scale)	8.550[a]	1.5742	5.960	12.266							

Table 8.3: Parameter estimates for soluble thrombomodulin

Parameter Estimates

Parameter	B	Std. Error	95% Wald Confidence Interval		Hypothesis Test			Exp(B)	95% Wald Confidence Interval for Exp(B)	
			Lower	Upper	Wald Chi-Square	df	Sig.		Lower	Upper
(Intercept)	3.484	2.3054	-1.035	8.002	2.284	1	.131	32.587	.355	2988.014
C182n6ct_1	-.004	.0016	-.007	-.001	6.947	1	.008	.996	.993	.999
Age	.006	.0179	-.029	.041	.120	1	.729	1.006	.972	1.042
FASTINGBLOODGlucose_1	.268	.1010	.070	.466	7.019	1	.008	1.307	1.072	1.593
BMI_1	-.011	.0523	-.114	.091	.048	1	.827	.989	.892	1.095
ProteinCarbonyl_1	-.294	.3025	-.887	.298	.947	1	.330	.745	.412	1.348
C183n3_1	.001	.0756	-.147	.150	.000	1	.984	1.001	.864	1.161
C18_1	.022	.0108	.001	.043	4.221	1	.040	1.022	1.001	1.044
LEPTINNgml	.035	.0357	-.034	.105	.988	1	.320	1.036	.966	1.111
CRPugml	-.202	.1163	-.430	.026	3.006	1	.083	.817	.651	1.027
Eselectinngml	.017	.0101	-.003	.037	2.731	1	.098	1.017	.997	1.037
C161_1	-.070	.0226	-.114	-.026	9.569	1	.002	.933	.892	.975
C181n9ct_1	.008	.0036	.001	.015	4.676	1	.031	1.008	1.001	1.015
(Scale)	3.857[a]	.7101	2.688	5.533						

Dependent Variable: SMEAN(solthrombomodulinngml)
Model: (Intercept), C182n6ct_1, Age, FASTINGBLOODGlucose_1, BMI_1, ProteinCarbonyl_1, C183n3_1, C18_1, LEPTINNgml, CRPugml, Eselectinngml, C161_1, C181n9ct_1

a. Maximum likelihood estimate.

Table 8.4: Parameter estimates for leptin

Parameter Estimates

Parameter	B	Std. Error	95% Wald Confidence Interval		Hypothesis Test			Exp(B)	95% Wald Confidence Interval for Exp(B)	
			Lower	Upper	Wald Chi-Square	df	Sig.		Lower	Upper
(Intercept)	13.229	4.6476	4.120	22.338	8.102	1	.004	556314.9	61.557	5.03E+9
C182n6ct_1	.004	.0037	-.003	.012	1.513	1	.219	1.005	.997	1.012
[Sex=M]	-3.093	1.1021	-5.253	-.933	7.877	1	.005	.045	.005	.393
[Sex=F]	0[a]	.	.	.	.	.	.	1	.	.
Age	-.006	.0325	-.070	.058	.036	1	.849	.994	.932	1.059
FASTINGBLOODGlucose_1	-.270	.1216	-.508	-.032	4.925	1	.026	.763	.601	.969
BMI_1	.043	.1045	-.162	.248	.172	1	.678	1.044	.851	1.282
ProteinCarbonyl_1	-2.218	.5162	-3.229	-1.206	18.459	1	.000	.109	.040	.299
C183n3_1	.028	.0837	-.136	.192	.113	1	.737	1.028	.873	1.212
C16_1	-.020	.0126	-.045	.005	2.550	1	.110	.980	.956	1.005
C18_1	.072	.0455	-.017	.161	2.481	1	.115	1.074	.983	1.174
(Scale)	16.532[b]	3.0184	11.559	23.645						

Dependent Variable: SMEAN(LEPTINNgml)
Model: (Intercept), C182n6ct_1, Sex, Age, FASTINGBLOODGlucose_1, BMI_1, ProteinCarbonyl_1, C183n3_1, C16_1, C18_1

a. Set to zero because this parameter is redundant.

b. Maximum likelihood estimate.

Table 8.5: Parameter estimates for BMI

Parameter Estimates

Parameter	B	Std. Error	95% Wald Confidence Interval		Hypothesis Test			Exp(B)	95% Wald Confidence Interval for Exp(B)	
			Lower	Upper	Wald Chi-Square	df	Sig.		Lower	Upper
(Intercept)	28.532	3.2348	22.191	34.872	77.794	1	.000	2.5E+12	4.34E+9	1.4E+15
C182n6ct_1	-.017	.0025	-.021	-.012	43.036	1	.000	.984	.979	.988
[Sex=M]	.524	1.1445	-1.719	2.768	.210	1	.647	1.689	.179	15.921
[Sex=F]	0[a]	.	.	.	.	.	.	1	.	.
Age	-.031	.0458	-.121	.058	.473	1	.492	.969	.886	1.060
C15_1	-.374	.2264	-.818	.070	2.728	1	.099	.688	.442	1.072
C181n9ct_1	.019	.0036	.012	.026	28.000	1	.000	1.019	1.012	1.026
C222_1	.200	.0287	.144	.256	48.570	1	.000	1.221	1.154	1.292
FASTINGBLOODGlucose_1	.174	.1184	-.058	.406	2.153	1	.142	1.190	.943	1.501
LEPTINNgml_1	.025	.0936	-.159	.208	.071	1	.791	1.025	.853	1.232
(Scale)	17.633[b]	3.2193	12.329	25.219						

Dependent Variable: SMEAN(BMI)
Model: (Intercept), C182n6ct_1, Sex, Age, C15_1, C181n9ct_1, C222_1, FASTINGBLOODGlucose_1, LEPTINNgml_1

a. Set to zero because this parameter is redundant.

b. Maximum likelihood estimate.

Table 8.6: Parameter estimates for fasting plasma glucose

Parameter Estimates

Parameter	B	Std. Error	95% Wald Confidence Interval		Hypothesis Test			Exp(B)	95% Wald Confidence Interval for Exp(B)	
			Lower	Upper	Wald Chi-Square	df	Sig.		Lower	Upper
(Intercept)	4.379	2.3368	-.201	8.959	3.511	1	.061	79.727	.818	7774.878
C182n6ct_1	-.004	.0027	-.010	.001	2.661	1	.103	.996	.990	1.001
BMI_1	.027	.0641	-.099	.153	.177	1	.674	1.027	.906	1.165
[Sex=M]	.503	.7459	-.959	1.965	.455	1	.500	1.654	.383	7.134
[Sex=F]	0[a]	.	.	.	.	.	.	1	.	.
Age	.036	.0237	-.010	.083	2.342	1	.126	1.037	.990	1.086
C16_1	.022	.0118	-.001	.045	3.486	1	.062	1.022	.999	1.046
C15_1	-.790	.2590	-1.297	-.282	9.295	1	.002	.454	.273	.754
C18_1	-.065	.0311	-.125	-.004	4.307	1	.038	.938	.882	.996
C183n3_1	.212	.0856	.045	.380	6.161	1	.013	1.237	1.046	1.463
(Scale)	11.078[b]	2.0225	7.745	15.844						

Dependent Variable: SMEAN(FASTINGBLOODGlucose)
Model: (Intercept), C182n6ct_1, BMI_1, Sex, Age, C16_1, C15_1, C18_1, C183n3_1

a. Set to zero because this parameter is redundant.

b. Maximum likelihood estimate.

Table 8.7: Parameter estimates for soluble E-Selectin

Parameter Estimates

Parameter	B	Std. Error	95% Wald Confidence Interval		Hypothesis Test			Exp(B)	95% Wald Confidence Interval for Exp(B)	
			Lower	Upper	Wald Chi-Square	df	Sig.		Lower	Upper
(Intercept)	82.792	35.1041	13.989	151.594	5.562	1	.018	9.0E+35	1189180	6.9E+65
C182n6ct_1	-.041	.0141	-.068	-.013	8.383	1	.004	.960	.934	.987
Age	-.484	.1691	-.816	-.153	8.209	1	.004	.616	.442	.858
FASTINGBLOODGlucose_1	1.872	.4341	1.021	2.723	18.598	1	.000	6.503	2.777	15.228
BMI_1	.197	.5931	-.966	1.359	.110	1	.740	1.217	.381	3.893
ProteinCarbonyl_1	-4.070	3.4827	-10.896	2.756	1.366	1	.243	.017	1.853E-5	15.732
C183n3_1	.926	.6323	-.313	2.165	2.144	1	.143	2.524	.731	8.717
LEPTINNgml	-.519	.7978	-2.083	1.045	.423	1	.515	.595	.125	2.843
CRPugml	.173	1.0881	-1.959	2.306	.025	1	.874	1.189	.141	10.032
C15_1	-1.791	1.7340	-5.189	1.608	1.066	1	.302	.167	.006	4.992
(Scale)	360.996[a]	66.4647	251.642	517.870						

Dependent Variable: SMEAN(Eselectinngml)
Model: (Intercept), C182n6ct_1, Age, FASTINGBLOODGlucose_1, BMI_1, ProteinCarbonyl_1, C183n3_1, LEPTINNgml, CRPugml, C15_1

a. Maximum likelihood estimate.